CHARACTERIZATION OF THE METAPLASTIC PROCESS IN THE STOMACH USING *IN VIVO* MODELS AND NOVEL NORMAL AND METAPLASTIC GASTRIC CELL LINES

By

Victoria Gail Weis

Dissertation

Submitted to the Faculty of the

Graduate School of Vanderbilt University

in partial fulfillment of the requirements

for the degree of

DOCTOR OF PHILOSOPHY

in

Cell and Developmental Biology

August, 2013

Nashville, Tennessee

Approved:

Christopher V. Wright

Richard M. Peek

Maureen A. Gannon

Chin Chiang

James R. Goldenring

ACKNOWLEDGEMENTS

I would first like to thank my mentor, Dr. James R. Goldenring for all the time and effort you have put into my training. Jim provided the support and mentoring for me to be an independent scientist. He allowed me to direct my project, but pushed me when I may have become complacent or made sure I had a back up when I took big risks. I would also like to thank Jim for encouraging me to voice my own opinions or ideas even if they meant trouble. Even more, thank you for all the support and understanding while I began the next stage of life as a mom. I couldn't have asked for a better mentor in navigating this new way of life.

I would also like to thank my committee members: Dr. Chin Chiang, Dr. Maureen Gannon, Dr. Richard Peek, and my chair, Dr. Christopher Wright. My committee always provided insightful feedback and helpful criticism in every meeting. Your guidance helped direct my work to what it is today. Dr. Peek was always willing to collaborate on needed projects and I am thankful for the help. I would like to especially thank Dr. Wright for inspiring me to be to the best scientist I can be. My training would not have been complete without the support and guidance of my committee. I would also like to thank Elaine Caine for all that she does. Elaine has done so much to make the life of a CDB student easier.

Members of the Goldenring lab have been instrumental in my training (and survival) through this entire process. Everyone was always willing to lend a hand or offer advice when needed. The friendly and helpful environment allowed me to learn so much about both science and life. Janice Williams was an excellent labmate who went above and beyond to teach me several techniques. I think I did extra tEM samples just so I could

visit her. Lynne Lapierre was always willing to answer all of my questions even if I interrupted Afternoon Tea Time. Her enthusiasm about polarization has considerably rubbed off on me and I cannot thank her enough. A big thanks goes to the Gastric Crew. Josane Sousa not only helped jump start my project when I was in a rut, but also provided friendship and support along the way. Christine Petersen's infectious cheerfulness was enough to pull me through on bad days. I feel much better knowing my cell culture 'babies' will be in good hands. I would also like to acknowledge Ki Taek Nam, our resident expert for everything. Always happy to look at slides, Ki Taek provided insight and unbiased opinions. I must thank him for his help on our trip to Korea, especially the baseball tickets. Also, many thanks to everyone else in the lab (past and present). There isn't enough space to even begin to show how important everyone has been to my training. I have enjoyed all of our discussions both scientific (controls?) and otherwise (dogs, cats, espresso, and many many others).

I would also like to acknowledge members of the Coffey lab. When I would run out of something, they would always let me borrow whatever I needed. Thanks to Emily Poulin for editing parts of this thesis. Jeff Franklin always had insightful feedback on my cell lines and provided much needed advice. Others in the Vanderbilt community must also be acknowledged. Thanks to Dr. Robert Whitehead for his expertise on the Immortomouse line and for making time to chat with me on his visits from Australia. And thanks to the late night custodial crew who always checked on me when I stayed late with my cells. They always brightened my night.

And lastly, thank you to my family and friends. My wonderful husband, Jared, is my rock. Without his steadfast support, I wouldn't be where I am today. He was always

accommodating and patient when I started running on ‘Tori’ time. Thank you! And thank you to our son, Jacob, for always reminding me to enjoy the moment. I can’t imagine graduate school without him. And I must also thank our ‘puppies’, Maya and Casper, for always providing stress relief at the end of the day.

Finally, I would like to acknowledge my funding sources. These studies were supported by grants from a Department of Veterans Affairs Merit Review Award, NIH grant RO1 DK071590, and an ARRA Supplement (DK071590-S1). This work was supported by core resources of the Vanderbilt Digestive Disease Center, (P30 DK058404) and the Vanderbilt-Ingram Cancer Center, and imaging supported by both the Vanderbilt Combined Imaging Shared Resource and the Shared Imaging Resource of the Vanderbilt Epithelial Biology Center.

TABLE OF CONTENTS

Page

LIST OF TABLES

LIST OF FIGURES

CHAPTER I

CURRENT UNDERSTANDING OF SPASMOLYTIC POLYPEPTIDE EXPRESSING METAPLASIA (SPEM) AND ITS STANDING IN THE PRENEOPLASTIC PROCESS

Adapted From: Weis, V.G. and Goldenring, J.R. Current understanding of SPEM and its standing in the preneoplastic process. Gastric Cancer. 2009;12(4):189-97.

Gastric adenocarcinoma is the second leading cause of cancer-related death worldwide (Pisani et al. 1999). Gastric resection remains the critical step in gastric cancer therapy. Accordingly, the early detection of early stage cancers remains a priority. However, the cellular mechanisms involved in the progression of preneoplastic events to gastric cancer remain unclear. This lack of a clear understanding of the neoplastic transition hampers efforts to discover better screening methods for populations at risk. Thus, a more extensive knowledge of the preneoplastic events could clearly reduce gastric cancer mortality. The following discussion reviews the emerging concepts on the origin of preneoplastic metaplasia and the factors that influence conversion of metaplasia towards neoplasia.

Oxyntic Atrophy, Metaplasia, and Gastric Adenocarcinoma

Chronic infection of the stomach with the gram-negative bacterium, *Helicobacter pylori*, is the leading proximate cause of gastric cancer in humans (Blaser et al. 1994a). Chronic *H. pylori* infection causes global changes in the gastric mucosa which can

eventually lead to gastric adenocarcinoma. These global changes result from the two major effects of chronic *H. pylori* infection: parietal cell loss (or oxyntic atrophy) and prominent inflammation. Oxyntic atrophy has a profound affect on the gastric mucosa because parietal cells play an important role in differentiation of other gastric lineages. Parietal cells are responsible for the secretion of a number of factors including amphiregulin, TGF-alpha, HB-EGF, and Shh (Beauchamp et al. 1989; Murayama et al. 1994; Abe et al. 1997; Jain et al. 2006a). Loss of parietal cell-derived signaling molecules disrupts the proper differentiation of other lineages such as the zymogen-secreting chief cells (Li et al. 1996). The second major result of chronic infection is prominent inflammation throughout the mucosa. Oxyntic atrophy along with prominent inflammation appear to be the prerequisites for progression to metaplasia and gastric adenocarcinoma (El-Zimaity et al. 2002).

Oxyntic atrophy in the setting of inflammation can progress to the development of metaplasia. In humans, two types of metaplasia can arise from the presence of oxyntic atrophy and inflammation: intestinal metaplasia and spasmolytic polypeptide expressing metaplasia (SPEM). Both intestinal metaplasia and SPEM have been associated with the progression to intestinal type gastric cancer (Hattori et al. 1979; Hattori et al. 1982; Hattori 1986; Correa 1988; Filipe et al. 1994; Takizawa et al. 1998; Schmidt et al. 1999; Xia et al. 2000; Yamaguchi et al. 2002; Halldorsdottir et al. 2003). Thus, a case can be made for oxyntic atrophy in association with prominent inflammation laying the groundwork for altered gastric lineages that are involved in the development of gastric cancer. However, the factors mediating progression from oxyntic atrophy to gastric cancer remain unclear. Intestinal metaplasia is characterized by the presence of intestinal

goblet cells in the stomach (Morson 1955). Because intestinal goblet cells are not normally present in the stomach, intestinal metaplasia was originally proposed as the pre-neoplastic metaplasia leading to intestinal type cancer (Correa 1988). Goblet cells in intestinal metaplasia express appropriate intestinal markers including Muc2 and Trefoil factor 3 (TFF3) (Ectors et al. 1986). However, investigations have identified a second possible pre-neoplastic metaplasia, SPEM. The mucous metaplastic lineages in SPEM display morphological characteristics more typical of deep antral gland cells or Brunner's glands, with expression of Muc6 and Trefoil Factor 2 (TFF2) (Schmidt et al. 1999). Despite the similarity between SPEM and the deep antral glands, no gastrin cells are observed in these glands. Recent studies have suggested that both SPEM and intestinal metaplasia may be pre-neoplastic metaplasias. In three separate studies, SPEM was associated with 90% of resected gastric cancers (Schmidt et al. 1999; Yamaguchi et al. 2001; Halldorsdottir et al. 2003). The exact influences promoting the sequential progression from oxyntic atrophy to metaplasia to dysplasia, however, remain unknown.

Parietal cell loss leads to metaplasia

The unresolved questions about the origin of oxyntic atrophy and its progression to gastric cancer are difficult to examine in humans, but mouse models are more amenable to answering these questions. As mentioned above, the most common predisposing factor for gastric cancer in humans is chronic *H. pylori* infections, resulting in oxyntic atrophy and prominent inflammation. The importance of both oxyntic atrophy and the inflammatory response has been examined in mice. Chronic infection of mice with *H. pylori* or with a different, but related, subspecies of *Helicobacter felis* (*H. felis*) results in profound loss of parietal cells and inflammation throughout the mucosa, similar

to that seen in humans (Fox et al. 1996; Wang et al. 1998; Fox et al. 2003). *H. felis*-infected C57BL/6 mice develop SPEM after 6 months of infection, demonstrating that oxyntic atrophy and inflammation can also lead to SPEM in mice (Figure 1). After 12 months of infection, the mice progress to gastritis cystica profunda, a dysplastic process in the fundic mucosa (Wang et al. 1998). Importantly, however, the infected mice never develop intestinal metaplasia, suggesting that SPEM is the pre-neoplastic metaplasia in mice. The direct cause of SPEM, however, is difficult to elucidate from this chronic model complicated by the presence of both of the major predisposing factors: oxyntic atrophy and prominent inflammation.

To isolate the role of oxyntic atrophy from the role of inflammation in the development of SPEM, administration of DMP-777 has been utilized to examine the role of acute oxyntic atrophy. DMP-777 is a cell permeant neutrophil elastase inhibitor that ablates parietal cells without inciting an inflammatory response. Loss of parietal cells is due to the secondary activity of DMP-777 as a parietal cell-specific protonophore. After 3 days of DMP-777 administration, mice develop oxyntic atrophy. The oxyntic atrophy gives rise to SPEM after 10 to 14 days of DMP-777 administration in the absence of inflammation (Nomura et al. 2004c). Thus, SPEM develops as a direct result of the loss of parietal cells (Figure 1). However, DMP-777-induced SPEM never progresses to dysplasia even after a year of administration (Goldenring et al. 2000). L635, another parietal cell-specific protonphore, lacks the neutrophil inhibition that DMP-777 possesses. Instead, administration of L635 results in oxyntic atrophy and a prominent inflammatory response that is similar to *H. felis* infection (Nam et al. 2010). SPEM develops after only 3 days of L635 administration. The rapid induction of SPEM from L635 administration is

the result of the inflammatory response that accompanies the parietal cell loss because without inflammation (as in DMP-777 administration) SPEM does not develop in 3 days (Nam et al. 2010). Although longer administration of L635 is not currently possible, the similarity of L635 administration and *H. felis* infection has led to the use of L635 as an initial alternative to long infection studies. Together, these findings suggest the important role of inflammation in the progression to gastric neoplasia. Furthermore, immunodeficient mice infected with *H. felis* do not develop oxyntic atrophy and thus do not develop SPEM or progress to dysplasia (Fox et al. 1993). In the case of pharmacological ablation of parietal cells, no inflammation is needed for parietal cell loss. More importantly, the parietal cell loss is sufficient for the development of SPEM.

Cellular Origin of Metaplasia

Although oxyntic atrophy leads to the emergence of SPEM, the cellular origin of SPEM was only recently discovered (Figure 1). Normal gastric cell lineages such as the acid secreting parietal cell and mucin secreting mucous neck cell are derived from progenitor cells located in the upper region of the gland (Karam 1993; Karam et al. 1993b; Karam et al. 1993c; Karam et al. 1993d; Karam et al. 1993e; Karam et al. 2003). As the post-mitotic mucous neck cells migrate towards the base of the gland, they alter their expression profiles as well as their morphology to redifferentiate into zymogen secreting chief cells (Figure 1) (Karam et al. 1993d; Ramsey et al. 2007). A previous study has shown that the transcription factor, *Xbp1* is necessary for the cessation of mucous cell marker expression and complete differentiation to chief cells (Huh et al. 2010). Furthermore, the transcriptions factor, *Mist1* is expressed in the last stages of this mucous

to chief cell differentiation and in mature chief cells (Figure 1). *Mist1* is required to establish the chief cell secretory machinery and thus for full maturation of chief cells (Ramsey et al. 2007). Because both mucous neck cells and chief cells have conventionally been thought of as post-mitotic, it had originally been suggested that SPEM cells arise from a cryptic progenitor cell located at the base of the gastric glands. However, recent studies have shown that the chief cells (or a subset of chief cells) transdifferentiate into SPEM cells (Nam et al. 2010). Indeed, the most reliable pattern for the emergence of SPEM following induced oxyntic atrophy has been the identification of cells at the bases of fundic glands expressing both intrinsic factor (a mouse chief cell marker) and TFF2 in different granules within the same cells (Nomura et al. 2004c). One recent study demonstrated that some SPEM cells express MIST1, a chief cell differentiation specific marker (Nozaki et al. 2008). The development of the Mist1-Cre mouse has now allowed for the investigation of chief cells as the cell of origin for SPEM. In this study, *Mist1* expressing chief cells lineage traced into SPEM regardless of the induction milieu (Nam et al. 2010). Oxyntic atrophy in both the absence and presence of inflammation results in chief cell transdifferentiation into SPEM. However, this study could not address the question if all chief cells or only a subset have the ability to transdifferentiate. The study by Nozaki et al. showed that SPEM cells located towards the base of the gland have an increase in the expression of minichromosome maintenance complex component 3 (MCM3), which is involved in initiation of genome replication. Occasionally, MCM3 positive cells were also observed at the bases of normal gastric glands in cells that co-expressed intrinsic factor, a chief cell marker in mice, suggesting that it may be a subset of chief cells that retain or possibly can reactivate the ability to

replicate (Nozaki et al. 2008). Recent studies in the intestine and gastric antrum have shown cells with leucine-rich repeat containing G-protein-coupled receptor 5 (*Lgr5*) transcriptional activity function like adult stem cells. Cells transcriptionally active for *Lgr5* expressed intrinsic factor and pepsinogen and were seen scattered in the lesser curvature of the stomach. However, upon administration of DMP-777 or L635, this subset of *Lgr5* expressing chief cells did not lineage map into SPEM (Nam et al.). Future studies are needed to investigate further the possibility that SPEM arises from a previous unidentified subset of chief cells as this data suggest different populations of chief cells exist.

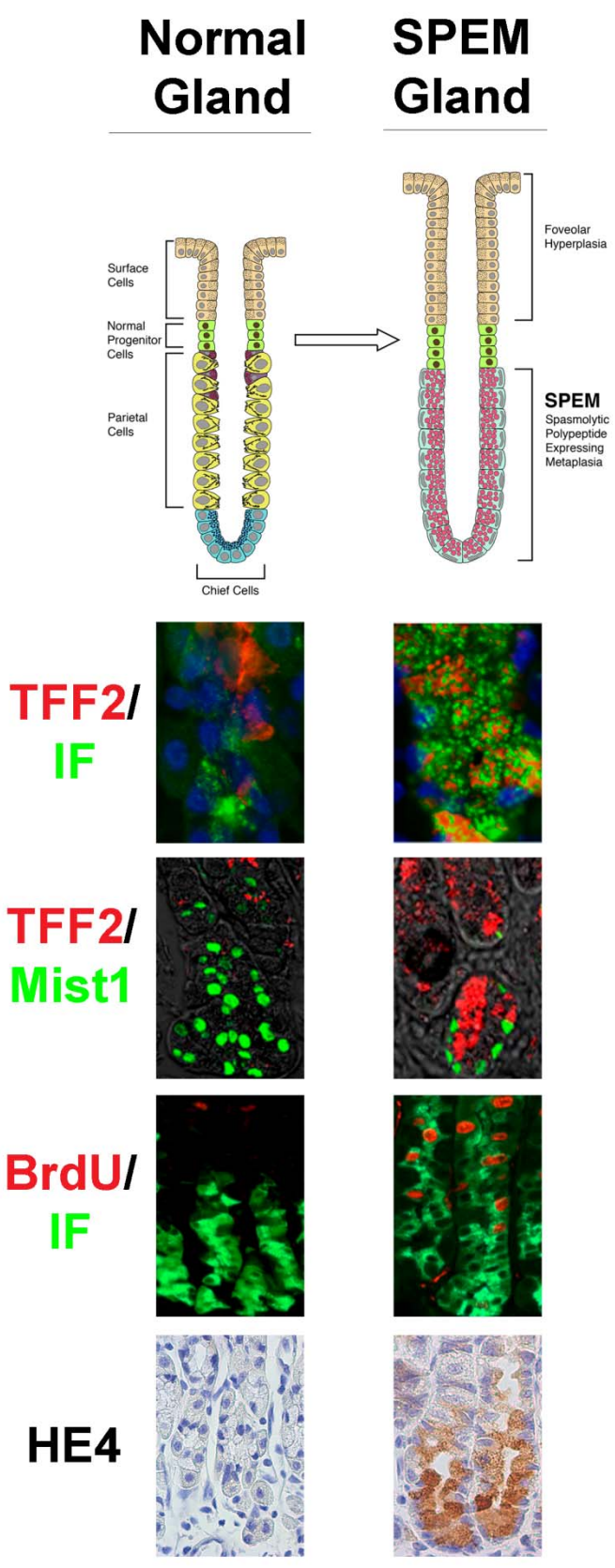
Normal Gland
SPEM Gland
Surface Cells
Normal Progenitor Cells
Parietal Cells
Chief Cells
Foveolar Hyperplasia
SPEM
Spasmolytic Polypeptide Expressing Metaplasia
TFF2/ IF
TFF2/ Mist1
BrdU/ IF
HE4

Figure 1. Comparison of normal fundic gastric glands and metaplastic SPEM glands in mice. The diagram at the top depicts alterations in gland lineages between normal and SPEM glands with emergence of SPEM and foveolar hyperplasia following loss of parietal cells. Panels below show immunostaining patterns for normal and SPEM-containing glands. TFF2 (red) expressing mucous neck cells redifferentiate into intrinsic factor (green) expressing chief cell at the base of normal glands. However, TFF2 expression is expanded to the base of SPEM glands and appears within cells that show dual staining for intrinsic factor. Mist1 (green) is a differentiated chief cell marker in normal gastric glands. However, Mist1 is also expressed in some TFF2-expressing SPEM cells, demonstrating transdifferentiation of chief cells. Although proliferation as detected by BrdU (red) is normally only in the progenitor zone of the upper normal gland, TFF2-expressing SPEM cells show clear proliferating cells also expressing intrinsic factor (IF). Previous studies have led to the identification of promising biomarkers of SPEM such as HE4. HE4 is not detected in normal chief cells or any normal fundic cells, but HE4 staining is strongly observed in SPEM.

The origin of intestinal metaplasia has been harder to elucidate because *Helicobacter* infection in mice does not result in intestinal metaplasia. However, *H. pylori* infection of other species, such as Mongolian gerbils, does induce intestinal metaplasia (Hirayama et al. 1996; Honda et al. 1998a). Moreover, *H. pylori* infection-induced intestinal metaplasia evolves into gastric cancer in older Mongolian gerbils (Honda et al. 1998b; Watanabe et al. 1998; Yoshizawa et al. 2007). Detailed examination of the histological progression of oxyntic atrophy to gastric cancer in the Mongolian gerbil has shed some light into the origin of intestinal metaplasia and its association with SPEM (Yoshizawa et al. 2007). After only 3 weeks of infection, the gerbils developed SPEM in the presence of oxyntic atrophy. The emergence of intestinal metaplasia followed later at 24 and 39 weeks of infection. Importantly, the sites of intestinal metaplasia were surrounded by the pre-existing SPEM. Moreover, single glands contained both intestinal metaplasia and SPEM (Yoshizawa et al. 2007). Similar developmental patterns of intestinal metaplasia have also been observed in humans (El-

Zimaity et al. 2001). The findings in these studies suggest that oxyntic atrophy results in the development of SPEM which in turn can then evolve into intestinal metaplasia (Figure 2). However, conclusive evidence of this progression has evaded researchers so far. Future studies in mouse models of SPEM and intestinal metaplasia are needed to trace this progression of metaplastic lineages to cancer. Until these studies are conducted, three hypotheses must be considered. First, each type of metaplasia (intestinal metaplasia or SPEM) may lead to a distinct type of cancer. For example, SPEM may progress to gastric type cancers while intestinal metaplasia proceeds to intestinal type cancers. Alternatively, one of the metaplasias could be the preneoplastic metaplasia, while the other is merely associated with cancer. The third hypothesis based on the Mongolian gerbil studies is that SPEM develops first, progresses to intestinal metaplasia, and finally evolves into gastric cancer. More extensive studies comparing both the transcript and protein expression patterns of metaplastic lineages to the patterns of gastric adenocarcinomas may provide insights into the links between metaplastic lineages and cancer.

Another aspect of this progression that must be considered, though not frequently mentioned, is the geographical origin of these metaplastic lesions within the stomach. SPEM and the resulting intestinal metaplasia found in *H. pylori* infected Mongolian gerbils initiated along the lesser curvature of the stomach and expanded towards the greater curvature during longer terms of infections (Yoshizawa et al. 2007). This concentration of metaplastic lineages along the lesser curvature has also been documented in humans (Sugimura et al. 1982; El-Zimaity et al. 2001). Additionally, *H. pylori* preferentially colonizes the lesser curvature both in mouse models and in humans

(Lee et al. 1997; Misra et al. 2000). This localization of metaplastic initiation in both rodents and humans may be the result of *Helicobacter sp.* colonization patterns. However, there may also be an underlying factor for this convergence on the lesser curvature that has yet to be discovered. For example, the cellular lineage composition of the lesser curvature may vary from the greater curvature to account for these differences in location of metaplastic initiation. Interestingly, the human stomach has not yet been extensively mapped out. It will be interesting to know the full extent of the differences in lineage distributions between the two curvatures and how they correspond with *H. pylori* colonization and the origin of metaplasia.

It is also necessary to consider the other geographical axis when examining the origin of metaplasias. Unlike the possible lineage differences between the two curvatures, there are known differences in the cell lineages between the fundus and the antrum of the stomach. Although parietal cells play a crucial signaling role in the fundus, they are not found in the antrum. Chief cells are also not located in the antrum. Instead, antral glands have a TFF2-expressing lineage that populates the base of the glands. The antrum also contains other cell lineages not found in the fundus such as gastrin expressing G-cells. Gastrin plays an important role in acid secretion as well as proliferation in the fundus (Johnson 1977; Wang et al. 1996). Knocking out gastrin creates a hypogastrinemic environment which results in a reduction in parietal cell mass in the fundus and chronic inflammation in the antrum. This antral inflammation leads to an increase in intestinal markers such as villin and MUC2, although goblet cell morphology is not seen. Eventually, tumors develop in the antrum in 12 month old gastrin-deficient mice (Zavros et al. 2005). Interestingly, another mouse model, the trefoil factor 1 (TFF1) knockout

mouse, also results in antral tumors, although more quickly. TFF1, unlike gastrin, is normally expressed in surface cells throughout the entire stomach. Mice lacking TFF1 expression develop antral tumors at 5 months of age (Lefebvre et al. 1996). Both mouse models suggest an important role for gastrin and TFF1 in maintaining normal differentiation of the antrum. A third mouse model combines the effect of gastrin and TFF1 loss. The gp130 mouse contains a mutation that inhibits protein tyrosine phosphatase (SHP2) binding to the interleukin 6 (IL-6) family co-receptor gp130. This binding inhibition results in decreases in gastrin and TFF1 expression as well as an increase in signal transducer and activator of transcription 3 (STAT3) expression. These aberrant expression patterns result in antral tumors at 6 weeks of age, which quickly extend into the fundus by around 17 weeks of age. Additionally, these tumors are accompanied by SPEM (Judd et al. 2004). Thus, the combined effect of gastrin loss with TFF1 loss accelerates the development of antral tumors in mice. Moreover, this model resembles antral tumor development in humans. Together gastric tumor models, in mice and Mongolian gerbils, demonstrate how metaplasias of the stomach and gastric cancer may originate and progress differently depending on the geographical location and possibly local regulatory signals.

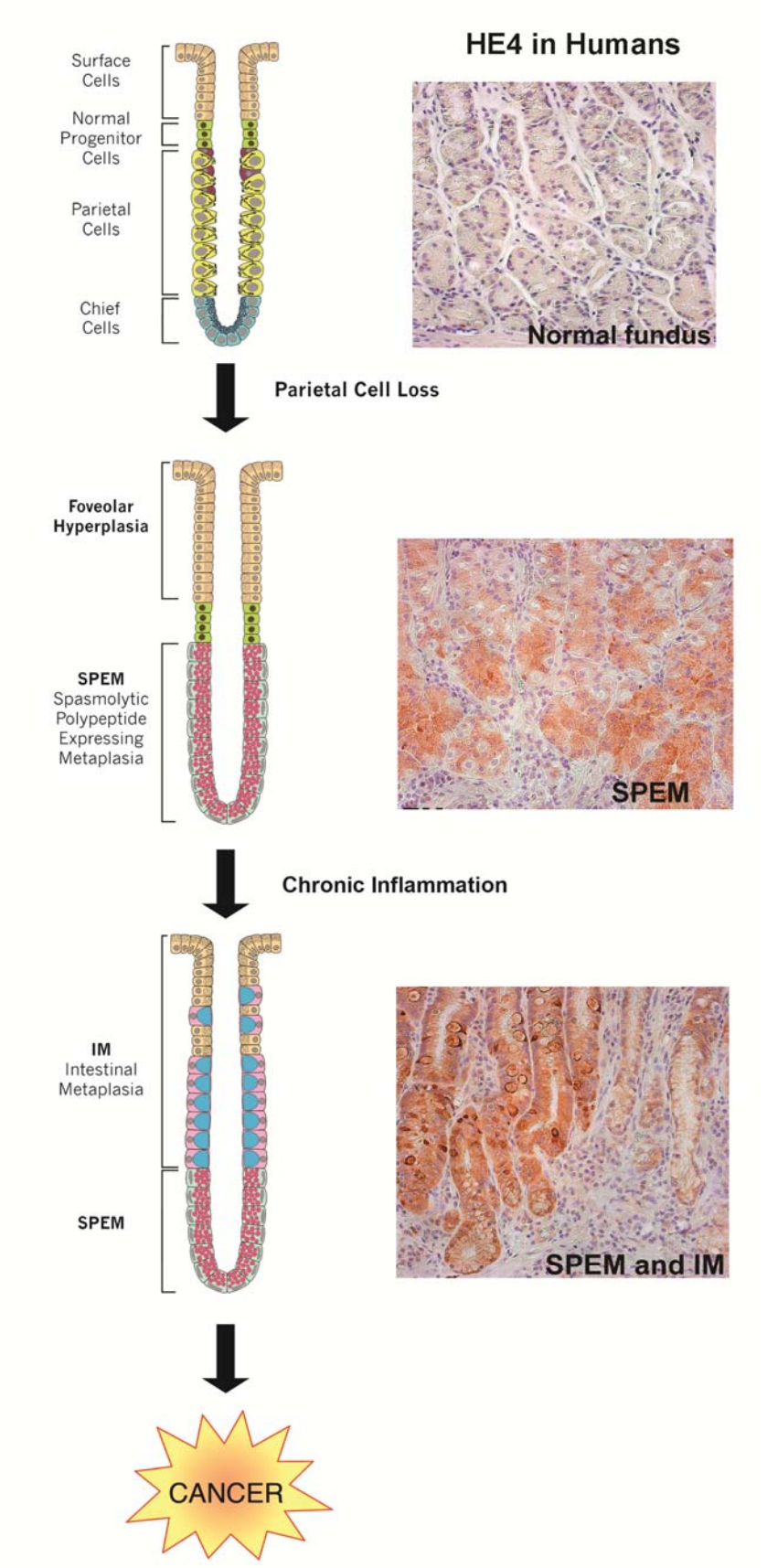
HE4 in Humans
Surface Cells
Normal Progenitor Cells
Parietal Cells
Chief Cells
Normal fundus
Parietal Cell Loss
Foveolar Hyperplasia
SPEM
Spasmolytic Polypeptide Expressing Metaplasia
SPEM
Chronic Inflammation
IM
Intestinal Metaplasia
SPEM
SPEM and IM
CANCER

Figure 2. Current model for the origin and progression of gastric metaplasias in humans. Studies have demonstrated that loss of parietal cells results in chief cell transdifferentiation and the SPEM emergence. In the presence of chronic inflammation from *H. pylori* infection, SPEM evolves into intestinal metaplasia then progresses on to gastric cancer. Establishment of biomarkers of these metaplastic lineages is a priority. Recent studies in mice identified HE4 as a SPEM biomarker. In humans, HE4 is not expressed in the cells of the normal fundus. However, HE4 is detected in both SPEM and intestinal metaplasia, supporting the hypothesis of SPEM progression to intestinal metaplasia.

Regulation of Metaplasia

While oxyntic atrophy is directly responsible for the development of SPEM, the emergence of SPEM can be altered by endocrine or paracrine regulation. As stated above, parietal cells produce instructive signaling for the growth and differentiation of the other gastric lineages. However, parietal cells also receive signals from other cell types in the gastric mucosa such as the previously mentioned gastrin secreting G cells and histamine secreting enterochromaffin-like (ECL) cells (Zimmerhackl et al. 1993; Andersson et al. 1998; Hinkle et al. 1999; Lindstrom et al. 2001; Samuelson et al. 2003; Chen et al. 2006a; Jain et al. 2006b). Gastrin stimulates ECL cell release of histamine, the primary stimulator of acid secretion from parietal cells (Chen et al. 2006a). Histamine secreted by the ECL cells also plays an important role in the differentiation of the gastric lineages (Appendix B) (Nozaki et al. 2009). At the same time, somatostatin cells coordinate inhibitory influences both on acid secretion and hormonal secretion (Chew 1983). Thus, parietal cells, G cells, somatostatin cells and ECL cells coordinate with each other to regulate the gastric mucosal milieu. Understandably then, the disruption of this balance of intramucosal factors affects the maturation of normal gastric lineages as well as the development of SPEM. For example, gastrin deficient mice develop SPEM after only one

day of DMP-777 administration, while it takes 10 days of DMP777 administration for the development of SPEM in wild type mice (Nomura et al. 2004c). Similarly, histidine-decarboxylase (HDC) deficient mice (which lack histamine) also have an accelerated development of SPEM upon administration of DMP-777 (Appendix B) (Nozaki et al. 2009). These studies highlight the complex coordination that occurs between the different cell lineages of the stomach.

Additionally, other intramucosal paracrine factors such as growth factors are important in the regulation of metaplasia. To examine the role of the epidermal growth factor (EGF) signaling pathway in the development of SPEM, the *waved-2* mouse was utilized, because it has a reduction in the EGF receptor tyrosine kinase activity. Upon administration of DMP-777, accelerated development of SPEM was observed in the *waved-2* mice (Ogawa et al. 2006). Further investigations into this signaling pathway demonstrated that different EGF receptor ligands affected the mucosal lineages differently. DMP-777-induced SPEM in TGFα-deficient mice developed similarly to that seen in wild type mice. In contrast, loss of amphiregulin led to accelerated SPEM development (Nam et al. 2007). Taken together, these findings demonstrate that emergence of SPEM is regulated by a complex coordination of both endocrine and paracrine factors. While loss of a single factor may alter SPEM development, no factor has been found to be solely responsible for the emergence of SPEM.

Metaplastic progression to gastric cancer

Inflammation plays an important role in the development and progression of SPEM. As stated before, while SPEM can develop in the absence of inflammation, it does not progress to dysplasia without inflammation. *Helicobacter* infections in mice

progress to dysplasia when prominent inflammation is present (Wang et al. 2000). The inflammatory response observed in these mice is composed mostly of a TH1 response (Mohammadi et al. 1996). Interestingly, further investigation into the components of inflammation has led to the discovery that the type of inflammatory response appears to be important in the progression to gastric cancer. In mice with a TH2 dominant inflammatory response to *H. felis* infection, the SPEM did not progress to dysplasia (Roth et al. 1999). Thus, a TH1 dominant inflammatory response is needed for progression of SPEM to dysplasia in mice. Other factors involved in the progression to neoplasia such as the necessary immune cells have been difficult to elucidate, possibly because of gaps in our knowledge of progression from metaplasia to dysplasia.

One recent study suggested a role for bone marrow derived cells (BMDCs) within this progression (Houghton et al. 2004a). This study found that BMDCs were recruited to the stomach during chronic *H. felis* infection. These recruited BMDCs appeared to engraft into the SPEM glands and progress to gastritis cystica profunda (Houghton et al. 2004a). No engraftment was observed in models of SPEM without inflammation, such as DMP-777 treatment. It also remains unclear whether BMDCs adopt the SPEM phenotype or actually fuse with SPEM cells during engraftment. At this time, it remains uncertain whether this engraftment of SPEM by BMDCs is specific to infection with the *H. felis* strain and there remains no strong evidence to support a role for BMDCs in the evolution of metaplasia or cancer in humans.

Another issue to consider is the concept of field cancerization and expansion of mutated clones. Field cancerization suggests that multiple stem cells form independent epithelial tumors (Slaughter et al. 1953). Application of this concept to SPEM and

intestinal metaplasia proposes that one of the stem cells in the gastric gland acquires a mutation. This mutated stem cell would then expand its mutated progeny until it eventually took over the gland and all the cell lineages present would have the mutation. The unit would then spread by gland fission creating a field of mutated gastric glands. A recent study applying this concept to intestinal metaplasia proposed that a gastric stem cell commits to the intestinal phenotype (McDonald et al. 2008). The progeny of the mutated stem cell would be seen mixed with normal gastric lineages as the stem cell proceeded to take over the gland. This could be one explanation for the mixed glands observed in the *H. pylori* infected Mongolian gerbils (Yoshizawa et al. 2007). It is possible that, while SPEM arises from transdifferentiation of the chief cells, intestinal metaplasia is derived from a mutated stem cell born in the context of SPEM. Alternatively, intestinal metaplasia may represent a further mucous cell metaplastic differentiation that predisposes to adoption and propagation lineages with genetic mutations. If these concepts are correct, then SPEM and intestinal metaplasia may represent sequential steps in the progression to gastric cancer.

Future studies may result in biomarker discovery

Given the clear association of metaplasias in the stomach with increased risk for gastric cancer, identification of markers of metaplasia and metaplastic progression to dysplasia is a clear priority for the development of effective screening methods that could identify pre-neoplasia. The discovery of preneoplastic biomarkers would be of great value for earlier detection and treatment of preneoplastic lesions. Recent studies have begun to identify a number of biomarkers that have implications for cancer outcome. For example, a recent study identified the secreted whey acidic protein (WAP) domain

protein, HE4 (WFDC2) as a putative biomarker (Nozaki et al. 2008). While there was no HE4 expression in normal gastric lineages, there was a prominent increase in expression in SPEM lineages from both DMP-777 treated and *H. felis* infected mice (Figure 1). Similarly, HE4 was expressed in metaplastic lineages in humans (Figure 2). Through examination of human tissue arrays, HE4 was found to have strong expression in 100% of both SPEM and intestinal metaplasias. Additionally, strong HE4 expression is maintained in a number of intestinal-type gastric cancers, making it a promising biomarker candidate. However, a more expansive array of biomarkers is still needed to increase the diagnostic specificity of metaplasias and preneoplastic events as well as expand our understanding of the metaplastic progression. As more biomarkers are established, diagnosis and treatments may be increasingly specialized based on the individual patient's biomarker expression patterns. Additionally, the discovery of new biomarkers will lead to a greater understanding into the molecular progression of normal gastric lineages to metaplasia (SPEM and intestinal metaplasia) to cancer.

Rationale and aims

Inflammation plays an important part in the progression to gastric adenocarcinoma. Utilizing pharmacological agents (DMP-777 and L635), the specific roles of parietal cell loss and inflammation could be investigated. Loss of parietal cells alone is sufficient for the transdifferentiation of chief cells into SPEM, while parietal cell loss accompanied by inflammation exacerbates the SPEM induction and progression. However, the molecular mechanisms of transdifferentiation in chief cells and SPEM progression have been difficult to elucidate with the currently available model systems. In Chapter II, SPEM lineages arising in different milieu were investigated for

commonalities and differences of phenotypically similar SPEM lineages. Transcriptional expression of acute SPEM without inflammation (DMP-777) or in the presences of inflammation (L635) and chronic SPEM with chronic inflammation were analyzed by gene microarray. We hypothesized that the presence or absence of inflammation as well as the length of time would result in differences among the SPEM lineages. However, all SPEM lineages would express a subset of transcripts, regardless of the surroundings in which it arose. To further investigate novel markers found in Chapter II, as well as previously identified factors involved in the induction of SPEM, we utilized the Immortomouse to develop two novel *in vitro* cell culture systems: ImChief and ImSPEM. Development of these lines would provide crucial *in vitro* models for investigations into the molecular mechanisms of chief cells and metaplasia of the stomach. To understand the progression of metaplasia, the cell of origin must also be examined. In Chapter IV, *Mist1* null mice were utilized to study the intrinsic characteristics of chief cells necessary for transdifferentiation into SPEM. Chief cells in *Mist1* null mice do not completely mature because they cannot maintain their secretory machinery. While previous investigations have focused on extrinsic factors acting upon chief cells, this study focuses on the function of chief cells themselves in SPEM induction. Overall, the studies presented here broaden our current understanding of the initiation and induction of metaplasia in the stomach. Furthermore, these studies provide novel *in vitro* models to study the molecular mechanisms and interactions of SPEM.

CHAPTER II

HETEROGENEITY IN MOUSE SPASMOLYTIC POLYPEPTIDE-EXPRESSING METAPLASIA LINEAGES IDENTIFIES MARKERS OF METAPLASTIC PROGRESSION

Appears as: Weis, V.G., Sousa, J.F., Lafleur, B.J., Nam, K.T., Weis, J.A., Finke, P.E., Ameen, N.A., Fox, J.G., and Goldenring, J.R. Heterogeneity in mouse spasmolytic polypeptide-expressing metaplasia lineages identifies markers of metaplastic progression. Gut. In press.

Introduction

Helicobacter pylori infection is the major predisposing factor for human gastric cancer (Blaser et al. 1994a). In humans, *H. pylori* infection causes a disruption in the gastric homeostasis by inducing prominent chronic inflammation and loss of parietal cells. The loss of parietal cells leads to two distinct types of mucous cell metaplasia: intestinal metaplasia and spasmolytic polypeptide-expressing metaplasia (SPEM). While intestinal metaplasia has conventionally been considered the primary neoplastic precursor to gastric cancer, SPEM is associated with 90% of resected gastric cancers (Schmidt et al. 1999; Yamaguchi et al. 2001; Halldorsdottir et al. 2003). Increasing evidence in humans and rodent models suggests that intestinal metaplasia develops in the presence of pre-existing SPEM, supporting the concept that SPEM is a neoplastic precursor (Yoshizawa et al. 2007; Nam et al. 2009; Goldenring et al. 2010).

Chronic *H. felis* infection in mice is a critical model for *H. pylori* infection in humans. After 6 months of *H. felis* infection, significant parietal cell loss accompanied by inflammation leads to the emergence of a proliferative SPEM lineage (Figure 3A). SPEM progresses to dysplasia after 1 year of infection without developing phenotypic intestinal metaplasia (Wang et al. 2000; Houghton et al. 2004a). Thus, all present evidence indicates that SPEM is the direct precursor to dysplasia in *H. felis*-infected mice. Several mouse models have previously been utilized to investigate SPEM induction in the setting of parietal cell loss. Of importance, an acute oxyntic atrophy model using the parietal cell-specific protonophore, DMP-777, allows for the separation of the roles of parietal cell loss and inflammation in the initiation of SPEM (Figure 3A) (Goldenring et al. 2000; Nomura et al. 2004c). Oral gavage administration of DMP-777 for 14 days induces SPEM as a direct result of parietal cell loss. However, DMP-777 also inhibits any inflammatory response because of its ability to potently inhibit neutrophil elastase resulting in SPEM that is less proliferative (Goldenring et al. 2000; Nomura et al. 2004c). DMP-777-induced SPEM fails to progress to dysplasia even after a year of administration (Goldenring et al. 2000). Thus, the DMP-777 model shows that parietal cell loss is sufficient for SPEM initiation, but inflammation is necessary for the progression of SPEM to dysplasia. In contrast, acute administration of L635, a protonophore analog of DMP-777 that lacks elastase inhibition, results in a prominent inflammatory response and induces a SPEM lineage phenotypically similar to *H. felis* infection (Figure 3A and Figure 4) (Nam et al. 2010). Analysis of the progression to dysplasia with chronic administration of L635 is not currently feasible due to limited supplies of the drug. These results have led to the concept that inflammatory cells drive the evolution of metaplasia

towards a more proliferative lineage and later to dysplasia. However, no studies have investigated differences in expression among phenotypic SPEM lineages.

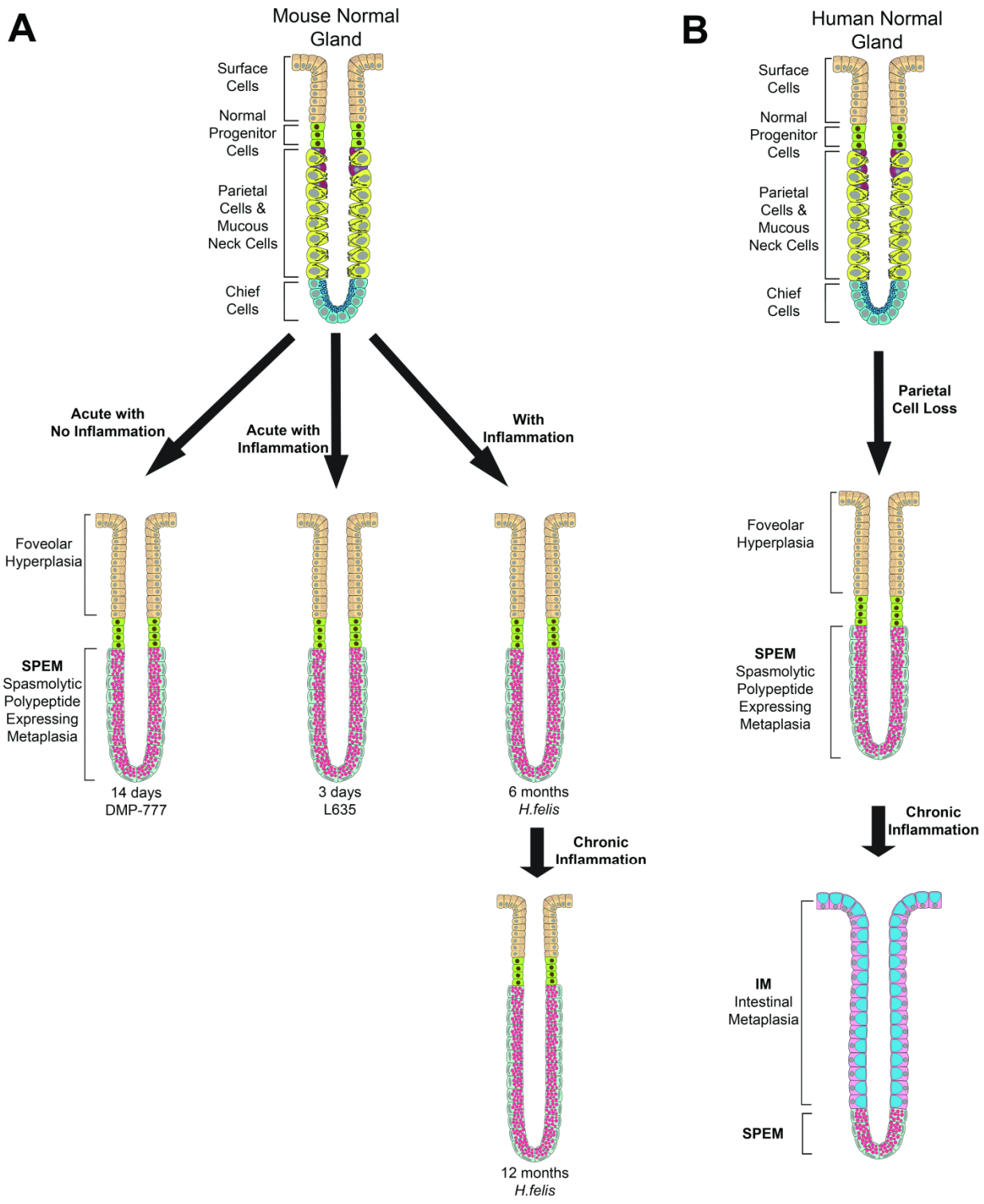
A
Mouse Normal Gland
Surface Cells
Normal Progenitor Cells
Parietal Cells & Mucous Neck Cells
Chief Cells
Acute with No Inflammation
Acute with Inflammation
With Inflammation
Foveolar Hyperplasia
SPEM
Spasmolytic Polypeptide Expressing Metaplasia
14 days
DMP-777
3 days
L635
6 months
H.felis
Chronic Inflammation
12 months
H.felis
B
Human Normal Gland
Surface Cells
Normal Progenitor Cells
Parietal Cells & Mucous Neck Cells
Chief Cells
Parietal Cell Loss
Foveolar Hyperplasia
SPEM
Spasmolytic Polypeptide Expressing Metaplasia
Chronic Inflammation
IM
Intestinal Metaplasia
SPEM

Figure 3. Models of phenotypic SPEM in mice and of metaplastic progression in humans. (A) The three mouse models used in these investigations all display phenotypic SPEM. DMP-777 administration is an acute model of parietal cell loss that results in SPEM without inflammation. L635 administration is also an acute model of SPEM; however, L635-induced SPEM is accompanied by prominent inflammation. *H. felis* infection is a SPEM model phenotypcially similar to L635 but with chronic inflammation. *H. felis* infection induces SPEM at 6 months but progresses with chronic inflammation to acquire intestinal characteristics. (B) In humans, loss of parietal cells leads to the emergence of SPEM. Intestinal metaplasia arises from SPEM under the influences of chronic inflammation.

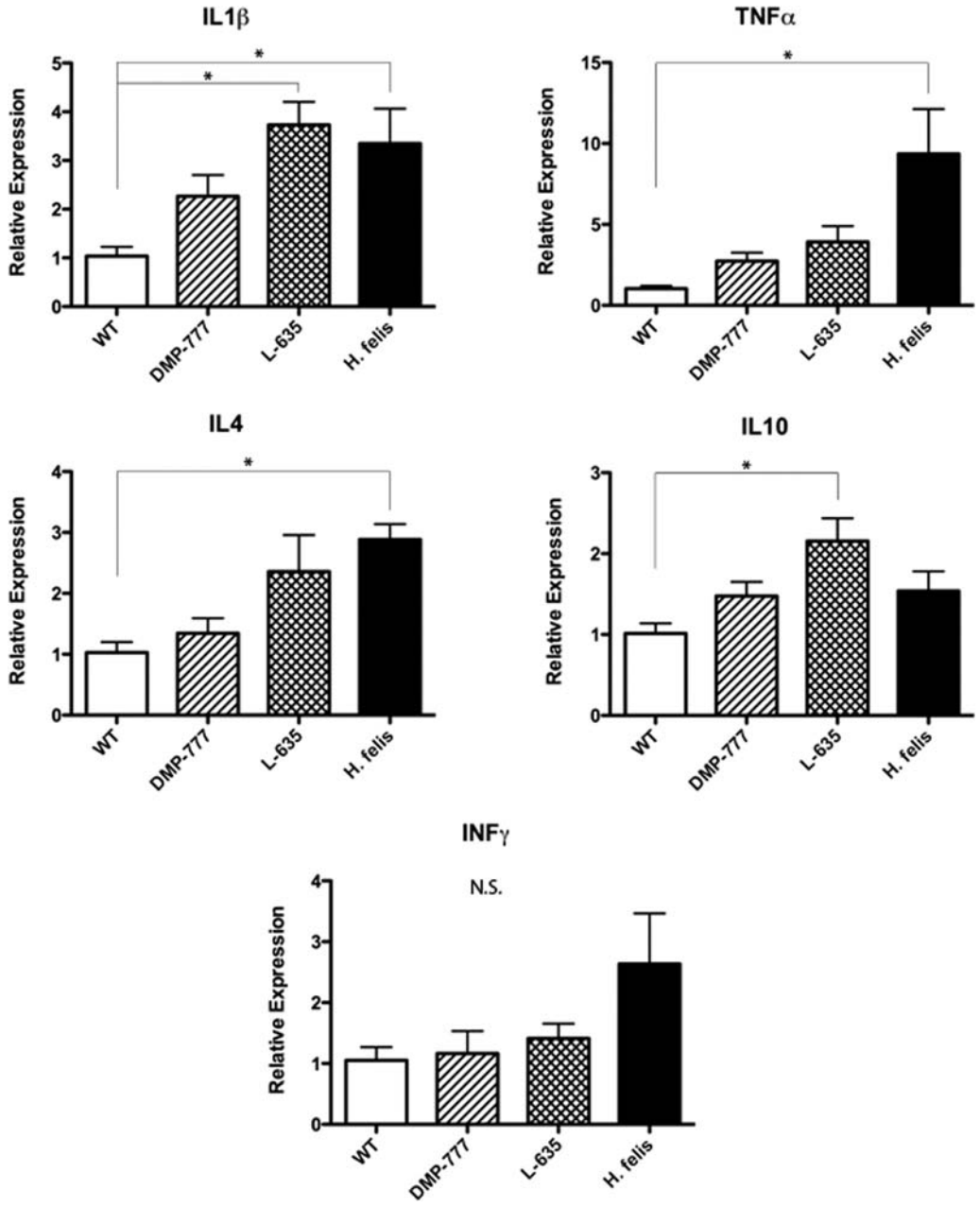

Figure 4. Expression of cytokines in the gastric mucosa of L-635–treated and H felis–infected mice. Transcript levels for tumor necrosis factor (TNF)-α, IL-1β, IL-4, IL-10, and interferon-γ were determined by real-time PCR in fundic RNA samples isolated from untreated wild-type (WT), DMP-777–treated, L-635–treated, and H felis–infected mice (n = 3 for all groups). Results are expressed as a ratio of the mean expression in wild-type mice (±standard error of the mean). *P < 0.05 vs untreated wild-type mice. Adapted from (Nam et al. 2010).

Recent studies have shed important light on the origins of SPEM lineages. Lineage mapping studies showed that SPEM arises through transdifferentiation of mature chief cells into mucous cell metaplasia (Nam et al. 2010). Nevertheless, these studies utilizing three SPEM models have indicated that differences exist among phenotypically similar SPEM lineages. *H. felis* infection-induced and L635-induced SPEM, both of which are associated with prominent inflammatory infiltrates, were derived almost completely from transdifferentiated chief cells. In contrast, phenotypic SPEM arising from DMP-777 administration showed two distinct component lineages: transdifferentiated chief cells at the gland bases and mucous neck cell hyperplasia in the neck region (Nam et al. 2010). Taken together, these studies suggest that transdifferentiation of chief cells to SPEM is common to all models, but the progression of metaplasia is significantly affected by the surrounding inflammatory milieu.

To investigate the different phenotypic SPEM lineages, we have compared transcriptional expression profiles for microdissected chief cells from untreated C57BL/6 mice with microdissected SPEM cells from mice after 6-12 months of *H. felis* infection, 3 days of L635 administration, or 14 days of DMP-777 administration. Specific comparison categories identified putative markers of SPEM emergence as well as metaplastic progression. Wfdc2 (HE4), the previously reported SPEM and intestinal metaplasia marker,(Nozaki et al. 2008) was upregulated in all SPEM models. Additionally, the disulfide-linked heterodimeric glycoprotein clusterin (Clu), which is expressed only at low levels in the progenitor zone of the normal stomach, was upregulated in all of the SPEM lineages in both mice and humans. SPEM models with inflammation showed upregulation of a number of biomarkers that also were previously

observed in human intestinal metaplasia (Lee et al. 2010). The ATP-binding cassette transporter, cystic fibrosis transmembrane conductance regulator (CFTR), was not found in normal gastric mucosa or SPEM without inflammation, but was upregulated in inflammatory SPEM. In humans, CFTR was expressed only in intestinal metaplasia, but not in normal mucosa or SPEM. Together, these findings indicate that distinct heterogeneity is present in different animal models of phenotypic SPEM. In addition, these investigations indicate that SPEM in the context of inflammation, especially with long-term infection with *H. felis* for greater than one year, acquires the expression of intestinal transcripts that resemble features of intestinal metaplasia in humans.

Methods

Mice

C57BL/6 mice obtained from Jackson Laboratories (Bar Harbor, ME) were used for all experiments. During the experiments, the mice were maintained with regular mouse chow and water *ad libitum* in a temperature-controlled room under a 12-hour light/dark cycle. The care, maintenance, and treatment of animals in these studies followed protocols approved by the Institutional Animal Care and Use Committee of Vanderbilt University.

Drug administration and H. felis challenge

DMP-777, a gift from DuPont Pharmaceuticals (Wilmington, DE), was formulated in 0.5% methylcellulose and administered orally as a gavage once daily at 350 mg/kg/day for 14 consecutive days. L635, dissolved in saline and orally administered as

a gavage once daily at 350 mg/kg/day for 3 consecutive days, was a gift from Merck & Co, Inc (Rahway, NJ). *H. felis* was grown in brucella broth containing 5% fetal bovine serum overnight. Bacteria were collected by centrifugation. After fasting overnight, 6 week old mice were inoculated 3 times every other day by oral gavage with 10^8 *H. felis* cells in 0.2 ml of brucella broth.

Gene microarray analysis

DMP-777 or L635 was administered by oral gavage to groups of six 7 month old C57BL/6 male mice. Another group of 6 mice (2 males and 4 females) were *H. felis* infected for 6-12 months. Untreated C57BL/6 male mice were used as controls. Chief cells from control mice or SPEM lineages at the base of glands from treated mice were laser capture microdissected from frozen sections of fundic stomach. Total RNA was isolated from microdissected cells with Picopure RNA Isolation Kit (Arcturus, Mountain View, CA). The Nugen WT Pico Kit (San Carlos, CA) was used to reverse transcribe and amplify 25 ng of total RNA for each sample. Fragmented and labeled samples were hybridized to Affymetrix Mouse Gene 1.0ST arrays (Santa Clara, CA) using standard Affymetrix protocols. The raw gene expression data (.cel files) were converted to expression values using the Affy function in R (http://www.bioconductor.org). Once expression values were obtained, we filtered the features that have at least 25% samples with intensities above 100 fluorescent units and inter-quartile range of at least 0.5 (removal of outliers and non-specific intensities). The $\log_2$-based expression levels were then compared on the resulting features using ebayes moderated t-tests implemented in the limma package. These p-values were ranked and a candidate feature list was compiled, using False Discovery Rate adjusted p-value cut-offs obtained by the linear

step-up method described by Hochberg and Benjamini (Hochberg et al. 1990). The generated candidate lists were then compared to each other to create the comparison categories (Table 1 and Supplemental Table 1 - Supplemental Table 5).

Quantitative real time polymerase chain reaction

From 3 male mice per group, total RNA was extracted from the gastric fundus using TRIzol (Invitrogen, Carlsbad, CA) according to the manufacturer's instructions. For each sample, 1 μg of total RNA was treated with RQ1 RNase-free DNase (Promega, Madison, WI) and then reverse-transcribed using Superscript III reverse transcriptase (Invitrogen, Carlsbad, CA). Quantitative real time polymerase chain reaction (qRT-PCR) was performed with EXPRESS SYBR GreenER quantitative PCR SuperMix (Invitrogen, Carlsbad, CA) using specific primers in an ABI StepOnePlus Real-Time PCR System (Applied Biosystems, Foster City, CA). The specific primer sequences and concentrations are listed in Supplemental Table 6. Each sample was run in triplicate following cycling conditions indicated by the SYBR Green supermix manufacturer's protocol. Relative expression analysis was performed as previously reported (Nam et al. 2010). In short, using TATA–box-binding protein as an endogenous control and the mean value of the control mouse samples as a reference, the $2^{-\Delta\Delta}$ cycle threshold method was used to compare samples. Statistical significance ($P < 0.05$) between the groups was determined using the Mann-Whitney *U* test.

Immunohistochemistry

Excised stomachs from mice were frozen in liquid nitrogen or fixed in 4% paraformaldehyde overnight and embedded in paraffin. For paraffin embedded samples,

antigen retrieval was performed using Target Retrieval solution (DakoCytomation, Glostrup, Denmark). For frozen samples (for GSII lectin and CFTR antibodies), 7 μm thick sections were air dried then fixed in 4% paraformaldehyde (for GSII lectin) or 2% paraformaldehyde (for CFTR) for 10 minutes. Immunostaining was performed using the following primary antibodies incubated at 4°C overnight: mouse anti-TFF2 (1:500; a gift from Dr Nicholas Wright, Cancer UK, London, England), mouse anti-pan-cytokeratin (1:500, Abcam, Cambridge, MA), goat anti-clusterin α (1:2500, Santa Cruz Biotechnology, Santa Cruz, CA), rabbit anti-CFTR (1:500),(Ameen et al. 2000) and mouse anti-CFTR clone M3A7 (1:40, Santa Cruz Biotechnology, Santa Cruz, CA). Detection for immunohistochemistry was performed with 3,3-diaminobenzidine using a kit from Vector Laboratories (Burlingame, CA). For immunofluorescence, Alexa594 conjugated GSII lectin (Molecular Probes, Eugene, OR), Cy3-goat anti-mouse IgM antibody, Cy5-goat anti-mouse IgG antibody (Jackson ImmunoResearch, West Grove, PA), and Alexa488 donkey anti-goat IgG (Invitrogen, Carlsbad, CA) were used at 1:500. Slides were mounted with ProLong Gold Antifade Reagent with DAPI (Invitrogen). Sections were analyzed using Zeiss Axiophot microscope equipped with an Axiovision digital imaging system (Zeiss, Jena GmBH, Germany) or an Olympus FV1000 confocal microscope (Tokyo, Japan) and tissue arrays were analyzed using the Ariol SL-50 automated slide scanner (Genetix, San Jose, CA).

Statistical analysis

A tissue array of normal gastric fundic mucosa (n=15) and metaplasias (SPEM and intestinal metaplasia, n=37) resected at University of Tokyo (Leys et al. 2006) was used for analysis of clusterin expression. Each core was identified as having normal

glands, SPEM, intestinal metaplasia or a combination. The TMA section used for analysis had 25 cores with normal glands, 20 with SPEM and 11 with intestinal metaplasia. Samples were considered positive if the glands displayed the staining pattern described: progenitor region of normal glands, throughout SPEM glands, or a few cells at the base of intestinal metaplasia glands. A percentage was calculated as the number of positive cores out of a total number of cores with SPEM or intestinal metaplasia. For initial expression analysis in cancer, a tissue array comprised of 44 gastric cancers resected at Vanderbilt Medical Center (Leys et al. 2006) was scored as positive or negative using immunohistochemistry. For this analysis, 16 intestinal-type cancer cores and 7 diffuse-type cancer cores were scored. A core was considered positive if clusterin staining was detected in any part of the gland besides the progenitor region. A second gastric adenocarcinoma tissue array with 450 patient samples resected at Seoul National University Hospital was used for correlation studies (SNUH-2004-GC; SuperBioChips, Seoul, Korea) (Lee et al. 2010). Stained sections were scanned using the Ariol SL-50 (Genetix, San Jose, CA). CellProfiler (Lamprecht et al. 2007) (Broad Institute, Cambridge, MA) was then used to detect the percentage of epithelial cells positive for clusterin immunostaining using pan-cytokeratin as a reference for the total number of epithelial cells (Figure 5). All counted cells had nuclei as detected by DAPI.

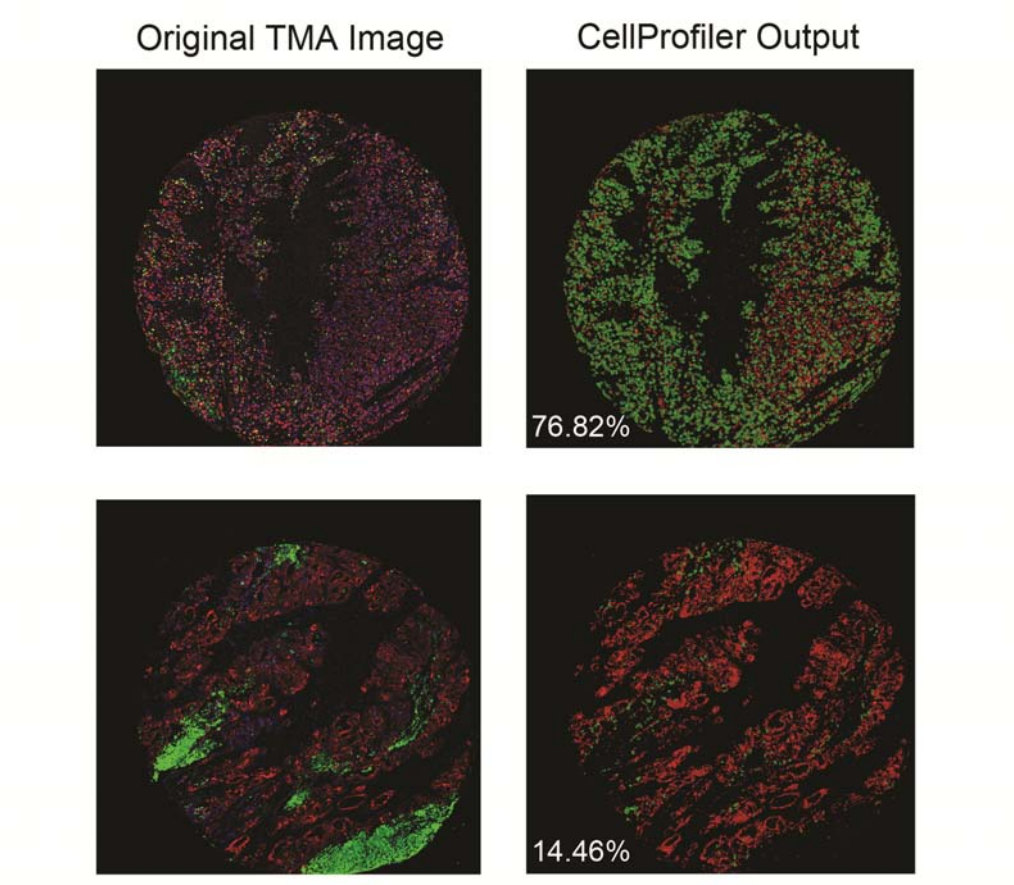

Figure 5. Representative images of tissue array cores and CellProfiler expression detection. Each core was individually processed with CellProfiler. Pan-cytokeratin (red) was used to identify epithelial cells and DAPI for nuclei. CellProfiler detected the number of clusterin (green) positive epithelial cells with nuclei. The left panels are a representative TMA core images and the right panels are the CellProfiler renderings of the detected expression. In the CellProfiler renderings (right panels), red represents epithelial cells with nuclei as detected by pan-cytokeratin staining and green is detectable clusterin staining. The percentage of clusterin positive epithelial cells was used for correlation studies of clusterin expression.

Cox proportional hazards models were used to evaluate the association between percent of clusterin positive epithelial cells and survival. All models included pathologic stage as defined by American Joint Committee on Cancer (AJCC). We transformed the percentage of positive clusterin staining using the square root transformation to reduce

variability. Restricted cubic splices (rcs) were used to allow for more flexibility in the relationship between positive staining and survival. Analysis of variance models were fit for clusterin levels and prognostic indicators including stage, Lauren grade, metastasis, and histopathology. Pair-wise differences for all statistically significant prognostic indicators were performed at the 0.05 level of significance.

Results

Gene microarray analysis of phenotypic SPEM lineages with and without inflammation

To compare the expression profiles of SPEM lineages arising in different milieus, we used laser capture microdissection to isolate chief cells from control untreated mice and SPEM cells at the bases of glands from mice treated with DMP-777, L635, or *H. felis* infection. These SPEM models were selected based on their distinct characteristics such as length of treatment (acute versus chronic) and progression to dysplasia (presence versus absence of inflammation) (Figure 3A), so that the commonalities and differences among the different phenotypic SPEM lineages could be analyzed. Levels of isolated mRNA transcripts from the microdissected cells were measured with Affymetrix gene microarrays. Five comparison categories were established based on the SPEM model characteristics (as mentioned above) to analyze upregulated transcripts associated with either the emergence or progression of SPEM (listed in Table 1 with heat maps of each group shown in Figure 6). The Pan-SPEM and Acute SPEM categories focus on transcripts upregulated with the induction of SPEM. Transcripts upregulated in all SPEM

lineages as compared to chief cells are markers indicative of the initiation of SPEM (Pan-SPEM). Eight transcripts were upregulated in Pan-SPEM including the secreted glycoprotein, clusterin (Clu) and the previously reported SPEM marker, whey acidic protein 4-disulfide core domain 2 (Wfdc2, also known as HE4) (Nozaki et al. 2008). In the previous study, we identified HE4 as a marker of SPEM and intestinal metaplasia that was not found in the normal stomach (Nozaki et al. 2008). The Acute SPEM comparison, comprised of transcripts increased in acute SPEM lineages (DMP-777 and L635-induced SPEM) versus chief cells, revealed transcripts that initially increase in SPEM induction, but decrease in chronic SPEM lineages. Acute SPEM identified 5 additional transcripts upregulated in the initiation of SPEM (Table 1), which included fidgetin-like 1 (Fignl1), a transcript previously reported as upregulated in gastrin-deficient mice treated with DMP-777 (Nozaki et al. 2008).

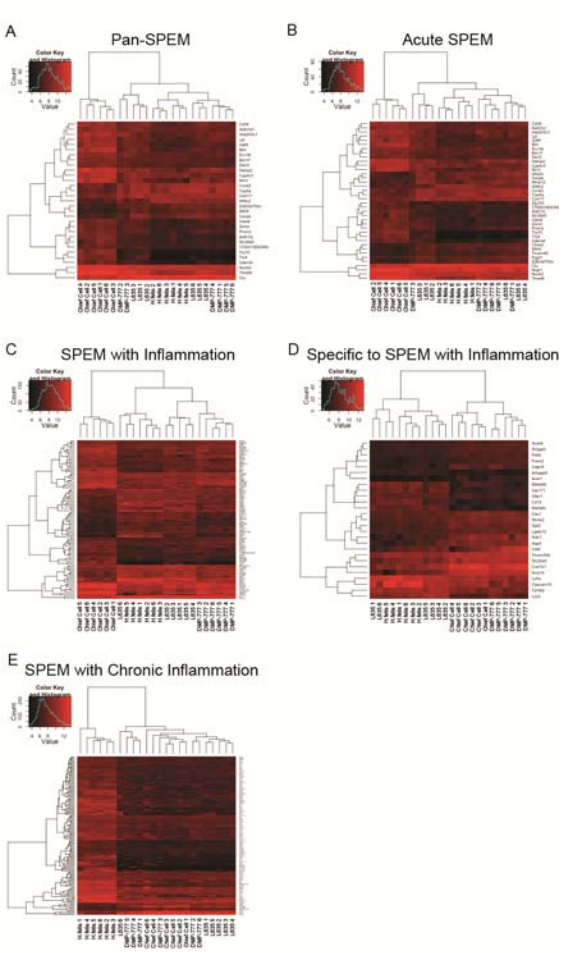

Figure 6. Heat map analysis of each comparison category. Heat map analysis was performed on each comparison category: Pan-SPEM (A), Acute SPEM (B), SPEM with Inflammation (C), Specific to SPEM with Inflammation (D), and SPEM with Chronic Inflammation (E). Clustering of samples is shown in each panel.

Table 1. Upregulated transcripts in three mouse models of SPEM. Normal chief cells and SPEM lineages from 3 SPEM models were compared by gene microarray (6 mice per group). Five comparison categories were established: Pan-SPEM (I), Acute SPEM (II), SPEM with Inflammation (III), Specific to SPEM with Inflammation (IV), and SPEM with Chronic Inflammation (V). The linear fold change in each sample group is listed as compared to the column marked with a bullet point (•). In Categories I, II, and III, fold changes are upregulated as compared to Chief Cells. Category IV changes are compared to DMP-777. In Category V, listed transcripts are upregulated in *H. felis* as compared to each of the other groups; thus fold changes are shown as relative downregulation in the respective groups. Asterisks denote transcripts previously found upregulated in human metaplasias of the stomach (Lee et al. 2010).

I. Pan-SPEM				
	Chief Cells	DMP-777	L635	*H.felis*
*Ccnb2	●	2.01	2.55	1.82
*Cenpk	●	1.35	2.60	1.27
Clu	●	1.04	1.58	1.38
Cxcl17	●	1.50	1.81	1.56
Slfn9	●	1.33	2.18	1.33
*Top2a	●	1.95	2.92	2.11
Traf4	●	1.75	2.18	1.59
Wfdc2	●	1.62	1.50	3.12
II. Acute SPEM				
	Chief Cells	DMP-777	L635	
Chek2	●	1.23	1.42	
Fignl1	●	1.19	1.93	
Mmp12	●	1.91	2.79	
Tmem48	●	0.78	1.76	
Ube2c	●	1.61	2.88	
III. SPEM with Inflammation				
	Chief Cells		L635	*H.felis*
*Cftr	●		3.14	5.78
*Ctss	●		1.24	2.03
*Dmbt1	●		2.72	2.77
Etv5	●		2.01	3.13
*Gpx2	●		2.36	3.00
*Mad2l1	●		2.12	1.78
*Prom1	●		0.73	1.44
IV. Specific to SPEM with Inflammation				
		DMP-777	L635	*H.felis*
Arhgap9		●	0.84	0.77
Cd14		●	1.53	2.72
Ceacam10		●	0.36	2.17
Glipr1		●	0.98	0.84
Gpr171		●	1.89	2.17
Ly6a		●	0.75	1.26
Lyz2		●	2.53	1.97
Ms4a6b		●	1.45	1.94
Ms4a6c		●	2.13	2.03
Tyrobp		●	1.47	1.15
V. SPEM with Chronic Inflammation				
	Chief Cells	DMP-777	L635	*H.felis*
*Casp1	-4.10	-4.45	-4.32	●
*Ceacam1	-3.44	-3.05	-2.28	●
*Gpa33	-2.93	-2.74	-3.60	●
*Il18r1	-3.09	-1.66	-1.99	●
*Itga2	-2.87	-2.61	-2.81	●
*Muc4	-3.74	-3.34	-3.77	●
*Pigr	-5.37	-3.29	-3.16	●
*Vil1	-2.59	-2.26	-2.60	●

Because previous studies have indicated that SPEM cannot progress to dysplasia in the absence of inflammation,(Goldenring et al. 2000; Oshima et al. 2005) transcripts putatively involved in the progression of SPEM were identified with comparisons focusing on SPEM accompanied by inflammation (L635- and *H. felis*-induced SPEM). Transcripts increased in L635- and *H. felis*-induced SPEM versus chief cells are listed as "SPEM with Inflammation," whereas the comparison of inflammatory SPEM to non-inflammatory SPEM (DMP-777-induced SPEM) identified "Specific to SPEM with Inflammation" transcripts. The "SPEM with Chronic Inflammation" category compares *H. felis*-induced SPEM to acute SPEM models (with and without inflammation) and chief cells. Ten transcripts were upregulated in the Specific to SPEM with Inflammation comparison. The SPEM with Inflammation and SPEM with Chronic Inflammation categories yielded numerous upregulated transcripts (43 and 131, respectively) (selected transcripts listed in Table 1). Pathway analysis of the comparison categories only identified an increase in interferon-γ associated genes in SPEM with Chronic Inflammation (Figure 7). As a whole, these gene microarray studies demonstrated that phenotypic SPEM lineages did indeed demonstrate distinct differences in transcript expression.

To narrow the lists for further investigation, we compared the upregulated transcripts to transcripts previously reported as upregulated in microdissected human metaplasias of the stomach (SPEM or intestinal metaplasia) by gene microarray (Lee et al. 2010) (Table 1). Nine transcripts from SPEM with Inflammation, including the chloride transporter, cystic fibrosis transmembrane conductance regulator homolog (CFTR), were also upregulated in human metaplasia, while 17 common transcripts were

found for SPEM with Chronic Inflammation. Only 3 other transcripts from the other comparison categories, topoisomerase (DNA) IIα (Top2a), cyclin B2 (Ccnb2), and centromere protein K (Cenpk), were also upregulated in the human metaplasia microarrays. Thus, we found considerable overlap in transcripts associated with SPEM with Inflammation in mice and those associated with metaplasias in humans.

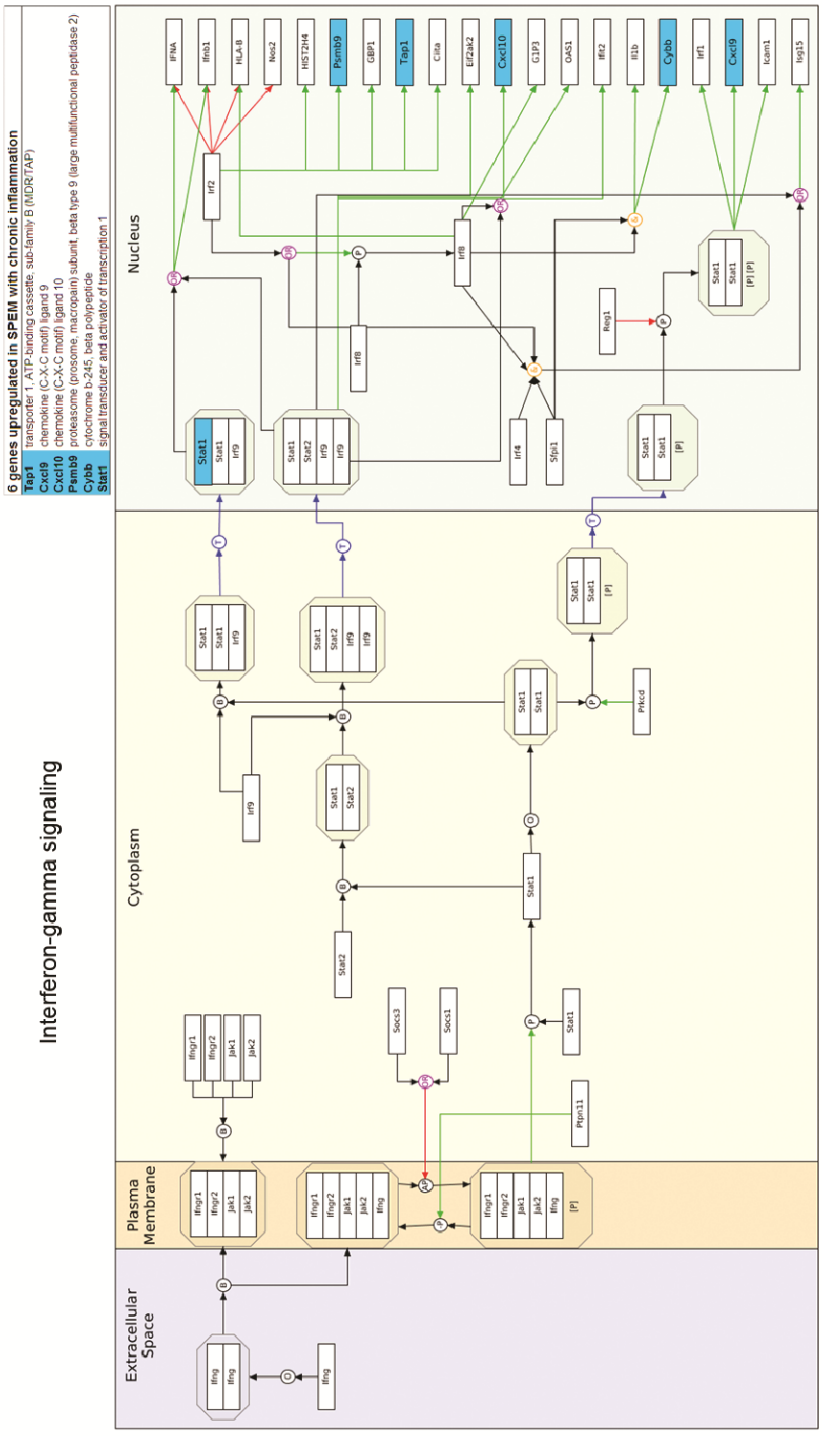

Figure 7. Pathway analysis of SPEM with Chronic Inflammation. Pathway characteristics were analyzed by examining WIKIpathways database for transcripts in each of the comparison categories using WebGestalt. The SPEM with Chronic Inflammation category was enriched with interferon-γ associated genes.

Quantitative PCR analysis of upregulated transcripts

Quantitative real-time PCR (qRT-PCR) was used to evaluate further selected upregulated transcripts from each of the comparison categories (Figure 8 and Figure 9 - Figure 13). *H. felis*-induced SPEM was divided into two time points (6 and 12 months) to distinguish between the earlier stages of SPEM and chronic SPEM. In these studies, regions of whole gastric fundus were used for qRT-PCR, rather than microdissected samples. While this approach failed to validate all transcripts from the categories, it allowed for analysis of and insight into upregulation on a more global scale. The poorly understood gene, schlafen 9 (Slfn9), from the Pan-SPEM category was significantly upregulated in all SPEM models versus normal gastric mucosa (Figure 8A). HE4 expression showed an increasing trend in all SPEM models, but failed to reach statistical significance in all individual comparisons. Clusterin was significantly upregulated in acute SPEM models, and there was a trend towards upregulation in 12 month *H. felis* infection-induced SPEM (Figure 8A). All five Acute SPEM transcripts were significantly increased in DMP-777- and L635-induced SPEM versus normal mucosa (Figure 8B and Figure 10). The six transcripts in SPEM with Inflammation that were upregulated in human metaplasias of the stomach were tested along with a selected transcript, ets variant gene 5 (ETV5), which was the only transcription factor found in the category (Figure 8C and Figure 11). Many of the transcripts, including CFTR and ETV5, were validated as significantly upregulated in SPEM with inflammation as compared to normal mucosa. CFTR expression increased over 100-fold in 12 month *H. felis* infection-induced SPEM. Notably, ETV5 was significantly upregulated in L635- and 6 month *H. felis* infection-induced SPEM, but decreased to near normal levels after 12

months of *H. felis* infection. Similar to Pan-SPEM transcripts, not all of the Specific to SPEM with Inflammation transcripts followed the trend found in the microarray data with statistical significance (Figure 8D and Figure 12). Expression of carcinoembryonic antigen-related cell adhesion molecule 10 (Ceacam10) and TYRO protein tyrosine kinase binding protein (Tyrobp) expression was significantly increased in inflammatory SPEM models as compared to the non-inflammatory SPEM model. While others such as glioma pathogenesis-related 1 (Glipr1) and the two members of the membrane-spanning 4-domains subfamily A, member 6B and member 6C (Ms4a6b and Ms4a6c), followed the trend, but did not achieve statistical significance. Five transcripts from SPEM with Chronic Inflammation that were also upregulated in human metaplasias of the stomach (Nomura et al. 2004c) were selected for qRT-PCR analysis (Figure 8E and Figure 13). Four of these transcripts, including villin 1 (Vil1), were significantly upregulated in the 12 month *H. felis* infection-induced SPEM model compared to the other sample groups (acute SPEM models and control). Together, these results provide a consistent profile of the alterations in the expression of the transcripts in each comparison category, and thus classify gene expression characteristics of SPEM with and without inflammatory influence.

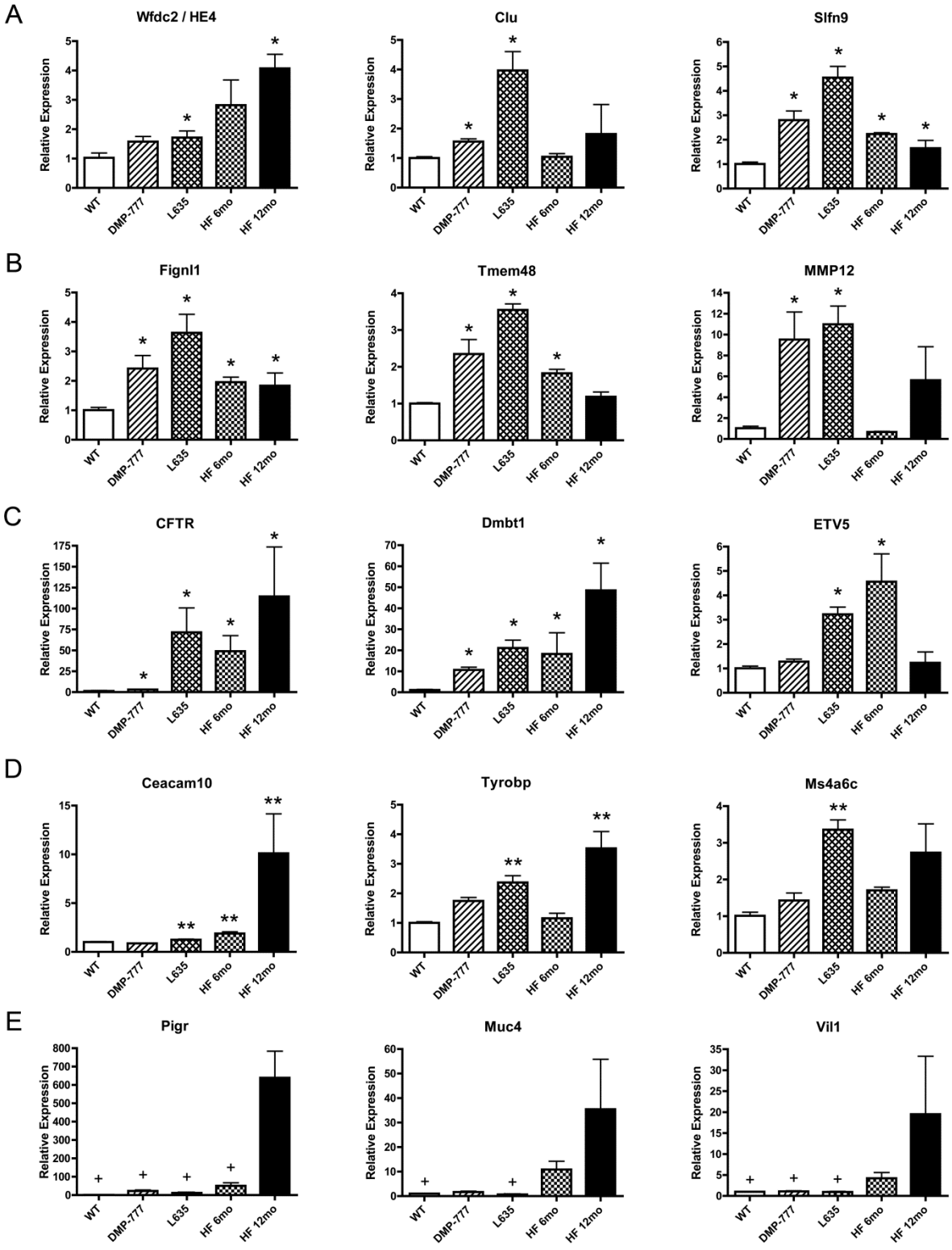
A
Wfdc2 / HE4
Clu
Slfn9
B
FignI1
Tmem48
MMP12
C
CFTR
Dmbt1
ETV5
D
Ceacam10
Tyrobp
Ms4a6c
E
Pigr
Muc4
Vil1
Relative Expression
WT
DMP-777
L635
HF 6mo
HF 12mo

Figure 8. Quantitative Real Time PCR assay of selected upregulated transcripts from each comparison category. Expression of selected upregulated transcripts from each category was assessed by qRT-PCR in RNA isolated from the whole fundic stomach (3 mice per group). Pan-SPEM (A) and Acute SPEM (B) transcripts were associated with the emergence of SPEM, while SPEM with Inflammation (C), Specific to SPEM with Inflammation (D), and SPEM with Chronic Inflammation (E) relate to the progression of SPEM lineages. Results are shown as fold change as compared to the mean value of the control group (labeled WT). Single asterisks in A, B, and C signify significant upregulation as compared to WT. Double asterisks in D are significant as compared to DMP-777-induced SPEM. Significance in E (+) is noted as compared to 12 month *H. felis* infection. All values are shown as means +/- standard error of the mean, SE. ($p < 0.05$ by Mann-Whitney U test).

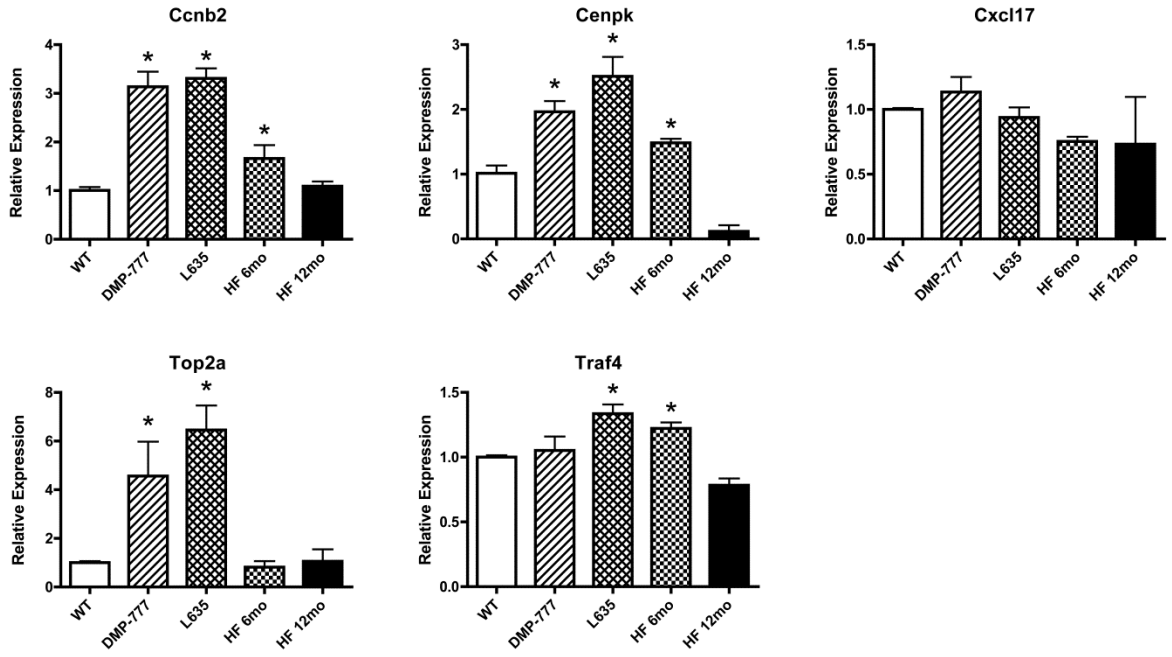

Figure 9. Quantitative Real Time PCR of transcripts in the Pan-SPEM category. Global expression of upregulated transcripts from each category was assessed by qRT-PCR as in Figure 2. The SPEM models were compared to WT (n=3, mean+/- standard error of the mean, SE). (*$p < 0.05$ by Mann-Whitney U test).

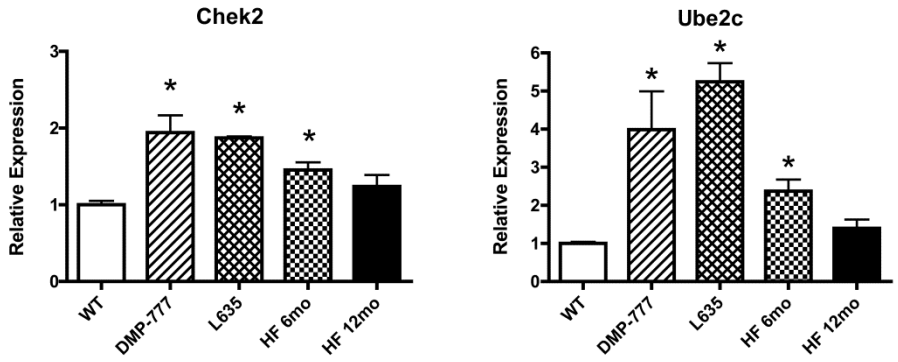

Figure 10. Quantitative Real Time PCR of transcripts in the Acute SPEM category. Global expression of upregulated transcripts from each category was assessed by qRT-PCR as in Figure 2. The acute SPEM models (DMP-777 and L635) were compared to WT (n=3, mean +/- standard error of the mean, SE). (*$p < 0.05$ by Mann-Whitney U test).

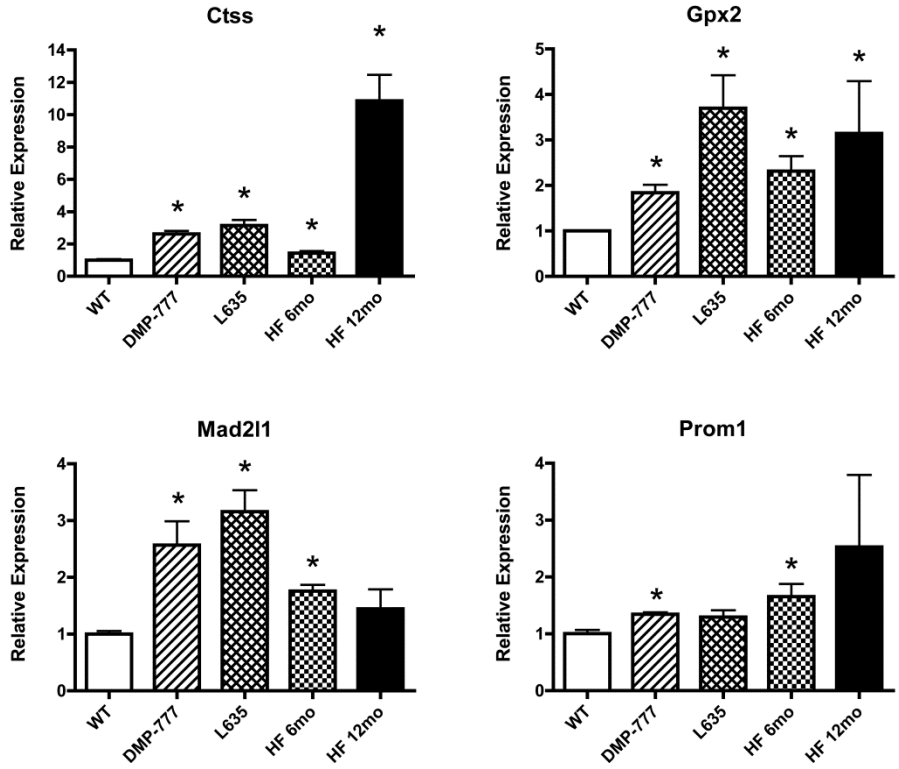

Figure 11. Quantitative Real Time PCR of transcripts in the SPEM with Inflammation category. Global expression of upregulated transcripts from each category was assessed by qRT-PCR as in Figure 2. The inflammatory SPEM models (L635 and *H.felis*) were compared to WT (n=3, mean +/- standard error of the mean, SE). (*$p < 0.05$ by Mann-Whitney U test).

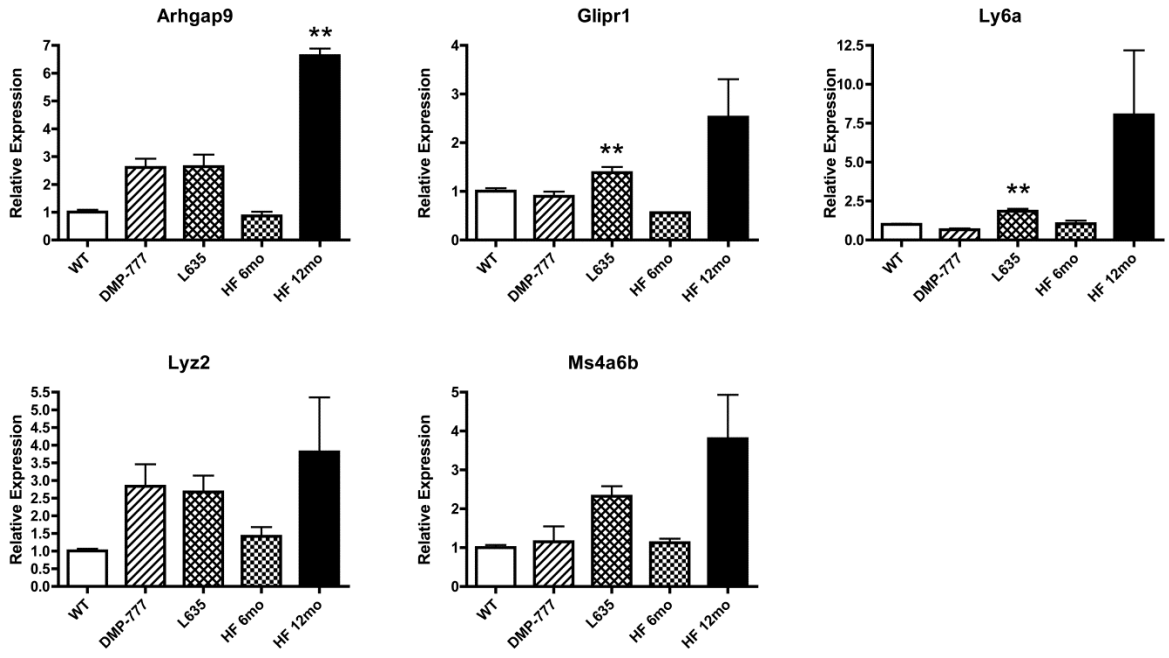

Figure 12. Quantitative Real Time PCR of transcripts in the Specific to SPEM with Inflammation category. Global expression of upregulated transcripts from each category was assessed by qRT-PCR as in Figure 2. The inflammatory SPEM models (L635 and *H.felis*) were compared to the non-inflammatory SPEM model (DMP-777) (n=3, mean +/- standard error of the mean, SE). (**p < 0.05 by Mann-Whitney U test).

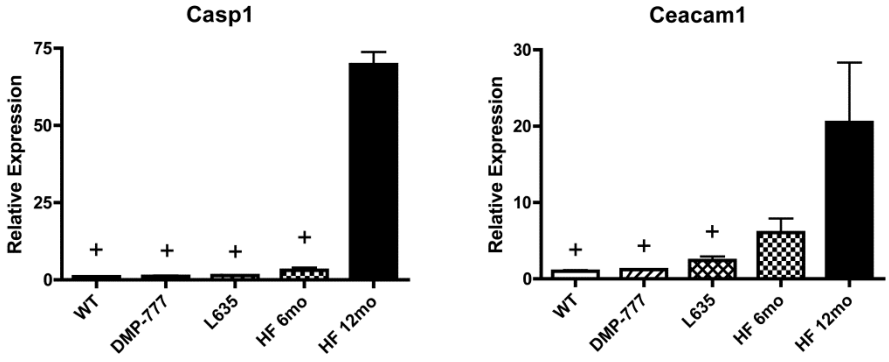

Figure 13. Quantitative Real Time PCR of transcripts in the SPEM with Chronic Inflammation category. Global expression of upregulated transcripts from each category was assessed by qRT-PCR as in Figure 2. Each group is compared to 12 month *H.felis* infection-induced SPEM (n=3, mean +/- standard error of the mean, SE). (+p < 0.05 by Mann-Whitney U test).

Clusterin expression is increased in all SPEM lineages

Based on antibody availability, we selected clusterin from the Pan-SPEM category to investigate protein expression profiles of the induction of SPEM. Clusterin is a ubiquitously expressed secreted glycoprotein thought to be involved in a variety of cellular processes such as tissue remodeling, differentiation, cytoprotection, and anti-apoptosis (Collard et al. 1987; Aronow et al. 1993; Ahuja et al. 1994; McLaughlin et al. 2000; Lee et al. 2011; Fjeldbo et al. 2012). In untreated mice, clusterin staining was observed at low levels only in cells in the isthmus of the oxyntic glands (Figure 14). Some clusterin positive cells co-labeled with the first few TFF2-expressing mucous neck cells. In all SPEM models, clusterin was strongly expressed throughout the SPEM lineages (Figure 14). Differences in the upregulation of clusterin mRNA versus detectable protein suggests clusterin mRNA is processed differently between the SPEM lineages. Together, these results demonstrate that clusterin protein expression is a marker of SPEM regardless of the causation or surrounding milieu of chief cell transdifferentiation to SPEM.

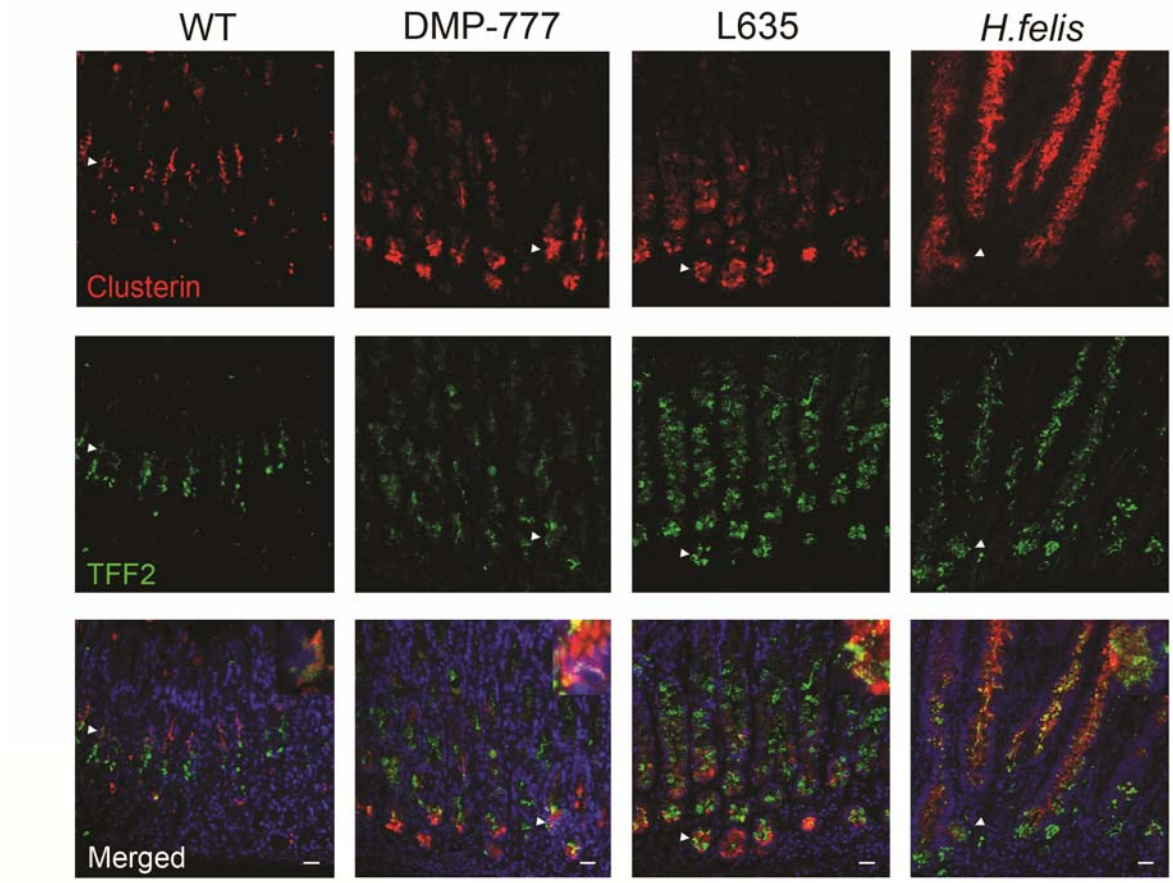

Figure 14. Expression of Clusterin in normal murine gastric mucosa and SPEM models. Sections of C57BL/6 mouse fundic mucosa were immunostained with antibodies against clusterin (top panels, red) and TFF2 (middle panels, green). In WT mice, clusterin was expressed in cells located in the isthmus and co-labeled with TFF2 in a small number of cells (arrowheads and higher magnification inset). Clusterin expression was detected throughout all SPEM lineages (14 day DMP-777 administration, 3 day L635 administration, and 12 month *H. felis* infection) (arrowheads and higher magnification insets). DAPI (blue). Bar = 20 μm.

Upregulation of CFTR expression is observed only in SPEM with inflammation

To investigate possible markers for the progression of SPEM lineages, we examined the expression of CFTR, the most upregulated transcript in SPEM with inflammation as detected by qRT-PCR. CFTR is an ATP-gated chloride channel that is

found on the apical membrane of epithelial cells including intestinal crypt cells (Ameen et al. 2000). As assessed by immunohistochemistry, CFTR was not detected in the normal gastric fundus (Figure 15) confirming previous investigations (McDaniel et al. 2005). Although CFTR mRNA was increased in all SPEM lineages, DMP-777-induced SPEM lineages lacked detectable CFTR protein expression. However, expression of CFTR protein was observed in the apical membranes of the inflammatory SPEM lineages induced by either L635 administration or *H. felis* infection, which both have large increases in CFTR mRNA expression (Figure 15). Similar expression was seen following 6 months and 12 months of *H. felis* infection (data not shown). These results show a difference in expression patterns between the inflammatory and non-inflammatory SPEM lineages and suggest that CFTR is a marker of advanced proliferative SPEM that may possess the ability to progress towards dysplasia.

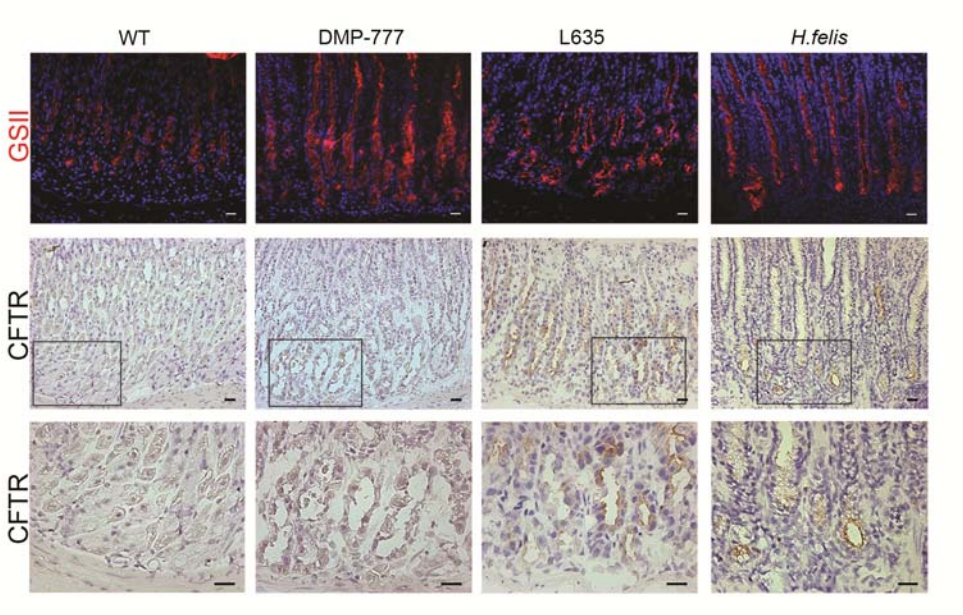

Figure 15. Expression of CFTR in normal murine gastric mucosa and SPEM models. Frozen sections of C57BL/6 mouse fundic mucosa were immunostained with either GSII lectin (a mucous neck cell and SPEM marker) or an antibody against CFTR to investigate CFTR protein expression in SPEM. Top Panel: GSII (green) labels mucous neck cells in WT stomach mucosa and SPEM at the bases of glands in each of the SPEM models. Middle and Bottom Panels: Frozen sections immunohistochemical staining for CFTR showed no CFTR expression was detected in either WT mucosa or non-inflammatory SPEM (DMP-777-induced SPEM). The inset shows magnification of the bases of glands. CFTR expression was detected on the apical membranes of SPEM cells accompanied by inflammation (3 day L635 administration and 12 month *H. felis* infection). Scale bars = 20 μm.

Clusterin and CFTR expression in human metaplasias of the stomach and gastric cancer

Based on the murine data, we examined the expression of clusterin and CFTR in human gastric tissues. Clusterin was expressed in a pattern similar to that observed in murine tissue. In normal human gastric mucosa, clusterin was detected in the isthmus region of fundic glands (Figure 16A). Some dual-labeling with TFF2 was observed in cells near the upper neck region of oxyntic glands, similar to our observations in mouse.

In metaplasias of the stomach, clusterin had a robust granular pattern throughout SPEM glands, but was limited to a few cells at the base of glands when detected in intestinal metaplasia (Figure 16B). These clusterin positive intestinal metaplasia cells did not express TFF2. In a tissue array of metaplasias from the human gastric fundus, 90% of cores with SPEM and 46% with intestinal metaplasia (18/20 and 5/11, respectively) were positive for the respective clusterin staining patterns. In a small cohort of gastric adenocarcinomas collected at Vanderbilt, clusterin was expressed in 56.5% of cancers (9/16 intestinal-type and 4/7 diffuse-type). A second cohort of 450 Korean patient samples, predominately early stage cancers, was used to assess clusterin as a prognostic biomarker. Clusterin staining was quantified by calculating the percentage of keratin-staining epithelial cells in each sample that were clusterin positive (Figure 16C and Figure 5). There was a statistically significant association between percent of clusterin positive epithelial cells and stage. Specifically, there were pairwise differences between all comparisons except stage 1 versus 3, and stage 3 versus 4 (Figure 16D). Both positive clusterin staining and stage were associated with survival (p-values of .0232 and < 0.0001, respectively). Clusterin was modeled using a restricted cubic spline with 4 knots. While the second knot (consisting of 23-43% clusterin positive epithelial staining) correlated with longer survival time, the 43-95% staining group was associated with shorter survival time (Figure 16E). Further, the model including both stage and percent clusterin staining had a c-index of 0.86, which is essentially equivalent to an area under the ROC curve (demonstrating good prediction).

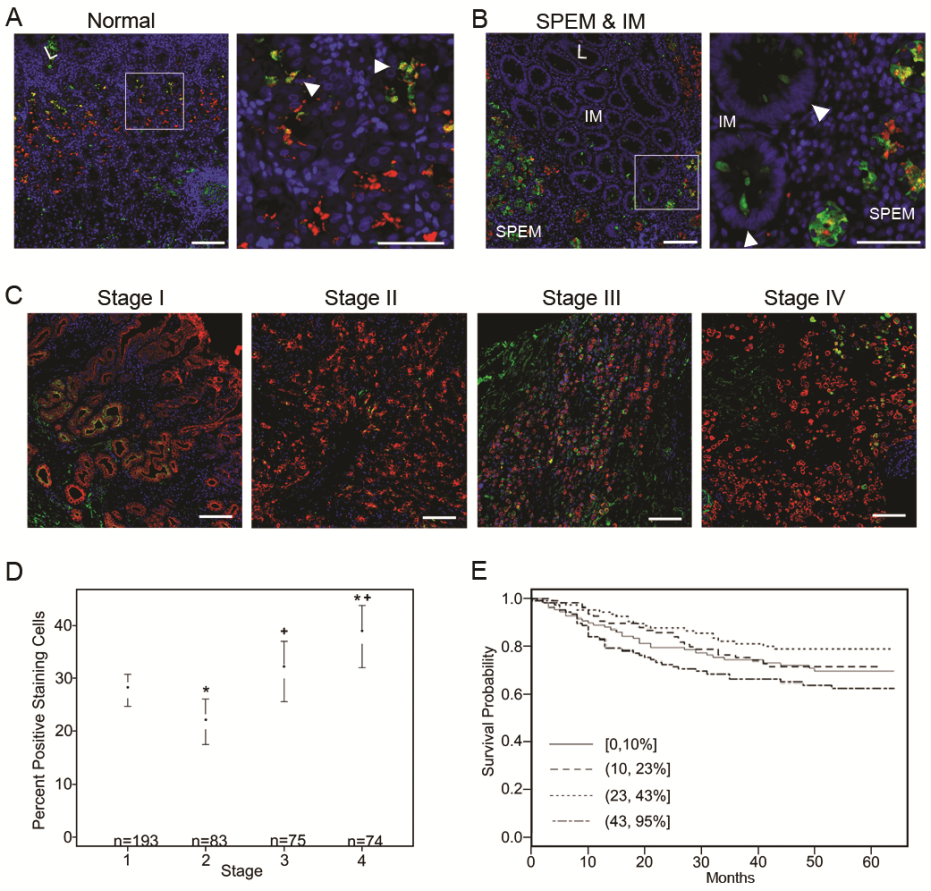

Figure 16. Clusterin expression in human normal gastric mucosa, metaplasia of the stomach, and gastric cancer. (A) In normal glands, clusterin (green) was detected in the isthmus and in a few cells dual-labeled with TFF2 (red) as seen in the inset (arrowheads in top right panel). The sample shown was taken from the University of Tokyo metaplasia array. (B) Clusterin was prominently expressed throughout SPEM glands as marked by TFF2 in red. In intestinal metaplasia, clusterin was limited to a few cells at the base of glands (designated by arrowheads in bottom right panel). These staining patterns were found in 90% of SPEM samples and 45% of intestinal metaplasia samples on the University of Tokyo metaplasia tissue array. Left panel scale bar = 100 μm. Inset panel scale bar = 50 μm. (C) Representative images from a human gastric cancer TMA show clusterin (green) expression in gastric cancer cells in each stage. Pan-cytokeratin staining (red) marks epithelial cells. Clusterin expression was present in all stages of cancer (I-IV) with averages of 27.75%, 21.82%, 31.32%, and 37.94% clusterin positive epithelial cells, respectively. DAPI (blue). Bar = 100 μm. (D) The percentage of clusterin positive epithelial cells was statistically significantly related to tumor stage by analysis of variance ($p = 0.05$). There were significant differences in clusterin staining between stage 1 compared to stages 2 and 4 (labeled with *) and stage 2 versus stages 3 and 4 (labeled with +). (E) Estimated survival curves of clusterin by staining percentage categorized into 4 quartiles. The highest staining quartile (43-95% clusterin positive epithelial cells) correlated with the worst survival outcome.

CFTR expression was also investigated to understand the correlation between murine and human gastric metaplasias. Similar to murine expression patterns, CFTR was undetectable in normal gastric mucosa (Figure 17). Conversely, CFTR was not observed in human SPEM even though it was accompanied by prominent inflammation. Nevertheless, intestinal metaplasia showed strong CFTR expression in the apical membranes throughout the glands. An analysis of CFTR expression in adenocarcinomas using tissue arrays was not possible because all available antibody reagents only perform well in frozen sections. Nevertheless, taken together with the murine tissue data, these results suggest a correlation between SPEM with inflammation in mice and intestinal metaplasia in humans, supporting the hypothesis that murine SPEM with inflammation is more advanced and acquires intestinal characteristics.

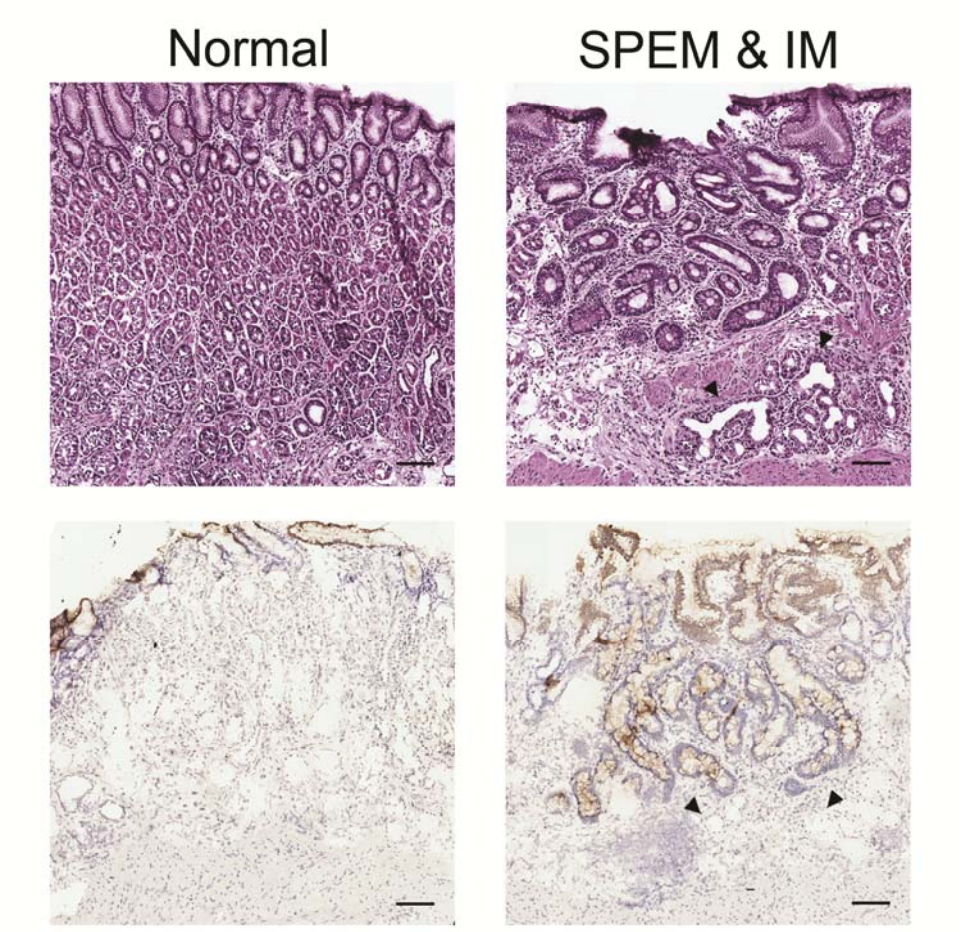

Figure 17. CFTR expression in human normal gastric mucosa and in metaplasia of the human stomach. Frozen sections of human stomach were immunostained with an antibody against CFTR (bottom panels). Top panels are H&E staining of sections for orientation and morphology. CFTR was absent from normal mucosa (bottom left) and SPEM lineages (designated by arrowheads in right panels). The diffuse cytoplasmic immunoreactivity seen in surface cells is nonspecific as CFTR is localized to apical membranes. However, expression was observed in intestinal metaplasia (bottom right). Due to limitations of the CFTR antibody and the lack of availability of frozen adenocarcinoma samples, CFTR expression was not evaluated in cancers. Bar = 100 μm.

Discussion

Chronic *H. pylori* infection in humans results in the loss of parietal cells accompanied by prominent inflammation. Loss of parietal cells from the gastric mucosa results in a disruption of the homeostasis that, under normal conditions, promotes orderly differentiation and maturation of oxyntic gland lineages. Our previous data have shown that parietal cell loss without inflamamtion (DMP-777 treatment) results in the transdifferentiation of chief cells into SPEM (Nam et al. 2010), possibly as a transient and local injury response mechanism. However, when SPEM becomes chronic, under the continuing influence of chronic inflammation as in the setting of *H. pylori* infection, SPEM progresses to dysplasia. Although SPEM alone is not sufficient for progression to dysplasia, it is necessary for the initiation of carcinogenesis cascade. Thus, metaplastic cell lineages such as SPEM and intestinal metaplasia are considered neoplastic precursors. Intestinal metaplasia arises in the presence of pre-existing SPEM (Yoshizawa et al. 2007; Goldenring et al. 2010) suggesting a progression from SPEM to intestinal metaplasia and then to neoplasia. The mechanisms of the induction and progression of metaplasias in the stomach remain poorly understood. A number of investigators have utilized chronic *H. felis* infection in mice as a major model for the development of metaplasia in the stomach and progression to dysplasia (Lee et al. 1990; Wang et al. 2000; Houghton et al. 2004a; Nam et al. 2010; Oshima et al. 2011; Varon et al. 2011). *H. felis* infected mice do not develop phenotypic intestinal metaplasia, but instead SPEM progresses directly to dysplasia (Wang et al. 2000; Houghton et al. 2004a). The present investigation indicates that, while phenotypic intestinal metaplasia may not develop from SPEM in *H. felis*-infected mice, over time the SPEM lineages do begin to express intestinal transcripts,

including CFTR and villin. Thus, while these lineages may not display all of the characteristics of goblet cells and absorptive cells as in human intestinal metaplasia, they do represent further alterations towards more intestinal characteristics that correlate with susceptibility to the development of dysplasia (Figure 3).

Studies using DMP-777 and L635 have shown that parietal cell loss is sufficient to induce SPEM, but the presence of inflammation is necessary for the progression of SPEM to a more proliferative metaplasia as well as to gastritis cystica profunda/dysplasia (Fox et al. 1993; Goldenring et al. 2000; Nam et al. 2010). Differences in the timescale for SPEM emergence as well as proliferation and dysplastic potential suggest that the surrounding milieu significantly affects the SPEM lineages. Previously, differences among phenotypically similar SPEM lineages have not been investigated. In this study, we analyzed the transcriptional expression of three SPEM models, establishing expression profiles for each lineage model. Specific comparisons of these profiles identified commonalities and differences among the SPEM lineages arising in different milieus. Thirteen transcripts were upregulated in two comparison categories (Pan-SPEM and Acute SPEM) indicative of SPEM initiation. Two of these, the secreted glycoprotein Wfdc2/HE4 and the poorly characterized ATPase Fignl1, were previously reported as upregulated in SPEM from gastrin null mice after only 1 day of DMP-777 treatment (Nozaki et al. 2008). Another secreted glycoprotein, clusterin, was also upregulated in SPEM. Similar to HE4, clusterin was prominently expressed in all SPEM lineages. A recent study has shown that clusterin upregulation may in part be induced by gastrin (Fjeldbo et al. 2012), which is elevated in our mouse models of SPEM. However, clusterin is also upregulated in SPEM from DMP-777 treated gastrin null mice (data not

shown), indicating that gastrin-independent pathways exist for clusterin upregulation. Although the mechanisms for clusterin upregulation are unclear, clusterin represents a specific marker of SPEM induction in the gastric oxyntic mucosa.

Comparisons of expression profiles of the inflammatory SPEM models identified putative markers of advanced SPEM. In particular, prominent upregulation of CFTR was observed in both inflammatory SPEM models, but was undetectable in normal glands and in the non-inflammatory DMP-777-induced SPEM lineages. This represents the first definite expression difference among phenotypic SPEM lineages. Along with the other changes in intestinal transcripts such as villin, these findings suggest that inflammation elicits upregulation of genes, such as CFTR, which are more characteristic of the duodenum. As inflammation is required for progression of metaplasia to dysplasia, it follows that SPEM accompanied by prominent inflammation acquires intestinal metaplastic markers. Moreover, a recent study from Varon et. al. suggested *Helicobacter*-induced metaplasia advances after 75 weeks to express Muc2, an intestinal metaplasia marker, in the upper portions of glands (Varon et al. 2011). The comparisons in the present study represent expression profiles that can be used to distinguish differences among phenotypic SPEM lineages such as the more advanced SPEM with intestinal characteristics (SPEM-IC) that is susceptible to progression to dysplasia. It remains unclear at this time whether proteins such as clusterin and CFTR represent markers of the metaplastic process or whether they directly contribute to the progression of disease. Direct analysis of these questions remains problematic because there are no *in vitro* models of normal chief cells and metaplastic lineages (SPEM and IM). Nevertheless, we anticipate that the rapid induction of metaplasia following L635

treatment will aid future examination of candidate protein influences using mouse strains with targeted gene disruption.

Taken together, the identification of differences among the expression profiles of phenotypic SPEM lineages illustrates the need to characterize in greater detail SPEM lineages found in the various models of metaplasia of the stomach and gastric cancer. Although SPEM was initially underappreciated as a preneoplastic lesion, recent investigations have illustrated the high prevalence of SPEM in numerous mouse models of gastric homeostasis and gastric cancer (Oshima et al. 2004; Katz et al. 2005; Oshima et al. 2006; Jain et al. 2008; Keeley et al. 2010; Ito et al. 2011). The loss of Klf4 in glandular tissues results in the development a SPEM phenotype in the absence of inflammation (Katz et al. 2005). Similar to DMP-777- induced SPEM, SPEM in Klf4-deficient mice does not acquire intestinal characteristics (such as Muc2 or villin expression) nor does it progress to dysplasia. Samuelson et. al. reported that the loss of Hip1r in parietal cells resulted in apoptotic loss of parietal cells and chief cells (Jain et al. 2008; Keeley et al. 2010). A SPEM lineage accompanied by inflammatory infiltrates emerged at 5 weeks of age (Jain et al. 2008; Keeley et al. 2010). Expression of intestinal features such as Muc2 and villin is unknown in this SPEM model; however, this model is of interest for comparison to L635-induced SPEM (an acute SPEM model with inflammation). *K19-C2mE* transgenic mice, which overexpress COX-2 and microsomal prostaglandin E synthase-1 (mPGES-1), develop SPEM at 12 weeks of age and then progress to tumors at 48 weeks (Oshima et al. 2004). The addition of WntI expression (*K19-WntI/C2mE* or Gan mice) resulted in SPEM at 5 weeks of age progressing to dysplastic tumors at 20 weeks (Oshima et al. 2006). In these models, development of

mucosal lesions was associated with prominent macrophage infiltrates similar to *H. felis*-induced SPEM. In contrast to all SPEM models utilized in this study, mice deficient for Runx3 develop a SPEM phenotype without prominent inflammation and without loss of parietal cells. Although there is no inflammatory infiltrate, cells at the base of some SPEM glands expressed intestinal markers, Muc2 and CDX2 (Ito et al. 2011), which are not seen in our metaplasia models. This model is of interest for comparison because of the progression of SPEM to acquire intestinal characteristics without the presence of inflammation or loss of parietal cells. The markers identified in our present investigations should provide reference points for analysis of the metaplastic lineages that arise in these other mouse models.

By establishing commonalities and differences in the expression patterns in our three murine SPEM models, we were able to find novel potential biomarkers of metaplasia in the human stomach (Clusterin and CFTR). While all SPEM lineages in mice expressed clusterin, we found that 90% of SPEM and 46% of intestinal metaplasia in humans expressed clusterin. In human intestinal metaplasia, clusterin localized to a few cells at the base of the intestinal metaplasia, which is the region suggested as a transitional and proliferative area of intestinal metaplasia arising from SPEM (Goldenring et al. 2010). Clusterin may be acting in an anti-apoptotic or cytoprotective manner to help maintain this transitional niche. Clusterin upregulation was maintained in the majority of intestinal-type and diffuse-type cancers. Correlation between clusterin expression and stage was U-shaped suggesting clusterin functions differently in the different stages of cancer, a pattern previously observed in other types of cancers (Rizzi et al. 2010). Adverse patient outcome was associated with the highest percentage of

clusterin expression, which was more frequently seen in late stage cancers. This study supports the recent findings that high clusterin expression in late stage gastric cancers correlated with a poor outcome (Bi et al. 2010). Therefore, clusterin is a useful biomarker for SPEM and an adverse prognostic marker for adenocarcinomas. Conversely, CFTR expression was absent in human SPEM, but was upregulated in intestinal metaplasia. These findings show that expression profiles in murine SPEM with inflammation (SPEM-IC) overlap with human intestinal metaplasia, suggesting that SPEM-IC is a more advanced SPEM lineage (Figure 3). Further investigation of murine SPEM lineages will provide greater insight into the heterogeneity of SPEM as well as the progression of early stage SPEM to SPEM-IC in mouse and, by analogy, to the progression of SPEM to intestinal metaplasia in humans.

In summary, we have established distinct expression profiles of SPEM with or without inflammation that illustrate similarities among all SPEM lineages and differences in SPEM lineages with the potential for progression to dysplasia in mice. From these profiles, clusterin upregulation was verified as a biomarker of SPEM and poor patient outcome. Additionally, CFTR was identified as a biomarker of SPEM with inflammation in mice and intestinal metaplasia in humans. The expression profiles of SPEM lineages with inflammation, especially *H. felis* infection-induced SPEM, identified a more advanced SPEM lineage in mice that has adopted some intestinal characteristics. These studies support a model of metaplastic progression in mice that begins with the induction of SPEM and advances to SPEM with intestinal characteristics (SPEM-IC) that may have dysplastic potential. The studies also indicate that the mouse model of chronic *H. felis* infection does mimic the analogous human condition of *H. pylori* infection suggesting a

progression of parietal cell loss to initiation of SPEM to further metaplastic progression towards intestinalizing metaplasia in the presence of inflammatory influences.

CHAPTER III

NOVEL IN VITRO CHIEF CELL AND SPEM CULTURES PROVIDE A MODEL FOR CHARACTERIZATION OF METAPLASIA IN THE STOMACH

Appears as: Weis, V.G., Petersen, C.P., Mills, J.C., Drapkin, R.I., Tuma, P.L., Whitehead, R.H., and Goldenring, J.R. Novel in vitro chief cell and SPEM cultures provide a model for characterization of metaplasia in the stomach. Manuscript in preparation.

Introduction

Homeostasis in the stomach relies on a balance of the production and maintenance of multiple cell lineages, such as the acid-producing parietal cells, mucous-secreting neck cells, and zymogen-secreting chief cells. In the normal stomach, mucous neck cells transdifferentiate into chief cells as they progress towards the base of the gastric glands (Karam et al. 1993d; Ramsey et al. 2007). Parietal cells are thought to secrete factors that control this maturation of chief cells (Beauchamp et al. 1989; Murayama et al. 1994; Abe et al. 1997; Jain et al. 2006a) because the absence of parietal cells results in loss of chief cells (Li et al. 1996). However, the specific factors responsible for chief cell maturation and homeostasis of are unclear. Studies using *in vivo* models and *in vitro* primary culture models to investigate these specific factors show the effects of a specific factor on the whole tissue level. Using these techniques, several studies have attempted to elucidate such factors and have determined various aspects of chief cell function, such as signals that regulate zymogen secretion (Langley 1882; Hirschowitz 1967; Koelz et al. 1982; Raufman et al. 1983; Berger et al. 1985; Sutliff et al. 1986; Raufman et al. 1987). The molecular pathways that regulate zymogen secretion were established further with

pharmacological agents that activate specific steps of recognized signaling pathways, such as elevation of cAMP or Ca^{2+} levels (Muallem et al. 1986; Raufman et al. 1986; Brown et al. 1987; Matozaki et al. 1988; Tsunoda et al. 1988). However, the trafficking pathways involved in secretion are still unknown. The majority of these studies utilized isolated primary chief cells, which precludes molecular studies. Therefore, it has proven difficult to elucidate the molecular pathways and interactions of the factors involved in the maturation and function of chief cells due to the lack of an *in vitro* model that can be easily manipulated.

In damage or disease, the homeostasis of the stomach is disrupted and chief cells trandifferentiate into spasmolytic polypeptide-expressing metaplasia (SPEM) (Nomura et al. 2004a; Nomura et al. 2004c; Nozaki et al. 2008; Nam et al. 2010). Acute SPEM is thought to be a protective mechanism for repairing local damage; however, in the presence of inflammation, SPEM progresses to more advanced metaplasia (Fox et al. 1993; Goldenring et al. 2000; Wang et al. 2000; El-Zimaity et al. 2001; Houghton et al. 2004a; Oshima et al. 2005; Yoshizawa et al. 2007; Nam et al. 2010; Varon et al. 2011). In humans, SPEM gives rise to intestinal metaplasia which can progress to cancer (Hattori et al. 1979; Hattori et al. 1982; Hattori 1986; Correa 1988; Filipe et al. 1994; Takizawa et al. 1998; Schmidt et al. 1999; Xia et al. 2000; Yamaguchi et al. 2002; Halldorsdottir et al. 2003). In mice, however, SPEM does not progress to phenotypic intestinal metaplasia. Instead, SPEM progresses to "SPEM with intestinal characteristics" (SPEM-IC), which is the mouse version of intestinal metaplasia (Weis et al. 2013). Administration of DMP-777, an elastase inhibitor and protonophore, results in parietal cell loss without inflammation (Nomura et al. 2004c), and SPEM develops after 10-14 days. Even after

two years of daily DMP-777 administration, SPEM never progresses to dysplasia (Goldenring et al. 2000). In contrast, administration of L635, a protonophore analogue of DMP-777 that lacks elastase inhibition, results in SPEM with a prominent inflammatory response after three days (Nam et al. 2010). In contrast to DMP-777, L635-induced SPEM begins to acquire some intestinal transcripts (Weis et al. 2013). Furthermore, *H. felis*-infected mice develop SPEM with chronic inflammation that expresses even more intestinal transcripts (SPEM-IC) (Varon et al. 2011; Weis et al. 2013). After approximately 12 months of infection, SPEM-IC progresses to dysplasia (Wang et al. 1998; Wang et al. 2000; Houghton et al. 2004a; Nam et al. 2010; Varon et al. 2011). These three models have been used to elucidate expressional changes in the induction of SPEM and the progression to SPEM-IC and dysplasia.

Numerous studies have identified a variety of putatively important factors in chief cell homeostasis and function or induction and progression of SPEM. However, no *in vitro* models of chief cells or metaplasia of the stomach currently exist, which has significantly hindered specific investigations into the molecular mechanisms of the numerous factors identified in a multitude of studies. *In vitro* models are desperately needed to elucidate such mechanisms. The availability of the Immortomouse (Jat et al. 1991), makes the establishment of such *in vitro* models now possible (Whitehead et al. 1994; Whitehead et al. 2008; Kohn et al. 2010). The Immortomouse is a transgenic mouse that has an interferon-γ (IFNγ) inducible expression of a temperature sensitive T-antigen (Jat et al. 1991). The presence of IFNγ induces expression of the immortalizing T-antigen. At the permissive temperature of 33°C, the T-antigen folds correctly and immortalizes the cells. However, at the non-permissive temperature of 39°C, IFNγ is

removed and residual T-antigen misfolds, returning the cultures to a more 'primary-like' state. The Immortomouse has been successfully used to establish cell lines from various tissues, including the stomach (Whitehead et al. 1994; Allen et al. 2000; Whitehead et al. 2008; Whitehead et al. 2009; Kohn et al. 2010). However, these stomach cell lines do not express any chief cell or SPEM cell characteristics, but more closely resembles gastric surface cells (Whitehead et al. 2009), while another is a gastric stromal cell line (Whitehead, R.H., unpublished). In this study, we have developed and characterized the first *in vitro* models of chief and SPEM cells that are invaluable to expanding our understanding of the molecular mechanisms of chief cell homeostasis and the metaplastic process.

Using a modified protocol previously used for chief cell isolation (Tashima et al. 2009), our cell isolates were enriched for either chief cells or SPEM cells to remove contamination of other cell types. We established a chief cell line (ImChief) from untreated Immortomice and a SPEM cell line (ImSPEM) from L635-treated Immortomice. ImChief and ImSPEM cells expressed only the appropriate cell lineage markers. Additionally, ImSPEM cells polarize on transwells and form cystic structures when grown in Matrigel. Utilizing our two novel *in vitro* cell culture models, gene expression comparisons reveal a novel subapical marker of SPEM, MAL2. As a protein necessary for transcytosis, MAL2 is the first trafficking protein identified as upregulated in SPEM.

Methods

Animals and cell isolation buffers

Immortomice (tsA58SV40 T antigen transgenic; (Jat et al. 1991) Charles River Laboratories, Wilmington, MA, USA) were maintained on a C57- BL/6 background. Mice were euthanized at 12-16 weeks of age. Chief cells were isolated from four untreated female Immortomice. For SPEM cell isolation, L635 dissolved in saline was orally administered as a gavage once daily at 350 mg/kg/day for three consecutive days to three female Immortomice. L635 was a gift from Merck & Co, Inc (Rahway, NJ). All procedures were performed under Vanderbilt IACUC-approved animal protocols. Solutions for cell isolation were made from a basic buffer of 0.5 mM NaH_2PO_4, 1 mM Na_2HPO_4, 20 mM $NaHCO_3$, 70 mM NaCl, 5 mM KCl, 50 mM HEPES, and 11 mM glucose in water. Medium A is 2 mM EDTA and 2% BSA (fraction V and globulin free A-9418; Sigma-Aldrich, St. Louis, MO) in basic buffer. Medium B is 1 mM $CaCl_2$, 1.5 mM $MgCl_2$ and 2% BSA (fraction V and globulin free) in basic buffer.

Cell isolation and culture

Chief cells and SPEM cells were isolated by sequential digestions as described previously by others (Tashima et al. 2009). Stomachs were excised, inverted, washed in ice cold 1X PBS, and tied off at the antrum and the forestomach. Unwanted tissue from the antrum and the forestomach were then removed. Medium A containing 2.5 mg/mL of protease type XIV (Sigma-Aldrich) was injected into the stomach until fully inflated (500-800 μl). The inflated stomachs were incubated in a series of solutions for 30 minutes each in a 37°C shaking water bath (Fractions 1-5). First, they were submerged in

Medium A without protease (Fraction 1) followed by three changes of Medium B (Fractions 2-4). For fraction 5, stomachs were incubated in Medium B with 0.5 mg/mL of DNase I (Sigma-Aldrich) and then vigorously shaken by hand for 30 seconds. A 500 µL aliquot from each fraction was fixed with 4% paraformaldehyde at 4°C for 20 minutes to verify cell types in each fraction. To confirm cell isolation from the mucosa, stomachs were fixed in 4% paraformaldehyde and paraffin embedded for immunohistochemical analysis.

Chief cells and SPEM cells were found to be enriched in fractions 4 and 5. To remove tissue clumps, fractions 4 and 5 were filtered through a 100 µm cell strainer. These fractions were centrifuged for 5 minutes at 1000 rpm and resuspended in a 1:1 mixture of Ham's F-12 and Dulbecco's minimum essential medium containing 10% heat-inactivated FBS, 8 µg/mL ITS, 1 µg/mL hydrocortisone, 100 U/mL penicillin and streptomycin, 100 µg/mL MycoZap Plus-PR (Lonza, Rockland, ME), 1 ng/mL EGF, 1 ng/mL bFGF, 10 ng/mL HGF, and 5 U/mL interferon-γ (IFNγ). Growth factors and IFNγ were purchased from PeproTech (Rocky Hill, NJ). Cells were plated on collagen (PureCol; Advanced BioMatrix, San Diego, CA) coated 96-well and 24-well plates at varying densities (10,000-60,000 cells for 96 well plates and 50,000 to 200,000 cells for 24 well plates) and incubated at 33°C with 5% CO_2. Cells were passaged at a 1:2 dilution as needed using trypsin with EDTA. Various cellular morphologies were observed and further purified by sequential higher dilution passages (1:3-5) or with trypsin-soaked cloning disks. Each morphology was analyzed by qPCR to verify cell type. Colonies with the desired expression profile were selected. Cells were maintained at 33°C in the media described above.

For immunostaining analysis, cells were plated at confluency on collagen-coated coverslips or transwell filters and cultured at 39°C for 1 week. For 3D culture experiments, 25,000 cells were suspended in 1:1 mixture of media (without IFNγ) and Matrigel (9.9 mg/mL stock; Sigma-Aldrich) and grown in 48-well plates at 39°C for 3-5 weeks. IFNγ was removed from the media for all experiments at 39°C.

Transfections of cells

For transfection of ImChief cells, Amaxa Nuclefactor (Lonza, Allendale, NJ), FuGene 6 (Promega, Madison, WI), TurboFect (Thermo Scientific, Glen Burnie, MD), and Effectene (Qiagen, Valencia, CA) were tested (Table 2). For the Amaxa Nucleofactor System, 500,000 cells were transfected with 2 μg of an EGFP plasmid according to manufacturer's protocol using Kit T and program T-030. Cells were incubated at 33°C and media was changed after 24 hours. Transfection efficiency was calculated 48 hours after transfection. For FuGene 6, TurboFect, and Effectene, cells were grown to approximately 70% confluency at 33°C overnight. Cells were then transfected with an EGFP plasmid according to manufacturer's protocols and incubated at 33°C. Again, media was changed after 24 hours and efficiencies were calculated after 48 hours. Efficiencies were calculated as the number of GFP positive cells out of the total number of cells. For *Mist1* transfections, 2 μg of an MIST1-EGFP plasmid (Bredemeyer et al. 2009) was transfected using the Amaxa Nucleofactor System as stated above. After transfection, cells were incubated at 39°C for 3 days.

Table 2. Transfection efficiency of ImChief cells by various transfection methods. ImChief cells were transfected with an EGFP plasmid via different transfection methods to test transfection capabilities. After 48 hours of transfection, GFP expression was examined. Efficiency was calculated by the number of GFP-expressing cells out of the number of cells counted (>850 cells). The Amaxa Nucleofactor method resulted in the highest transfection efficiency.

Transfection Method	DAPI	GFP	Transfection Percentage
Amaxa	2921	856	29.3%
FuGene 6	1207	50	4.1%
TurboFect	1411	24	1.7%
Effectene	878	23	2.6%

RNA extraction, reverse transcription and real time PCR

For characterization experiments, cells were plated on collagen coated dishes and incubated at 39°C for one week. Initial ImSPEM characterization used cells grown at 33°C. Final characterization (Table 3) used cells incubated at 39°C for one week. Cells were washed with 1X PBS and RNA was extracted with TRIzol (Invitrogen, Carlsbad, CA) according to the manufacturer's instructions. The RNA (1 μg) was treated with RQ1 RNase-free DNase (Promega, Madison, WI) and then reverse-transcribed using the Advantage RT-for-PCR kit (Clontech, Palo Alto, CA). Advantage 2 PCR kit (Clontech) was used for all PCR amplifications (unless stated otherwise) using gene specific primers and the following protocol: denature for 5 minutes at 94°C, amplification for 40 cycles of 20 seconds at 94°C, 20 seconds at 60°C, and 20 seconds at 68°C, and final extension for 5 minutes at 68°C. Reactions were then visualized on a 2% agarose gel. For quantitative RT-PCR, 1 μg of total RNA was treated with RQ1 RNase-free DNase (Promega, Madison, WI) and then reverse-transcribed using Superscript III reverse transcriptase (Invitrogen, Carlsbad, CA). Quantitative real time polymerase chain reaction (qRT-PCR)

was performed with EXPRESS SYBR GreenER quantitative PCR SuperMix (Invitrogen, Carlsbad, CA) using specific primers in an ABI StepOnePlus Real-Time PCR System (Applied Biosystems, Foster City, CA). Each sample was run in triplicate following cycling conditions indicated by the SYBR Green supermix manufacturer's protocol. TATA–box-binding protein (TBP) was used as an endogenous control and reference for verification of sufficient cDNA in the reaction.

Immunofluorescence analysis

The following primary antibodies were used in this study: sheep anti-Pepsinogen II (1:1000; Abcam, Cambridge, MA), rabbit anti-RAB3D (1:50; ProteinTech Group Inc, Chicago, IL), rabbit anti-HE4 (1:2000) (a gift from Dr. Ronny Drapkins, Harvard Medical School, Boston, Massachusetts), mouse IgM anti-TFF2 (1:1000; Abcam), mouse anti-E-cadherin (1:200; BD Tranduction Laboratories, Lexington, KY), mouse anti-p120 (1:200; BD Transduction Laboratories), rat anti-ZO1 (1:400; Developmental Studies Hybridoma Bank, University of Iowa, Iowa City, IA), and rabbit anti-MAL2 (1:1000) (In et al. 2010). Fluorescent secondary antibodies (Cy3 and Cy5; Jackson ImmunoResearch Laboratories, West Grove, PA and Alexa-488, -594, and -647; Invitrogen, Carlsbad, CA) were used at 1:500 to visual primary antibodies. For coverslips and transwells, cells were washed with PBS and fixed with 4% paraformaldehyde for 20 minutes at room temperature. Cells were blocked/extracted with 10% normal donkey serum (Jackson ImmunoResearch Laboratories) and 0.3% Triton X-100 for 30 minutes at room temperature. Primary antibodies were diluted in 1% serum and 0.05% Tween-20 and incubated overnight at 4°C. Cells were washed three times with PBS and incubated with secondary antibodies in 1% serum for one hour at room temperature. After three washes

with PBS, coverslips or transwells were mounted with ProLong Gold plus 4′,6-diamidino-2-phenylindole (DAPI; Invitrogen). Matrigel plugs were moved to 0.5 mL microcentrifuge tubes, washed 3 times with PBS to remove media from the plug, and fixed in 4% paraformaldehyde for one hour at room temperature. After three washes with PBS, plugs were blocked/extracted with 10% normal donkey serum and 0.3% Triton X-100 rotating for one hour at room temperature. Plugs were washed twice with PBS and 0.05% Tween-20 and then rotated overnight at 4°C with primary antibodies. After two washes with PBS and Tween-20, plugs were incubated with secondary antibodies for four hours rotating at room temperature. They were then washed four times with PBS and Tween-20, washed twice with PBS, and mounted in Prolong Gold plus DAPI on a glass slide with a coverslip. For all Matrigel plugs, tubes were centrifuged for one minute at 6000 rpm between each step to collect all fragments of the Matrigel. All primary and secondary antibodies used for Matrigel plugs were diluted in 1% normal donkey serum. All images of cells were captured with an Olympus FV1000 confocal microscope (Cell Imaging Shared Resource, Vanderbilt University, Nashville, TN).

For immunostaining in tissue, human and mouse stomachs were obtained as previously reported (Leys et al. 2006; Weis et al. 2013). For mouse tissue, 4% paraformaldehyde-fixed paraffin-embedded stomachs from untreated control mice, 14-day DMP-777 treated mice, three-day L635 treated mice, and 6-12-month *Helicobacter felis* infected mice were used. A tissue array of metaplasias (SPEM and intestinal metaplasia, n=19) resected at University of Tokyo (Leys et al. 2006) was used for analysis of MAL2 expression. A tissue array comprised of 44 gastric cancers resected at Vanderbilt Medical Center Sections was used for analysis of expression in gastric cancer

(Leys et al. 2006). Eleven intestinal-type cancer cores were analyzed. Sections were heated at 60°C for 30 minutes, allowed to cool to room temperature, deparaffinized in Histo-Clear (National Diagnostics, Atlanta, GA), and rehydrated. Antigen retrieval was performed using Target Retrieval solution (DakoCytomation, Glostrup, Denmark). Slides were blocked overnight at 4°C with serum-free protein block (DakoCytomation). Primary antibodies were incubated overnight at 4°C in antibody diluent with background reducing components (DakoCytomation). Sections were washed in PBS and incubated with secondary antibodies for one hour at room temperature. After washing in PBS, sections were mounted in Prolong Gold plus DAPI. Images of tissue were captured with a Zeiss Axio Imager M2 microscope (Jena GmBH, Germany) outfitted with a Spot Xplorer camera (SPOT Imaging Solutions, Sterling Heights, Michigan) using either a 20X NA 0.8 or 40X NA 0.95 Plan-Apochromat objective (Zeiss).

Western blot analysis

Cells were plated at confluency and incubated at 39°C for one week. For analysis of media, cells were washed and fresh media was added for 24 hours. After 24 hours on the cells, media was collected and stored at -80°C. For analysis of cell lysates corresponding to the media analysis, protein was isolated from the plated cells with TRIzol according to the manufacturer's instructions. For overexpression experiments, protein was isolated in a lysis buffer of 50 mM Tris (pH 8.0), 150 mM NaCl, and 0.5% SDS in PBS plus phosphatase inhibitors. Lysates were rocked for 30 minutes at 4°C and then centrifugated for 15 minutes at 4°C. The protein-containing supernatants were transferred to new tubes. The protein concentration of the cell lysates was measured by bicinchoninic acid (BCA) method using the Pierce BCA protein assay reagent (Pierce,

Rockford, IL). A total protein amount of 20 μg of each cell lysate sample and an aliquot of 15 μL of media was suspended in 1X SDS sample buffer. Samples were resolved in a 10% Bis-Tris NuPAGE Novex 1.0 mm gel (Life Technologies, Carlsbad, CA) and transferred to an Immobilon-P PVDF membrane (Millipore, Billerica, MA). Blots were blocked with 5% dry milk powder in Tris-buffered saline and 0.05% Tween-20 (TBS-T). Primary antibodies were diluted in 2.5% dry milk powder/TBS-T and incubated overnight at 4°C. After four washes in TBS-T, blots were incubated with horseradish peroxidase-conjugated secondary antibodies (Jackson ImmunoResearch) for one hour at room temperature. Blots were then washed four times with TBS-T and once with TBS only. Specific labels were detected with enhanced chemiluminescence reagents (Pierce, Rockford, IL) and BioMax ML film (Kodak, Rochester, NY). For sequential probing, blots were washed with TBS-T and stripped with ReBlot Plus Strong Antibody Stripping Solution (Millipore) for 20 minutes at room temperature. After two washes of TBS-T, blots were again blocked and probed as described. Cell lysate bands were normalized to the control bands of either rabbit anti–voltage-dependent anion-selective channel protein 1 (VDAC1)/porin (1:1000; Abcam) or β-actin (1:1000; Sigma-Aldrich).

Gene microarray analysis

ImChief cells and ImSPEM cells were plated at approximately 80% confluency on collagen coated flasks and incubated at 39°C for one week. Cells were detached with Trypsin and EDTA and washed twice with PBS. Total RNA was isolated with the *mir*Vana miRNA Isolation Kit (Life Technologies) following manufacturer's protocol. cDNA was reverse transcribed from 130 ng of RNA using the Ambion WT Expression Kit (Life Technologies). Standard Affymetrix protocols were used to fragment and label

5.5 µg of cDNA. Samples were then hybridized to the Affymetrix mouse gene 1.0ST array (Santa Clara, California). Data was analyzed on an Affymetrix Expression Console v. 1.1 using a RMA normalization to produce log base 2 values. Statistical significance was determined by unpaired Student's *t*-tests ($p \leq 0.05$) with GeneSpring software (Agilent Technologies, Wilmington, DE) using Benjamini-Hochberg MTC (Hochberg et al. 1990). Fold changes of the top 25 increased genes are listed in Table 4.

Table 3. Transcriptional expression of lineage specific markers in ImChief and ImSPEM cells. ImChief cells and ImSPEM cells were cultured at 39°C for one week. Both cultures express the epithelial markers *Krt8* and *Krt18*. ImChief cells express all chief cell markers except *Gif*. Other lineage markers are not expressed, demonstrating the specificity of the ImChief cell line. Similarly, ImSPEM cells express SPEM markers and some SPEM-IC markers (*Cftr* and *PigR*), but lack markers of other lineages. Additionally, the ImChief and ImSPEM cell lines did not express intestine and antral-specific markers (*Pdx1* and *Cdx2*) showing the cultures were not contaminated with intestinal or antral cells.

Cell Lineage	Marker	ImChief	ImSPEM
Epithelial Cell	Krt 8	+	+
Epithelial Cell	Krt 18	+	+
Chief Cell	Mist1	+	-
Chief Cell	PGC	+	-
Chief Cell	Rab3d	+	+
Chief Cell	Gif	-	-
Surface Cell	Muc5ac	-	-
Parietal Cell	H/K ATPase	-	-
Endocrine Cell	ChgA	-	-
Neck Cell / SPEM	Tff2	-	+
SPEM	He4	-	+
SPEM	Clu	-	+
SPEM-IC	Cftr	-	+
SPEM-IC	Dmbt1	-	-
SPEM-IC	PigR	-	+
SPEM-IC	Vil1	-	-
Antral Cell / Duodenum	Pdx1	-	-
Duodenum	Cdx2	-	-

Results

Establishment of an immortalized chief cell line (ImChief)

Stomachs from four female Immortomice were digested in serial fractions to obtain an enriched population of chief cells. As previously reported (Tashima et al. 2009), chief cells were found predominately in fractions 4 and 5. Chief cells constituted 73% of the cells found in the enriched fractions (Figure 18). To establish a chief cell line, these Immortomouse chief cells enriched fractions were cultured on collagen-coated plates at the permissive temperature (33°C) in the presence of IFNγ, which induces expression of the temperature sensitive T antigen transgene. At the permissive temperature, the T antigen protein folds correctly and causes in 'immortalization' of the cells. Colonies with an epithelial-like morphology (a cobblestone appearance) appeared after several passages. These colonies were further purified using sequential higher dilution passages and isolation with cloning disks. Although stromal cells could not be completely removed, detection of epithelial markers cytokeratins 8 and 18 (*Krt8* and *Krt18*) confirms epithelial cells are predominantly present in the culture (Figure 19). The transcriptional profile of the cell line was analyzed by PCR to verify the composition of the gastric cell types in the culture. Lineage markers for the various cell types of the stomach were examined in cells cultured at the non-permissive temperature (39°C) for one week. Transcriptional analysis of the cell culture reveals the expression of the chief cell-specific markers *Mist1*, pepsinogen C (*Pgc*), amylase 2 (*Amy2*), and *Rab3d*, but not gastric intrinsic factor (*Gif*) (Figure 19). However, the cells do not express the mucous neck cell markers *Muc6* and *Tff2*, thus ruling out the presence of mucous neck cells,

which normally differentiate into chief cells *in vivo*. Furthermore, markers of foveolar cells, parietal cells, and endocrine cells were not detected (Figure 19). The expression of chief cell markers and lack of all other lineage markers demonstrates the predominance of chief cells and the absence of other gastric cell lineages; thus the culture was appropriately designated ImChief (Im-Immortomouse, Chief-Chief cells). This expression pattern was retained for at least 50 passages suggesting the chief cell phenotype is stable. A previous report from *in vivo* murine stomach showed that upon the loss of parietal cells, chief cells transdifferentiate into SPEM cells and begin expressing HE4 (Nozaki et al. 2008). Of note, although parietal cells are not present in the *in vitro* cell culture, ImChief cells do not transdifferentiate, as determined by the lack of *He4* transcriptional expression (Figure 19).

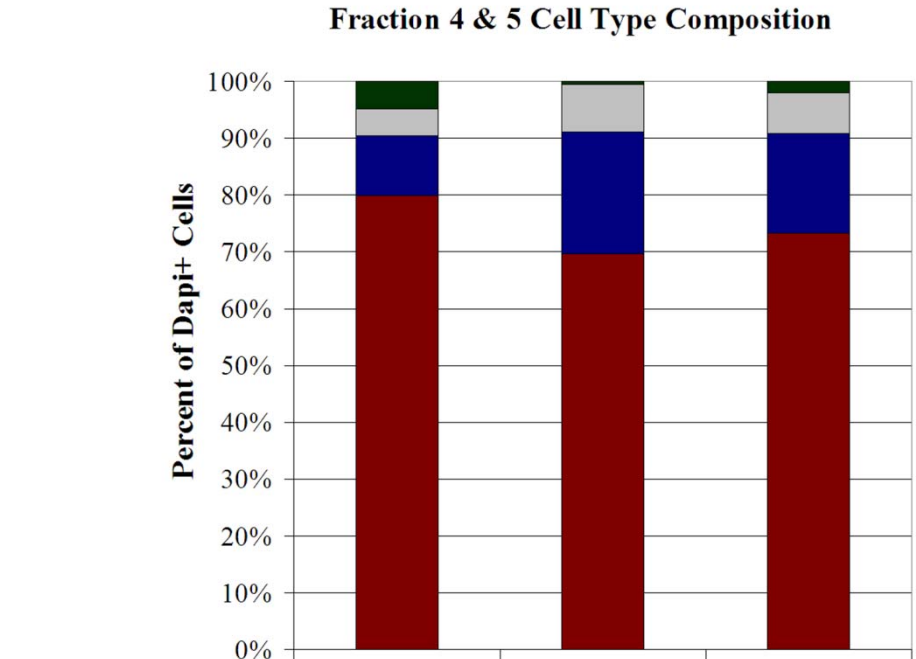

	Fraction 4	Fraction 5	Total
Unidentified Cell Type	4.78%	0.51%	1.99%
Mucous Neck Cells	4.78%	8.40%	7.14%
Parietal Cells	10.53%	21.37%	17.61%
Chief Cells	79.90%	69.72%	73.26%

Figure 18. Cell type composition of fractions 4 and 5 of stomach digestion. An aliquot from fractions 4 and 5 of the cell isolate were fixed with 4% PFA and spun down onto a slide using a cytospin centrifuge. After drying the slides, cells were immunolabeled with H/K-ATPase (parietal cell marker), TFF2 (mucous neck cell marker), PGC (chief cell marker), and DAPI (nuclei). Fraction 4 had the highest enrichment of chief cells at 79.9%, while fraction 5 had 69.7%. The percentage of parietal cells increased between fraction 4 and 5 (from 10.5% to 21.4%). Although fraction 5 had an increase in parietal cells, fractions 4 and 5 (together 73.3% chief cells) were both used for plating and culturing of chief cells. This allowed for a higher total number of chief cells for plating and presumably, parietal cells would not survive in culture over time.

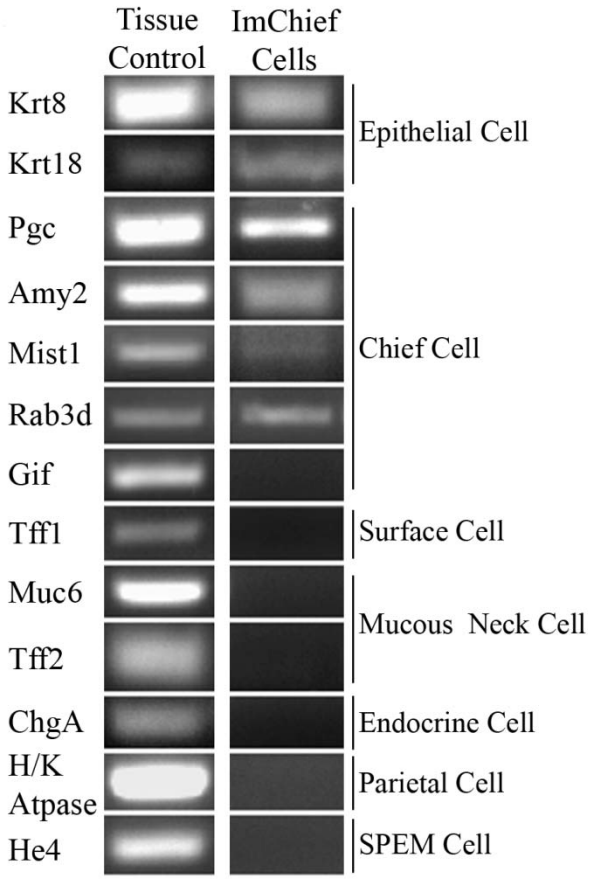

Figure 19. Expression of gastric cell lineage markers in ImChief cells. ImChief cells were grown at 39°C for one week. cDNA made from an *H. felis*-infected stomach was used for a positive control. ImChief cells expressed the epithelial markers, *Krt8* and *Krt18*. They also expressed all chief cell markers except *Gif*. Although the expression is low, the chief cell specific marker, *Mist1*, is expressed. ImChief cells did not detectably express markers for other gastric cell types (surface cells, parietal cells, mucous neck cells, endocrine cells, or SPEM cells). The lack of *He4* shows ImChief cells do not transdifferentiate into SPEM in this culture system. This expression pattern shows ImChief cells have a similar expression pattern to *in vivo* chief cells.

In vivo chief cells produce and secrete vesicles that contain zymogens, such as pepsinogen. Recent studies have shown RAB3D co-localizes with these secretory vesicles, suggesting a role in exocytosis of the zymogens (Tang et al. 1996). To examine

whether ImChief cells possess the secretory components found *in vivo*, cells at both the permissive and non-permissive temperatures were probed for pepsinogen (PGC) and RAB3D. Immunostaining revealed that ImChief cells produce pepsinogen vesicles at both temperatures (Figure 20). Furthermore, RAB3D co-labeled these pepsinogen vesicles. These findings confirm that ImChief cells produce the necessary secretory components. The localization of RAB3D predominately on pepsinogen vesicles suggests that ImChief cells may also actively secrete zymogen vesicles, however more studies are needed. Additionally, ImChief cells appear to express more RAB3D and pepsinogen co-positive vesicles at the non-permissive temperature (39°C) than at the permissive temperature (33°C) (Figure 20). At 39°C, the temperature sensitive T antigen misfolds and thus no longer immortalizes the cells, significantly decreasing proliferation of ImChief cells after approximately three days at 39°C whereby cells cannot be passaged (data not shown). Although further validation of increased vesicle production at 39°C is needed, these observations indicate that ImChief cells cease proliferation and subsequently may become more differentiated and 'primary-like' at the non-permissive temperature. Taken together, these data demonstrate that ImChief cells retain significant characteristics of *in vivo* chief cells.

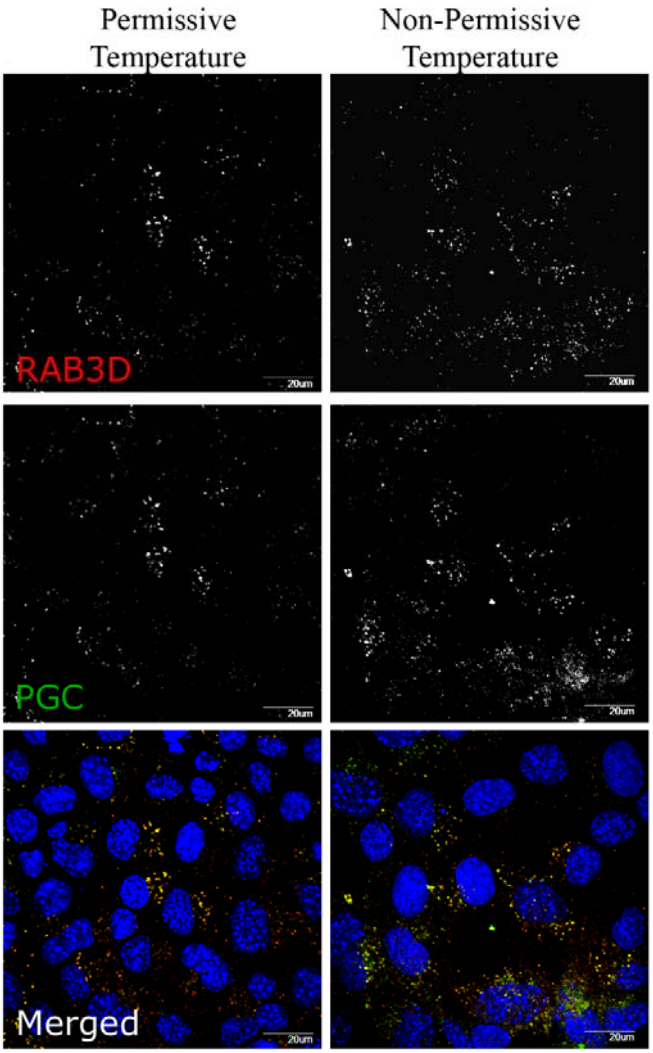

Figure 20. RAB3D and PGC expression in ImChief cells at the permissive and non-permissive temperatures. ImChief cells were plated on collagen-coated coverslips and incubated at either 33°C (permissive) or 37°C (non-permissive) for one week. Cells were immunolabeled with RAB3D (top row and red in merged panel) and PGC (middle row and green in merged panel). RAB3D and PGC co-labeled vesicles in ImChief cells at both temperatures (bottom row). However, at the non-permissive temperature, ImChief cells express more co-labeled vesicles, suggesting they become more differentiated. DAPI (blue).

Mist1 overexpression demonstrates the utility of the ImChief cell line

We sought to determine the utility of ImChief cells as a tool for investigating molecular mechanisms of chief cells. First, the ability of ImChief cells to be transfected was tested with multiple established transfection protocols. As seen in Table 2, ImChief cells were sucessfully transfected by multiple transfection methods with varying transfection efficiencies. Although the transfection efficiency for all methods was low, an electroporation transfection method (Amaxa Nucleofactor) resulted in the highest efficiency (29%). To further establish the utility of ImChief cells as an *in vitro* chief cell model, we chose to perform preliminary studies examining the function of *Mist1*, a chief cell-specific transcription factor. Previous studies in both mouse stomach and human gastric cancer cell lines have shown that *Mist1* is required for the formation of pepsinogen granules (Ramsey et al. 2007; Tian et al. 2010). To examine if ImChief cells would function in a similar manner, cells were transfected with a human *Mist1* plasmid (Tian et al. 2010). A preliminary western blot suggests that *Mist1* overexpression in ImChief cells induces an increase in endogenous pepsinogen (PCG) levels (Figure 21). Furthermore, the metaplasia marker, HE4, remained undetectable upon *Mist1* overexpression (Figure 21). The lack of HE4 upregulation indicates ImChief cells will not readily become metaplastic from simple manipulations such as transfection. These preliminary results suggest the ImChief cell line functions similarly to *in vivo* chief cells and can be used for the investigation of specific molecular mechanisms in chief cells.

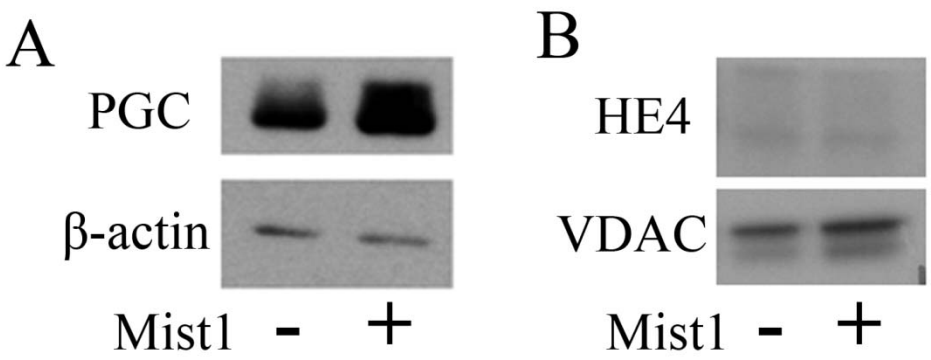

Figure 21. PGC and HE4 expression in protein lysates from ImChief cells overexpressing MIST1. ImChief cells were transfected with a Mist1-EGFP plasmid or a control EGFP plasmid and cultured at 39°C for three days (n=1). 20 μg of protein lysate was probed for PGC or HE4. β-actin and VDAC were used as loading controls. Overexpression of MIST1 increased PGC expression. HE4 expression was not detected, showing that simple manipulation of ImChief cells does not cause them to transdifferentiate into SPEM.

Immortalized SPEM cell line (ImSPEM) retains in vivo SPEM characteristics

A recent study profiling multiple human gastric cell lines showed that the KatoIII cell line retained expression of some metaplastic markers (Tan et al. 2011). However, the KatoIII line expresses a mixture of SPEM and intestinal metaplasia markers, and therefore cannot be appropriately used as an *in vitro* cell culture model for studying the signaling pathways and molecular mechanisms of SPEM. Accordingly, we developed and characterized a more definitive *in vitro* model of SPEM. To establish a SPEM cell line, the successful approach used for the establishment of the ImChief line was again utilized. SPEM was induced in three female Immortomice by oral gavage of L635 for three days. Stomachs were inverted and digested in serial fractions. Again, fractions 4 and 5 were enriched with the cell type of interest. Cells were plated on collagen-coated plates at 33°C with IFNγ and passaged (at 1:2) as needed. Multiple epithelial-like morphologies

emerged in the culture. Each morphology was purified individually by sequential higher dilution passages. Unlike the ImChief cell purification, cloning disks were not needed because the epithelial-like cells in the SPEM cell enriched cultures expanded more quickly than the contaminating stromal-like cells. Epithelial origin was confirmed by transcriptional expression of *Krt8* and *Krt18* (Figure 22). Additionally, all cultures were negative for *Pdx1* expression, verifying the cells as derived from the fundus of the stomach and not the antrum or duodenum (Table 3). Expression of specific cell lineage markers was investigated to identify the cell types present in each culture. Differences in the expression of the differentiated gastric cell markers were detected among the different purified cultures. All cultures expressed the SPEM lineage markers *Tff2* and *He4*; however, a few cultures expressed other differentiated gastric cell markers as well (data not shown). This type of expression profile may result for a multitude of reasons. For example, these cultures may contain multiple differentiated gastric cell types that are proliferating, or a progenitor cell with the ability to give rise to multiple lineages. For the present study, we focused on the cell cultures that expressed SPEM markers, but lacked expression of other lineage markers, as they represented purified SPEM cell cultures. The expression levels of the SPEM markers varied among the different SPEM cultures (data not shown). Therefore, from the different SPEM cultures, the culture with the most prominent expression of the SPEM markers *Tff2* and *He4* (Figure 22) as compared to the other cultures was selected and designated ImSPEM (Im-Immortomouse, SPEM-Spasmolytic Polypeptide Expressing Metaplasia).

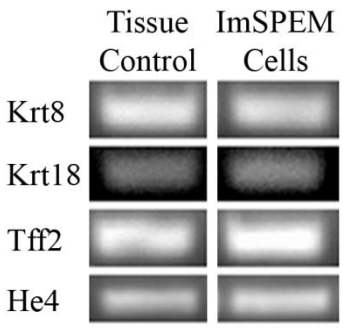

Figure 22. Transcript expression of SPEM markers in ImSPEM cells. Cells were cultured at 33°C for one week for initial expression characterization. Expression of the SPEM markers *He4* and *Tff2* was analyzed in ImSPEM cells. ImSPEM cells express the epithelial markers (*Krt8* and *Krt18*) and the SPEM markers.

Multiple *in vivo* SPEM characterististics were evaluated in order to fully validate the newly established ImSPEM line. One distinct property of *in vivo* SPEM cells is re-entry into the cell cycle. Although chief cells are post-mitotic, upon transdifferentiation to SPEM, SPEM cells begin to proliferate. Aptly, upon return to a more primary-like culture at 39°C without IFNγ, ImSPEM cells continue to proliferate. ImSPEM cells can be maintained and passaged at 39°C without IFNγ for at least one month, signifying that ImSPEM cells possess an intrinsic proliferative property similar to *in vivo* SPEM cells. Another characteristic of L635-derived SPEM is the acquisition of intestinal transcripts. Previously, we have shown transcriptional heterogeneity among SPEM lineages from different murine models of SPEM (Weis et al. 2013). Briefly, SPEM lineages derived in the presence of inflammation progress to SPEM-IC (SPEM with Intestinal Characteristics) by acquiring intestinal transcripts such as *Cftr*, *Dmbt1*, and eventually *Vil1* and *PigR*. To characterize the metaplastic state of ImSPEM cells, expression of selected previously

reported SPEM (by real time PCR) and SPEM-IC (by qRT-PCR) markers were evaluated at the non-permissive temperature (39°C). ImSPEM cells expressed all SPEM markers that were tested by real time PCR (Table 3). The SPEM-IC markers *Cftr* and *PigR* were expressed at low levels while *Vil1*, *Dmbt1*, and *Cdx2* were not expressed at all (Table 3) as tested by qRT-PCR. This expression profile matches that of SPEM-IC cells *in vivo*.

Although ImSPEM cells retain the transcriptional profile of *in vivo* SPEM, we further characterized the ImSPEM line by analyzing protein expression of key SPEM markers. When chief cells transdifferentiate into SPEM, SPEM cells begin producing TFF2 vesicles and HE4 vesicles. To date, HE4 expression is the most prominent and specific marker of SPEM induction *in vivo*. Thus, TFF2 and HE4 expression in ImSPEM cells was investigated. Immunostaining revealed ImSPEM cells expressed both TFF2 and HE4 that localized to cytoplasmic vesicles (Figure 23). To confirm HE4 expression in ImSPEM cells, western blots of protein lysates were probed for HE4. Replicate protein lysates show HE4 expression in ImSPEM cells, but not ImChief cells (Figure 23). Moreover, because HE4 is known to be secreted *in vivo*, we tested for HE4 detection in the conditioned media as a measure of functional secretory machinery in the ImSPEM line. ImSPEM cells were grown at 39°C for one week. ImChief cells were used as a negative control as they do not express HE4. After one week at 39°C, fresh media was incubated on the cells for 24 hours. Western blot analysis of the 24 hour conditioned media reveals HE4 detection in ImSPEM media, but not ImChief media, showing ImSPEM cells have functional secretory machinery (Figure 23). Taken together, these data demonstrate ImSPEM cells possess many of the characteristics displayed by *in vivo* SPEM lineages and provides a novel *in vitro* model of this metaplastic cell type.

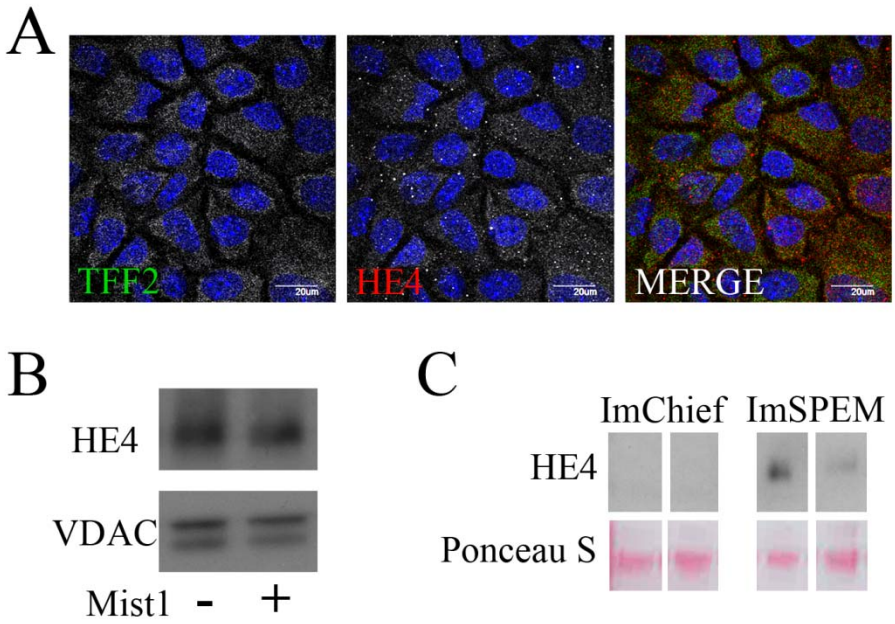

Figure 23. Expression of SPEM protein markers, TFF2 and HE4. Immunolabeling of ImSPEM cells (A), ImSPEM protein lysate (B), and conditioned media (C) reveal expression and secretion of SPEM markers. (A) Cells were grown on collagen-coated coverslips at 39°C for one week. ImSPEM cells express individual TFF2 and HE4 vesicles similar to *in vivo* SPEM. (B) Cells were transfected with a Mist1-EGFP or GFP control plasmid and grown at 39°C for three days. 20 µg of protein lysate was immunolabeled for HE4 and VDAC (loading control). ImSPEM protein lysates confirm HE4 expression. Furthermore, MIST1 overexpression does not cause SPEM to revert back to chief cells, as there is no change in HE4 expression. (C) ImChief and ImSPEM cells were grown on collagen-coated transwells at 39°C for one week. Fresh media was added for 24 hours. The 24 hour conditioned media from ImChief cells and ImSPEM cells show secretion of HE4 from ImSPEM cells. Replicates for ImChief and ImSPEM cells are shown. Ponceau S staining is shown as a loading control.

Gene microarray comparison of ImChief and ImSPEM identifies Mal2 as a novel subapical marker of metaplasia

Gene microarray analysis was used to compare the complete transcriptional profiles of ImChief cell and ImSPEM cells grown at 39°C without IFNγ for one week. Cells grown at 39°C were selected because of more primary-like (and possibly more

'differentiated') state. Additionally, effects from the T-antigen-induced immortalization are minimized, as it is no longer active at this temperature. Levels of mRNA transcripts from triplicates of each cell line were measured with Affymetrix gene microarrays. Comparison of ImChief and ImSPEM expression profiles identified new putative markers of the metaplastic process. Table 4 lists the top 25 transcripts upregulated in ImSPEM cells as compared to ImChief cells. *Mal2*, the third most upregulated transcript in ImSPEM, is increased by 113 fold. Previous reports have shown that MAL2 protein is required for the transcytosis pathway and is normally localized to the subapical compartment in polarized cells (de Marco et al. 2002; Marazuela et al. 2004a; Marazuela et al. 2004b; Marazuela et al. 2004c; de Marco et al. 2006; Ramnarayanan et al. 2007; In et al. 2010; Ramnarayanan et al. 2011). We chose to further validate the upregulation and localization of MAL2 in the mouse stomach due to its potential as a novel subapical marker of SPEM.

Table 4. Gene microarray comparison of ImChief and ImSPEM cells. ImChief cells and ImSPEM cells were incubated at the non-permissive temperature (39°C) for one week. Transcriptional expression was analyzed by gene microarray. The top 25 transcripts upregulated in ImSPEM cells compared to ImChief cells reveal putative new markers of SPEM. The normalized expression level in the respective cell line is shown as well as the fold change.

Gene Symbol	ImChief Expression Level	ImSPEM Expression Level	Fold change
Ppbp	5.91	13.85	244.85
Krt5	6.81	13.80	127.20
Mal2	5.85	12.68	113.25
Krt6a	6.61	13.17	94.35
Trim29	6.60	13.07	89.06
Cldn4	7.28	13.48	73.53
Dsg3	5.81	11.99	72.20
Spink5	6.18	12.32	70.83
Rab25	6.76	12.77	64.46
Vsnl1	6.79	12.77	63.39
Krt14	7.57	13.50	61.07
Krt17	7.60	13.53	60.73
Tacstd2	6.68	12.58	59.53
Serpinb5	5.84	11.70	57.83
Il1a	5.29	11.13	57.20
Xist	5.87	11.71	57.18
Dsp	6.64	12.47	57.00
Cdh1	6.76	12.44	51.21
Cdh3	6.67	12.26	48.17
Trex2	6.81	12.32	45.36
Mpzl2	6.47	11.97	45.34
1600029D21Rik	7.35	12.85	45.01
Rab15	6.46	11.89	43.22
Clic3	7.01	12.41	42.06
Gpx2	6.53	11.90	41.43

First, we examined the expression of MAL2 in normal murine gastric glands. In untreated control mice, MAL2 immunoreactivity was detected in the subapical compartment of mucous neck cells and surface cells (Figure 24). A diffuse cytoplasmic staining pattern was also detected in parietal cells (co-stain with H/K-ATPase not shown)

and there was low MAL2 expression in chief cells (Figure 24). To thoroughly investigate MAL2 expression in SPEM, we utilized three models of SPEM: 14 days DMP-777 treatment, three days L635 treatment, and 12 month *H. felis* infection. As previously reported, acute SPEM without inflammation is induced by DMP-777 treatment, while L635 administration results in SPEM with prominent inflammation (Nomura et al. 2004c; Nam et al. 2010). *H. felis* infection was used as a model of chronic inflammation and SPEM that progresses to SPEM-IC (Varon et al. 2011; Weis et al. 2013). As shown in Figure 24, MAL2 expression is increased and located subapically in SPEM lineages from all three models as well as gastritis cystica profunda in 12 month *H. felis*-infected mice. These findings not only validate MAL2 as a new marker of SPEM, but also as a novel marker of polarized vesicle trafficking in SPEM. Although several studies have elucidated the expression profile of SPEM (Lee et al. 2003; Judd et al. 2004; Nomura et al. 2004b; Nomura et al. 2004c; Ogawa et al. 2006; Nam et al. 2007; Nozaki et al. 2008; Nozaki et al. 2009; Lee et al. 2010; Weis et al. 2013), the discovery of MAL2 provides the first insight into the possible factors and mechanisms involved in transcytosis and secretion in SPEM cells.

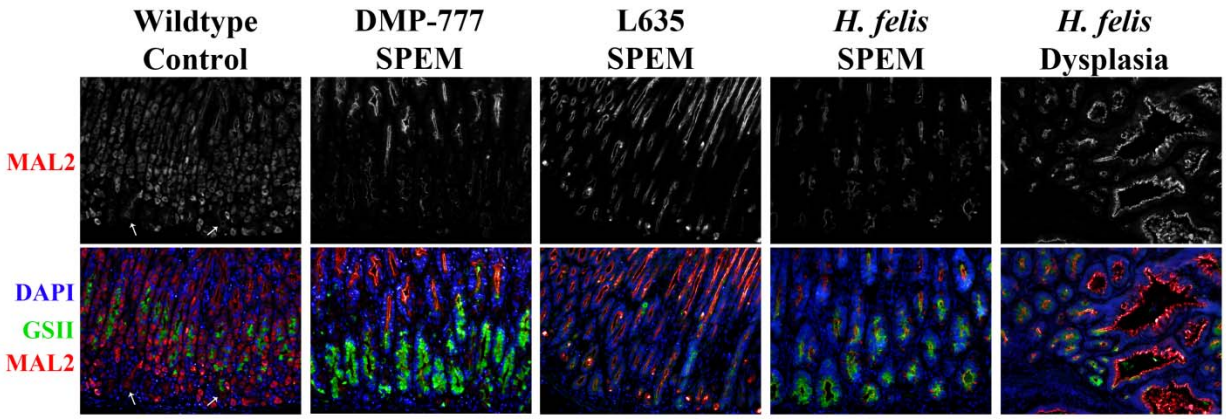

Figure 24. Expression of MAL2 in normal murine gastric mucosa and SPEM models. Sections of C57BL/6 mouse fundic mucosa were immunostained with MAL2 (top panel and red in bottom merged panel) and GSII lectin (a mucous neck cell and SPEM marker) (green). MAL2 images were taken at the same exposure for each sample (top row). MAL2 was expressed most strongly in parietal cells, which demonstrated a dispersed cytoplasmic localization. Weaker subapical staining was observed in mucous cells (surface and neck cells and to a lesser extent chief cells in the normal mucosa (arrows). In all SPEM models (DMP-777, L635, and *H.* felis), MAL2 expression was increased in the SPEM models as compared to the chief cells in the normal mucosa and localized to the subapical compartment in SPEM cells marked by GSII lectin. A region of dysplasia (gastritis cystica profunda) in the *H. felis* infected mouse also showed strong expression of MAL2. All images were taken with a 20X objective. DAPI (blue).

To investigate MAL2 expression in human metaplasias of the stomach, a tissue microarray with mixture of SPEM and intestinal metaplasia samples was probed for MAL2 (Figure 25). MAL2 was expressed in SPEM and localized to the subapical region. In intestinal metaplasia, MAL2 was localized to the same subapical compartment. In human, 12 out of 12 samples of SPEM and 7 out of 7 samples of intestinal metaplasia expressed MAL2 (Figure 25). A gastric cancer tissue microarray was also immunostained to investigate MAL2 expression in intestinal type gastric cancers (Figure 25). Subapical expression of MAL2 was found in 9 out of 11 intestinal type gastric cancers (Figure 25). Overall, in both mouse and human, MAL2 is a novel marker of metaplasia in the stomach

and understanding its role in transcytosis could provide valuable knowledge about the mechanisms involved in the metaplastic process.

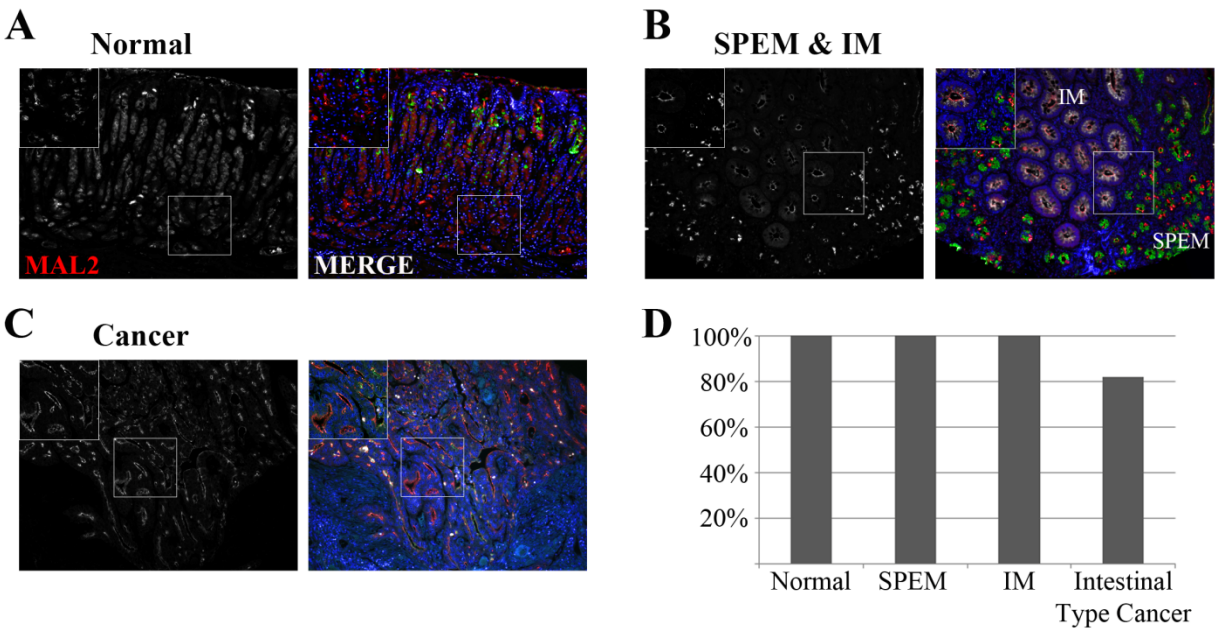

Figure 25. MAL2 expression in normal human gastric mucosa, metaplasia, and cancer. A tissue microarray of normal gastric mucosa (A), SPEM (B), and intestinal metaplasia (B) and a microarray of gastric cancer (C) was labeled with MAL2 (red, first panel), GSII lectin (green), and DMBT1 (an intestinal metaplasia marker) (white). All images were taken with a 10X or 20X (insets shown in upper left corners) objective. The second panels are the merged images. (A) MAL2 was expressed in the subapical compartment of mucous cells and chief cells in the normal mucosa Parietal cells expressed MAL2 in a diffuse cytoplasmic pattern. (B) SPEM (GSII-green) and intestinal metaplasia (DMBT1-white) displayed subapical localization of MAL2. MAL2 expression was increased in SPEM and intestinal metaplasia (IM). (C) A representative image of intestinal type cancer from the gastric cancer tissue microarray. In cancer, MAL2 was subapically expressed. (D) The percentage of samples of normal chief cells, SPEM, intestinal metaplasia, and intestinal type cancer samples that expressed MAL2 was calculated. 100% of chief cells (13/13), SPEM (12/12) and intestinal metaplasias (7/7) expressed MAL2. MAL2 expression was found in 82% of intestinal type gastric cancers (9/11). DAPI (blue).

ImSPEM cells polarize and form cystic structures

The microarray and MAL2 data suggest transcytosis plays an important role in metaplasia. Therefore, we assessed the polarization ability of ImSPEM cells. ImSPEM cells were plated near confluency on collagen-coated transwells and incubated at 39°C for one week. On transwell filters, ImSPEM cells remain very flat (approximately 5 μM tall) and vary between forming a monolayer and a bilayer of cells. In bilayers, the bottom layer consists of numerous smaller cells, while the upper layer has fewer, but distinctly larger and flatter cells. Adherens junction proteins p120 and E-cadherin localized to the lateral membranes of all cells in both cell layers. However, the lower layer of cells had jagged and irregular junctions, while the top layer displayed a smooth and continuous pattern (Figure 26). Additionally, F-actin is concentrated at the membrane of the cells in the top layer. In the bottom layer, distinct lateral membrane expression was detected, as well as lower intensity apical localization (Figure 27). This pattern suggests differences in polarization within the ImSPEM cells. Cells in the monolayer have similar patterning to the cells in the bilayer. To investigate the extent of polarization, tight junctions were examined with ZO1 immunostaining (Figure 26). Because of varying cell heights and the complications of two cell layers, ZO1 staining was unclear in bilayers. However, in the monolayer regions, ZO1 was localized to the top of the lateral membranes of the cells (Figure 26), demonstrating that ImSPEM cells polarize and possibly establish a transition between the lateral and apical membrane. Overall, these data show ImSPEM cells on transwells vary between forming a monolayer and a bilayer of two distinct layers that establish adherens and tight junctions. In the bilayer, the bottom layer of cells appears to polarize and becomes taller, while the top layer of cells establishes more continuous and

distinct junctions. Furthermore, cells in the monolayer establish tight junctions showing polarization.

Determining the degree of polarization of ImSPEM cells proved difficult as there are no reported apical markers in SPEM. Without the discovery of MAL2 as a subapical SPEM marker, studies of ImSPEM polarization would have been impeded. However, we are able to utilize the newly validated SPEM marker, MAL2, to determine if ImSPEM cells designate an apical side for transcytosis. Again, ImSPEM cells were grown on collagen-coated transwells at 39°C for one week. MAL2 expression was limited to the upper layer of cells and the monolayer (Figure 27). Furthermore, MAL2 localized to the subapical regions of the cells. This specific subapical localization of MAL2 demonstrates that ImSPEM cells define an apical side. As described above, HE4 is secreted from ImSPEM cells and can be detected in the media by western blot analysis. To determine directionality of HE4 secretion and further confirm polarization of the cells, ImSPEM cells were grown on collagen-coated transwells at 39°C for one week. Fresh media was added for 24 hours to the apical and basal sides of the transwells. Media from both sides was collected separately and 15 μL was probed for HE4 by western blot; HE4 secreted protein was only detected in the apical conditioned media (Figure 27). These findings show ImSPEM cells delineate an apical membrane for secretion, thus confirming the ability of ImSPEM cells to polarize when grown on transwell filters.

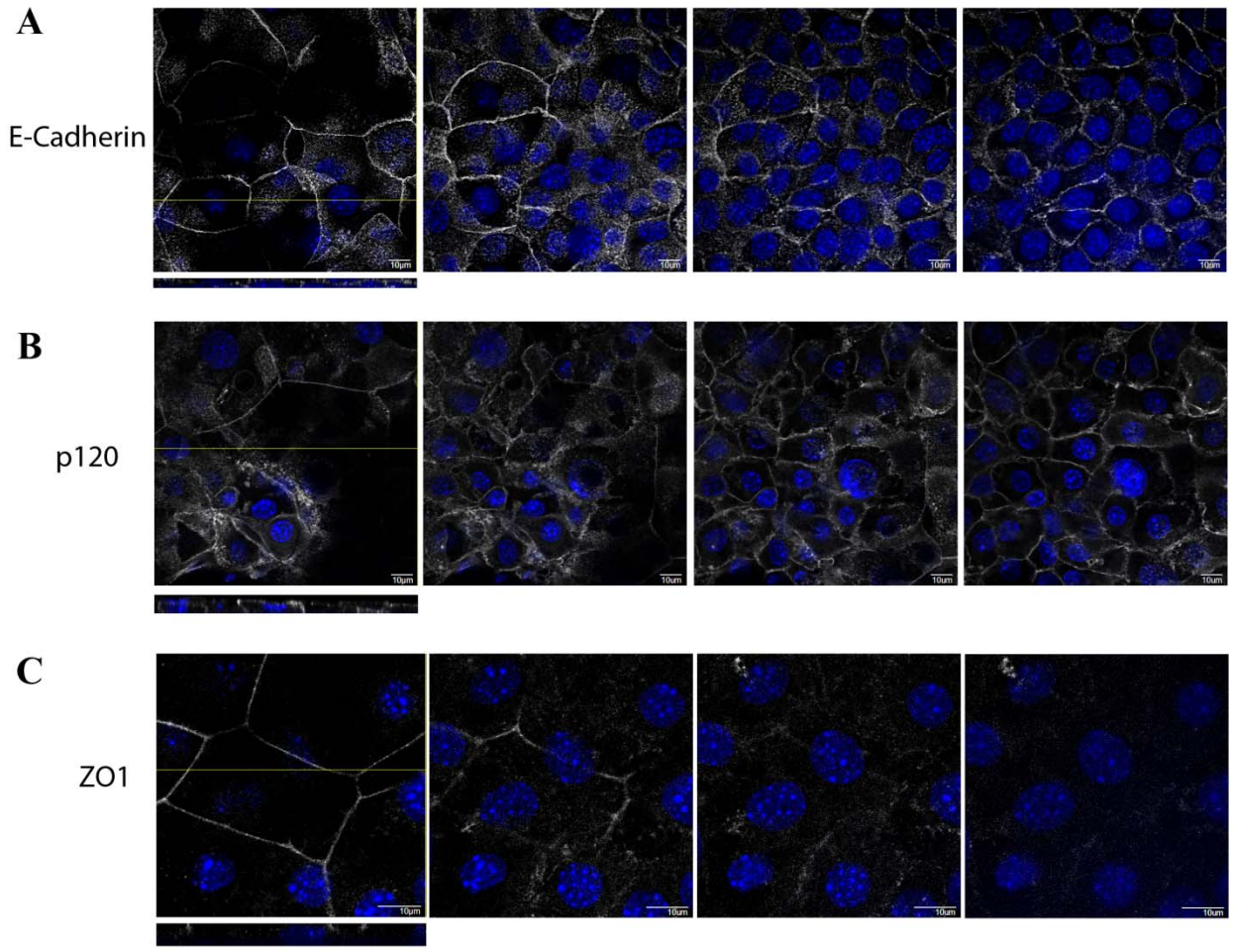

Figure 26. Polarization of ImSPEM cells on transwells. ImSPEM cells were grown on collagen-coated transwell at 39°C for one week. Cells were immunolabeled for E-cadherin (A), p120 (B), and ZO1 (C). Expression patterns were analyzed using Z-stacks of the transwells. ImSPEM cells grew in either a monolayer (C) or bilayer of cells (A-C). Serial images taken 1 μm apart are shown. (A) ImSPEM cells in a bilayer displayed lateral staining for E-cadherin. Cells on the top layer exhibited more continuous adherence junction staining while cells in the bottom layer had more jagged staining. The specific lateral membrane expression can be seen in the Z-axis (first panel). (B) p120 was also localized to the lateral membrane in a similar pattern to E-cadherin. (D) ZO1 staining was examined in an area of monolayer growth because the varying thickness and size of cells in the bilayer made localization of ZO1 staining ambiguous. In the monolayer, cells expressed ZO1 on the upper edge of the lateral membrane demonstrating the establishment of tight junctions in the correct location. DAPI (blue).

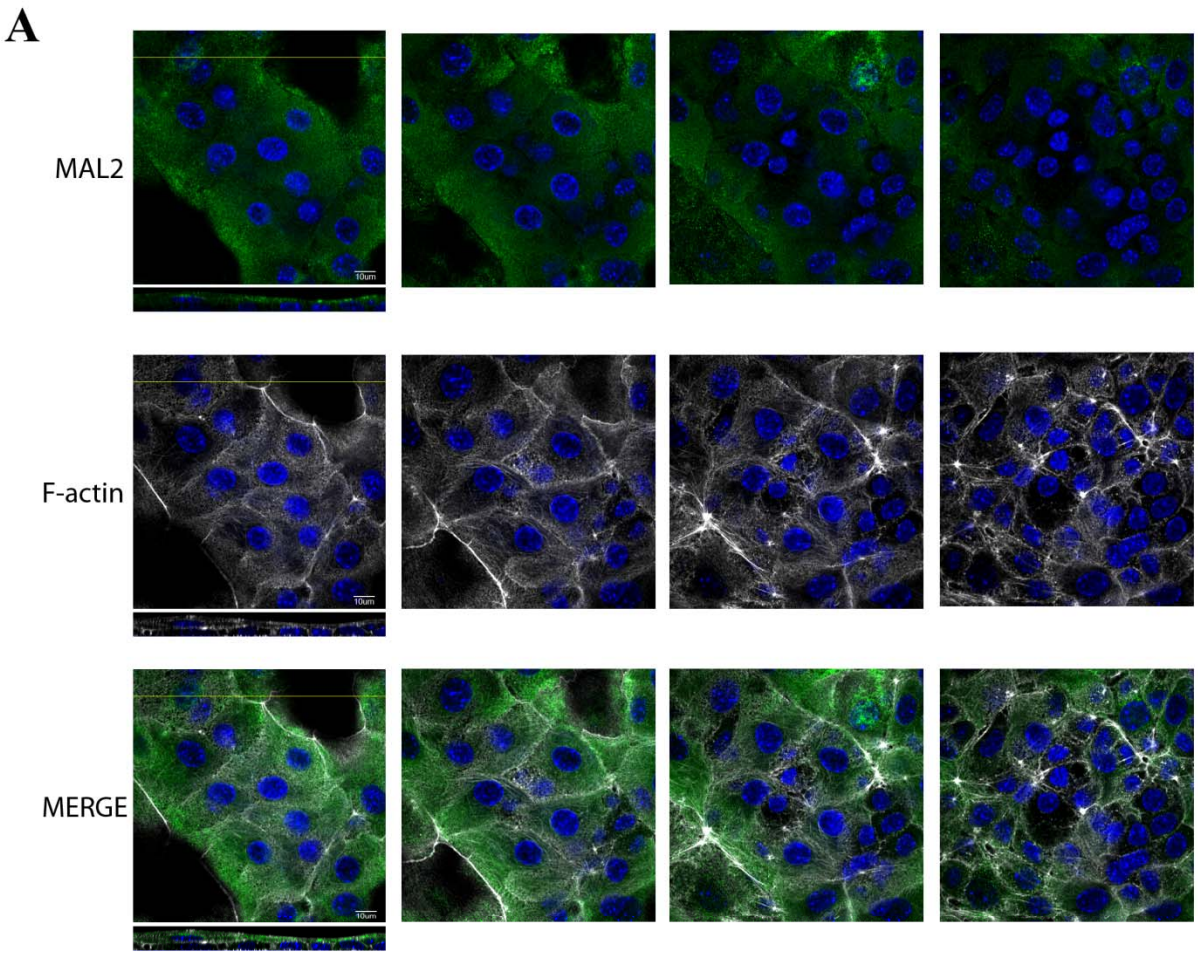
A
MAL2
F-actin
MERGE
10um
B
Apical
Basal
HE4
Ponceau S

Figure 27. Apical polarization in ImSPEM cells. ImSPEM cells were grown on collagen-coated transwell at 39°C for one week. (A) Cells were immunolabeled with MAL2 (green) and actin (phalloidin) (white). Expression patterns were analyzed using Z-stacks of the transwells. Serial images taken 1 μm apart are shown. MAL2 was localized to the subapical region of ImSPEM cells. In the bilayer of cells, MAL2 was only detected in the cells of the top layer. DAPI (blue). (B) After one week at 39°C, fresh media was added for 24 hours to apical and basal compartments of the transwells. Media was collected and cell debris was removed. 15 μL of the 24 hour conditioned media was probed for HE4 by western blot. HE4 was detected only in the apical media, demonstrating directional secretion. Ponceau S staining is shown as a loading control.

Utilizing the 3D culture model of suspension in Matrigel, the extent of growth and polarization of ImSPEM cells was examined. ImSPEM cells were suspended in Matrigel at a 1:1 dilution with media. Cells were then incubated at 39°C until large structures were apparent. This varied from three to six weeks. By light microscopy, spherical cellular structures can be identified. While some strictly proliferating cells form multicellular spheroids, other structures appear to be cup-shaped or exhibit hollowed interiors (Figure 28). The ability to form indentions and hollowed areas further confirms the polarization capacity of ImSPEM cells. The size and shape of the hollowed areas varied. Initial attempts to retrieve intact Matrigel plugs for immunofluorescent studies failed because the plugs were no longer polymerized enough to hold their shape. Therefore, the semi-liquid contents of each well were gently centrifuged to collect all cells and fragments of the Matrigel. The structures in the Matrigel held together during the centrifugation such that immunostaining analysis could be performed, however they may have been slightly flattened. As seen by F-actin immunolabeling, the cystic structures consist of various layers of cells with some areas having only one cell layer while others have multiple layers (Figure 28). Serial images from Z-stacks of these structures reveal areas of open

cavities that are void of actin staining and nuclei. These findings reveal that ImSPEM cells not only grow but can form cystic structures in Matrigel.

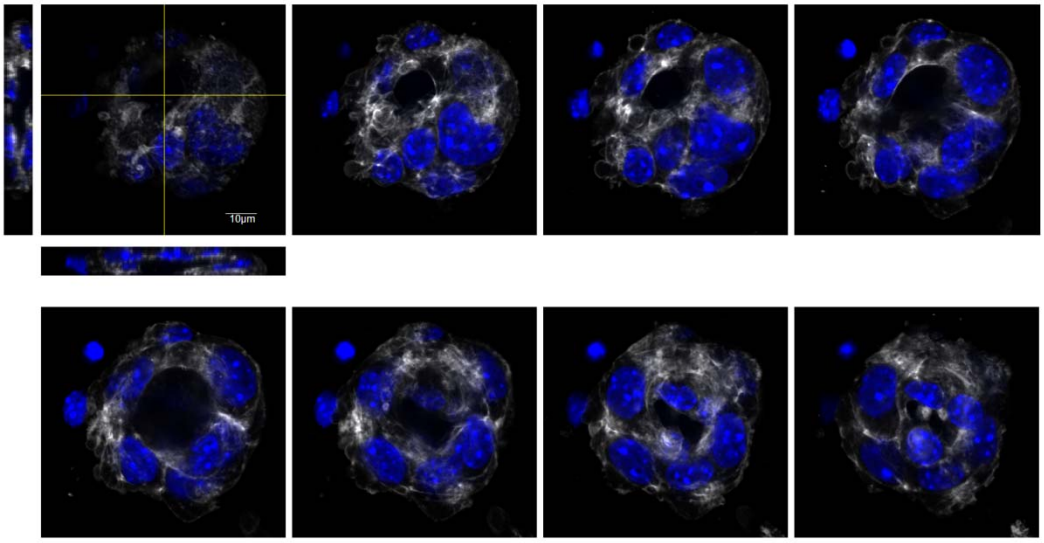

Figure 28. ImSPEM cystic structures in 3D Matrigel culture. ImSPEM cells were suspended in Matrigel and grown at 39°C. Cystic structures appeared at three to six weeks. Cells were immunostained for actin (phalloidin). Serial images through the cysts (0.5 µm apart) are shown. An opening inside the structures is clearly evident from the lack of actin staining and nuclei. This shows ImSPEM cells polarize to form cystic structures in 3D Matrigel cultures. DAPI (blue).

Discussion

The stomach maintains homeostasis through a complex network of both cell autonomous and nonautonomous signaling pathways. Numerous studies have been conducted on specific signaling molecules and how their alterations affect the normal stomach cell types (Beauchamp et al. 1989; Murayama et al. 1994; Li et al. 1996; Abe et al. 1997; Nomura et al. 2004a; Nomura et al. 2004c; Jain et al. 2006a; Nozaki et al. 2008;

Nam et al. 2010). Recent studies have shown that damage or disease in the stomach can cause chief cells to transdifferentiate into SPEM. Thus, a new focus has been placed on understanding the molecular mechanisms involved in chief cell homeostasis and metaplastic transdifferentiation. After the discovery of the chief cell secretory mechanism (Langley 1882; Hirschowitz 1967; Koelz et al. 1982; Raufman et al. 1983; Berger et al. 1985; Muallem et al. 1986; Raufman et al. 1986; Sutliff et al. 1986; Brown et al. 1987; Raufman et al. 1987; Matozaki et al. 1988; Tsunoda et al. 1988), progress toward understanding other molecular events and signals in chief cell homeostasis and function has been slow. Studies into the mechanisms that underlie this homeostasis, as well as transdifferentiation into SPEM have been hampered by the sole reliance on *in vivo* mouse models. While *in vivo* models are important for studying complex signaling networks and the role of specific genes or signaling pathways on a whole tissue scale, it is difficult to identify specific molecular interactions or gene dynamics on a cellular level. Therefore, *in vitro* cell culture studies are greatly needed to help uncover such phenomena. There is currently one established cell line of a normal gastric epithelial cell type called ImSt (also developed from the Immortomouse); however, this cell line does not express lineage specific markers for parietal cells, mucous neck cells, or chief cells and thus is presumably a cell culture model of gastric surface cells (Whitehead et al. 2009). Currently, human gastric cancer cell lines are used in the majority of gastric *in vitro* studies (Bredemeyer et al. 2009; Wei et al. 2010; Chaturvedi et al. 2011; Fujii et al. 2012; Noto et al. 2013). However, these lines have inherent disadvantages for use in understanding the role of genes in gastric homeostasis or the metaplastic process. For example, previous studies investigating the function of the chief cell specific transcription

factor *Mist1* in vesicle maturation used human gastric cancer cell lines (Tian et al. 2010) because of the lack of *in vitro* models of normal chief cells. As *Mist1* is typically lost early in the progression to gastric cancer (Lennerz et al. 2010), the cancer cell lines used do not express *Mist1*, therefore a *Mist1* stably expressing cell line had to be established and pepsinogen, a significant component of secretory vesicles, also had to be transfected into the cells in order to study the regulation of vesicle formation in these cells (Tian et al. 2010). The establishment of the novel ImChief cell line now allows such studies to be conducted in an *in vitro* chief cell model that closely resembles *in vivo* chief cells. ImChief cells become more differentiated and primary-like at the non-permissive temperature of 39°C, allowing study of endogenous proteins and differentiation and secretion mechanisms. Additionally, for overexpression or knockdown experiments, we have shown that ImChief cells can be transfected effectively with a plasmid of interest. Thus, the ImChief cell line is an essential *in vitro* chief cell model that allows for the study of factors (endogenous and exogenous) that are difficult to study using currently available resources, such as mouse models and gastric cancer cell lines.

When parietal cells are lost, chief cells transdifferentiate into SPEM possibly as a protective mechanism (Nomura et al. 2004a; Nomura et al. 2004c; Nozaki et al. 2008; Nam et al. 2010). In the presence of chronic inflammation, SPEM can progress to intestinal metaplasia in the human (El-Zimaity et al. 2001); however, the mechanisms of induction or progression of SPEM are unknown. Due to the absence of SPEM cell culture models, there is currently a lack of *in vitro* methods to study the metaplastic process in the stomach. A recent study profiled the transcriptional expression of several gastric cancer cell lines. KATOIII cells retained a more metaplastic profile than the other cell

lines as measured by expression of several SPEM and intestinal metaplasia markers (Tan et al. 2011). While KATOIII cells are a better *in vitro* model for metaplasia than other cancer cell lines, expression of intestinal metaplasia markers prohibits separation of studies of SPEM from intestinal metaplasia. The establishment of the novel ImSPEM cell line fills this void of a SPEM-specific *in vitro* cell culture model. Numerous studies in the mouse of either loss or overexpression of specific genes have identified multiple proteins that result in the development of SPEM (Judd et al. 2004; Nomura et al. 2004c; Oshima et al. 2004; Katz et al. 2005; Ogawa et al. 2006; Oshima et al. 2006; Nam et al. 2007; Jain et al. 2008; Nozaki et al. 2008; Nozaki et al. 2009; Keeley et al. 2010; Lee et al. 2010; Ito et al. 2011). Moreover, *Helicobacter* infection studies have revealed roles for the immunological response that is important in the metaplastic progression. Upon infection, the gastric mucosa is infiltrated with immune cells, such as macrophages and neutrophils, and the expression of secreted cytokines (most notably, IL-1β and TNF-α) are increased. However, specific molecular interactions and cellular effects of specific genes, cytokines, or immune cells are obfuscated in complex *in vivo* models. Such effects on SPEM can now be investigated in this novel ImSPEM cell culture model. For example, our lab is currently utilizing ImSPEM cells to investigate the capacity of the transcription factor *Mist1* to initiate SPEM reversal back to chief cells. Preliminary data indicates there is no change in HE4 expression in cell lysates, suggesting *Mist1* alone is not capable of reversing SPEM (Figure 23). Moreover, purified cytokines or isolated immune cells can also be co-cultured with ImSPEM cells to study their role in metaplasia. Similar to investigations of the role of extrinsic factors, ImSPEM cells can also be used to study the intrinsic properties and mechanisms of SPEM. The evidence that ImSPEM cells function

similarly to their *in vivo* counterparts allows for targeted mechanistic studies of previously identified intrinsic proteins putatively important in the metaplastic process. For instance, since ImSPEM cells secrete HE4, one of the few specific markers of SPEM, elucidation of its secretory mechanisms are now possible. Additionally, in previous studies, we have identified transcriptional upregulation of *Mmp12*, a secreted elastase, in acute SPEM (Weis et al. 2013). Disintegration of the 3D Matrigel plugs suggests that ImSPEM cells actively secrete a factor (or multiple factors) that is capable of extracellular matrix degradation. Therefore, it is possible that MMP12 may be an essential secreted protein involved in this matrix degradation. Such extrinsic and intrinsic studies into the mechanisms of SPEM are now possible with the development of the novel *in vitro* cell culture model, ImSPEM.

Several gene microarray studies by our lab and others have yielded numerous insights into the induction and progression of SPEM in both the mouse and human (Nomura et al. 2004a; Nozaki et al. 2008; Lee et al. 2010). Based on these previous successes, we compared the ImChief cell line to the ImSPEM cell line with gene microarray analysis. From this analysis, we established a list of putative markers of SPEM. MAL2 immunostaining in murine tissue revealed an increase in subapical expression in SPEM cells. A previous study from our lab has characterized a progression of SPEM to acquire intestinal characteristics (SPEM-IC) in the mouse (Weis et al. 2013). Although further validation is necessary, immunostaining of murine SPEM models suggests *H. felis*-induced SPEM (SPEM-IC) expresses the highest levels of MAL2 in our three SPEM models. Our previous study concluded that SPEM-IC is the mouse version of intestinal metaplasia that is found in humans (Weis et al. 2013). Accordingly, both SPEM

and intestinal metaplasia in the human express MAL2 with the highest expression in intestinal metaplasia. Furthermore, 82% of intestinal type gastric cancers (9/11) expressed MAL2. MAL2 is a multispan transmembrane protein that is necessary for transcytosis in polarized epithelial cells. In ImSPEM cells, MAL2 was localized to the subapical compartment, confirming the ability of ImSPEM cells to polarize on transwells. Because of its known role in transcytosis, studies of MAL2 in ImSPEM cells will provide unique insights into the little known trafficking mechanisms of SPEM. Understanding the trafficking machinery and other molecular mechanisms of SPEM will broaden our understanding of the metaplastic progression and may lead to areas of clinical intervention in the future. Moreover, while we have identified a new SPEM marker from the microarray analysis, investigation of other putative genes may also provide novel insights into the molecular machinery of SPEM.

An underlying concern of cell culture models is that the majority of studies are conducted in 2D cultures, which may not be relevant to the *in vivo* system. However, in the case of the ImChief cell line, many characteristics of the chief cells will remain obscure without the use of an *in vitro* model system. Due to the predominant reliance on *in vivo* models throughout the literature, numerous animal model systems exist to validate potential findings from the ImChief cell line. Recent advances made in propagating enteroids from the intestine (Sato et al. 2009), have generated considerable interest in culturing enteroids or gastroids from the stomach. However, propagation techniques for gastric enteroids or gastroids have not been refined. In contrast, the ImSPEM cell line consists of a known and thoroughly characterized cell type that has the ability to grow as a 3D culture in Matrigel, forming polarized cystic structures. Thus, ImSPEM cells in 3D

culture can be used to assess a wide array of traits, such as proliferation, polarization, and cyst or gland formation. Overall, we have established and thoroughly characterized two novel *in vitro* cell lines: chief cells (ImChief) and SPEM cells (ImSPEM). These studies have shown the utility of ImChief and ImSPEM cell lines as vital model systems for studying intrinsic and extrinsic factors involved in both gastric homeostasis and the metaplastic process.

CHAPTER IV

LOSS OF *MIST1* IMPEDES CHIEF CELL TRANSDIFFERENTIATION INTO SPEM

Appears as: Weis, V.G., Petersen, C.P., Mills, J.C., and Goldenring, J.R. Loss of Mist1 impedes chief cell transdifferentiation into SPEM. Manuscript in preparation.

Introduction

Gastric glands consist of multiple cell lineages that are derived from progenitor cells that reside in the isthmus region of the glands. The cells emerge from the progenitor region and differentiate as they migrate away (Karam et al. 1993a; Karam et al. 1993c; Karam et al. 1993d). Acid-secreting parietal cells migrate downward towards the base and reside in the neck region of the gland (Karam et al. 1992). Mucous neck cells also migrate towards the base of the glands. As they exit the neck region of the gland, mucous neck cells switch their secretory machinery and transdifferentiate into zymogen-secreting chief cells that continue to mature until they reach the base of the gland (Karam et al. 1993d). During this transdifferntiation, the cells begin to expand their rough endoplasmic reticulum (rER) and extend their apical membranes to establish a more pyramidal shape (Karam et al. 1993d; Ramsey et al. 2007; Bredemeyer et al. 2009). This transdifferentiation is accompanied by the replacement of mucous filled vesicles with zymogen containing vesicles (Karam et al. 1993d; Ramsey et al. 2007). Approximately two transition cells (GSII lectin and intrinsic factor dual positive) are observed per gastric gland (Karam et al. 1993d; Ramsey et al. 2007). The transcription factor, XBP1, is

required for establishment of the rER and termination of the mucous neck cell vesicles (Huh et al. 2010). Accordingly, without XBP1 expression, cells retain mucous neck cell markers and thus do not fully differentiate into chief cells. XBP1 also induces expression of the chief cell specific transcription factor, MIST1 (Huh et al. 2010). MIST1 is involved in the expansion of the apical membrane and generation of secretory vesicles (Ramsey et al. 2007). While XBP1 is required for chief cells to differentiate from mucous neck cells, MIST1 is necessary for chief cells to fully mature as they migrate to the base of the gland. When MIST1 expression is lost, chief cells still cease expression of mucous neck cell markers (GSII lectin) but retain fewer and smaller zymogen vesicles as well as have defects in apical expansion (Ramsey et al. 2007). Thus, without MIST1, chief cells cannot maintain their secretory machinery and do not fully mature.

Disruptions in the homeostasis of these lineages are associated with the metaplastic process in the stomach. Metaplasias and gastric malignancies are associated with *Helicobacter* infections (Blaser et al. 1994b; Correa et al. 2010). *Helicobacter* infections result in oxytnic atrophy (parietal cell loss) and a prominent inflammatory response. In humans, two types of metaplasias arise: spasmolytic polypeptide expressing metaplasia (SPEM) and intestinal metaplasia (Correa 1988; Schmidt et al. 1999). Recent studies have shown that SPEM develops initially and then gives rise to intestinal metaplasia (Yoshizawa et al. 2007; Goldenring et al. 2010). *Helicobacter* infected mice develop SPEM after 6 months of infection and progress to dysplasia after 12 months (Wang et al. 2000; Houghton et al. 2004b). However, the mice do not develop phenotypic intestinal metaplasia (no goblet cells are present). Instead, in the presence of chronic inflammation, SPEM evolves to a more proliferative and advanced state designated

"SPEM with intestinal characteristics" (SPEM-IC) (Weis et al. 2013). SPEM-IC expresses intestinal transcripts and appears to be the mouse analog to intestinal metaplasia in humans (Weis et al. 2013). However, the mechanisms involved in this metaplastic progression are unclear.

Our lab has developed two acute SPEM induction models in animals to analyze the initiation of SPEM in the absence or presence of inflammation. Administration of the protonophore, DMP-777, results in parietal cell loss without an inflammatory response, presumably because DMP-777 inhibits elastase (Nomura et al. 2005b). After 14 days of treatment, two zones of mucous cells appear: mucous neck cell hyperplasia (GSII lectin expression) and SPEM that has transdifferentiated from chief cells (GSII lectin and intrinsic factor expression) (Nam et al. 2010). This model demonstrates that loss of parietal cells is sufficient for SPEM induction. However, DMP-777 induced SPEM never progresses to dysplasia, even after a year of administration (Goldenring et al. 2000). Taken together, the DMP-777 and *Helicobacter* (*H. felis*) SPEM models demonstrate the necessity of inflammation for progression to dysplasia. However, the lengthy time (at least 6 months) required for *H. felis* to induce SPEM is prohibitive to studying SPEM in the presence of inflammation in multiple mouse models. Our lab has characterized an acute SPEM model with a prominent inflammatory response (Nam et al. 2010). Administration of L635, a DMP-777 analog that lacks elastase inhibition, induces chief cell transdifferentiation into SPEM accompanied by prominent inflammation in three days. L635 induced SPEM expresses some intestinal transcripts, such as *Cftr* and *Dmbt1*, at levels similar to 6 month *H. felis* induced SPEM (Weis et al. 2013). Furthermore, L635 induced SPEM exhibits increased proliferation, resembling *H. felis* induced SPEM (Nam

et al. 2010). This demonstrates a more advanced SPEM induction by L635 over DMP-777. These two acute SPEM models, DMP-777 and L635 administration, can be used to efficiently investigate the initiation and progression of SPEM.

Chronic inflammation has been shown to be an important extrinsic signal in the metaplastic progression of the stomach. Investigations of *Helicobacter* infections have determined elevations of inflammatory cytokines (Nam et al. 2010; Quiding-Jarbrink et al. 2010); however the complex signaling networks as well as the individual effects of these cytokines is unclear. Among chronic inflammation induced SPEM models, such as *Helicobacter* infection or *Hip1r* null mice, currently only the pro-inflammatory cytokine interferon-γ (IFNγ) has been shown to be necessary for the induction of SPEM (Yamamoto et al. 2004; Tu et al. 2011; Liu et al. 2012). Additionally, investigations of normal gastric homeostasis regulators have failed to identify the necessity of a specific gene for the development of SPEM (Mulder et al. 1991; Nomura et al. 2005b; Ogawa et al. 2006; Nam et al. 2007). All of these studies (including the study detailed in Appendix B) focus on the necessity of extrinsic signals and factors that act upon 'passive' chief cells for transdifferentiation into SPEM. However, studies of the required native intrinsic mechanisms and gene expression of the chief cell for SPEM induction are severely lacking. Here, we suggest a more active role for chief cells through an intrinsic secretory contribution to the complex signaling involved in the metaplastic progression of the stomach.

As *Mist1* is necessary for the development of fully mature chief cells, in this study, *Mist1* null mice are used to investigate the necessity of mature chief cells with fully established secretory machinery for the initiation of SPEM. DMP-777 and L635 were

administered to *Mist1* null mice and control mice. DMP-777 treated *Mist1* null mice exhibited an increase in GSII lectin and intrinsic factor (GIF) dual positive cells. These cells resembled 'neck to chief' transition cells found in the normal stomach. However, focal areas displayed some characteristics of SPEM, such as a small increase in proliferating GSII lectin and GIF dual positive cells. Significant parietal cell loss and inflammation occurred with L635 administration of *Mist1* null mice, similar to L635 treated control mice. Proliferation in L635 treated *Mist1* null mice was similar to DMP-777 treatment of null mice in both quantity and localization. No increase in GSII lectin and GIF co-positive cells was found in the L635 treated *Mist1* null mice. Instead, the majority of glands in L635 treated *Mist1* null mice retain chief cells along the base of the glands, indicating that *Mist1* null mice do not develop SPEM from parietal cell loss or inflammation as readily as control mice.

Methods

Mice

C57BL/6 mice obtained from Jackson Laboratories (Bar Harbor, ME) were used as controls. *Mist1* null mice were maintained on a C57BL/6 background. During the experiments, the mice were maintained with regular mouse chow and water *ad libitum* in a temperature-controlled room under a 12-hour light/dark cycle. The care, maintenance, and treatment of animals in these studies followed protocols approved by the Institutional Animal Care and Use Committee of Vanderbilt University.

Drug Administration

DMP-777, a gift from DuPont Pharmaceuticals (Wilmington, DE), was formulated in 0.5% methylcellulose and administered orally as a gavage once daily at 350 mg/kg/day. Control mice (n=3) and and *Mist1* null mice (n=5) were treated for 14 consecutive days. L635, dissolved in saline and orally administered as a gavage once daily at 350 mg/kg/day, was a gift from Merck & Co, Inc (Rahway, NJ). Control mice (n=3) and *Mist1* null mice (n=3) were treated for three consecutive days.

Immunofluorescence

Excised stomachs from mice were fixed in 4% paraformaldehyde overnight and embedded in paraffin. Sections were heated at 60°C for 30 minutes and then cooled to room temperature for 30 minutes. Tissue was deparaffinized and rehydrated. Antigen retrieval was performed using Target Retrieval solution (DakoCytomation, Glostrup, Denmark). Slides were blocked using protein block serum-free (DakoCytomation) for one hour at room temperature. Immunostaining was performed using the following primary antibodies incubated at 4°C overnight: goat anti-intrinsic factor (1:1000, a gift from Dr David Alpers, Washington University, St. Louis, Missouri, USA) and rat immunoglobulin G (IgG) anti-Ki-67 (1:50, Dako). Detection was performed using fluorescent secondaries or fluorescent conjugated GSII lectin (Molecular Probes, Eugene, OR) for 1 hour at room temperature. Slides were mounted with ProLong Gold Antifade Reagent with DAPI (Invitrogen). Sections were analyzed using Zeiss Axiophot microscope equipped with an Axiovision digital imaging system (Zeiss, Jena GmBH, Germany) or using the Ariol SL-50 automated slide scanner (Genetix, San Jose, CA). Quantification of the average number of cells immunostaining for Ki67, GSII lectin, and

intrinsic factor per gland was done by manual counts. All counted cells had nuclei as detected by DAPI. The number of dual positive cells (Ki67 and GSII lectin or GSII lectin and intrinsic factor) was counted only in well oriented glands in which the entire length of the gland was visible and void of any tangential cross sectioning. On average, five glands were counted from one representative mouse in each sample group. Due to the complexity of the calculations, the counts presented in this study are representative quantifications of the observations made from multiple mice in each group.

Results

Acute SPEM induction in the absence of inflammation in Mist1 null mice

DMP-777, a protonophore with elastase inhibition, was administered by oral gavage to control mice and *Mist1* null mice for 14 days. Parietal cell loss and presence of the various gastric cell lineages was analyzed by PAS staining. In PAS stained sections of untreated control mice, parietal cells are light pink, chief cells are blue, and mucous neck cells are a dark magenta color (data not shown). SPEM cells also stain as a dark magenta color similar to mucous neck cells, though SPEM cells are predominately located at the base of glands in regions of parietal cell loss. The patterning of cells in untreated *Mist1* null mice differs slightly from control mice. As previously reported (Ramsey et al. 2007), *Mist1* null mice have a small increase in transition cells (mucous neck to chief cells), an increase of parietal cells localized near the base, and aberrant chief cell structure. However, the cell types stain the same as control mice by PAS (Figure 29). Control mice treated with DMP-777 had significant parietal cell loss (Figure 29). Loss of blue stained chief cells from the base of glands can also be seen. The chief cells are replaced with

magenta colored cells at the base of the glands, indicative of SPEM cells (Figure 29). Previous reports have shown these as SPEM cells derived from transdifferentiated chief cells (Nam et al. 2010). DMP-777 treatment of *Mist1* null mice also results in a reduction of parietal cells as compared to untreated control and *Mist1* null mice. However, fewer parietal cells are lost in treated *Mist1* null mice as compared to treated control mice (Figure 29). The amount of parietal cell loss varied throughout the fundus of *Mist1* null mice, suggesting a more focal effect of DMP-777. Mucous neck cells increase in number and extend further down the gland, although not to the base. Furthermore, while the number of chief cells decreases, treated *Mist1* null mice still retain some chief cells at the base of most glands in the fundus, suggesting a failure of fully induced SPEM (Figure 29).

Quantification of the cell lineages throughout the fundus of control and *Mist1* null mice was performed to show differences of the lineages between treated and untreated mice. Although at least 3 mice from each group were manually examined, counts represented here are from one representative mouse from each group. GSII lectin (mucous neck cell and SPEM marker) and intrinsic factor (GIF) were utilized to examine the cell lineages in the fundus of control and *Mist1* null mice. GSII lectin labels mucous neck cells and SPEM cells, while GIF is a chief cell specific marker that persists in early SPEM lesions. In untreated control mice, as mucous neck cells migrate towards the base of glands, they quickly switch from expression of mucins (detected by GSII lectin) to GIF expression during transdifferentiation into chief cells (Figure 30). Approximately two transition cells that co-express mucous neck cell and chief cell markers can be found in a normal gastric gland. GIF expression continues to increase as the chief cells mature towards the base (Figure 30). As previously reported (Ramsey et al. 2007), *Mist1* null

mice have an increase in transition cells (5-6 per gland) corresponding to a delay in transdifferentiation to chief cells (Figure 30). Furthermore, emerging from the transition zone, chief cells have a sudden decrease in GIF expression (Figure 30) (Ramsey et al. 2007). This loss of expression is due to the inability of chief cells to establish the secretory machinery in the absence of MIST1 (Ramsey et al. 2007).

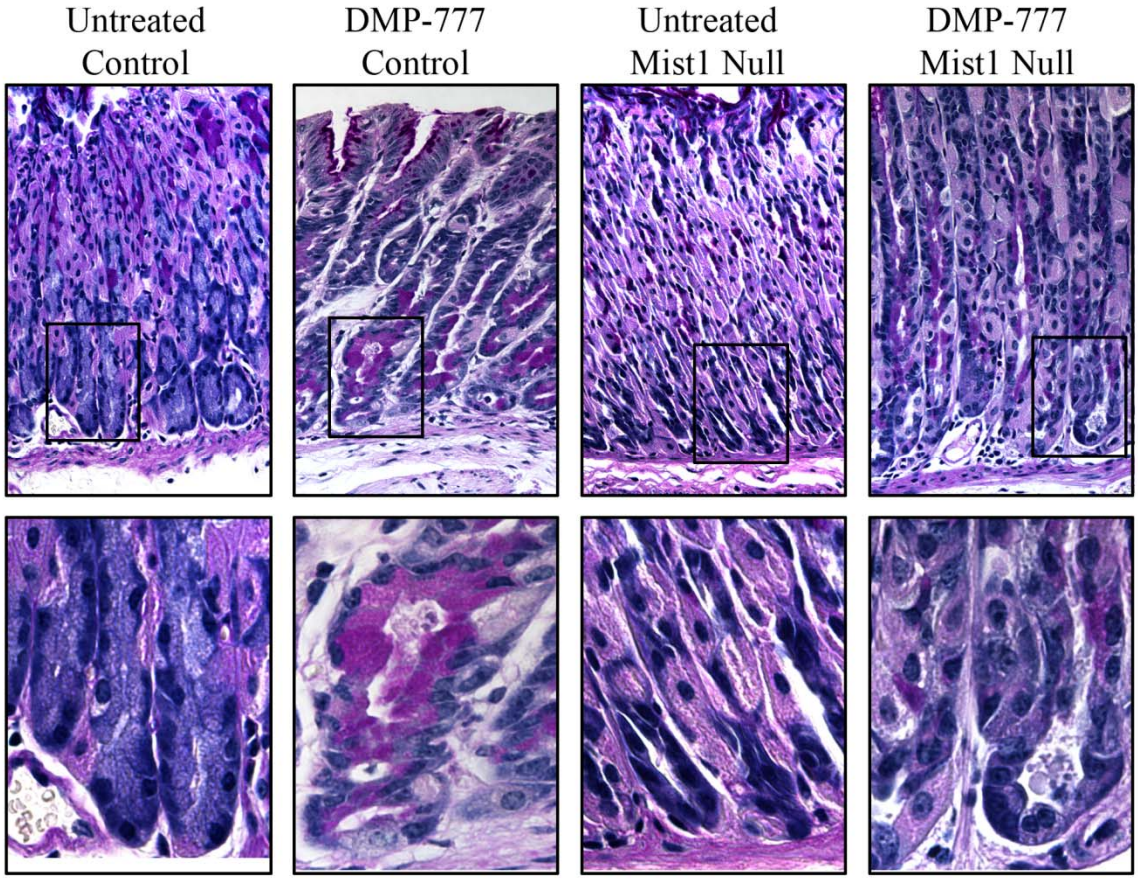

Figure 29. PAS staining of untreated and DMP-777 treated control and *Mist1* null mice. DMP-777 was administered to control mice and *Mist1* null mice for 14 days to induce SPEM. Images in top row were taken with a 20X objective. Black box highlights area imaged with 40X objective for the bottom row. DMP-777 treatment in control mice causes significant parietal cell loss. Magenta colored SPEM cells replace the blue stained chief cells at the base of glands. While magenta staining is extended closer to the base in *Mist1* null mice, small blue stained chief cells remain at the base of glands.

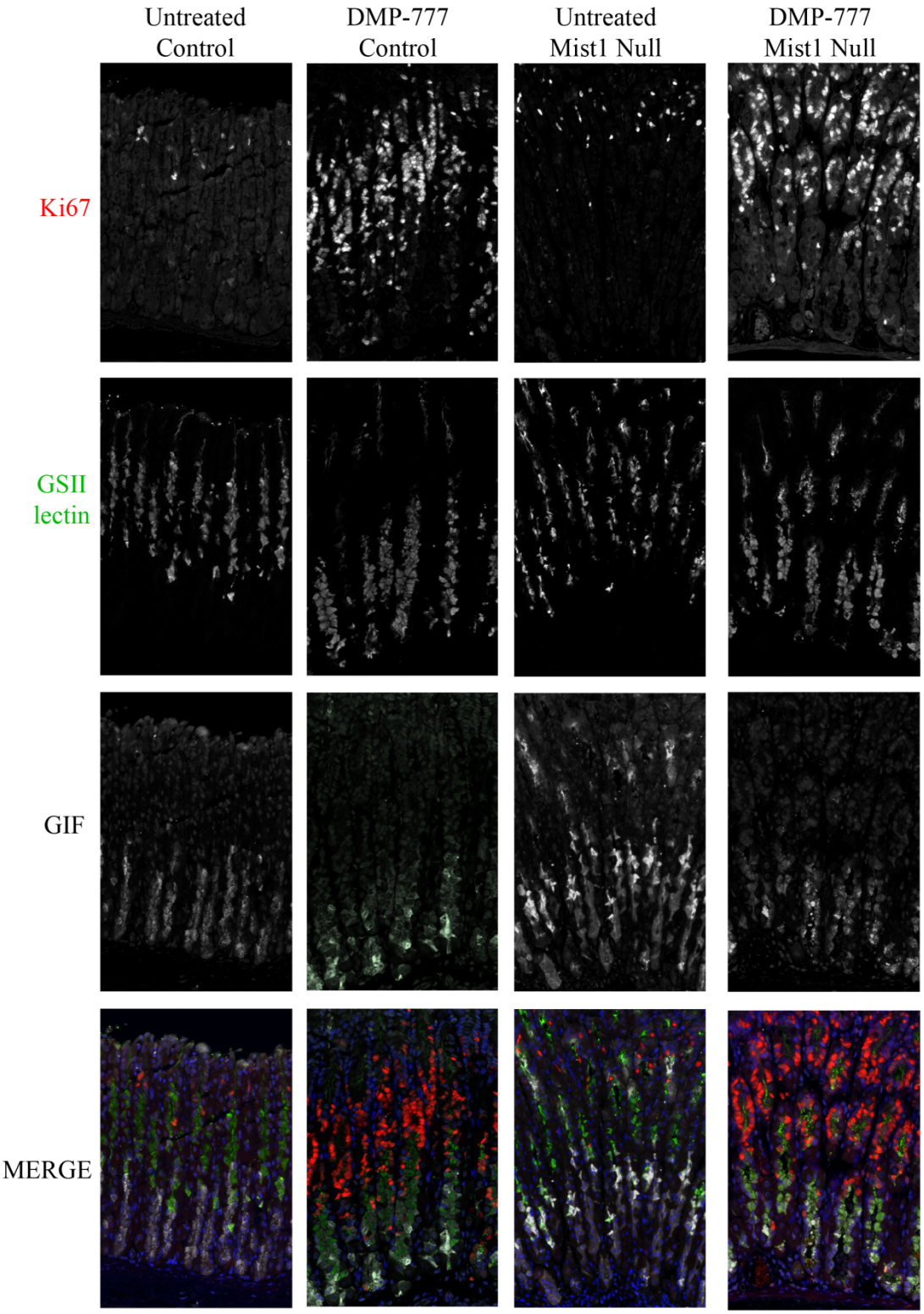
Untreated Control
DMP-777 Control
Untreated Mist1 Null
DMP-777 Mist1 Null
Ki67
GSII lectin
GIF
MERGE

Figure 30. Proliferation of SPEM (GSII lectin positive) cells after DMP-777 administration. Sections were immunostained for Ki67, GSII lectin, and GIF. For GIF images, the exposure was equal in all captured images. Untreated controls and *Mist1* null mice have low levels of proliferation localized only to the progenitor region and distinct separate regions of GSII lectin and GIF immunolabeling. DMP-777 treated control mice have an increase in the number of GSII lectin and GIF dual positive cells at the base of glands representing the induction of SPEM. Moreover, these mice had an increase in proliferation that was predominately located in the mucous neck cell hyperplasia (GSII lectin positive cells in the middle of the glands). However, occasional triple positive cells can be found at the base of glands. DMP-777 treated *Mist1* null mice have a similar expression pattern as the DMP-777 treated control mice. Of note, GIF expression levels at the base of glands in DMP-777 treated *Mist1* null mice appear higher than found in DMP-777 treated control mice and thus more closely resemble transition cells (GSII lectin and GIF dual positive cells) in the untreated *Mist1* null mouse. DAPI (blue).

DMP-777 administration to control mice results in an increase of GSII lectin and GIF co-labeling cells at the base of glands (Figure 30). When chief cells transdifferentiate into SPEM, they begin to re-express mucous neck cell markers (Nozaki et al. 2008; Nam et al. 2010), accounting for the increase in dual positive cells (~3.5 fold increase). DMP-777 treated *Mist1* null mice also have an increase in co-expressing cells compared to untreated null mice (Figure 30). However, it is a smaller increase (~2.3 fold) than found in control mice treated with DMP-777. Additionally, the co-expressing cells in the DMP-777 treated *Mist1* null mice have high GIF expression, resembling the transition cells in untreated null mice (Figure 30). If these dual positive cells were SPEM cells from transdifferentiated *Mist1* null chief cells, they would presumably lack the machinery for such high GIF expression because lack of *Mist1* results in loss of high GIF in chief cells. These findings suggest *Mist1* null mice predominately have an accumulation of transition cells instead of the induction of SPEM in the setting of acute parietal cell loss.

Another characteristic of the induction of SPEM is an increase in proliferation of GSII lectin positive cells. Tissue was immunostained for Ki67 (proliferation), GSII lectin

(mucous neck cell and SPEM), and GIF (chief cell and early SPEM lesions). Untreated control mice had less than one Ki67 and GSII dual positive cell per gland (Figure 30). When present, the co-positive cell was located at the junction of the progenitor and neck zone. Thus, this dual labeling cell is an emerging immature mucous neck cell. Upon the induction of DMP-777 induced SPEM, there is a 22.1 fold increase of proliferating GSII lectin labeled cells (Figure 30). This increase appears to predominately come from the mucous neck cell hyperplasia zone of DMP-777 treated glands (GSII lectin positive, GIF negative). However, there is also an increase in GSII lectin positive SPEM cells at the base that label with Ki67 (Figure 30). Similarly to control mice, untreated *Mist1* null mice have approximately one proliferating immature mucous neck cell per gland. Conversely, Ki67 and GSII lectin dual positive cells only increase 5.2 fold in DMP-777 treated *Mist1* null mice. While SPEM cells at the base of glands (GSII lectin and GIF positive) have a small increase in proliferation, this increase is again mainly in the mucous neck cell hyperplasia (Figure 30). Although further spatial quantification of GSII lectin and Ki67 labeling is needed, the increase in number of dual positive cells between untreated and DMP-777 treated is considerably less in *Mist1* null mice than in control mice. Together, these findings suggest *Mist1* null mice are resistant to the development of SPEM.

Effects of parietal cell loss and prominent inflammation in Mist1 null mice

Loss of *Mist1* appears to impede the induction of SPEM initiated by the loss of parietal cells in the absence of inflammation. Previous studies have shown L635 administration, a DMP-777 analog without elastase inhibition, induces parietal cell loss accompanied by a prominent inflammatory response. SPEM derived from L635 treatment

for only three days expresses some intestinal transcripts, suggesting that it is a more advanced SPEM subtype (also called SPEM-IC). Therefore, control and *Mist1* null mice were treated with L635 for three days to investigate the induction of SPEM or SPEM-IC in *Mist1* null mice in the presence of inflammation. As seen by PAS staining, L635 treated control mice have significant parietal cell loss with a prominent inflammation response (Figure 31). The normal gastric cell lineages are replaced with SPEM cells transdifferentiated from chief cells (Nam et al. 2010). In contrast to DMP-777 induced SPEM, the entire region below the progenitor zone is composed of SPEM cells in L635 treated mice (Nam et al. 2010). *Mist1* null mice treated with L635 also show significant parietal cell loss and inflammation (Figure 31). However, prominent magenta staining at the base of the glands, indicative of SPEM, was not seen; instead, small blue stained cells resembling chief cells were present (Figure 31).

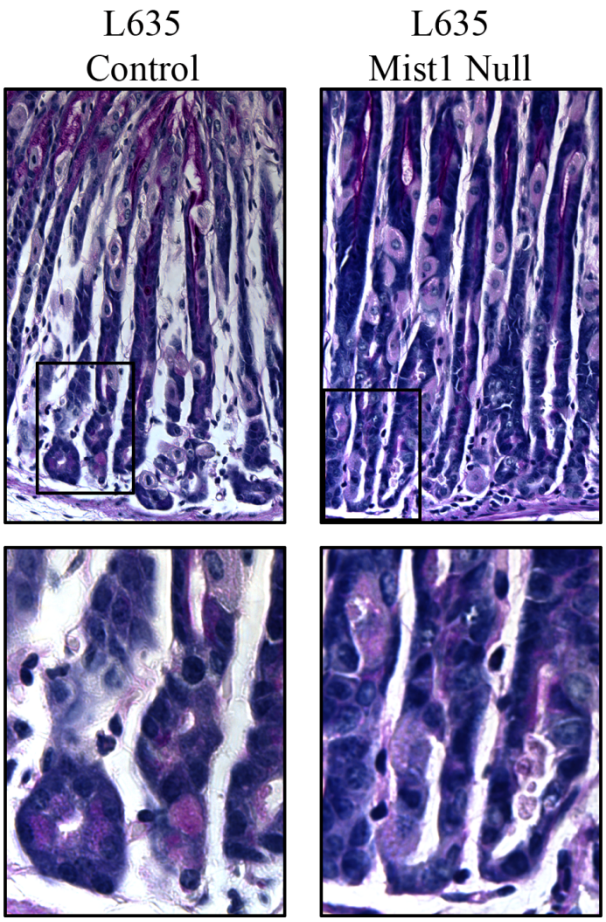

Figure 31. PAS staining of L635 treated control and *Mist1* null mice. L635 was administered to control mice and *Mist1* null mice for three days to induce SPEM. Images in top row were taken with a 20X objective. Black box highlights area imaged with 40X objective for the bottom row. L635 administration caused significant parietal cell loss in both control and *Mist1* null mice. Magenta colored SPEM cells replace the blue stained chief cells at the base of glands. Note that L635 induced SPEM cells do not stain as bright magenta as DMP-777 induced SPEM cells. However in *Mist1* null mice, small blue stained chief cells were still found at the base of glands, suggesting a failure to transdifferentiate into SPEM. PAS staining of untreated control and *Mist1* null mice is previously shown in Figure 29.

The cell lineages in L635 treated control and *Mist1* null mice were then analyzed by immunostaining for GSII lectin and GIF. In L635 treated control mice, GSII immunolabeling extends to the base of glands. L635 induced SPEM is completely

comprised from transdifferentiated chief cells (Nam et al. 2010). GIF expression is significantly decreased and then lost from the SPEM cells due to the advanced stage of L635 induced SPEM (Figure 32). Even with this rapid GIF loss, L635 treated control mice have a 2.98 fold increase in GSII lectin and GIF dual positive cells (Figure 32). Conversely, although L635 treated *Mist1* null mice also have a significant decrease in parietal cells, GSII lectin is not found at the base of all glands in the fundus, and GIF expression is still found at the base (Figure 32). In fact, it appears there are fewer glands with GSII lectin at the base in L635 treated *Mist1* null mice than null mice treated with DMP-777. Quantification verified no change in GSII lectin and GIF dual positive cells between untreated and L635 treated *Mist1* null mice. The short time course of treatment (3 days) may account for the lack of a change in co-positive cells in L635 treated *Mist1* null mice as compared to DMP-777 treated null mice.

L635 induced SPEM in control mice displays a 16.2 fold increase in proliferation of the GSII lectin positive SPEM cells as seen by Ki67 immunostaining (Figure 32). In contrast to DMP-777 induced SPEM, proliferation is seen throughout the entire length of L635 induced SPEM glands in control mice (Figure 32). *Mist1* null mice also have an increase in proliferation when treated with L635. While there is a small increase in proliferation of GSII lectin and GIF dual positive cells, the majority of the 4.7 fold increase is in the upper GSII lectin positive cells similar to DMP-777 induced proliferation (Figure 32). These findings suggest the presence of inflammation during parietal cell loss does not exacerbate SPEM induction or progression to SPEM-IC in *Mist1* null mice.

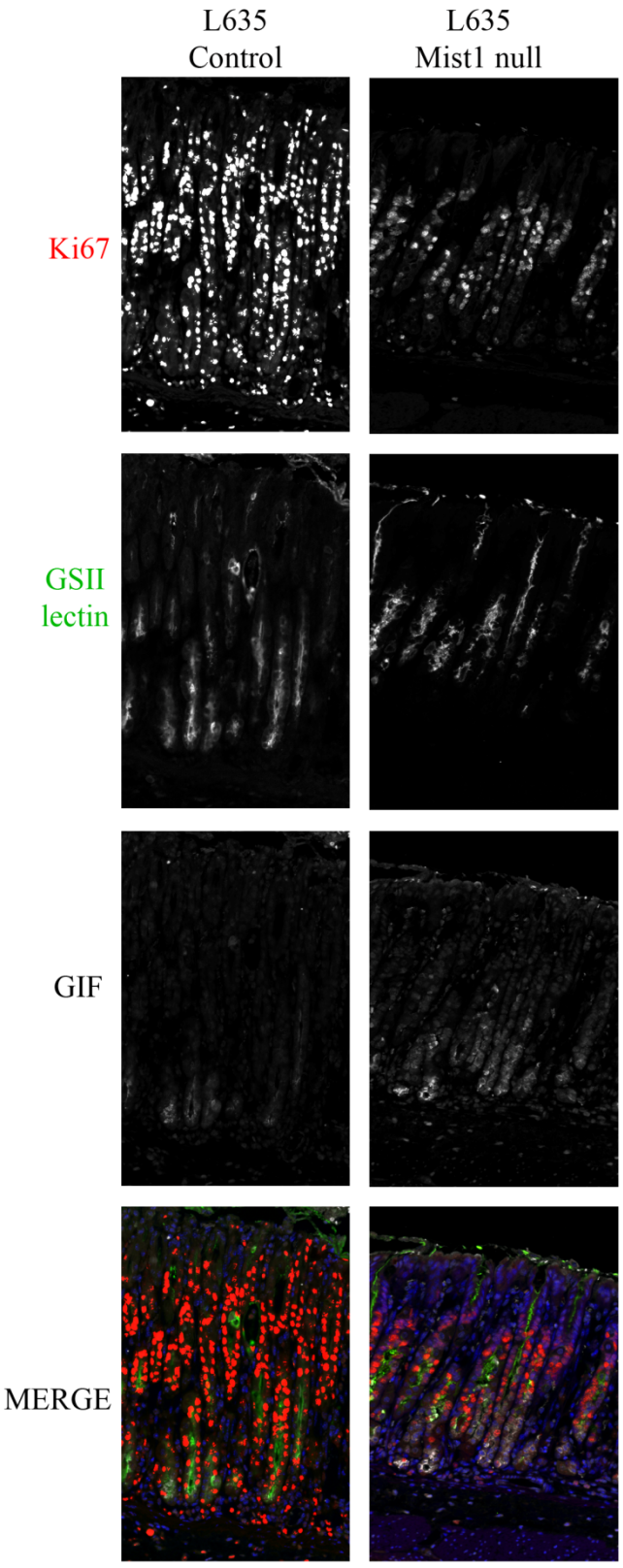
L635
Control
L635
Mist1 null
Ki67
GSII
lectin
GIF
MERGE

Figure 32. Proliferation of L635 induced SPEM (GSII lectin positive) cells. Sections were immunostained for Ki67, GSII lectin, and GIF. For GIF images, the exposure was the same in all captured images. Untreated controls and *Mist1* null mice are previously shown in Figure 30. L635 administration induces a proliferative SPEM lineage in control mice. As seen in the first column, proliferation is seen throughout the length of the SPEM glands. While L635 treated *Mist1* null mice also had an increase in proliferation, these cells were predominately localized in the upper regions of GSII lectin staining. Occasional triple positive cells were also observed. Additionally, the number of GSII lectin and GIF dual positive cells did not change in L635 treated *Mist1* null mice as compared to untreated null mice. DAPI (blue).

Discussion

Disruption of the homeostasis of the stomach leads to changes in the cell lineages in the glands. Loss of the acid-secreting parietal cells results in chief cell transdifferentiation into SPEM cells (Nomura et al. 2005b; Nozaki et al. 2008; Nam et al. 2010). The presence of inflammation during oxyntic atrophy advances SPEM to SPEM with intestinal characteristics (SPEM-IC) ,which is the mouse analog of the progression of SPEM to intestinal metaplasia in humans (Weis et al. 2013). Because SPEM gives rise to intestinal metaplasia in the progression to gastric cancer in humans, SPEM is considered a preneoplastic lesion (Goldenring et al. 2010). However, the mechanisms necessary for this metaplastic progression are unclear. Several studies have attempted to elucidate factors involved; however, most have focused on the role of extrinsic influences such as immune cells and other signaling molecules (Mulder et al. 1991; Nomura et al. 2005b; Ogawa et al. 2006; Nam et al. 2007; Tu et al. 2011). While these studies broaden our understanding of the complex networks in the progression to SPEM, the involvement of the native intrinsic chief cell mechanisms and gene expression are unknown. In this

study, we have investigated the necessity of mature chief cells with properly functioning secretory machinery.

Chief cells in *Mist1* null mice fail to establish their secretory machinery resulting in immature chief cells that have decreased GIF and pepsinogen expression (Ramsey et al. 2007). Initially, one may expect *Mist1* null mice to develop SPEM faster, as aberrant chief cells may more readily transdifferentiate into reparative SPEM cells. However from the studies presented here, *Mist1* null mice display a decrease in SPEM induction potential (Figure 33). Distinguishing between 'neck to chief' transition cells and SPEM cells is difficult because they both co-label with GSII lectin and GIF (Ramsey et al. 2007; Nozaki et al. 2008). For this reason, we also examined proliferation of GSII lectin positive cells because transition cells have not been shown to proliferate (Karam et al. 1993d; Ramsey et al. 2007). DMP-777 treatment of null mice did increase the number of proliferating GSII lectin positive cells as well as cells co-labeled with GSII lectin and GIF. The majority of the proliferating cells were located in the mucous neck cell hyperplasia region of GSII lectin labeling. Furthermore, the GIF expression levels in the dual positive cells (GSII lectin and GIF) resembled the levels found in the 'neck to chief' transition cells found in untreated *Mist1* null mice. If *Mist1* null chief cells at the base of glands differentiated into SPEM, the cells would presumably lack the secretory machinery for such levels of GIF expression. Additionally, because GIF decreases and is eventually lost in SPEM, there is no rationale for the cells to setup the necessary secretory machinery through alternative pathways. There are two explanations for the potential origin of these cells. The reduction of parietal cells may cause a failure of 'neck to chief' transition cells to completely differentiate into chief cells, thus resulting in an

accumulation of transition cells that express mucous neck cell markers (GSII lectin) and chief cell markers (GIF). However, triple positive cells (Ki67, GSII lectin, and GIF) can still be found at the base of glands, demonstrating that SPEM is capable of developing in *Mist1* null mice, albeit to a lesser degree. A second possibility is that only a subset of chief cells in the *Mist1* null mouse has the ability to transdifferentiate into SPEM. The newly differentiated chief cell just emerging from the transition zone (before it has lost its secretory abilities) may give rise to the proliferating SPEM cells found in DMP-777 treated null mice. Overall, our data shows *Mist1* null mice are capable of developing SPEM but not as readily as control mice.

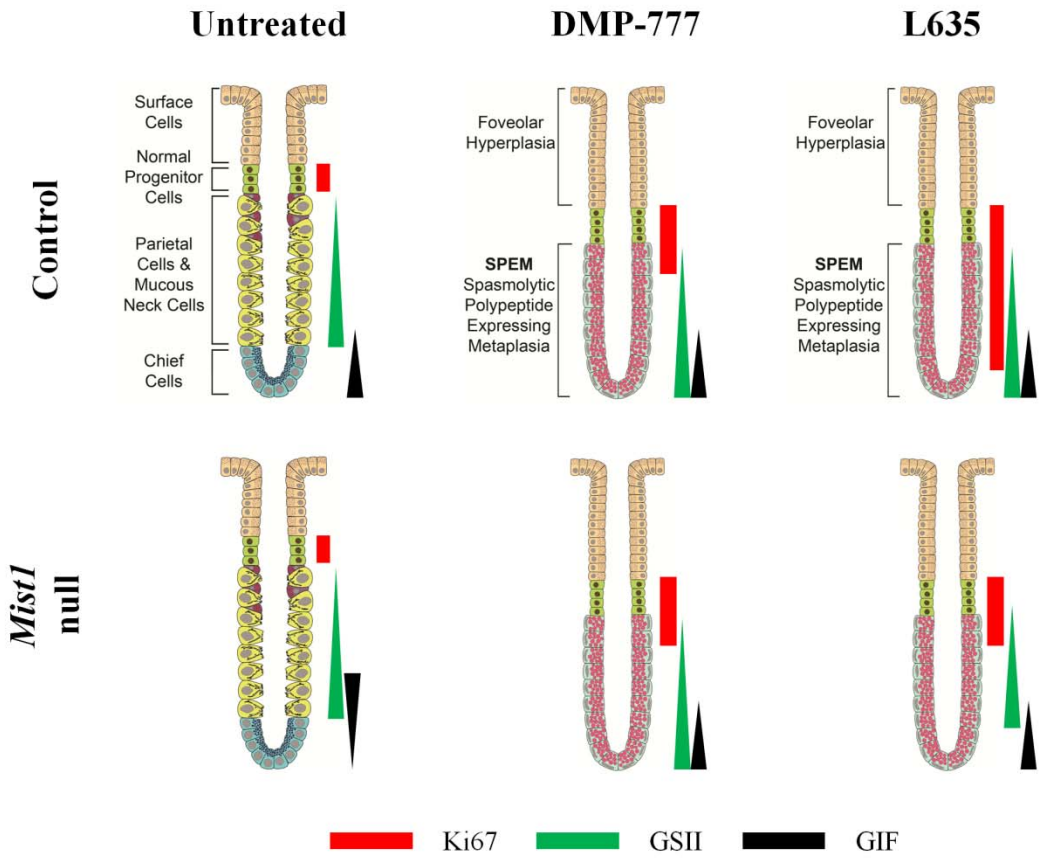

Figure 33. Diagram of expression patterns in untreated and treated control mice and *Mist1* null mice. This model depicts the staining pattern for Ki67 (red), GSII lectin (green), and GIF (black). DMP-777 and L635 treated *Mist1* null glands are depicted with a SPEM gland only to show a loss of parietal cells (not the induction of SPEM). DMP-777 treated control mice have increased proliferation in the mucous neck cell hyperplasia region while dual labeled SPEM cells (GSII lectin and GIF) are present at the base of the glands. Proliferation is seen in SPEM cells throughout the length of the gland in L635 treated control mice. In *Mist1* null mice treated with DMP-777, proliferation is increased the upper GSII lectin region. Dual positive cells (GSII lectin and GIF) that resemble transition cells found in the untreated *Mist1* null mouse are found at the base of the glands. L635 administration to *Mist1* null mice results in an increase proliferation similar to that seen in DMP-77 treatment. Furthermore, there was no change in the number of dual positive cells (GSII lectin and GIF).

Parietal cell loss in the presence of inflammation can induce a more proliferative and advanced SPEM in only three days (Nam et al. 2010; Weis et al. 2013). L635 was

administered to *Mist1* null mice to determine if the additional stimulus of inflammation accompanied with parietal cell loss could induce SPEM or SPEM-IC. Administration of L635 in null mice increased the number of proliferating GSII lectin positive cells but not GSII lectin and GIF dual positive cells. Additionally, many glands retained distinct separation of GSII lectin labeled neck cells and GIF expressing chief cells. While proliferating GSII lectin and GIF positive cells towards the base of glands could be seen, proliferation in L635 treated null mice was predominately observed in the upper GSII lectin positive region, similar to DMP-777 treatment. It is possible that the proliferating GSII lectin labeled cells in the upper neck region represents mucous neck cell hyperplasia as seen in DMP-777 treated mice. Overall, parietal cell loss by either drug induced a similar level and localization of proliferation in null mice, but it appears that dual positive (GSII lectin and GIF) cells do not increase after only three days of parietal cell loss even under the influence of inflammation. Even if only a subset of chief cells is capable of transdifferentiation, more SPEM cells (labeled by GSII lectin and GIF) would be expected from L635 treatment because of the influence of inflammation. This data further supports that the increase of dual positive cells in DMP-777 treated null mice may predominately arise from an accumulation of transition cells that fail to become chief cells instead of chief cells transdifferentiating into SPEM. Thus, our data suggests *Mist1* null mice are resistant to developing SPEM. However, when parietal cells are lost, a small subset of newly differentiated chief cells may become SPEM. After three days, even in the presence of inflammation, the majority of chief cells remain unchanged, suggesting that the loss of chief cells after 14 days of parietal cell loss is replaced by an accumulation of transition cells.

The studies presented here focus on the necessary intrinsic properties and characteristics of chief cells for SPEM induction. Without *Mist1*, chief cells cannot properly maintain their secretory machinery. The current investigations show *Mist1* null mice are resistant to SPEM induction. Because *Mist1* is exclusively expressed in chief cells in the stomach, this resistance is solely due to their defects. Of note, *Mist1* is also expressed in mature plasma cells, however recent studies have shown loss of *Mist1* does not cause defects in these cells (Capoccia et al. 2011). The prevailing assertion of studies in the stomach literature is that the signaling networks from other cell types (e.g. immune and parietal cells) are the driving force of the metaplastic progression and chief cells are merely passive participants. However, *Mist1* null mice with aberrant maturation and secretion are resistant to SPEM induction suggesting that normal chief cells secrete signals to help coordinate the transition to SPEM. Overall, these studies demonstrate the first intrinsic characteristic of chief cells necessary for the induction of SPEM. Furthermore, chief cells are not purely passive participates but instead contribute to the complex signaling involved in the metaplastic progression of the stomach.

CHAPTER V

CONCLUSIONS AND FUTURE DIRECTIONS

Conclusions

Aberrations of gastric homeostasis are associated with various gastric diseases, such as ulcers and adenocarcinomas. *Helicobacter pylori* (*H. pylori*) infections are a common cause of these aberrations in humans (Blaser et al. 1994b; Correa et al. 2010). Chronic inflammation and loss of the acid-secreting parietal cells (oxyntic atrophy) results from *H. pylori* infections. Without the differentiation signaling pathways from the parietal cells, chief cells transdifferentiate into SPEM, possibly as a localized repair mechanism (Nomura et al. 2004a; Nomura et al. 2004c; Nozaki et al. 2008; Nam et al. 2010). However, under chronic inflammatory influences, SPEM gives rise to intestinal metaplasia (Yoshizawa et al. 2007; Goldenring et al. 2010). In this milieu, gastric adenocarcinomas can develop. Similar to humans, *Helicobacter* infections in mice lead to oxyntic atrophy with a prominent inflammatory response, and SPEM develops after six months of infection (Wang et al. 2000; Houghton et al. 2004b). Phenotypic intestinal metaplasia does not develop in mice; instead, SPEM progresses directly to dysplasia after 12 months of infection (Wang et al. 2000; Houghton et al. 2004b). Previous studies comparing expression profiles of normal chief cells and *Helicobacter* induced SPEM have identified upregulated genes (Nomura et al. 2004b; Nam et al. 2010; Quiding-Jarbrink et al. 2010). Other manipulations of gastric homeostasis, such as disruptions of the EGFR signaling pathway and drug induced oxyntic atrophy can also cause SPEM (Goldenring et al. 2000; Nomura et al. 2004c; Nam et al. 2010). However, the

mechanisms involved in the development of SPEM are unclear. The work presented here has lead to novel discoveries and tools that have expanded our understanding of SPEM. Investigations into both the heterogeneity of SPEM lineages and *Mist1* null mice have led to a new model of metaplastic progression in the mouse as well as the novel concept that chief cells are active participants that require secretory machinery for transdifferentiation into SPEM. Additionally, novel *in vitro* chief cell and SPEM cell models were developed and now provide necessary tools to elucidate molecular mechanisms of chief cells and SPEM. These studies have also revealed novel metaplasia markers.

Heterogeneity of phenotypic SPEM lineages

Differing expression patterns and characteristics have been reported for SPEM lineages from different settings(Weis et al. 2013). These differences have confounded our understanding of SPEM induction. In the first study presented here, three models of SPEM induction (DMP-777 administration, L635 administration, and *H. felis* infection) were chosen for transcription expression analysis. These three distinct models were chosen based on their distinct characteristics, such as length of treatment (acute versus chronic) and progression to dysplasia (presence versus absence of inflammation). DMP-777 treatment initiates SPEM in only 14 days without inducing an inflammatory response. Acute SPEM accompanied by prominent inflammation is induced by L635 administration. Lastly, *H. felis* infection was utilized as a chronic SPEM induction method with chronic inflammation. Gene microarray analysis revealed an expression profile common to all SPEM lineages, as well as a profile specific to SPEM with inflammation, indicative of progression towards more advanced SPEM. Eight transcripts were upregulated in all SPEM lineages regardless of the surrounding milieu. A previously reported (Nozaki et al.

2008) SPEM marker, whey acidic protein 4-disulfide core domain 2 (*Wfdc2*, also known as *He4*), was found to be upregulated in all SPEM lineages. Clusterin (*Clu*) was also upregulated in all SPEM lineages. In normal gastric glands, CLU protein was expressed at low levels in the progenitor zone. Upon SPEM induction, CLU expression was upregulated in SPEM in all three murine models. In humans, upregulated CLU protein expression as compared to normal glands was found in SPEM (18/20) and intestinal metaplasia (5/11). In intestinal metaplasia, CLU labeled small cells near the SPEM to intestinal metaplasia transition. Clusterin expression was retained in 56.5% of gastric cancers (9/16 intestinal-type and 4/7 diffuse-type). Furthermore, highest expression of CLU (43-95% of epithelial cells positive for CLU) correlated with shorter survival time. Thus, the comparison of SPEM lineages identified a novel SPEM marker. Additionally, we compared SPEM developed in the presence of inflammation to normal chief cells. *Cftr* transcription was upregulated in L635 and *H. felis* induced SPEM. CFTR protein was expressed only in murine SPEM accompanied by inflammation. In humans, CFTR was expressed in intestinal metaplasia, but not SPEM. Moreover, intestinal associated transcripts, such as *Muc4*, *Vil1*, and *PigR* were upregulated in 12 month *H. felis* infected mice. These findings identified a more advanced SPEM that acquires intestinal transcripts, which could potentially progress to dysplasia. This lineage has been denoted SPEM-IC (SPEM with intestinal characteristics). Thus, this study has led to a shift in the metaplastic paradigm in the stomach. SPEM is induced upon parietal cell loss, but under the influence of chronic inflammation, SPEM progresses to SPEM-IC, which is a more advanced and proliferative metaplasia. Because dysplasia arises directly from SPEM in mice, SPEM-IC represents the mouse equivalent of intestinal metaplasia in humans. The

transcriptional profiles established in this study can now be utilized to better characterize the stage of SPEM lineages found in other murine metaplasia models. Furthermore, the categories of transcripts identified in these expressional comparisons provide putative factors for future investigations.

Establishment of in vitro models of chief cells and SPEM cells

While we, along with others, have identified putative factors and signaling pathways involved the induction and progression of SPEM (as described above)(Nomura et al. 2004a; Nozaki et al. 2008; Lee et al. 2010; Nam et al. 2010; Weis et al. 2013), mechanistic studies of their roles have been limited to the utilization of *in vivo* models. Previously, normal gastric chief cell or metaplasia cell lines did not exist. Most *in vitro* studies use human gastric cancer cell lines with inherent disadvantages or isolated primary cells that lack manipulation capabilities (such as overexpression) (Bredemeyer et al. 2009; Wei et al. 2010; Chaturvedi et al. 2011; Fujii et al. 2012; Noto et al. 2013). Utilizing the Immortomouse (Jat et al. 1991), we developed two cell lines to fill this deficit. A chief cell line, ImChief, was established and characterized. Immortomice were also treated with L635 to establish the SPEM cell line, ImSPEM. ImChief cells express all chief cell markers except intrinsic factor (*Gif*) and lack expression of all other gastric lineage markers. Pepsinogen C and RAB3D containing vesicles are produced in ImChief cells. At the non-permissive temperature, the number of these vesicles appears to increase and proliferation ceases, showing that ImChief cells become more differentiated. ImSPEM cells express the SPEM markers, *Tff2* and *He4*, but not other stomach specific lineage markers. TFF2 vesicles and HE4 vesicles are seen in ImSPEM cells. In fact, HE4 is apically secreted into the conditioned media of the cells, demonstrating that ImSPEM

cells establish secretory machinery that traffics to the specified apical membrane. Immunostaining of junctional markers (p120, E-CAD, and ZO1) validates the polarization of ImSPEM lines grown on transwells. Furthermore, ImSPEM cells form cystic structures with hollow centers when grown in Matrigel at the non-permissive temperature. Gene microarray comparison of ImChief and ImSPEM cells has revealed several genes putatively upregulated in SPEM. Protein expression of the third most increased transcript, *Mal2* (a transcytosis protein), was examined in tissue and the cell lines. MAL2 expression was increased in murine and human metaplasias of the stomach. 82% of intestinal type gastric cancers also expressed MAL2. MAL2 localized to the subapical region of SPEM cells in tissue. Additionally, MAL2 was localized to the subapical zone of ImSPEM cells. MAL2's known role in transcytosis may help elucidate trafficking mechanisms in SPEM. Overall, both ImChief and ImSPEM exhibit characteristics of their respective *in vivo* counterparts and thus are indispensible *in vitro* models. These cell lines can be utilized for a multitude of studies, such as: chief cell homeostasis, roles of extrinsic factors in the metaplastic progression, or molecular mechanisms of SPEM, such as vesicular trafficking.

Loss of Mist1 impedes SPEM induction

Culture of ImChief cells has already led to a new route of investigation in SPEM induction. Although loss of parietal cells in the mouse is sufficient to induce SPEM, ImChief cells removed from their niche (and associated signals from parietal cells) do not readily transdifferentiate into SPEM in culture. During analysis of transcriptional expression of ImChief cells, low expression of the transcription factor *Mist1* was observed. We hypothesized that this low expression resulted in immature chief cells as

previously reported in *Mist1* null mice (Ramsey et al. 2007) and that mature chief cells were necessary for transdifferentiation into SPEM. To test this theory, *Mist1* null mice were treated with DMP-777 or L635. Null mice treated with DMP-777 had an increase in proliferating GSII lectin positive cells as well as GSII lectin and GIF dual positive cells. The proliferating GSII lectin cells predominately localized to the mucous neck cell hyperplasia zone, although proliferating GSII lectin and GIF co-labeled cells were occasionally observed at the base of glands. The majority of GSII lectin and GIF dual positive cells found at the base of the glands resembled 'neck to chief' transition cells found in untreated mice. L635 treatment of null mice also increases proliferating GSII lectin positive cells. Although proliferation is seen throughout the glands in L635 treated control mice, localization in treated null mice was similar to patterning observed in the DMP-777 treated null mice. Furthermore, there was no change in the number of GSII lectin and GIF co-labeled cells. Instead, distinct regions of chief cells remained. These data indicate that *Mist1* null mice are resistant to the induction of SPEM, although SPEM is not completely inhibited. Taken together, these studies suggest a model in which only the newest differentiated *Mist1* null chief cell just emerging from the transition zone has the ability to transdifferentiate. These may be the origin of the proliferating GSII lectin and GIF co-positive cells. However, the majority of chief cells do not trandifferentiate because they quickly lose their secretory machinery in the absence of *Mist1*. The increase in GSII lectin and GIF dual labeled cells in DMP-777 treatment of null mice may indicate an accumulation of transition cells. This accumulation is not seen in L635 treatment, as it may take longer than three days for the resident chief cells to be replaced by the transition cells. These findings show that chief cells are not passive participants in the induction of

SPEM, because without their secretory machinery they exhibit a decrease in SPEM. Thus, chief cells are an active contributor in the development of SPEM.

Overall, these studies have significantly expanded our understanding of the induction and progression of SPEM. Comparison of the heterogeneity among SPEM lineages has elucidated novel markers of metaplasia as well as identification of a mouse analog to intestinal metaplasia in humans (SPEM-IC). Additionally, indispensible and novel *in vitro* chief cell and SPEM cell models were established and are now available for future studies. These cell lines have already led to the discovery that mature chief cells with functional secretory machinery are necessary for the induction of SPEM. Thus, this body of work has made great strides in furthering our understanding of metaplasia in the stomach.

Future directions

Characterization of SPEM lineages in other murine models

As detailed above, the studies presented here have significantly enhanced our understanding of SPEM induction and progression. Many exciting directions for future studies have emerged from them. Of note, the identification of SPEM-IC as a more advanced metaplasia in the murine stomach has led to a new model for studying metaplastic progression in the mouse. Future *in vivo* studies can more accurately report the stage of metaplasia that arises from various manipulations. One important future study to expand this model is to characterize additional SPEM lineages that arise from different mouse models. Of note, *gastrin* null mice develop SPEM after only three days of DMP-777 (Nomura et al. 2004c). Another distinctive mouse model that develops

SPEM is the *Runx3* null mouse. *Runx3* null mice have a prominent inflammatory infiltration in the gastric mucosa and develop what appears to be SPEM at the base of glands. However, they retain parietal cells throughout the fundus (Ito et al. 2011). The expressional profile of this SPEM lineage may help identify SPEM transcripts upregulated because of inflammation but not parietal cell loss. Furthermore, Varon et. al. recently reported on several *Helicobacter* infections in mouse (Varon et al. 2011) that would be of interest for further characterization utilizing the transcript profiles established in our studies. Together, these studies would further our understanding of the induction of SPEM and progression to SPEM-IC. The findings would directly relate to the progression to intestinal metaplasia in humans. With the recent increase in attention given to SPEM in various mouse models, characterizing each SPEM lineage using the profiles established here would help unify the understanding of SPEM characteristics as well as pinpoint the stage of metaplastic progression in each mouse model.

Using ImChief and ImSPEM cells to study homeostasis and the metaplastic process

As alluded to in the *Mist1* null mouse studies, the necessity of mature chief cells in the induction of SPEM could focus future studies to the intrinsic properties of chief cells. ImChief cells can be used to study this requirement. While one would expect this transdifferentiation to happen in culture in the absence of parietal cell signals, ImChief cells did not transdifferentiate *de novo*. As noted in Chapter 3, overexpression of *Mist1* to drive ImChief cells towards further maturity also did not induce SPEM. However, another more powerful transcription factor such as *Xbp1* (upstream of *Mist1*) may promote complete maturation of ImChief cells. ImChief cells could be transfected with *Xbp1* to induce maturation. It is possible that this overexpression will push the ImChief

cells to a mature state that could then lead to transdifferentiation into SPEM. This study would greatly support the findings in the *Mist1* null mice. Furthermore, if *Xbp1* expression does push ImChief cells to complete maturation, it may then be possible to study pepsinogen secretion mechanisms. While much progress has previously been made in understanding pepsinogen secretion, new studies have been difficult due to a lack of *in vitro* models with manipulation capabilities. *Xbp1* overexpressing ImChief cells could renew efforts in this area and further understanding of the genes and factors that regulate pepsinogen secretion and how it is altered in disease.

These novel ImChief and ImSPEM cell lines can be utilized for investigations of any gene of interest involved in gastric homeostasis or metaplasia. In addition, these *in vitro* models can be used to discern the specific factors from the complex network involved in the induction and progression of metaplasia in the stomach. Studies investigating the inflammatory response in metaplasia must sort out the influences from several different sources (i.e. types of immune cells such as neutrophils, macrophages, etc). Ongoing studies in our lab have suggested that macrophages are the key inflammatory cell for the induction of SPEM. Thus, macrophages would be a notable choice for co-culturing experiments with ImChief and ImSPEM cells. Resident macrophages in the normal stomach as well as circulating macrophages that infiltrate the gastric mucosa after L635 treatment or *Helicobacter* infections could be isolated. The isolated macrophages on ImChief and ImSPEM cells could be co-cultured to investigate their effects in a controlled and less variable environment. Cells could be cultured in the same plate to analyze the necessity of direct interaction or in opposing compartments of transwells for paracrine signaling investigations. If an effect is detected through paracrine

signaling, a cytokine array may be used to elucidate the factors secreted into the media. This framework could also investigate possible feedback loops from chief cells, such as signals the chief or SPEM cells relay back to macrophages or other cell types.

Inflammatory cells are not the only avenue of exciting co-culturing studies. Upon the eradication of *Helicobacter* infection, the gastric mucosa reverts to normal lineages (Matsumoto et al. 2005; Nishizawa et al. 2007). This reversal was also observed 14 days after cessation of DMP-777 of L635 administration(Nomura et al. 2004c). It is presumed that parietal cells, once they begin to repopulate the gastric glands, resume directing the differentiation of chief cells. As no increase in cell death is observed during this reversal, it is inferred that SPEM cells can revert into chief cells. Thus, a primary parietal cell culture model could be isolated and co-cultured with ImSPEM cells. Utilizing established protocols, parietal cells remain viable for up to one week (Chew et al. 1989; Soroka et al. 1993; Agnew et al. 1999). If parietal cells are the driving force for SPEM reversal to chief cells, one would expect ImSPEM cells to decrease SPEM markers and begin expressing differentiated chief cell markers, such as *Mist1*. Furthermore, if ImSPEM cells did begin reverting to chief cells, it could by theorized that a secreted factor from parietal cells acts upon the ImSPEM cells causing upregulation of chief cell differentiation genes. Novel parietal cell secreted factors may be identified through this avenue. Additionally, transcriptional profiling of the actively reverting cells may reveal novel genes that are upregulated to drive chief cell differentiation. Identification of novel genes involved in the maturation of chief cells will contribute to our understanding of chief cell homestasis as well as their transdifferentiation into SPEM. Conversely, from previous DMP-777 studies, it has been theorized that the dying parietal cells secrete factors that could signal

chief cells to transdifferentiate. Thus, while normal functioning parietal cells may be able to reverse ImSPEM cells, dying parietal cells may push ImChief cells to SPEM. Again, these studies could be completed using isolated primary parietal cells in combination with ImChief cells.

Other immortalized gastric cell lines

Many co-culturing experiments could be proposed with the novel ImChief and ImSPEM cell lines. As mentioned above, many experiments of interest would involve frequent isolation of new parietal cells. An alternative to continuous replenishment is to develop an immortalized parietal cell line. We have had success using the Immortomouse to develop a chief cell line and a SPEM cell line. While SPEM cells have an innate proliferative ability, chief cells were thought to be post-mitotic. Thus, chief cells were originally thought to be difficult to culture and that immortalization would not be possible. The establishment of the ImChief cell line has refuted this theory. Similarly, a parietal cell line has conventionally been thought to be too difficult to develop. However, with the availability of the Immortomouse and an H/K ATPase Cre ERT2 transgenic mouse (Xiao et al.) (parietal cell specific expression), an enriched GFP expressing parietal cell population could be sorted, isolated, and cultured. Preliminary observations from the development of the ImSPEM cell line suggest that an immortalized parietal cell culture may be possible. During the development of the ImSPEM cell line, a few subclones expressed *H/K ATPase* transcripts, even after several passages. Initially, these cells were of no interest as we focused on establishing a SPEM cell line. Therefore, we actively reduced and ultimately eliminated these cells from the cultures. Establishing a parietal cell line would not only bolster future studies of the ImChief and ImSPEM cell

lines, but also provide a novel *in vitro* model system for studying trafficking and acid secretion. Ultimately, an aspiration would be to have an immortalized cell line of each of the major gastric fundic cell lineages (parietal cell, mucous neck cell, chief cell, and SPEM cell). With all of these cell lines available, a multitude of molecular mechanism and co-cultures could be investigated. Interest in culturing enteroids and organoids continues to increase; but, establishing protocols for sustained culturing for gastric lineages has proven difficult. If Immortomouse lines of parietal cells, mucous neck cells, and chief cells were all available, they could be studied in a 3D matrix such as Matrigel that may provide an *in vitro* system for studying gastric gland dynamics.

Possible interactions and roles of MMP12 in SPEM induction and progression

Initial characterization of ImSPEM cells grown in 3D Matrigel revealed cystic structures. While this finding presents a novel system to investigate polarization in SPEM, an atypical occurrence was found. When grown in Matrigel, ImSPEM cells degraded the Matrigel such that it could no longer retain its shape. Because ImSPEM cells were shown to properly function and secret HE4, we theorized that ImSPEM cells could secrete other factors that may degrade the surrounding matrix, such as matrix metalloproteinases (MMP's). From our comparison of acute SPEM lineages, we found *Mmp12* transcription was upregulated in L635 induced SPEM. *Mmp12* has been linked to emphysema and other inflammatory diseases in the lung (Molet et al. 2005). In fact, *Mmp12* deficiency resulted in macrophages being unable to degrade extracellular matrices and invade tissues (Shipley et al. 1996). Recent studies have also suggested cooperative interaction between MMP12 and neutrophil elastase (Shapiro et al. 2003). In the lung, it appears that neutrophil elastase (NE) activates MMP12 and degrades the tissue inhibitor of

metalloproteinase-1 (TIMP1) (a MMP12 inhibitor). From this data, we have hypothesized that MMP12 is a pro-inflammatory protein that is partially responsible for the prominent influx of macrophages and thus advanced stage of L635 induced SPEM. Furthermore, *Mmp12* transcription was also upregulated in DMP-777 induced SPEM. However, neutrophil elastase inhibition by DMP-777 may block NE from activating MMP12 and inhibiting TIMP1. Future studies could explore the interaction between MMP12 and NE as well as their role in inflammation. Neutrophil elastase null mice and *Mmp12* null mice could be treated with L635 and analyzed for the activation of NE or MMP12. These studies could provide insight into novel interactions between immune cells as well as identify specific factors and their mechanisms that contribute to the inflammatory influence on SPEM.

Longitudinal analysis of inflammation in Helicobacter infections

Because inflammation is such an important part of the metaplastic progression in the human stomach, many investigations have attempted to elucidate pathways involved in the complex inflammatory network. *Helicobacter* infections in mice remain the primary model for studying effects of chronic inflammation in SPEM and SPEM-IC. However, *Helicobacter* infections can be problematic due to inefficient colonization and lengthy incubation periods (six months) without confirmation of infection. Many diseases in other organs are also associated with inflammation, and research in these tissues has led to development of analysis techniques for presence and degree of inflammation. These tools allow the researcher to longitudinally study the progression of inflammation in a disease model of interest. For example, positron emission tomography (PET) imaging with [18F]fluorodeoxyglucose (FDG-PET) has been used to follow the

inflammatory burden in cystic fibrosis patients (Chen et al. 2006b). The use of such a tool to evaluate the presence and amount of inflammation in the stomach of *Helicobacter* infected mice would allow researchers to closely track the dynamics of inflammation in the stomach without having to euthanize a mouse. It would also allow earlier detection of failed colonization, thus saving time and resources. Longitudinal analysis of the inflammatory load in the stomach may also provide unique insights into correlations between the amount and length of time of the inflammatory response to the stage of metaplastic progression (SPEM or SPEM-IC). For example, the amount of inflammation may be a stronger influence on metaplastic progression than the length of time of inflammation. Furthermore, these imaging techniques may lead to a more profound understanding of the dynamic progression of metaplasia and the association with inflammation.

Conclusion

There are many exciting directions and possibilities for future studies investigating metaplasia of the stomach. The future studies described above allow for the greatest impact on our understanding of gastric homeostasis and metaplastic progression. Overall, the work presented here has identified novel markers of metaplasia, established a new model of SPEM progression, developed indispensible *in vitro* models, and determined the intrinsic chief cell characteristics required for transdifferentiation into SPEM.

APPENDIX A

SUPPLEMENTAL TABLES

Supplemental Table 1. Upregulated and downregulated transcripts in Pan-SPEM. List of transcripts upregulated or downregulated in all three SPEM models compared to WT.

Pan SPEM							Fold Change		
							WT vs	WT vs	WT vs
Probe	Direction	DMP777	*H.felis*	L635	WT_CC	Gene Symbol	DMP-777	*H.felis*	L635
12442_at	down in WT	9.79	9.60	10.33	7.78	Ccnb2	2.01	1.82	2.55
21973_at	down in WT	9.52	9.68	10.49	7.57	Top2a	1.95	2.11	2.92
51944_at	down in WT	7.64	7.47	8.06	5.88	D2Ertd750e	1.75	1.59	2.18
67701_at	down in WT	8.48	9.99	8.36	6.86	Wfdc2	1.62	3.12	1.50
232983_at	down in WT	9.82	9.87	10.12	8.31	Cxcl17	1.50	1.56	1.81
60411_at	down in WT	7.93	7.85	9.18	6.58	Cenpk	1.35	1.27	2.60
237886_at	down in WT	7.01	7.01	7.85	5.68	Slfn9	1.33	1.33	2.18
12759_at	down in WT	12.42	12.76	12.96	11.38	Clu	1.04	1.38	1.58
53322_at	up in WT	11.16	11.16	11.11	12.31	Nucb2	-1.15	-1.16	-1.20
70377_at	up in WT	7.21	6.93	6.85	8.53	Derl3	-1.31	-1.60	-1.68
67080_at	up in WT	6.25	5.90	6.38	7.62	1700019D03Rik	-1.37	-1.73	-1.25
15077_at	up in WT	8.82	7.13	7.86	10.29	Hist2h3c1	-1.47	-3.16	-2.43
67475_at	up in WT	7.80	7.44	7.51	9.28	Ero1lb	-1.48	-1.84	-1.77
192212_at	up in WT	6.85	5.96	7.44	8.36	Prom2	-1.51	-2.41	-0.93
16956_at	up in WT	8.14	6.56	7.72	9.68	Lpl	-1.54	-3.13	-1.96
110695_at	up in WT	7.91	7.43	8.48	9.54	Aldh7a1	-1.63	-2.12	-1.07
14711_at	up in WT	6.52	5.87	6.66	8.18	Gnmt	-1.66	-2.31	-1.51
54420_at	up in WT	6.63	5.58	6.91	8.32	Cldn8	-1.69	-2.74	-1.41
17952_at	up in WT	7.06	7.43	7.25	8.88	Birc1f	-1.82	-1.45	-1.63
209837_at	up in WT	6.11	5.85	6.18	7.94	Slc38a5	-1.83	-2.09	-1.76
66438_at	up in WT	9.41	7.84	9.10	11.27	Hamp2	-1.86	-3.43	-2.17
66269_at	up in WT	11.07	9.79	11.49	12.94	Tmed6	-1.87	-3.14	-1.45
12491_at	up in WT	8.24	7.25	8.84	10.18	Cd36	-1.94	-2.93	-1.34
14397_at	up in WT	5.55	4.64	6.20	8.04	Gabra4	-2.49	-3.41	-1.84
216188_at	up in WT	6.01	5.74	6.00	8.52	Aldh1l2	-2.51	-2.78	-2.51
14566_at	up in WT	7.12	6.25	7.65	9.82	Gdf9	-2.69	-3.57	-2.17
68404_at	up in WT	8.17	6.88	8.88	10.92	Nrn1	-2.75	-4.04	-2.04
102294_at	up in WT	8.15	8.64	8.75	10.90	Cyp4v3	-2.76	-2.26	-2.15
12144_at	up in WT	7.24	6.57	8.12	10.70	Blm	-3.46	-4.13	-2.58
22074_at	up in WT	4.39	3.55	5.83	8.58	Try4	-4.20	-5.04	-2.75
436522_at	up in WT	4.69	4.24	5.31	9.05	Try10	-4.36	-4.81	-3.75

Supplemental Table 2. Upregulated and downregulated transcripts in Acute SPEM. List of transcripts upregulated or downregulated in DMP-777- and L635- induced SPEM as compared to WT.

Acute SPEM						Fold Change	
Probe	Direction	DMP777	L635	WT_CC	Gene Symbol	WT vs DMP-777	WT vs L635
21973_at	down in WT	9.52	10.49	7.57	Top2a	1.95	2.92
68612_at	down in WT	8.32	9.59	6.71	Ube2c	1.61	2.88
17381_at	down in WT	8.59	9.47	6.68	Mmp12	1.91	2.79
60411_at	down in WT	7.93	9.18	6.58	Cenpk	1.35	2.60
12442_at	down in WT	9.79	10.33	7.78	Ccnb2	2.01	2.55
51944_at	down in WT	7.64	8.06	5.88	D2Ertd750e	1.75	2.18
237886_at	down in WT	7.01	7.85	5.68	Slfn9	1.33	2.18
60530_at	down in WT	7.71	8.44	6.51	Fignl1	1.19	1.93
232983_at	down in WT	9.82	10.12	8.31	Cxcl17	1.50	1.81
72787_at	down in WT	6.41	7.40	5.64	Tmem48	0.78	1.76
12759_at	down in WT	12.42	12.96	11.38	Clu	1.04	1.58
67701_at	down in WT	8.48	8.36	6.86	Wfdc2	1.62	1.50
50883_at	down in WT	7.29	7.48	6.06	Chek2	1.23	1.42
192212_at	up in WT	6.85	7.44	8.36	Prom2	-1.51	-0.93
110695_at	up in WT	7.91	8.48	9.54	Aldh7a1	-1.63	-1.07
53322_at	up in WT	11.16	11.11	12.31	Nucb2	-1.15	-1.20
67080_at	up in WT	6.25	6.38	7.62	1700019D03Rik	-1.37	-1.25
56312_at	up in WT	12.00	11.95	13.28	Nupr1	-1.28	-1.34
12491_at	up in WT	8.24	8.84	10.18	Cd36	-1.94	-1.34
54420_at	up in WT	6.63	6.91	8.32	Cldn8	-1.69	-1.41
66269_at	up in WT	11.07	11.49	12.94	Tmed6	-1.87	-1.45
14711_at	up in WT	6.52	6.66	8.18	Gnmt	-1.66	-1.51
17952_at	up in WT	7.06	7.25	8.88	Birc1f	-1.82	-1.63
70377_at	up in WT	7.21	6.85	8.53	Derl3	-1.31	-1.68
209837_at	up in WT	6.11	6.18	7.94	Slc38a5	-1.83	-1.76
67475_at	up in WT	7.80	7.51	9.28	Ero1lb	-1.48	-1.77
244556_at	up in WT	6.03	5.96	7.73	Zfp791	-1.70	-1.78
14397_at	up in WT	5.55	6.20	8.04	Gabra4	-2.49	-1.84
16956_at	up in WT	8.14	7.72	9.68	Lpl	-1.54	-1.96
68404_at	up in WT	8.17	8.88	10.92	Nrn1	-2.75	-2.04
102294_at	up in WT	8.15	8.75	10.90	Cyp4v3	-2.76	-2.15
14566_at	up in WT	7.12	7.65	9.82	Gdf9	-2.69	-2.17
66438_at	up in WT	9.41	9.10	11.27	Hamp2	-1.86	-2.17
15077_at	up in WT	8.82	7.86	10.29	Hist2h3c1	-1.47	-2.43
216188_at	up in WT	6.01	6.00	8.52	Aldh1l2	-2.51	-2.51
12144_at	up in WT	7.24	8.12	10.70	Blm	-3.46	-2.58
22074_at	up in WT	4.39	5.83	8.58	Try4	-4.20	-2.75
436522_at	up in WT	4.69	5.31	9.05	Try10	-4.36	-3.75

Supplemental Table 3. Upregulated and downregulated transcripts in SPEM with Inflammation. List of transcripts upregulated or downregulated in L635- and *H.felis*-induced SPEM as compared to WT.

SPEM with inflammation						Fold Change	
						WT vs	WT vs
Probe	Direction	*H.felis*	L635	WT_CC	Gene Symbol	*H.felis*	L635
12638_at	down in WT	10.32	7.68	4.54	Cftr	5.78	3.14
19695_at	down in WT	10.66	9.70	6.32	Reg3g	4.33	3.38
12738_at	down in WT	9.08	7.14	5.58	Cldn2	3.49	1.55
12505_at	down in WT	10.05	8.74	6.75	Cd44	3.29	1.98
104156_at	down in WT	10.02	8.90	6.90	Etv5	3.13	2.01
67701_at	down in WT	9.99	8.36	6.86	Wfdc2	3.12	1.50
14776_at	down in WT	11.81	11.16	8.80	Gpx2	3.00	2.36
12945_at	down in WT	11.84	11.80	9.07	Dmbt1	2.77	2.72
12475_at	down in WT	8.77	7.57	6.04	Cd14	2.72	1.53
229323_at	down in WT	8.44	8.16	6.26	Gpr171	2.17	1.89
21897_at	down in WT	8.08	7.47	5.93	Tlr1	2.15	1.54
75974_at	down in WT	9.84	8.58	7.69	Dock11	2.15	0.89
21973_at	down in WT	9.68	10.49	7.57	Top2a	2.11	2.92
56615_at	down in WT	9.90	8.98	7.79	Mgst1	2.10	1.18
13040_at	down in WT	11.42	10.63	9.39	Ctss	2.03	1.24
73656_at	down in WT	7.97	8.07	5.94	Ms4a6c	2.03	2.13
17105_at	down in WT	9.45	10.01	7.48	Lyz2	1.97	2.53
14841_at	down in WT	7.34	7.47	5.38	Gsg2	1.95	2.08
17476_at	down in WT	9.59	8.88	7.74	Mpeg1	1.85	1.14
12442_at	down in WT	9.60	10.33	7.78	Ccnb2	1.82	2.55
27214_at	down in WT	8.79	8.72	6.99	Dbf4	1.80	1.72
56150_at	down in WT	9.58	9.92	7.80	Mad2l1	1.78	2.12
12523_at	down in WT	7.56	7.05	5.78	Cd84	1.78	1.27
19255_at	down in WT	9.11	8.94	7.35	Ptpn2	1.76	1.59
217946_at	down in WT	7.51	7.25	5.82	Cdca7l	1.70	1.43
16411_at	down in WT	7.20	6.75	5.51	Itgax	1.69	1.23
21825_at	down in WT	8.92	8.85	7.28	Thbs1	1.64	1.57
51944_at	down in WT	7.47	8.06	5.88	D2Ertd750e	1.59	2.18
232983_at	down in WT	9.87	10.12	8.31	Cxcl17	1.56	1.81
20288_at	down in WT	7.86	7.96	6.31	Msr1	1.55	1.66
15201_at	down in WT	8.03	9.58	6.56	Hells	1.47	3.02
19126_at	down in WT	12.21	11.49	10.76	Prom1	1.44	0.73
12260_at	down in WT	7.89	7.91	6.49	C1qb	1.40	1.42
12759_at	down in WT	12.76	12.96	11.38	Clu	1.38	1.58
68774_at	down in WT	6.92	7.27	5.56	Ms4a6d	1.36	1.72
14127_at	down in WT	7.68	7.98	6.35	Fcer1g	1.33	1.63
237886_at	down in WT	7.01	7.85	5.68	Slfn9	1.33	2.18
60411_at	down in WT	7.85	9.18	6.58	Cenpk	1.27	2.60
17869_at	down in WT	9.45	10.33	8.21	Myc	1.24	2.12
12527_at	down in WT	9.93	9.82	8.74	Cd9	1.19	1.08
22177_at	down in WT	10.18	10.50	9.03	Tyrobp	1.15	1.47
68533_at	down in WT	10.22	10.63	9.32	Mphosph6	0.91	1.31
64138_at	down in WT	8.87	9.09	8.03	Ctsz	0.84	1.06
216440_at	up in WT	9.40	8.80	10.18	Os9	-0.78	-1.39

Supplemental Table 3 cont.

72333_at	up in WT	6.62	6.62	7.40	Palld	-0.79	-0.79
20454_at	up in WT	6.83	6.56	7.63	St3gal5	-0.80	-1.07
77975_at	up in WT	10.07	9.56	10.91	Tmem50b	-0.84	-1.35
70028_at	up in WT	7.91	7.78	8.77	Dopey2	-0.86	-0.99
66663_at	up in WT	8.83	8.91	9.73	Uba5	-0.90	-0.83
218214_at	up in WT	7.12	7.17	8.05	Aof1	-0.94	-0.88
217337_at	up in WT	9.33	9.33	10.28	Srp68	-0.95	-0.95
107351_at	up in WT	5.98	6.04	6.95	Kank1	-0.97	-0.91
12036_at	up in WT	7.95	8.10	9.00	Bcat2	-1.05	-0.91
66119_at	up in WT	9.34	9.32	10.44	Tomm6	-1.10	-1.12
53322_at	up in WT	11.16	11.11	12.31	Nucb2	-1.16	-1.20
18604_at	up in WT	8.01	7.86	9.17	Pdk2	-1.16	-1.31
72039_at	up in WT	8.41	8.32	9.64	Mccc1	-1.23	-1.32
67041_at	up in WT	9.85	10.12	11.24	Oxct1	-1.39	-1.12
209027_at	up in WT	6.20	6.15	7.61	Pycr1	-1.41	-1.47
320718_at	up in WT	9.12	8.50	10.54	Slc26a9	-1.42	-2.04
108682_at	up in WT	7.14	7.29	8.57	Gpt2	-1.44	-1.28
17952_at	up in WT	7.43	7.25	8.88	Birc1f	-1.45	-1.63
70377_at	up in WT	6.93	6.85	8.53	Derl3	-1.60	-1.68
73647_at	up in WT	6.20	6.18	7.83	Capn9	-1.63	-1.64
104776_at	up in WT	8.77	9.09	10.41	Aldh6a1	-1.64	-1.32
66885_at	up in WT	8.22	8.09	9.86	Acadsb	-1.65	-1.78
67080_at	up in WT	5.90	6.38	7.62	1700019D03Rik	-1.73	-1.25
16008_at	up in WT	6.40	6.93	8.18	Igfbp2	-1.78	-1.25
67475_at	up in WT	7.44	7.51	9.28	Ero1lb	-1.84	-1.77
11806_at	up in WT	10.36	10.63	12.29	Apoa1	-1.92	-1.65
338521_at	up in WT	8.62	9.13	10.55	Fa2h	-1.93	-1.42
319229_at	up in WT	6.78	7.64	8.74	Sctr	-1.96	-1.10
209837_at	up in WT	5.85	6.18	7.94	Slc38a5	-2.09	-1.76
110695_at	up in WT	7.43	8.48	9.54	Aldh7a1	-2.12	-1.07
102294_at	up in WT	8.64	8.75	10.90	Cyp4v3	-2.26	-2.15
14711_at	up in WT	5.87	6.66	8.18	Gnmt	-2.31	-1.51
192212_at	up in WT	5.96	7.44	8.36	Prom2	-2.41	-0.93
30956_at	up in WT	6.49	7.52	8.94	Aass	-2.44	-1.42
54150_at	up in WT	6.91	6.78	9.37	Rdh7	-2.47	-2.59
17341_at	up in WT	6.38	7.22	8.94	Bhlha15	-2.56	-1.72
11829_at	up in WT	6.53	7.38	9.17	Aqp4	-2.64	-1.79
54420_at	up in WT	5.58	6.91	8.32	Cldn8	-2.74	-1.41
216188_at	up in WT	5.74	6.00	8.52	Aldh1l2	-2.78	-2.51
12577_at	up in WT	7.62	8.48	10.45	Cdkn1c	-2.83	-1.97
12865_at	up in WT	9.30	9.86	12.22	Cox7a1	-2.92	-2.36
12491_at	up in WT	7.25	8.84	10.18	Cd36	-2.93	-1.34
16956_at	up in WT	6.56	7.72	9.68	Lpl	-3.13	-1.96
66269_at	up in WT	9.79	11.49	12.94	Tmed6	-3.14	-1.45
15077_at	up in WT	7.13	7.86	10.29	Hist2h3c1	-3.16	-2.43
14397_at	up in WT	4.64	6.20	8.04	Gabra4	-3.41	-1.84
66438_at	up in WT	7.84	9.10	11.27	Hamp2	-3.43	-2.17
14566_at	up in WT	6.25	7.65	9.82	Gdf9	-3.57	-2.17
16517_at	up in WT	7.64	8.61	11.29	Kcnj16	-3.65	-2.68
68404_at	up in WT	6.88	8.88	10.92	Nrn1	-4.04	-2.04
12144_at	up in WT	6.57	8.12	10.70	Blm	-4.13	-2.58
69191_at	up in WT	8.38	10.68	13.01	Pdia2	-4.63	-2.34
436522_at	up in WT	4.24	5.31	9.05	Try10	-4.81	-3.75
22074_at	up in WT	3.55	5.83	8.58	Try4	-5.04	-2.75

Supplemental Table 4. Upregulated and downregulated transcripts in Specific to SPEM with Inflammation. List of transcripts upregulated or downregulated in L635- and *H.felis*-induced SPEM as compared to DMP-777-induced SPEM.

Inflammatory SPEM specific						Fold Change	
Probe	DIRECTION	*H.felis*	L635	DMP	Gene Symbol	*H.felis* vs DMP-777	L635 vs DMP-777
12475_at	down in WT	8.77	7.57	6.04	Cd14	2.72	1.53
229323_at	down in WT	8.44	8.16	6.26	Gpr171	2.17	1.89
26366_at	down in WT	12.39	10.58	10.22	Ceacam10	2.17	0.36
73656_at	down in WT	7.97	8.07	5.94	Ms4a6c	2.03	2.13
17105_at	down in WT	9.45	10.01	7.48	Lyz2	1.97	2.53
69774_at	down in WT	8.80	8.31	6.86	Ms4a6b	1.94	1.45
110454_at	down in WT	11.69	11.17	10.42	Ly6a	1.26	0.75
22177_at	down in WT	10.18	10.50	9.03	Tyrobp	1.15	1.47
73690_at	down in WT	7.89	8.03	7.05	Glipr1	0.84	0.98
216445_at	down in WT	6.58	6.65	5.81	Arhgap9	0.77	0.84
13012_at	up in WT	7.82	8.01	7.92	Cst8	-0.10	0.09
100705_at	up in WT	6.87	6.91	7.48	Acacb	-0.61	-0.57
72333_at	up in WT	6.62	6.62	7.40	Palld	-0.79	-0.79
20454_at	up in WT	6.83	6.56	7.63	St3gal5	-0.80	-1.07
56072_at	up in WT	7.19	7.35	8.03	Lgals12	-0.83	-0.67
77975_at	up in WT	10.07	9.56	10.91	Tmem50b	-0.84	-1.35
242022_at	up in WT	5.97	6.28	6.92	Frem2	-0.95	-0.64
12389_at	up in WT	7.90	7.94	8.95	Cav1	-1.05	-1.01
20535_at	up in WT	7.57	7.80	8.79	Slc4a2	-1.22	-0.99
171168_at	up in WT	5.07	5.37	6.30	Acer1	-1.24	-0.93
320718_at	up in WT	9.12	8.50	10.54	Slc26a9	-1.42	-2.04
108682_at	up in WT	7.14	7.29	8.57	Gpt2	-1.44	-1.28
73647_at	up in WT	6.20	6.18	7.83	Capn9	-1.63	-1.64
54150_at	up in WT	6.91	6.78	9.37	Rdh7	-2.47	-2.59
11829_at	up in WT	6.53	7.38	9.17	Aqp4	-2.64	-1.79
12865_at	up in WT	9.30	9.86	12.22	Cox7a1	-2.92	-2.36
16517_at	up in WT	7.64	8.61	11.29	Kcnj16	-3.65	-2.68

Supplemental Table 5. Upregulated and downregulated transcripts in SPEM with Chronic Inflammation. List of transcripts upregulated or downregulated in *H.felis*-induced SPEM as compared to the other 3 groups (WT, DMP-777, and L635).

SPEM with chronic inflammation							Fold Change		
Probe ID	DIRECTION	WT	DMP-777	L635	*H.felis*	Gene Symbol	WT vs *H.felis*	DMP-777 vs *H.felis*	L635 vs *H.felis*
780960_at	up in *H.felis*	5.26	5.05	4.23	10.59	Gm10885	5.33	5.54	6.36
404737_at	up in *H.felis*	6.43	7.97	6.32	12.44	Igl-J1	6.00	4.47	6.12
629842_at	up in *H.felis*	3.83	3.71	3.60	9.37	Gm15449	5.54	5.66	5.77
24108_at	up in *H.felis*	5.53	5.86	5.43	10.72	Ubd	5.19	4.86	5.29
16098_at	up in *H.felis*	4.39	4.66	4.28	9.52	Igkv1-117	5.13	4.86	5.24
16069_at	up in *H.felis*	7.13	6.98	6.12	11.16	Igj	4.03	4.18	5.04
243420_at	up in *H.felis*	6.47	6.05	5.60	10.61	Gm4964	4.14	4.55	5.01
229927_at	up in *H.felis*	5.28	5.32	4.83	9.72	Clca4	4.43	4.39	4.89
667865_at	up in *H.felis*	5.30	5.76	4.91	9.71	Igk-V19-17	4.41	3.95	4.80
384514_at	up in *H.felis*	4.25	5.43	4.13	8.91	Gm1418	4.67	3.49	4.78
108022_at	up in *H.felis*	4.63	5.19	4.34	9.02	Igk-V19-15	4.39	3.83	4.69
225594_at	up in *H.felis*	4.79	4.55	4.76	9.36	Gm4841	4.57	4.82	4.60
240327_at	up in *H.felis*	6.99	6.46	6.19	10.70	Gm4951	3.71	4.24	4.51
15930_at	up in *H.felis*	5.39	5.34	4.93	9.37	Ido1	3.98	4.03	4.45
12502_at	up in *H.felis*	5.27	5.78	5.19	9.61	Cd3g	4.34	3.83	4.42
16142_at	up in *H.felis*	6.83	6.93	6.71	11.10	Igl-V1	4.26	4.17	4.39
15000_at	up in *H.felis*	6.84	6.49	6.18	10.55	H2-DMb2	3.72	4.07	4.37
14038_at	up in *H.felis*	5.47	5.59	6.13	10.48	Expi	5.01	4.89	4.35
16145_at	up in *H.felis*	7.79	8.83	7.52	11.85	Igtp	4.06	3.02	4.33
60440_at	up in *H.felis*	7.33	7.05	7.44	11.77	Iigp1	4.43	4.71	4.33
12362_at	up in *H.felis*	6.00	5.66	5.79	10.11	Casp1	4.10	4.45	4.32
14938_at	up in *H.felis*	5.79	4.82	4.99	9.26	Gzma	3.47	4.45	4.28
14469_at	up in *H.felis*	6.76	7.18	6.09	10.35	Gbp2	3.59	3.17	4.26
110785_at	up in *H.felis*	7.83	8.76	7.80	12.03	Igl-C1	4.20	3.27	4.23
17002_at	up in *H.felis*	5.10	5.05	4.76	8.79	Ltf	3.69	3.74	4.03
368204_at	up in *H.felis*	5.34	5.38	6.50	10.40	Khdc1a	5.06	5.02	3.90
667597_at	up in *H.felis*	4.34	4.08	3.95	7.75	BC023105	3.41	3.67	3.80
140474_at	up in *H.felis*	6.13	6.54	6.10	9.88	Muc4	3.74	3.34	3.77
14998_at	up in *H.felis*	6.77	6.81	7.11	10.88	H2-DMa	4.10	4.07	3.76
110786_at	up in *H.felis*	7.43	6.78	6.10	9.85	Igl-C2	2.43	3.07	3.75
15953_at	up in *H.felis*	7.63	7.98	7.43	11.16	Ifi47	3.53	3.18	3.72
68891_at	up in *H.felis*	6.32	6.50	6.75	10.46	Cd177	4.15	3.96	3.71
59290_at	up in *H.felis*	7.51	7.70	6.84	10.44	Gpa33	2.93	2.74	3.60
17329_at	up in *H.felis*	6.48	6.53	6.76	10.33	Cxcl9	3.86	3.80	3.57
17472_at	up in *H.felis*	7.14	6.59	6.67	10.13	Gbp4	2.99	3.55	3.46
667550_at	up in *H.felis*	6.43	6.22	6.88	10.35	Gm8698	3.91	4.13	3.46
80797_at	up in *H.felis*	6.10	6.94	5.71	9.13	Clca2	3.03	2.19	3.41
20210_at	up in *H.felis*	5.91	6.12	6.76	10.14	Saa3	4.23	4.02	3.39
16149_at	up in *H.felis*	8.17	8.04	8.37	11.75	Cd74	3.58	3.71	3.39
71724_at	up in *H.felis*	5.31	4.64	4.57	7.92	Aox3	2.60	3.27	3.35

Supplemental Table 5 cont.

692161_at	up in *H.felis*	6.02	6.21	6.49	9.81	Igkv19-93	3.79	3.60	3.32
192201_at	up in *H.felis*	5.68	5.62	5.16	8.47	Wfdc15b	2.79	2.85	3.31
631323_at	up in *H.felis*	6.13	6.58	5.91	9.19	Gm12250	3.06	2.61	3.28
18703_at	up in *H.felis*	7.27	9.35	9.48	12.64	Pigr	5.37	3.29	3.16
76074_at	up in *H.felis*	7.22	7.05	7.84	11.00	5830443L24Rik	3.78	3.95	3.16
242851_at	up in *H.felis*	5.43	5.87	4.78	7.83	Gnat3	2.41	1.97	3.06
15944_at	up in *H.felis*	6.78	7.39	6.99	9.99	Irgm1	3.21	2.60	3.00
16398_at	up in *H.felis*	6.27	6.54	6.33	9.15	Itga2	2.87	2.61	2.81
16912_at	up in *H.felis*	9.41	9.88	8.97	11.77	Psmb9	2.37	1.89	2.80
110557_at	up in *H.felis*	7.20	7.36	7.05	9.80	H2-Q6	2.60	2.44	2.75
74424_at	up in *H.felis*	6.71	7.35	6.40	9.15	Tmc5	2.44	1.80	2.75
14961_at	up in *H.felis*	9.55	9.18	9.79	12.53	H2-Ab1	2.97	3.35	2.74
20304_at	up in *H.felis*	7.87	7.67	7.92	10.58	Ccl5	2.70	2.91	2.66
55932_at	up in *H.felis*	6.32	6.39	5.64	8.29	Gbp3	1.97	1.90	2.65
12638_at	up in *H.felis*	4.54	5.90	7.68	10.32	Cftr	5.78	4.42	2.64
15040_at	up in *H.felis*	7.79	7.98	7.50	10.13	H2-T23	2.34	2.15	2.63
20846_at	up in *H.felis*	8.15	8.66	8.08	10.70	Stat1	2.55	2.04	2.62
14960_at	up in *H.felis*	9.43	9.19	9.77	12.38	H2-Aa	2.95	3.19	2.61
22349_at	up in *H.felis*	7.14	7.47	7.13	9.73	Vil1	2.59	2.26	2.60
12266_at	up in *H.felis*	8.84	9.04	8.93	11.50	C3	2.67	2.46	2.57
258508_at	up in *H.felis*	5.82	5.94	6.20	8.78	Olfr99	2.96	2.83	2.57
20715_at	up in *H.felis*	5.41	5.55	5.56	8.09	Serpina3g	2.68	2.54	2.54
15019_at	up in *H.felis*	5.95	5.18	6.23	8.58	H2-Q8	2.63	3.40	2.35
235952_at	up in *H.felis*	6.89	7.42	6.69	9.02	Gm189	2.13	1.60	2.33
14067_at	up in *H.felis*	6.46	7.45	7.73	10.02	F5	3.55	2.57	2.29
26365_at	up in *H.felis*	7.04	7.43	8.20	10.48	Ceacam1	3.44	3.05	2.28
21354_at	up in *H.felis*	6.33	6.67	6.40	8.68	Tap1	2.35	2.01	2.28
14969_at	up in *H.felis*	7.85	7.79	8.15	10.43	H2-Eb1	2.58	2.64	2.28
16913_at	up in *H.felis*	7.28	7.57	7.70	9.95	Psmb8	2.67	2.38	2.25
56045_at	up in *H.felis*	9.65	9.96	9.17	11.39	Samhd1	1.75	1.43	2.22
245684_at	up in *H.felis*	5.81	5.71	5.84	8.03	Cnksr2	2.22	2.32	2.19
14999_at	up in *H.felis*	10.38	10.40	10.52	12.71	H2-DMb1	2.33	2.31	2.18
15945_at	up in *H.felis*	6.12	6.08	6.24	8.41	Cxcl10	2.29	2.33	2.17
12363_at	up in *H.felis*	6.51	6.47	7.40	9.57	Casp4	3.06	3.10	2.17
14962_at	up in *H.felis*	7.45	8.08	7.62	9.77	Cfb	2.32	1.69	2.16
320679_at	up in *H.felis*	6.05	6.64	6.18	8.29	Samd12	2.25	1.65	2.11
99633_at	up in *H.felis*	7.04	7.01	6.40	8.51	Lphn2	1.47	1.50	2.11
12517_at	up in *H.felis*	6.19	6.39	5.85	7.93	Cd72	1.74	1.54	2.08
12870_at	up in *H.felis*	6.01	6.05	6.40	8.47	Cp	2.46	2.42	2.07
13058_at	up in *H.felis*	7.01	7.69	7.86	9.90	Cybb	2.90	2.21	2.04
71893_at	up in *H.felis*	6.19	6.39	6.79	8.80	Noxo1	2.61	2.41	2.01
16182_at	up in *H.felis*	6.01	7.43	7.10	9.10	Il18r1	3.09	1.66	1.99
22375_at	up in *H.felis*	9.14	9.44	9.06	11.05	Wars	1.90	1.60	1.99

Supplemental Table 5 cont

12774_at	up in *H.felis*	5.44	6.08	5.93	7.90	Ccr5	2.46	1.82	1.97
16633_at	up in *H.felis*	5.57	5.64	5.98	7.93	Klra2	2.36	2.29	1.94
12738_at	up in *H.felis*	5.58	5.96	7.14	9.08	Cldn2	3.49	3.12	1.94
14964_at	up in *H.felis*	9.77	10.04	9.23	11.17	H2-D1	1.40	1.13	1.94
668139_at	up in *H.felis*	6.60	6.68	6.72	8.66	Gm8995	2.05	1.98	1.94
236573_at	up in *H.felis*	6.85	6.28	6.96	8.89	BC057170	2.05	2.62	1.93
80901_at	up in *H.felis*	6.72	6.85	6.46	8.39	Cxcr6	1.66	1.53	1.92
16362_at	up in *H.felis*	6.90	6.91	6.56	8.47	Irf1	1.57	1.56	1.90
102084_at	up in *H.felis*	6.00	6.28	6.08	7.97	NA	1.98	1.69	1.89
17076_at	up in *H.felis*	6.14	6.38	6.40	8.26	Ly75	2.12	1.89	1.86
21946_at	up in *H.felis*	9.40	9.40	9.70	11.54	Pglyrp1	2.13	2.14	1.84
107526_at	up in *H.felis*	7.13	6.62	6.67	8.49	Gimap4	1.36	1.87	1.82
26366_at	up in *H.felis*	10.22	8.95	10.58	12.39	Ceacam10	2.17	3.44	1.81
75345_at	up in *H.felis*	5.23	5.31	5.62	7.43	Slamf7	2.21	2.12	1.81
12268_at	up in *H.felis*	6.50	6.76	6.81	8.60	C4b	2.10	1.84	1.79
21838_at	up in *H.felis*	7.24	7.19	7.14	8.92	Thy1	1.68	1.74	1.78
16186_at	up in *H.felis*	6.39	6.50	6.80	8.52	Il2rg	2.13	2.02	1.72
12364_at	up in *H.felis*	6.29	6.03	5.77	7.47	Casp12	1.18	1.44	1.70
75568_at	up in *H.felis*	6.32	6.87	8.69	8.78	Capsl	2.45	1.91	1.68
18805_at	up in *H.felis*	7.69	13.38	7.62	9.27	Pld1	1.58	1.08	1.65
14991_at	up in *H.felis*	7.23	7.27	7.24	8.88	H2-M3	1.65	1.61	1.64
67701_at	up in *H.felis*	6.86	8.48	8.36	9.99	Wfdc2	3.12	1.50	1.62
19264_at	up in *H.felis*	7.12	7.55	8.06	9.64	Ptprc	2.52	2.09	1.59
219151_at	up in *H.felis*	6.42	6.81	6.81	8.31	Scara3	1.89	1.50	1.50
56434_at	up in *H.felis*	8.38	8.59	8.26	9.75	Tspan3	1.37	1.16	1.49
108670_at	up in *H.felis*	6.81	6.97	6.80	8.26	Epsti1	1.45	1.29	1.46
210293_at	up in *H.felis*	6.21	6.27	6.70	8.16	Dock10	1.95	1.89	1.46
16407_at	up in *H.felis*	5.60	5.89	5.92	7.36	Itgae	1.76	1.47	1.44
67092_at	up in *H.felis*	6.56	6.27	6.46	7.90	Gatm	1.34	1.63	1.43
240725_at	up in *H.felis*	6.85	6.62	6.64	8.08	Sulf1	1.22	1.45	1.43
246256_at	up in *H.felis*	5.32	5.59	5.83	7.25	Fcgr4	1.92	1.65	1.42
69146_at	up in *H.felis*	7.10	7.43	7.36	8.74	Gsdmd	1.64	1.31	1.38
77522_at	up in *H.felis*	7.87	8.04	7.90	9.26	Tmem213	1.39	1.22	1.36
101202_at	up in *H.felis*	6.10	6.14	6.18	7.48	Hepacam2	1.38	1.34	1.29
207474_at	up in *H.felis*	6.12	6.04	5.96	7.25	Kctd12b	1.13	1.21	1.29
12259_at	up in *H.felis*	7.02	7.51	7.38	8.66	C1qa	1.65	1.15	1.28
16401_at	up in *H.felis*	6.58	6.81	6.82	8.09	Itga4	1.51	1.28	1.27
75974_at	up in *H.felis*	7.69	8.38	8.58	9.84	Dock11	2.15	1.46	1.25
16792_at	up in *H.felis*	7.34	7.89	7.93	9.16	Laptm5	1.82	1.27	1.23
212167_at	up in *H.felis*	6.26	6.56	6.72	7.95	Pion	1.68	1.39	1.23
80898_at	up in *H.felis*	7.66	7.49	7.86	9.08	Erap1	1.42	1.59	1.22
12475_at	up in *H.felis*	6.04	6.22	7.57	8.77	Cd14	2.72	2.54	1.20
15277_at	up in *H.felis*	6.40	6.62	6.53	7.67	Hk2	1.28	1.06	1.14
213233_at	up in *H.felis*	6.78	6.62	7.68	7.95	Tapbpl	1.18	1.33	1.13
12767_at	up in *H.felis*	8.28	8.39	8.57	9.67	Cxcr4	1.39	1.27	1.10
54445_at	up in *H.felis*	6.03	6.08	6.43	7.44	Unc93b1	1.41	1.36	1.00
16205_at	up in *H.felis*	6.12	5.76	6.01	6.96	Gimap1	0.84	1.20	0.95
19126_at	up in *H.felis*	10.76	8.18	11.49	12.21	Prom1	1.44	1.07	0.71
74430_at	down in *H.felis*	8.52	7.66	7.82	6.87	4930452B06Rik	-1.65	-0.80	-0.95
66270_at	down in *H.felis*	8.82	8.24	8.23	7.09	Fam134b	-1.74	-1.15	-1.14
66438_at	down in *H.felis*	11.27	9.41	9.10	7.84	Hamp2	-3.43	-1.57	-1.26
192212_at	down in *H.felis*	8.36	6.85	7.44	5.96	Prom2	-2.41	-0.90	-1.48
18778_at	down in *H.felis*	13.73	13.38	13.63	12.15	Pla2g1b	-1.58	-1.24	-1.48
66269_at	down in *H.felis*	12.94	11.07	11.49	9.79	Tmed6	-3.14	-1.28	-1.70
12955_at	down in *H.felis*	9.20	8.68	9.31	7.20	Cryab	-1.99	-1.47	-2.11
18947_at	down in *H.felis*	12.42	12.07	11.15	8.96	Pnliprp2	-3.47	-3.11	-2.19
14570_at	down in *H.felis*	9.42	9.03	9.27	6.97	Arhgdig	-2.45	-2.06	-2.30
545677_at	down in *H.felis*	12.37	9.29	10.35	5.77	Gm12888	-6.60	-3.52	-4.58
81600_at	down in *H.felis*	13.65	12.18	13.28	7.39	Chia	-6.25	-4.79	-5.88

Supplemental Table 6. Quantitative RT-PCR primer sequences. Specific primer sequences are listed with the concentrations used for qRT-PCR experiments.

Primer Name	Sequence	Final Concentration
Arhgap9 F	TGCTGCCTGACTTTCGTGATG	100 nM
Arhgap9 R	GCGGTCATTCGGTTCTTATCC	100 nM
Casp1 F	GAAAGACAAGCCCAAGGTGAT	200nM
Casp1 R	GGTGTTGAAGAGCAGAAAGCA	200nM
Ccnb2 F	TGAAGTCCTGGAAGTCATGC	100nM
Ccnb2 R	GAGGCCAGGTCTTTGATGAT	100nM
CD14 F	CTCTGTCCTTAAAGCGGCTTAC	100nM
CD14 R	GTTGCGGAGGTTCAAGATGTT	100nM
Ceacam1 F	CCTCAGCACATCTCCACAAAG	200nM
Ceacam1 R	TATAGCCGTAGTGTTTCCCTTG	200nM
Ceacam10 F	CTCCGATTTCTGTGCGATTTC	100 nM
Ceacam10 R	GTCCGTGGCAGATTGTGAAC	100 nM
Cenpk F	AATACTGGACACTCTTAACG	100nM
Cenpk R	GGATCTTAGTTGTCAGTTCAT	100nM
CFTR F	CTGGACCACACCAATTTTGAGG	100nM
CFTR R	GCGTGGATAAGCTGGGGAT	100nM
Chek2 F	TCGGCTATGGGCTCTTCA	200nM
Chek2 R	CGTCCTTCTCAACAGTGGTC	200nM
Clu F	CCAGCCTTTCTTTGAGATGA	100nM
Clu R	CTCCTGGCACTTTTCACACT	100nM
Ctss F	TCTATGACGACCCCTCCTG	200nM
Ctss R	TTGCCATCCGAATGTATCCTT	200nM
Cxcl17 F	AGGTGGCTCTTGGAAGGTG	100nM
Cxcl17 R	CTCTGGAGGGTCTTTGCGA	100nM
Dmbt1 F	ACCTCCTCACGGTGCTACAG	100 nM
Dmbt1 R	GCTTCTTCACATCCTCCACTG	100 nM
ETV5 F	GCTCTTGGTGCTAAGTAGGA	200nM
ETV5 R	TCTGATGGGTGGGTGACA	200nM
Fignl1 F	TTATATTCCCCTCCCAGAAGC	200nM
Fignl1 R	GCCAGAAAACCCATCAGACT	200nM
Glipr1 F	CCAGCTTCGGTCAAAAGTGAG	100 nM
Glipr1 R	TGGGTGTATCCGTGAATGCAG	100 nM
Gpx2 F	CAGGGCTGTGCTGATTGAG	200nM
Gpx2 R	CGGACATACTTGAGGCTGTTC	200nM
Ly6a F	GACTTCTTGCCCATCAATTACC	100 nM
Ly6a R	TTAGTACCCAGGATCTCCATAC	100 nM
Lyz2 F	GCCAGAACTCTGAAAAGGAATG	100 nM
Lyz2 R	CTTTGGTCTCCACGGTTGTAG	100 nM
Mad2l1 F	TGCTTACAACTACTGACCCCG	200nM
Mad2l1 R	ACTGCCATCTTTCAAGGACTTC	200nM
Mmp12 F	CATGAAGCGTGAGGATGTAGAC	200nM
Mmp12 R	CTAGTGTACCACCTTTGCCA	200nM
Ms4a6b F	TCCCTCCAATCTACACTTTACC	100 nM

Supplemental Table 6 cont.

Ms4a6b R	GACTTTGTCTCCGTGACGATG	100 nM
Ms4a6c F	AAAAGACGAGTCCCAGCCTAC	100 nM
Ms4a6c R	ATGGGACAGGAGGAACAGATG	100 nM
Muc4 F	GCTGCCTGTATTCTTGCCT	200nM
Muc4 R	ATGTTCTGGTGCTGCTGGA	200nM
Pigr F	GATTTGGGAGGCAATGACAAC	100nM
Pigr R	GCTTTCTTGGATTCTTCTGGC	100nM
Prom1 F	TGGATAACACAGGAAGGAAGAG	400nM
Prom1 R	CAGGGTAGAGGCAAATGTCAG	400nM
Slfn9 F	TCCTTAGTGGTGAAACGGTCT	100nM
Slfn9 R	TCAGGTTGCTCACTCTGGTTG	100nM
Tbp F	CAAACCCAGAATTGTTCTCCTT	100 nM or 200nM
Tbp R	ATGTGGTCTTCCTGAATCCCT	100 nM or 200nM
Tmem48 F	GCTGCTACAAATGGGAGGAT	200nM
Tmem48 R	CACGGAAGGCGTCTGACTA	200nM
Top2a F	CGAAATGGCTATGGAGCTAA	100nM
Top2a R	TATCTTTGTCCAGGCTTTGC	100nM
Traf4 F	CAGGTGTTAGGCTTGGCTATC	100nM
Traf4 R	CGATTAGGGCAGGGGACTA	100nM
Tyrobp F	GGTGTTGACTCTGCTGATTGC	100 nM
Tyrobp R	AAGCTCCTGATAAGGCGACTC	100 nM
Ube2c F	CAACATCTGCCTGGACATC	400nM
Ube2c R	CCTGCTTTGAATAGGTTTCTTGC	400nM
Vil1 F	TCAAAGGCTCTCTCAACATCAC	200nM
Vil1 R	GGTGCTGGAAGGAACAGG	200nM
Wfdc2/HE4 F	TGCCTGCCTGTCGCCTCTG	100nM
Wfdc2/HE4 R	TGTCCGCACAGTCCTTGTCCA	100nM

APPENDIX B

ALTERED GASTRIC CHIEF CELL LINEAGE DIFFERENTIATION IN HISTAMINE-DEFICIENT MICE

Appears as: Nozaki, K.[*], Weis, V.[*], Wang, T.C., Falus, A., and Goldenring, J.R. Altered gastric chief cell lineage differentiation in histamine-deficient mice. Am J Physiol Gastrointest Liver Physiol. 2009;296:G1211-G1220.

[*]co-first authors

Abstract

The orderly differentiation of cell lineages within gastric glands is regulated by a complicated interplay of local mucosal growth factors and hormones. Histamine secreted from enterochromaffin-like cells plays an important role in not only stimulated gastric acid secretion but also coordination of intramucosal growth and lineage differentiation. We have examined histidine-decarboxylase (HDC)-deficient mice, which lack endogenous histamine synthesis, to evaluate the influence of histamine on differentiation of fundic mucosal lineages and the development of metaplasia following induction of acute oxyntic atrophy. Stomachs from HDC-deficient mice and wild-type mice were evaluated at 8 wk and 12 mo of age. DMP-777 was administrated orally to 6-wk-old mice for 1 to 14 days. Sections of gastric mucosa were stained with antibodies against Mist1, intrinsic factor, H/K-ATPase, trefoil factor 2 (TFF2), chromogranin A, and Ext1 and for the cell cycle marker phospho-histone H3. HDC-deficient mice at 8 wk of age demonstrated a prominent increase in chief cells expressing Mist1 and intrinsic factor.

Importantly Mist1-positive mature chief cells were present in the midgland region as well as at the bases of fundic glands, indicating a premature differentiation of chief cells. Mice dually deficient for both HDC and gastrin showed a normal distribution of chief cells in fundic glands. Treatment of HDC-deficient mice with DMP-777 led to loss of parietal cells and an accelerated and exaggerated emergence of mucous cell metaplasia with the presence of dual intrinsic factor and TFF2-expressing cells throughout the gland length, indicative of the emergence of spasmolytic polypeptide-expressing metaplasia (SPEM) from chief cells. These findings indicate that histamine, in concert with gastrin, regulates the appropriate differentiation of chief cells from mucous neck cells as they migrate toward the bases of fundic glands. Nevertheless, histamine is not required for emergence of SPEM following acute oxyntic atrophy.

Introduction

In the normal gastric fundic mucosa, progenitor cells located in the upper gland neck give rise to four types of epithelial cells including pepsinogen-secreting zymogenic chief cells, acid-producing parietal cells, and two types of mucous cells, namely surface mucous cells and mucous neck cells. These lineages differentiate from three second-order progenitor cells, prepit, preparietal, and preneck cells (Karam et al. 1993b; Karam et al. 1993c; Karam et al. 1993d). Prepit cells give rise to surface mucous cells, which migrate toward the lumen and secrete trefoil factor family 1 and mucin 5 types A and C. Parietal cells differentiate from preparietal cells and in mice most of these acid-secreting cells migrate toward the base. The mucous neck cells differentiate from preneck cells and secrete spasmolytic polypeptide/trefoil factor 2 (TFF2) and MUC6. As mucous neck cells

migrate toward the bases of fundic glands, they redifferentiate into zymogenic chief cells, which secrete both pepsinogen and intrinsic factor in rodents (Karam et al. 1993d). The prezymogenic cells display granules showing features intermediate between those of neck cells and zymogenic chief cells (Karam et al. 1993d; Ramsey et al. 2007). Importantly, the transition between mucous neck cells and chief cells occurs without an intermediate transiently amplifying cell and appears to involve the induction of the expression of the transcription factor Mist1 (Ramsey et al. 2007).

Recent investigations have noted the critical influence of intrinsic mucosal growth factors on the differentiation of fundic cell lineages. A number of studies have suggested that gastrin, released from antral G cells, leads to the expansion of parietal cell lineages (Neuburger et al. 1972; Koh et al. 1997). Gastrin is also the major driver for the expansion of surface cell lineages in hypergastrinemic states (Nomura et al. 2005b). Similarly, elevation of transforming growth factor (TGF)-α, normally secreted by parietal cells, surface cells, and enterochromaffin-like (ECL) cells, leads to a marked expansion of surface cells and a reciprocal decrement in the differentiation of lineages in the deep glands (i.e., parietal cells, chief cells, and mucous neck cells) (Dempsey et al. 1992; Bockman et al. 1995; Sharp et al. 1995; Goldenring et al. 1996). Parietal cells secrete a number of other growth factors including the EGF receptor ligands, amphiregulin (Abe et al. 1997), heparin-binding EGF (Murayama et al. 1995), as well as sonic hedgehog (Zavros et al. 2007). Loss of parietal cells leads to a number of alterations in gastric lineages including an inhibition of mucous neck cell to chief cell differentiation as well as transdifferentiation of chief cell in spasmolytic polypeptide-expressing metaplasia (SPEM) (Nomura et al. 2005b; Nam et al. 2007; Nozaki et al. 2008). The loss of either

gastrin (Nomura et al. 2005b) or amphiregulin (Nam et al. 2007) or attenuation of EGF-receptor signaling (Ogawa et al. 2006) leads to accelerated emergence of SPEM following acute oxyntic atrophy. Thus loss of intrinsic growth factors may lead to global alterations in intramucosal signaling that are necessary for the normal response of the mucosa to injury or lineage loss.

Fundic endocrine cell lineages can also influence through release of hormones such as somatostatin and histamine. Somatostatin-deficient mice develop hyperplastic polyps (Zavros et al. 2005). H2-histamine receptor knockout mice develop a hypertrophic gastropathy with marked foveolar hyperplasia (Ogawa et al. 2003). Furthermore, previous investigations of mice with targeted deletion of histidine decarboxylase (HDC), the key enzyme for the production of histamine, have shown an increase in ECL cell numbers and expansion of parietal cells that appear small and less mature (Nakamura et al. 2004). Although previous investigations have suggested that parietal cell-derived influences are required for maturation of chief cells (Li et al. 1996), no investigations have identified particular paracrine influences that promote chief cell differentiation. We have now sought to characterize the lineage changes in HDC-deficient mice in more depth. Our studies have revealed a previously unrecognized marked increase in chief cell numbers in HDC-deficient mice. HDC-deficient mice showed a pattern of premature differentiation of mucous neck cells into mature chief cells in the neck region of the fundic glands. However, dual knockout mice deficient in both histamine and gastrin showed an amelioration of the premature chief cell differentiation phenotype. The chief cells that differentiated in neck region still appear to be susceptible to transdifferentiation into SPEM following acute oxyntic atrophy. All of these results indicate that the process

of chief cell differentiation from mucous neck cells is regulated by the combined influence of both histamine and gastrin.

Materials and methods

Animals

HDC-deficient mice were genotyped as previously described (Ohtsu et al. 2001) (primers used were sense, 5′-GAG CAC TGT CAG CGA ATC CAC-3′; wild-type allele antisense, 5′-GGC CGT GAG ATA AGC GTG ACC-3′; and HDC-deficient allele antisense, 5′-TGG GAT TAG ATA AAT GCC TGC TCT-3′). Gastrin-deficient mice were genotyped as previously described (Nomura et al. 2005b) (primers used were wild-type allele sense, 5′-TCC ATG CCT CTT TGT TGT TG-3′; gastrin-deficient allele sense, 5′-TCG TCA AGA AGG CGA TAG-3′; and antisense, 5′-CCA GAG GTA AAG GGC TGA CCA G-3′). HDC-deficient mice and gastrin-deficient mice were crossed, and dual HDC/gastrin-deficient mice (HDC−/−/Gastrin−/−) were established by genotyping. HDC-deficient mice and Balb/c mice (Jackson Laboratories, Bar Harbor, ME) were euthanized at 6 wk, 2 mo, 6 mo, or 12 mo of age. HDC−/−/Gastrin−/− dual knockout mice were euthanized at 8 wk of age. DMP-777 (a gift of DuPont Pharmaceuticals), formulated in 0.5% methylcellulose, was administrated orally to 6-wk-old mice (6 per group) as a gavage once daily at 350 mg/kg per day. Stomachs were excised and opened along the greater curvature and fixed with 4% paraformaldehyde and embedded in paraffin for immunohistochemical analysis. All breeding and procedures were performed under Vanderbilt University IACUC-approved animal protocols.

Immunohistochemical analysis

Excised stomachs embedded in paraffin were used for immunohistochemistry analysis. Deparaffinized sections were pretreated with antigen retrieval using Target Retrieval solution (Dako Cytomation, Glostrup, Denmark) or Trilogy antigen retrieval solution (Cell Marque, Austin, TX) at 120°C for 15 min, followed by immediate cooling using iced water. Sections were then treated with 2% blocking serum and incubated with the primary antibody overnight at 4°C. Immunostaining was performed with the following primary antibodies: murine monoclonal immunoglobulin M (IgM) anti-TFF2 (a gift from Sir Nicholas Wright; Cancer Research, London, UK; 1:1,000), rabbit anti-Mist1 (a gift from Dr. Jason C. Mills; Washington University, St Louis, MO; 1:2,000), murine monoclonal anti-H/K-ATPase (a gift from Dr. Adam J. Smolka; Medical University of South Carolina, Charleston, SC; 1:100,000), rabbit anti-chromogranin A (Zymed Laboratories, San Francisco, CA; 1:500), rabbit anti-exostoses 1 (Ext1; ProteinTech, Chicago, IL; 1:1,000), murine monoclonal anti-phospho-histone H3 (Cell Signaling Technology, Danvers, MA; 1:1,000), and rabbit anti-intrinsic factor (a gift from Dr. David Alpers; Washington University; 1:2,000). For immunohistochemistry with detection with diaminobenzidine, the sections were incubated with biotinylated secondary antibody followed by horseradish peroxidase-conjugated streptavidin. Chromogen was developed with diaminobenzidine (BioGenex Laboratories, San Ramon, CA). For immunohistochemistry with alkaline-phosphatase detection, the sections were incubated with biotinylated secondary antibody followed by alkaline phosphatase-conjugated avidin-biotin complex. Chromogen was developed with Vector Red Substrate (Vector Laboratories, Burlingame, CA). All sections were counterstained with Meyer's

hematoxylin. For immunofluorescence analysis, Cy3-goat anti-mouse IgM antibody, Cy5-goat anti-mouse IgG antibody (Jackson ImmunoResearch, West Grove, PA), and Alexa488 goat anti-rabbit IgG (Invitrogen, Carlsbad, CA) were used, and ProLong Gold Antifade Reagent with DAPI (Invitrogen) was used for nuclear counterstain and mounting medium. Sections were viewed and photographed on a Zeiss Axiophot microscope equipped with an AxioVision digital imaging system (Zeiss, Jena, Germany) or a FluoView FV1000 confocal microscope system (Olympus, Tokyo, Japan).
For quantitation of early maturation of chief cells, numbers of cells expressing only intrinsic factor cells between the first and last TFF2-staining mucous neck cells were determined for 10 glands in dual-labeled sections from three animals in each group (wild-type, HDC-deficient, and dual HDC/gastrin-deficient mice). Statistically significant differences were determined by a Student's t-test.

For quantitation of cell numbers, well-oriented sections from three animals from each group (wild-type,days 0, 1, 3, 7, and 14 of treatment; HDC knockout, days 0, 1, 3, 7, and 14 of treatment) were analyzed. Three gland units from the lesser curvature of the fundic mucosa, in each slide, were counted under fluorescent microscope (Zeiss). The average and standard deviation for cell numbers for each cell type were determined, and statistically significant differences were analyzed by Mann-Whitney U-test.

Results

HDC-deficient mice have prominent increases in ECL cells.

Previous investigations of HDC-deficient mice demonstrated mucosal hypertrophy with increases in parietal cells and ECL cells (Nakamura et al. 2004). We

observed a similar pattern of hypertrophy in the mucosa of all HDC knockout mice with a prominent increase in mucosal height in 8-wk-old animals (Figure 34, A and B). We noted a prominent increase in ECL cells marked by both chromogranin A (Figure 34, C and D) and Ext1 staining (Figure 34, E and F). Whereas ECL cells in wild-type mice were distributed more toward the bases of fundic glands, in HDC-deficient mice the ECL cells were distributed more broadly along the gland length. Nevertheless, we did not observe any instances of either nodular or linear hyperplasia patterns.

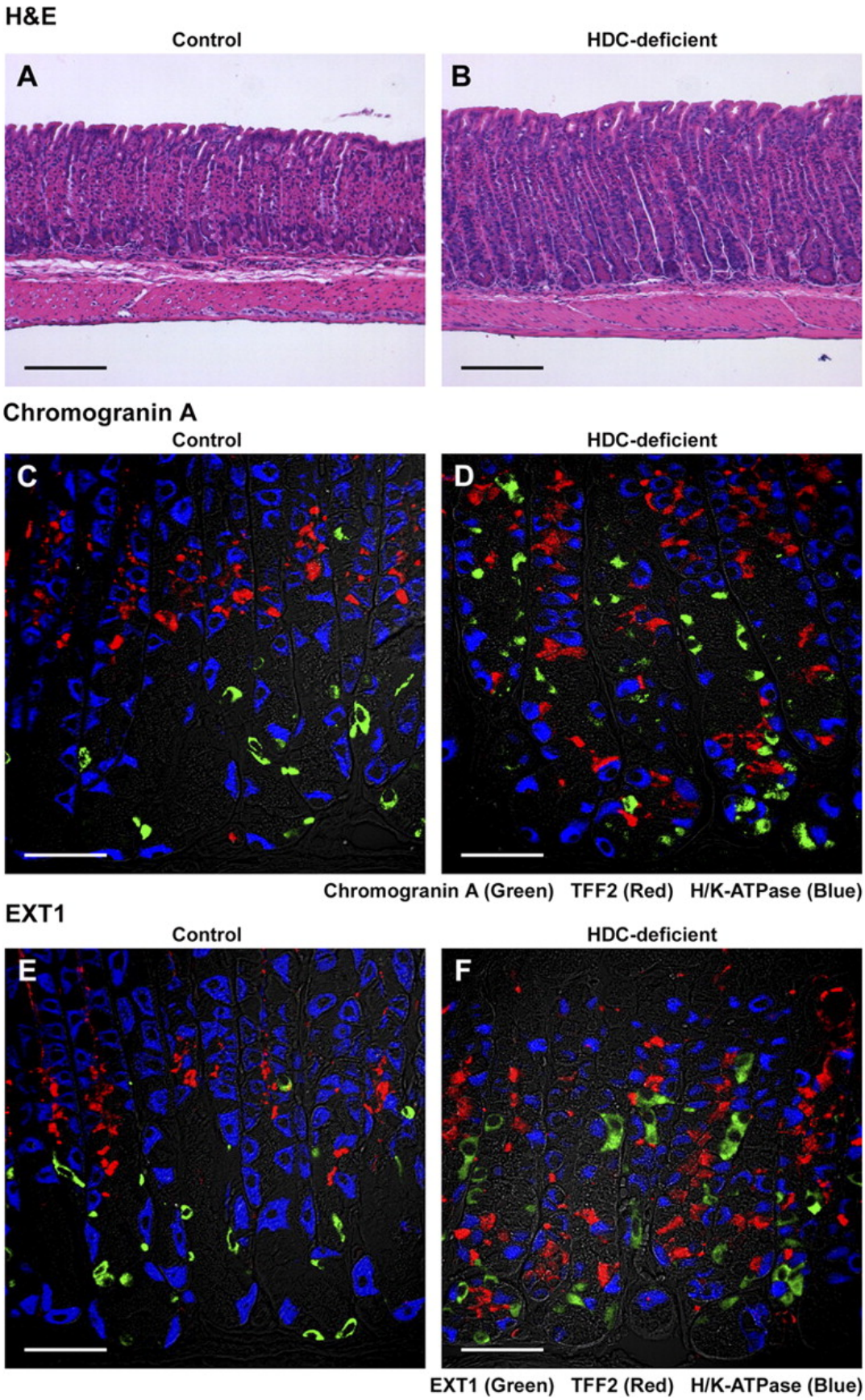
H&E
Control
HDC-deficient
A
B
Chromogranin A
Control
HDC-deficient
C
D
Chromogranin A (Green) TFF2 (Red) H/K-ATPase (Blue)
EXT1
Control
HDC-deficient
E
F
EXT1 (Green) TFF2 (Red) H/K-ATPase (Blue)

Figure 34. Characterization of the fundic mucosa of histidine-decarboxylase (HDC)-deficient mice. A: fundic mucosa of untreated wild-type mouse at 6 wk old (hematoxylin and eosin, H&E), which has normal architecture of fundic glands. B: fundic mucosa of an untreated 6-wk-old HDC-deficient mouse (H&E), which showed increased numbers of small parietal cells and chief cells. C and D: cells were triple stained for chromogranin A (green), trefoil factor 2 (TFF2) (red), and H/K-ATPase (blue). E and F: cells were tripled stained for exostoses 1 (Ext1) (green), TFF2 (red), and H/K-ATPase (blue). C and E: in wild-type mice, chromogranin A and Ext1-expressing endocrine cells were located mostly in the bases of fundic glands. D and F: in contrast, HDC-deficient mice showed increased numbers of endocrine cells that were distributed throughout the fundic gland length. Magnification bars: A and B = 160 μm; C–F = 40 μm.

HDC-deficient mice show a pattern of premature chief cell differentiation.

In examining the fluorescence stains for lineages in 8-wk-old mice, it became clear that, in addition to the broader distribution of ECL cells, there were significant alterations in other lineages. Most notably, there appeared to be two zones of TFF2-expressing mucous neck cells (Figure 35). The mucous neck cells in both zones were morphologically normal, but there also was a zone of intermediate cells that did not stain for TFF2; also, not all of these cells were accounted for by H/K-ATPase-expressing parietal cells (Figure 35E). We therefore investigated whether the intervening cells might be differentiated chief cells by assessing staining with antibodies against intrinsic factor (Figure 36), which is only expressed the zymogen granules of mature chief cells (Ramsey et al. 2007). In wild-type mice, intrinsic factor-expressing chief cells were observed only at the bases of glands, completely separate from TFF2-expressing mucous neck cells in the midgland (Figure 36, A–C). As noted previously, this phenotype is consistent with the differentiation of mucous neck into chief cells during migration toward the bases of glands (Karam et al. 1993d; Ramsey et al. 2007). In contrast, in 8-wk-old HDC-deficient mice, intrinsic factor-expressing chief cells were noted in both the midgland and at the

bases of fundic glands (Figure 36,D–F). This pattern of early chief cell differentiation was confirmed using staining for Mist1, a transcription factor, which is only expressed in mature chief cells (Figure 38). Supplemental information for this article is available at the American Journal of Physiology Gastrointestinal and Liver Physiology website. To quantitate this alteration in cell differentiation along the gland axis, we determined the number of intrinsic factor-positive cells lying between the first and last TFF2-expressing mucous neck cell in fundic glands from wild-type and HDC-deficient mice. Figure 37 demonstrates that, although few mature chief cells expressing intrinsic factor were identified within the mucous neck cell zone in wild-type mice, many mature chief cells were observed within the mucous neck cell region in HDC-deficient mice.

We also examined whether the mucosal phenotype could be explained by reactivation of mucosal progenitor cells. Figure 39 demonstrates that phospho-histone H3-expressing progenitor cells in both wild-type and HDC-deficient mice were only observed in the neck region of fundic glands. Similar results were also observed with Ki-67 staining (data not shown). These results suggested that a population of chief cells was maturing prematurely in the midgland region in the fundic mucosa of HDC-deficient mice.

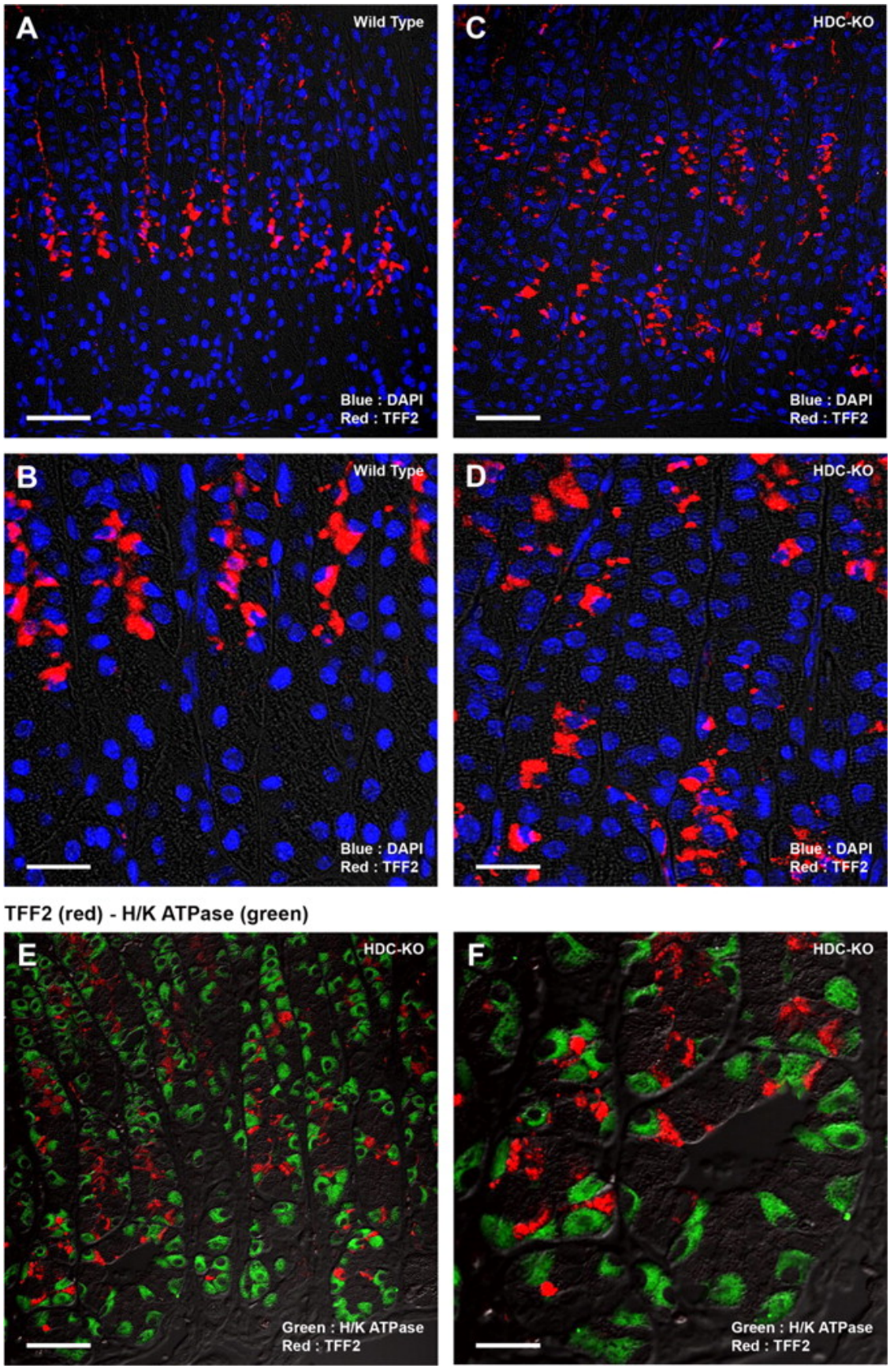
A
Wild Type
Blue : DAPI
Red : TFF2
C
HDC-KO
Blue : DAPI
Red : TFF2
B
Wild Type
Blue : DAPI
Red : TFF2
D
HDC-KO
Blue : DAPI
Red : TFF2
TFF2 (red) - H/K ATPase (green)
E
HDC-KO
Green : H/K ATPase
Red : TFF2
F
HDC-KO
Green : H/K ATPase
Red : TFF2

Figure 35. Characterization of TFF2-positive cells in HDC-deficient mice. A–D: sections of stomach from 8-wk-old wild-type and HDC-deficient [HDC knockout (KO)] mice were stained with antibodies against TFF2 (red), and nuclei were visualized with DAPI (blue). In the wild-type mice, TFF2 stained the mucous neck cells in the neck region (A, B). However, in HDC-deficient mice, TFF2-positive cells were located in two layers, not only in the neck region, but also deeper in the gland toward the base, forming two layers of TFF2-positive cells in the fundic glands (C, D). The two layers of TFF2-positive cells in HDC-deficient mice were separated from each other by a layer of nonstaining cells. E and F: HDC-deficient mouse fundic sections were stained for H/K-ATPase (green) and TFF2 (red). Note that parietal cells account for only some of the cells between the mucous neck cells. Magnification bars: A, C, and E = 40 μm; B, D, and F = 20 μm.

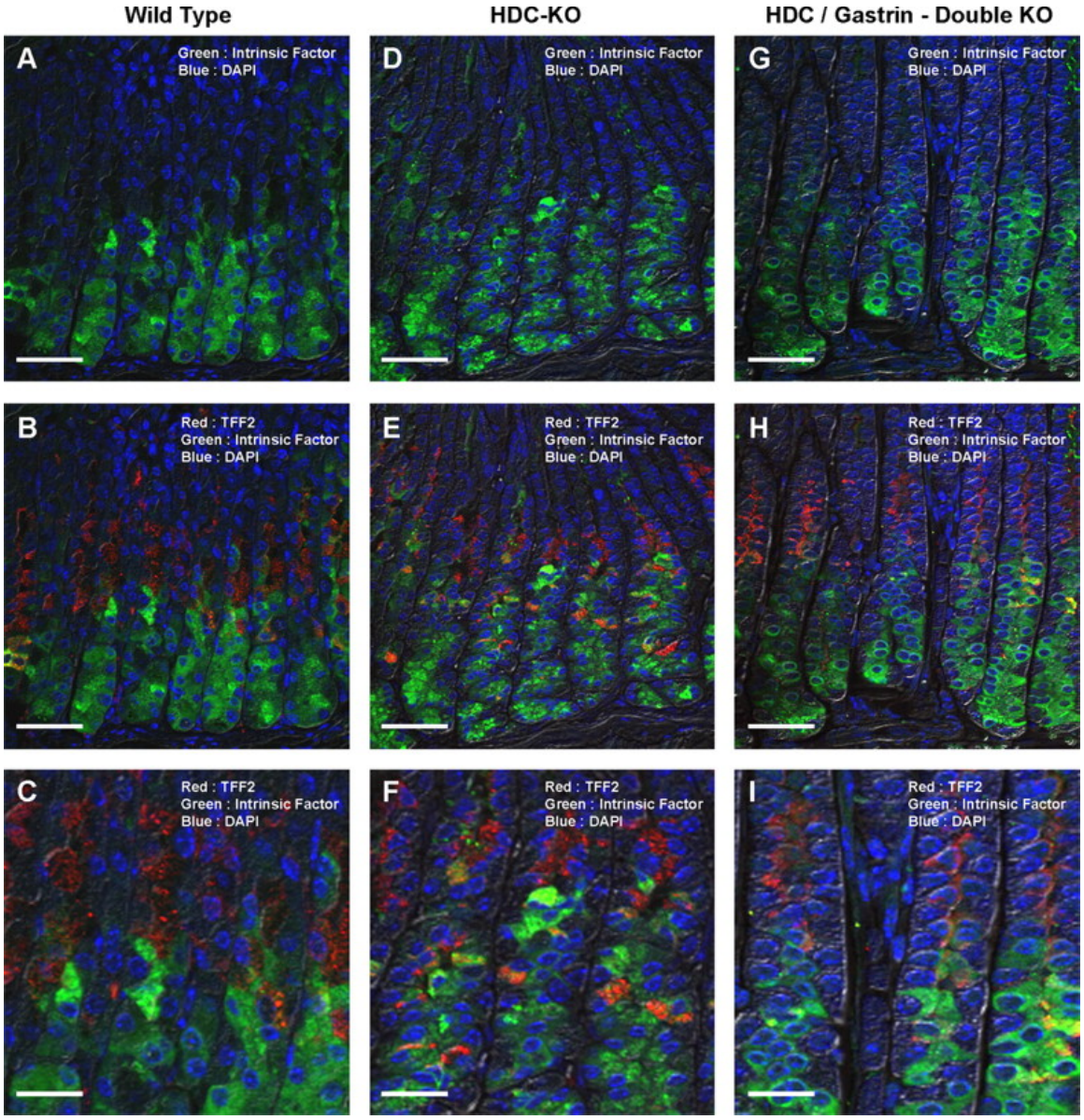

Figure 36. Aberrant location of intrinsic factor-positive mature chief cells in HDC-deficient mice. Sections of fundic mucosa from wild-type, HDC−/− and HDC−/− × gastrin−/− mice were immunostained for intrinsic factor (green) and TFF2 (red) along with DAPI staining of nuclei (blue). In the wild-type mice (A–C), intrinsic factor was positive in the cytoplasm of mature chief cells at bases of fundic glands. However, in 8-wk-old HDC knockout mice (D–F), intrinsic factor-positive cells were widely located along the fundic gland length in both the neck region and at the bases. In the dual HDC−/−× gastrin−/− mice (G–I), intrinsic factor-labeling mature chief cells were again predominantly located at the bases of fundic gland, deep to the mucous neck cell layer. Magnification bars: A, B, D, E, G, and H = 40 μm; C, F, and I = 20 μm.

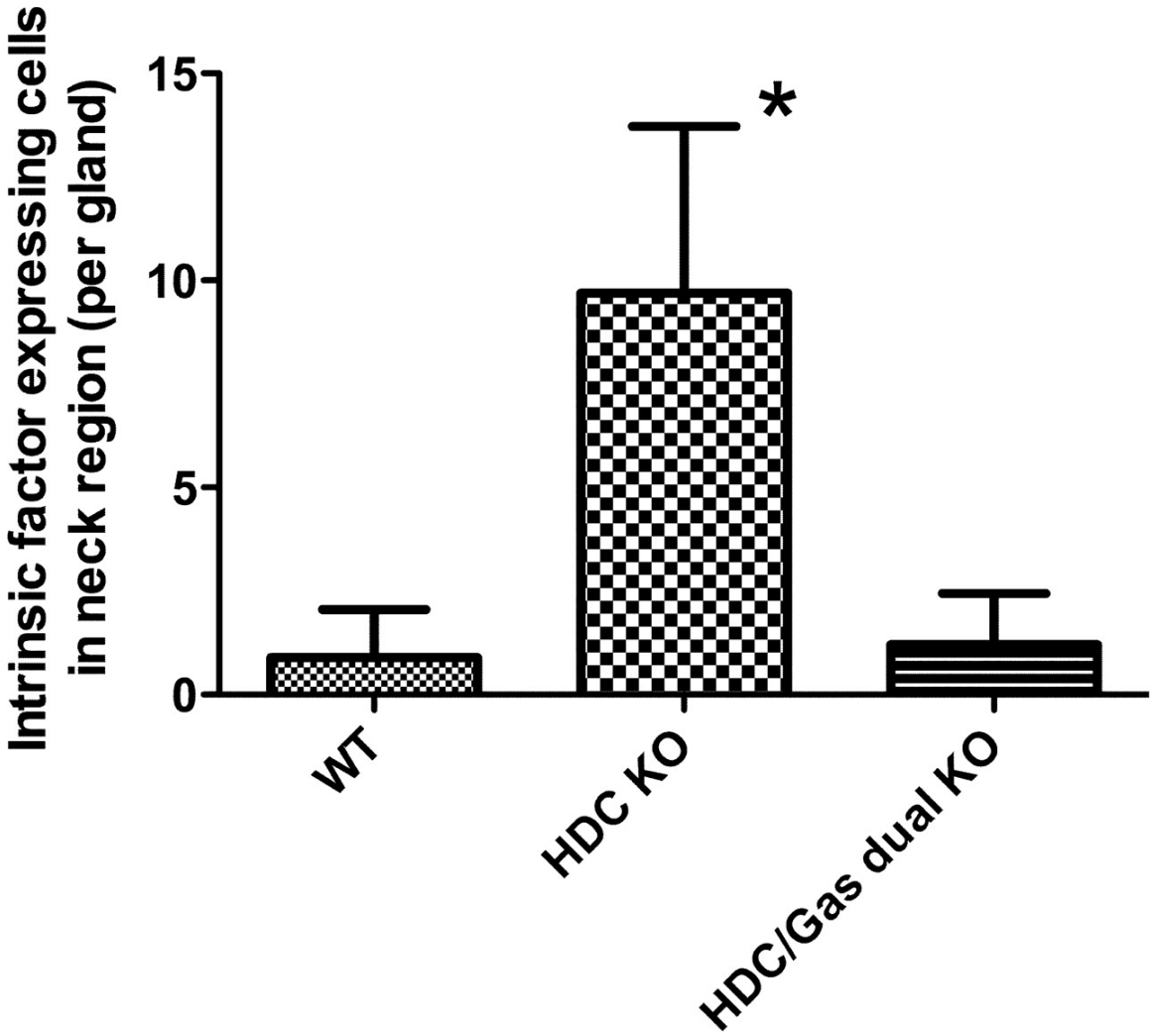

Figure 37. Premature maturation of chief cells in HDC-deficient mice. Intrinsic factor expression in mature chief cells within the neck region was assessed in sections stained for both intrinsic factor and TFF2 as in Figure 36. Neck region mature chief cells were counted as intrinsic factor-expressing cells located between the first and last TFF2-expressing mucous neck cells in each gland. Results are shown for mean cell numbers ± SD (*$P < 0.01$). Gas, gastrin.

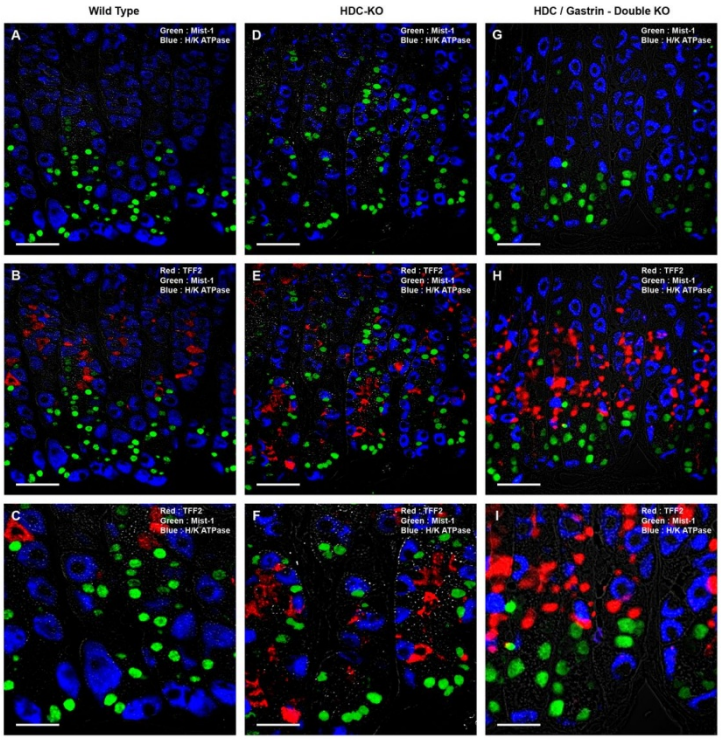

Figure 38. Aberrant location of Mist1 positive mature chief cells in HDC-deficient mice. Sections of fundic mucosa from wild type, HDC-/- and HDC-/- X gastrin-/- mice were immunostained for Mist1 (green), TFF2 (red) and H/K-ATPase (blue). In the wild type mice (A-C), Mist1 was positive in the nuclei of mature chief cells at bases of fundic glands. However, in 8-week-old HDC knockout mice (D-F), Mist1 positive cells were widely located along the fundic gland length in both the neck region and at the bases. In the dual HDC-/- X gastrin-/- mice (G-I), Mist1-labeling mature chief cells were again predominantly located at the bases of fundic gland, deep to the mucous neck cell layer. Magnification bars: A,B,D,E,G,H = 40 μm; C,F,I = 20 μm.

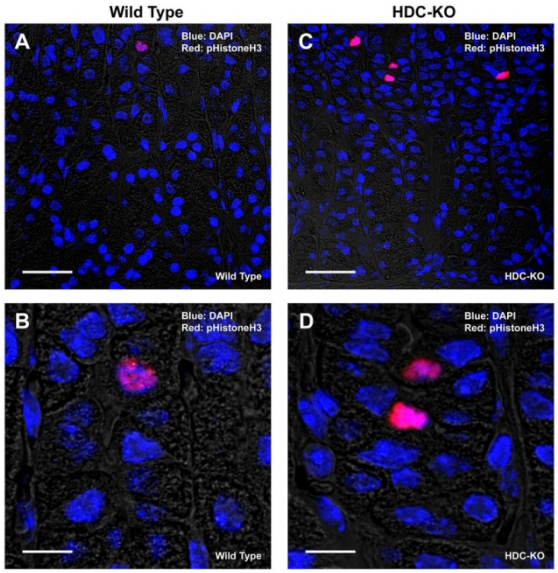

Figure 39. Characterization of mitotic cells in HDC-deficient mice. Sections of fundic mucosa from both wild type and HDC-deficient mice were stained with antibodies against phospho-Histone H3 (red) and counterstained with DAPI (blue). Both wild type (A,B) and HDC-deficient (C,D) mice showed phospho-Histone H3 staining cells in the neck region. Although the number of labeled cells in HDC-deficient mice was elevated, no proliferating cells were noted in the mid-gland or at the bases of fundic glands in either wild type or HDC-deficient mice. Magnification bars: A,C = 50 μm; B,D = 10 μm.

The secretion of histamine and gastrin are coregulated in the gastric mucosa to provide control of acid secretion. Previous investigations have determined that HDC-deficient mice have profound hypergastrinemia (Tanaka et al. 2002; Nakamura et al. 2004). Therefore, to analyze the influence of gastrin on the phenotype in histamine-deficient mice, we also examined the fundic mucosa of mice dually deficient in both histamine and gastrin (HDC−/− × gastrin−/− mice). In these dual knockout mice, we observed a normal distribution of lineages. Mucous neck cells were located in the midgland region distinctly separated from intrinsic factor-expressing chief cells that were located predominantly in the deep gland region (Figure 36, G–I). Although occasional intrinsic factor-expressing mature chief cells were still observed in the midgland, the cross of the HDC-deficient mice onto the gastrin knockout background significantly

ameliorated the phenotypic aberrations in the HDC-deficient mice as reflected by a decrease in intrinsic factor-expressing cells in the mucous neck cell zone of fundic glands (Figure 37). Similar results were also seen with Mist1 staining (Figure 38). These results indicate that the premature maturation of chief cells accrued from the coordinate influences of both a loss of histamine and hypergastrinemia.

Effects of acute parietal cell loss in HDC-deficient mice.

We have previously noted that acute loss of parietal cells using treatment with oral gavage of DMP-777 leads to mucous cell metaplasia through transdifferentiation of chief cells into SPEM. Following acute parietal cell losses, we observed marked increases in gastrin (Goldenring et al. 2000; Nomura et al. 2005b), and, because gastrin strongly stimulates histamine release, one would expect to observe elevated levels of tissue histamine release. Whereas we have recently demonstrated that loss of either gastrin or amphiregulin can promote the formation of SPEM (Nomura et al. 2005b; Nam et al. 2007) , the influence of histamine in promotion of metaplasia has not been examined. We therefore administered DMP-777 to HDC-deficient mice for 1–14 days (Figure 40). As with wild-type mice, DMP-777 elicited a rapid loss of parietal cells that was maximal by 3 days of treatment (Figure 40A). Although HDC-deficient mice showed almost twice the number of intrinsic factor-labeling chief cells compared with wild-type mice before treatment, in both groups we observed only small changes in intrinsic factor-expressing cells with DMP-777 treatment. We have previously noted that the appearance of cells expressing both intrinsic factor and TFF2 is the best reflection of the induction of SPEM following acute oxyntic atrophy (Nomura et al. 2005b; Nam et al. 2007) . In HDC-deficient mice treated with DMP-777, the appearance of dual labeling cells was

accelerated, and a significantly greater number of dual-expressing cells was observed in the HDC-deficient mice at all days of treatment. Figure 41 demonstrates that, although intrinsic factor-expressing chief cells were present in the untreated HDC-deficient mice, few cells were observed with dual staining for intrinsic factor and TFF2 (Figure 41C). In contrast, in DMP-777-treated HDC-deficient mice, dual intrinsic factor/TFF2-labeling cells were observed along the entire length of the fundic glands (Figure 41, F and I). These results suggest that histamine is not required for development of metaplasia induced by acute parietal cell loss. In addition, the findings indicate that chief cells that have matured prematurely in the neck region also can develop into metaplastic SPEM cells.

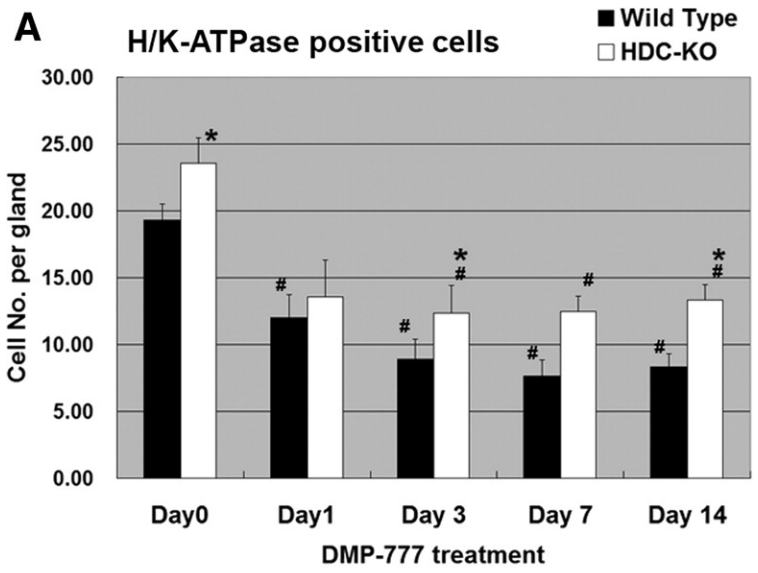
A
H/K-ATPase positive cells
Wild Type
HDC-KO
30.00
25.00
20.00
15.00
10.00
5.00
0.00
Cell No. per gland
Day0
Day1
Day 3
Day 7
Day 14
DMP-777 treatment

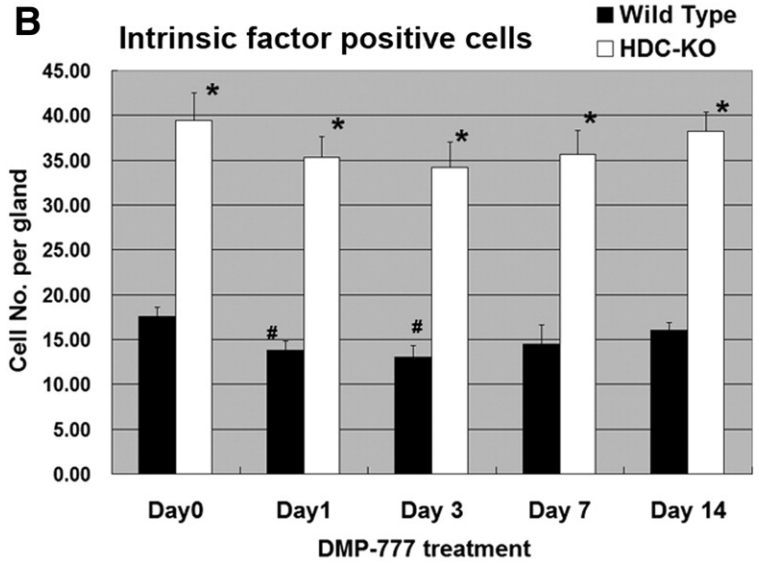
B
Intrinsic factor positive cells
Wild Type
HDC-KO
45.00
40.00
35.00
30.00
25.00
20.00
15.00
10.00
5.00
0.00
Cell No. per gland
Day0
Day1
Day 3
Day 7
Day 14
DMP-777 treatment

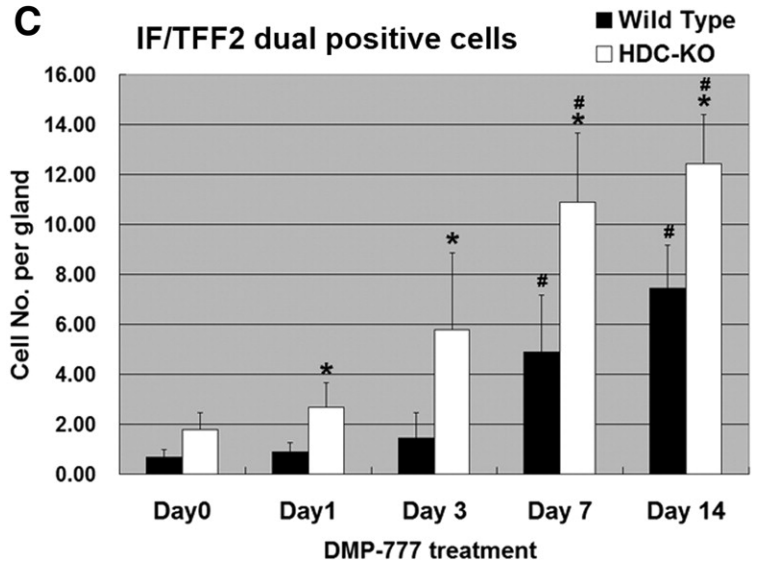
C
IF/TFF2 dual positive cells
Wild Type
HDC-KO
16.00
14.00
12.00
10.00
8.00
6.00
4.00
2.00
0.00
Cell No. per gland
Day0
Day1
Day 3
Day 7
Day 14
DMP-777 treatment

Figure 40. Alterations in cell lineages in HDC-deficient mice following acute atrophy oxyntic atrophy with DMP-777. Wild-type (solid bars) and HDC-deficient (open bars) mice were treated with DMP-777 for 0 to 14 days, and H/K-ATPase-staining parietal cells (A), intrinsic factor staining cells (B) and dual intrinsic factor (IF)/TFF2-staining cells (C) were quantitated. *$P < 0.05$ vs. wild-type (same treatment). #$P < 0.05$ vs. day 0 (untreated control).

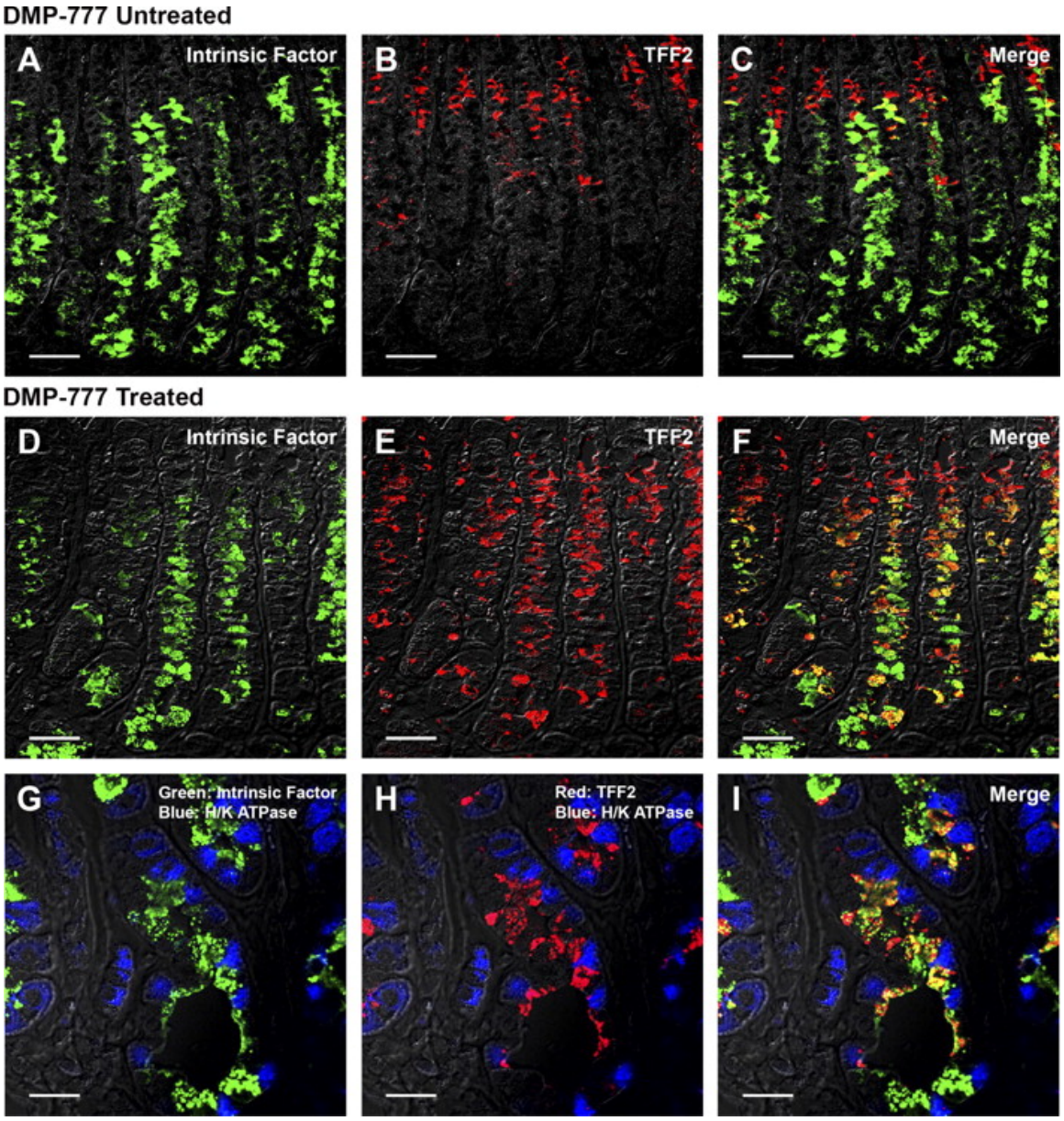

Figure 41. Characterization of fundic gland morphology in untreated or DMP-777-treated HDC-deficient mice. Sections of HDC-deficient mouse fundus from untreated (A–C) and DMP-777 treated (D–I) mice were stained for intrinsic factor (green), TFF2 (red), and H/K-ATPase (blue in G–I). As noted for Mist1 staining, the untreated HDC-deficient mice showed a marked increase in intrinsic factor-labeling chief cells throughout the length of the fundic glands. Little overlap with TFF2 labeling was observed except in the neck region. In contrast, after 14 days of treatment with DMP-777 to induce parietal cell loss, a large number of the intrinsic factor cells were also immunoreactive for TFF2 (D–F). Higher magnification of cells at the base of one gland showed that dual expressing cells show immunoreactivity for TFF2 and intrinsic factor in separate granules, a characteristic of spasmolytic polypeptide-expressing metaplasia cells. Magnification bars: A–F, 40 μm; G–I, 20 μm.

Older HDC-deficient mice show hyperplastic and metaplastic changes in the mucosa.

Previous investigations have reported that 9-mo-old HDC-deficient mice can develop hyperplastic changes in the fundus (Nakamura et al. 2004). We also examined HDC-deficient mice at over 1 yr of age. We did observe that all older mice showed regions of hyperplastic polyps along the greater curvature containing numerous parietal cells, chief cells, and mucous neck cells (Figure 43). Nevertheless, in 20% of the mice, we also observed other regions, especially along the lesser curvature, which showed marked mucous cell metaplasia with glands dominated by mucous cells that were reactive for both diastase-resistant periodic acid-Schiff (PAS) and Alcian blue (Figure 42, A–D). We have previously noted this phenotype in some forms of SPEM, and indeed the mucous cell metaplasia was strongly positive for TFF2 (Figure 42E). In contrast with the hyperplastic polyps on the greater curvature, these glands contained few parietal cells (Figure 42F). Chromogranin A-labeled ECL cells were observed along the gland length intermixed with the metaplasia (Figure 42, G and H). These results indicate that chronic absence of histamine in HDC-deficient may lead to global changes of both hyperplasia and metaplasia.

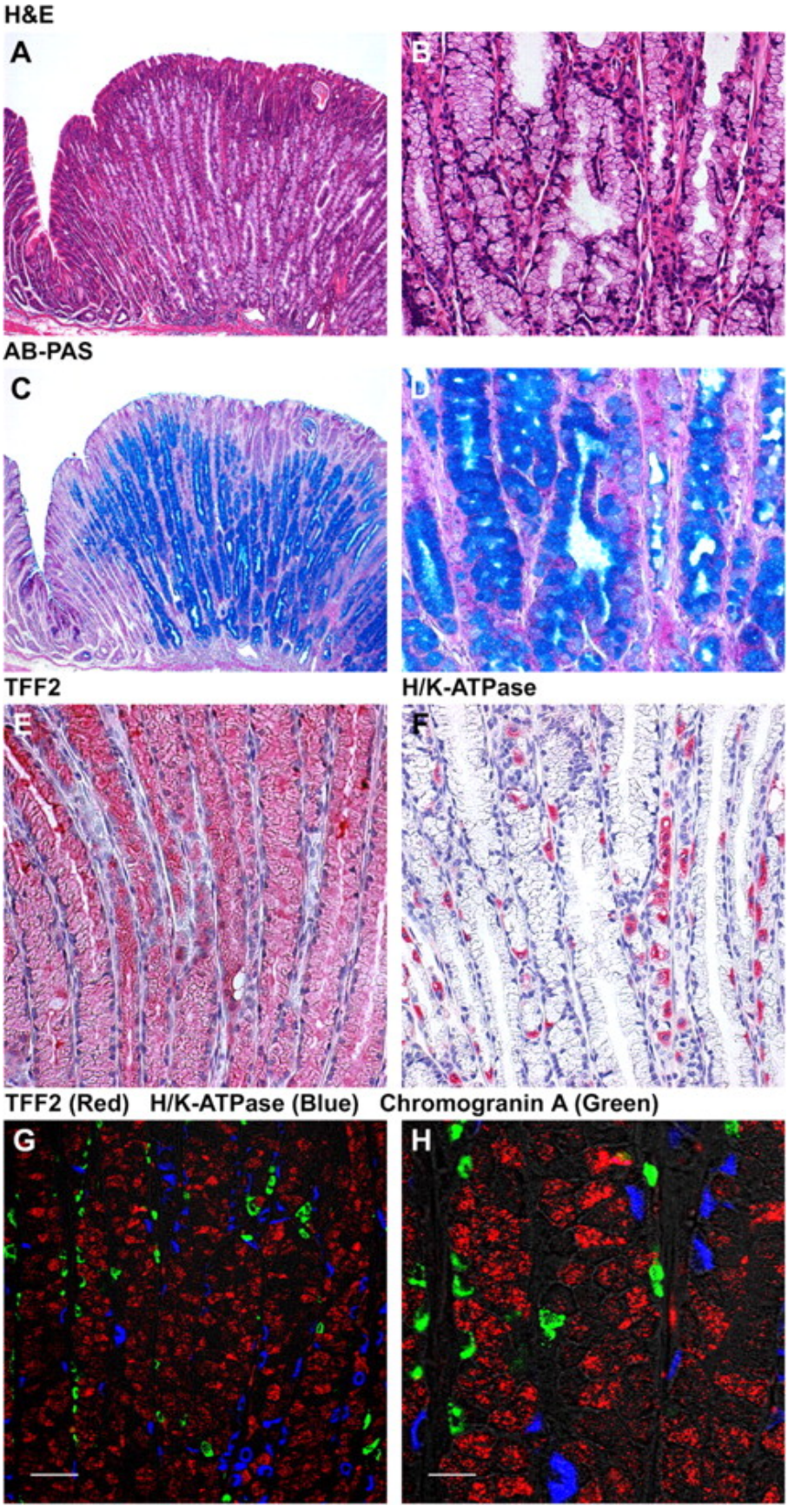
H&E
A
B
AB-PAS
C
D
TFF2
H/K-ATPase
E
F
TFF2 (Red) H/K-ATPase (Blue) Chromogranin A (Green)
G
H

Figure 42. One-year-old HDC-deficient mice showed metaplastic lesions. Sections of stomach from 1-yr-old HDC-deficient mice were examined by hematoxylin and eosin staining (A and B) or Alcian blue/periodic acid-Schiff (AB-PAS) (C and D) histochemical staining. Twenty percent of 1-yr-old mice showed mucous cell metaplasia that was dually positive for both PAS and Alcian blue in areas along the lesser curvature. Immunostaining of these metaplastic lesions showed strong staining of the mucous metaplasia for TFF2 (E) and relatively few H/K-ATPase immunoreactive parietal cells (F) that were extremely small. G and H: ECL cells were also interspersed in metaplastic glands stained with antibodies against chromogranin A (green), TFF2 (red), and H/K-ATPase (blue). Magnification bars: G, 40 μm; H, 20 μm.

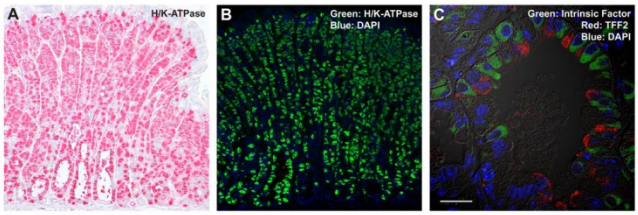

Figure 43. Hyperplastic polyps in HDC-deficient mice. (A) Immunohistochemical staining for H/K-ATPase (Alkaline phosphatase-Vector Red) (B) Immunofluorescence staining for H/K-ATPase (green) with nuclear counterstain with DAPI (blue). (C) Immunofluorescence staining against TFF2 (red) and Intrinsic Factor (green) with DAPI nuclear counterstain (blue). Along the greater curvature of all one year-old HDC-deficient mice, we observed hyperplastic polyps with expansion of parietal cell numbers. At the bases of glands in hyperplastic areas staining was observed for parietal cells (H/K-ATPase), chief cells (intrinsic factor) and mucous neck cells (TFF2). Magnification bar = 20 μM.

Discussion

Investigations over the past several years have led to the realization that cell lineage differentiation in fundic gastric glands is critically influenced by both hormonal factors as well as intrinsic mucosal growth factors. Intramucosal growth factors may have variable influences that are spatially heterogeneous as cells migrate from the progenitor zone in the neck to regions in the deeper glands. In particular, mucous neck cells differentiate initially in the neck from preneck cells and undergo a further differentiation into chief cells as they migrate toward the gland base (Karam et al. 1993d). Importantly,

mucous neck cell redifferentiation into chief cells occurs without any proliferating cell intermediate although a morphological prezymogenic cell can be identified (Karam et al. 1993d; Ramsey et al. 2007). Maturation of chief cells requires the expression of the transcription factor Mist1, and loss of Mist1 leads to a failure of complete differentiation of zymogenic cells in the deep glands (Ramsey et al. 2007). As chief cells migrate toward the base, they come under the influence of secreted paracrine factors from other lineages including parietal cells and ECL cells. These factors include a number of EGF receptor ligands and sonic hedgehog from parietal cells, as well as histamine and other growth factors secreted from ECL cells. A number of studies have indicated that the loss of parietal cells can alter the full differentiation of chief cells (Bockman et al. 1995; Li et al. 1996). However, the present investigation suggests that endocrine and intrinsic mucosal histamine production also have important influences on the differentiation of chief cells. Indeed, loss of histamine led to premature differentiation of chief cells in the neck region, before full migration to the base. The effects of histamine loss were also dependent on elevation of gastrin because breeding of HDC-deficient mice onto the gastrin-null background led to an amelioration of the premature chief cell differentiation phenotype. All of these results support the concept that the orchestration of fundic gland cell lineage differentiation requires a complex and coordinated influence of intrinsic and extrinsic growth factors.

Few studies have addressed the role of histamine as a regulator of gastric cell proliferation and differentiation. Previous investigations have suggested that histamine can regulate the proliferation of ECL cells (Modlin et al. 1996). Pharmacological inhibition of the H2-receptor leads to inhibition of acid secretion and elevated levels of

gastrin but is not associated with alteration in chief cell lineages. Similarly, knockout of the H2-histamine receptor leads to marked elevations in gastrin as well as increases in TGF-α and massive foveolar hyperplasia (Nakamura et al. 2004). This phenotype has been compared with that for transgenic overexpression of TGF-α, which also leads to massive foveolar hyperplasia (Bockman et al. 1995; Sharp et al. 1995; Goldenring et al. 1996; Nomura et al. 2005a).

Nevertheless, these mice do not show alterations in chief cell differentiation as seen in the HDC-deficient mice. All of these mice, as well as other models associated with hypergastrinemia, do not demonstrate early differentiation of chief cells (Minegishi et al. 2007). Importantly, because all of these models elevate gastrin, they would also be expected to raise histamine secretion. Thus most models of hypergastrinemia are likely dual models for hypergastrinemia with elevated histamine release (Figure 44). It is interesting to note that, although alterations in chief cell differentiation are not observed in hypergastrinemic insulin-gastrin transgenic mice at an early age, these mice do go on at a later age to develop SPEM and gastritis cystica profunda (Wang et al. 2000). In the HDC-deficient mouse, the gastric mucosa experiences hypergastrinemia in the absence of histamine (Nakamura et al. 2004) (Figure 44B). Interestingly, our studies have shown that the phenotype of premature differentiation and maturation in chief cells in the fundic gland neck was substantially ameliorated in dual HDC- and gastrin-deficient mice. These results suggest that the phenotype observed in HDC-deficient mice results from an imbalance in the influences of histamine and gastrin. Since a similar phenotype is not apparently observed in H2-receptor knockout mice (Ogawa et al. 2003; Minegishi et al. 2007), it seems likely that the loss of histamine may lead to alterations in signaling

through another histamine receptor. Perhaps the most likely candidate for this action would be through the H3-histamine receptor. The H3-histamine receptor is an autoreceptor on ECL cells and may regulate coordinated release of other ECL cell-paracrine factors (Kidd et al. 1996; Grandi et al. 2008). Alternatively, the loss of histamine secretion may in turn change the secretory pattern of other growth factors from parietal cells. In any case, these results again suggest that loss of one paracrine regulator such as histamine in the stomach can lead to global effects on amine, peptide, or growth factor secretion through various feed back loops. Disruption of these signaling loops alters the balance of lineage differentiation within gland units.

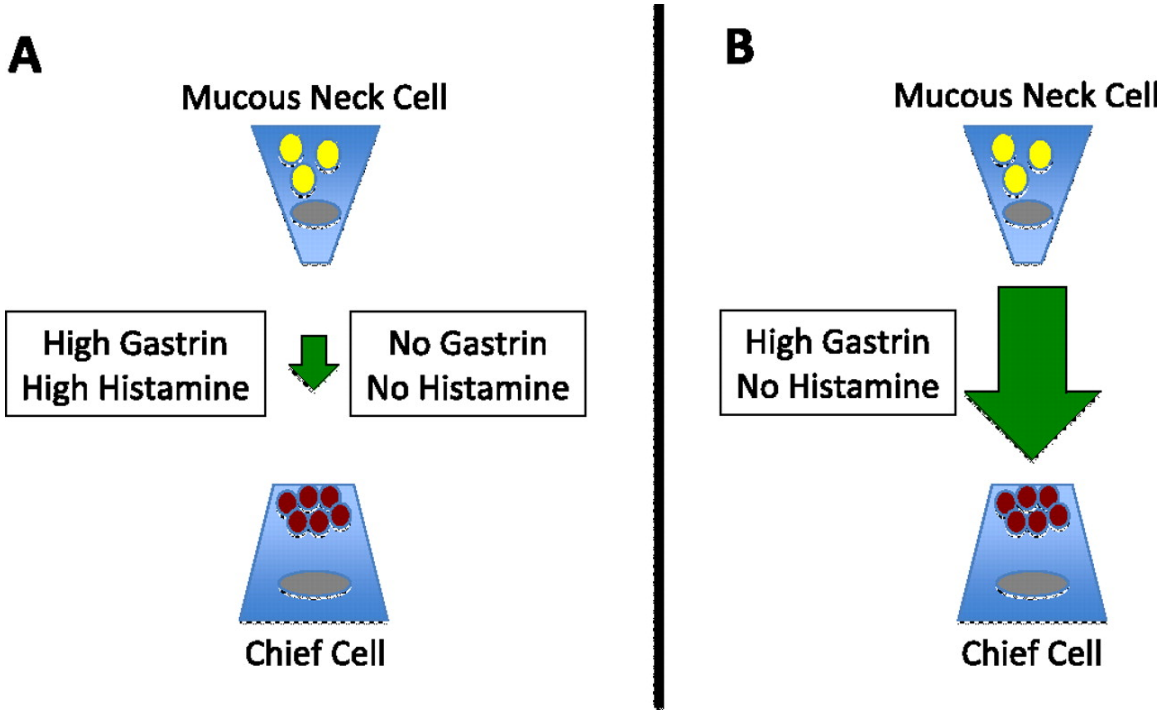

Figure 44. Model for regulation of chief cell differentiation by histamine and gastrin. A: most models of hypergastrinemia also elicit elevations in histamine. Thus, as in the normal gastric mucosa of wild-type mice, there is a balance of gastrin and histamine. B: in the HDC-deficient mice, hypergastrinemia exerts its effects in the context of an absence of histamine, leading to the observed premature differentiation of chief cells in the gland neck. In mice deficient for both histamine and gastrin, the balance is restored and chief cell lineage differentiation is normalized.

Previous studies have shown that acute oxyntic atrophy from treatment with the parietal cell-toxic compound DMP-777 leads to a rapid rise in serum gastrin and marked alterations in mucosal dynamics, leading to the emergence of SPEM (Goldenring et al. 2000; Nomura et al. 2005b; Nozaki et al. 2008). We have previously noted that SPEM developed more rapidly following DMP-777 treatment in gastrin- or amphiregulin-deficient mice (Nomura et al. 2005b; Nam et al. 2007) . Similarly, in HDC-deficient mice, acute oxyntic atrophy led to more rapid induction of SPEM and a greater amount of metaplasia within glands. The latter finding likely accrued from the increased baseline numbers of mature chief cells in the fundic glands of HDC-deficient mice. Accumulating evidence suggests that SPEM arises from both transdifferentiation of mature chief cells into mucous cell metaplasia as well as an arrest of mucous neck cell differentiation into chief cells (Nam et al. 2007; Nozaki et al. 2008). The results presented here indicate that mature Mist1-expressing chief cells, regardless of their position in the fundic glands of HDC-deficient mice, can undergo transdifferentiation manifested by dual expression of both intrinsic factor and TFF2 in separate granules within SPEM cells. Thus the ability to undergo transdifferentiation into mucous cell metaplasia appears to be an intrinsic characteristic of mature chief cells. Interestingly, whereas mucosal hyperplasia was the most characteristic pathological finding in older HDC-deficient mice, 20% of mice over 1 yr of age also showed metaplastic polyps along the lesser curvature. Thus it is possible that the expansion of the chief cell population may predispose over time to the development of oxyntic atrophy and metaplasia.

In summary, whereas previous investigations in HDC-deficient mice had documented age-dependent fundic mucosal hyperplasia, the present studies document

that the absence of intramucosal histamine production also leads to a remarkable premature differentiation in chief cells from mucous neck cells. HDC-deficient mice demonstrate a phenotype of increased mature chief cells located throughout the gastric gland. Although gastrin appears necessary for the development of this phenotype, it is does not appear to represent the sole mediator because hypergastrinemia alone does not elicit such an effect on chief cell differentiation. The small size of parietal cells suggests that they also do not undergo complete maturation (Nakamura et al. 2004). It appears likely that the combination of hypergastrinemia without histamine leads to an alteration in intramucosal signaling that regulates the timely differentiation of lineages as they migrate down the fundic glands.

REFERENCES

Abe, S., H. Sasano, K. Katoh, S. Ohara, T. Arikawa, T. Noguchi, S. Asaki, W. Yasui, E. Tahara, H. Nagura and T. Toyota (1997). Immunohistochemical studies on EGF family growth factors in normal and ulcerated human gastric mucosa. *Dig Dis Sci,* **42**(6): 1199-209.

Agnew, B. J., J. G. Duman, C. L. Watson, D. E. Coling and J. G. Forte (1999). Cytological transformations associated with parietal cell stimulation: critical steps in the activation cascade. *J Cell Sci,* **112 (Pt 16)**: 2639-46.

Ahuja, H. S., M. Tenniswood, R. Lockshin and Z. F. Zakeri (1994). Expression of clusterin in cell differentiation and cell death. *Biochem Cell Biol,* **72**(11-12): 523-30.

Allen, K. J., R. Reyes, K. Demmler, J. F. Mercer, R. Williamson and R. H. Whitehead (2000). Conditionally immortalized mouse hepatocytes for use in liver gene therapy. *J Gastroenterol Hepatol,* **15**(11): 1325-32.

Ameen, N., J. Alexis and P. Salas (2000). Cellular localization of the cystic fibrosis transmembrane conductance regulator in mouse intestinal tract. *Histochem Cell Biol,* **114**(1): 69-75.

Andersson, K., D. Chen, H. Mattsson, F. Sundler and R. Hakanson (1998). Physiological significance of ECL-cell histamine. *Yale J Biol Med,* **71**(3-4): 183-93.

Aronow, B. J., S. D. Lund, T. L. Brown, J. A. Harmony and D. P. Witte (1993). Apolipoprotein J expression at fluid-tissue interfaces: potential role in barrier cytoprotection. *Proc Natl Acad Sci U S A,* **90**(2): 725-9.

Beauchamp, R. D., J. A. Barnard, C. M. McCutchen, J. A. Cherner and R. J. Coffey, Jr. (1989). Localization of transforming growth factor alpha and its receptor in gastric mucosal cells. *J.Clin.Invest.,* **84**: 1017-1023.

Berger, S. and J. P. Raufman (1985). Prostaglandin-induced pepsinogen secretion from dispersed gastric glands from guinea pig stomach. *Am J Physiol,* **249**(5 Pt 1): G592-8.

Bi, J., A. L. Guo, Y. R. Lai, B. Li, J. M. Zhong, H. Q. Wu, Z. Xie, Y. L. He, Z. L. Lv, S. H. Lau, Q. Wang, X. H. Huang, L. J. Zhang, J. M. Wen and X. Y. Guan (2010). Overexpression of clusterin correlates with tumor progression, metastasis in gastric cancer: a study on tissue microarrays. *Neoplasma,* **57**(3): 191-7.

Blaser, M. and J. Parsonnet (1994a). Parasitism by the 'slow' bacterium Helicobacter pylori leads to altered gastric homeostasis and neoplasia. *J.Clin.Invest.,* **94**: 4-8.

Blaser, M. J. and J. Parsonnet (1994b). Parasitism by the "slow" bacterium Helicobacter pylori leads to altered gastric homeostasis and neoplasia. *J Clin Invest,* **94**(1): 4-8.

Bockman, D. E., R. Sharp and G. Merlino (1995). Regulation of terminal differentiation of zymogenic cells by transforming growth factor alpha in transgenic mice. *Gastroenterology.,* **108**: 447-454.

Bredemeyer, A. J., J. H. Geahlen, V. G. Weis, W. J. Huh, B. H. Zinselmeyer, S. Srivatsan, M. J. Miller, A. S. Shaw and J. C. Mills (2009). The gastric epithelial progenitor cell niche and differentiation of the zymogenic (chief) cell lineage. *Dev Biol,* **325**(1): 211-24.

Brown, M. R. and C. S. Chew (1987). Multiple effects of phorbol ester on secretory activity in rabbit gastric glands and parietal cells. *Can J Physiol Pharmacol,* **65**(9): 1840-7.

Capoccia, B. J., J. K. Lennerz, A. J. Bredemeyer, J. M. Klco, J. L. Frater and J. C. Mills (2011). Transcription factor MIST1 in terminal differentiation of mouse and human plasma cells. *Physiol Genomics,* **43**(3): 174-86.

Chaturvedi, R., M. Asim, J. Romero-Gallo, D. P. Barry, S. Hoge, T. de Sablet, A. G. Delgado, L. E. Wroblewski, M. B. Piazuelo, F. Yan, D. A. Israel, R. A. Casero, Jr., P. Correa, A. P. Gobert, D. B. Polk, R. M. Peek, Jr. and K. T. Wilson (2011). Spermine oxidase mediates the gastric cancer risk associated with Helicobacter pylori CagA. *Gastroenterology,* **141**(5): 1696-708 e1-2.

Chen, D., T. Aihara, C. M. Zhao, R. Hakanson and S. Okabe (2006a). Differentiation of the gastric mucosa. I. Role of histamine in control of function and integrity of oxyntic mucosa: understanding gastric physiology through disruption of targeted genes. *Am J Physiol Gastrointest Liver Physiol,* **291**(4): G539-44.

Chen, D. L., T. W. Ferkol, M. A. Mintun, J. E. Pittman, D. B. Rosenbluth and D. P. Schuster (2006b). Quantifying pulmonary inflammation in cystic fibrosis with positron emission tomography. *Am J Respir Crit Care Med,* **173**(12): 1363-9.

Chew, C. S. (1983). Inhibitory action of somatostatin on isolated gastric glands and parietal cells. *Am.J.Physiol.,* **245**: G221-G229.

Chew, C. S., M. Ljungstrom, A. Smolka and M. R. Brown (1989). Primary culture of secretagogue-responsive parietal cells from rabbit gastric mucosa. *Am J Physiol,* **256**(1 Pt 1): G254-63.

Collard, M. W. and M. D. Griswold (1987). Biosynthesis and molecular cloning of sulfated glycoprotein 2 secreted by rat Sertoli cells. *Biochemistry,* **26**(12): 3297-303.

Correa, P. (1988). A human model of gastric carcinogenesis. *Cancer Res.,* **48**: 3554-3560.

Correa, P., M. B. Piazuelo and K. T. Wilson (2010). Pathology of gastric intestinal metaplasia: clinical implications. *Am J Gastroenterol,* **105**(3): 493-8.

de Marco, M. C., F. Martin-Belmonte, L. Kremer, J. P. Albar, I. Correas, J. P. Vaerman, M. Marazuela, J. A. Byrne and M. A. Alonso (2002). MAL2, a novel raft protein of the MAL family, is an essential component of the machinery for transcytosis in hepatoma HepG2 cells. *J Cell Biol,* **159**(1): 37-44.

de Marco, M. C., R. Puertollano, J. A. Martinez-Menarguez and M. A. Alonso (2006). Dynamics of MAL2 during glycosylphosphatidylinositol-anchored protein transcytotic transport to the apical surface of hepatoma HepG2 cells. *Traffic,* **7**(1): 61-73.

Dempsey, P. J., J. R. Goldenring, C. J. Soroka, I. M. Modlin, R. W. McClure, C. D. Lind, D. A. Ahlquist, M. R. Pittelkow, D. C. Lee, E. P. Sandgren and et al. (1992). Possible role of transforming growth factor alpha in the pathogenesis of Menetrier's disease: supportive evidence form humans and transgenic mice. *Gastroenterology,* **103**(6): 1950-63.

Ectors, N. and M. F. Dixon (1986). The prognostic value of sulphomucin positive intestinal metaplasia in the development of gastric cancer. *Histopathology,* **10**(12): 1271-7.

El-Zimaity, H. M. T., H. Ota, D. Y. Graham, T. Akamatsu and T. Katsuyama (2002). Patterns of gastric atrophy in intestinal type gastric carcinoma. *Cancer.,* **94**: 1428-1436.

El-Zimaity, H. M. T., J. Ramchatesingh, M. A. Saeed and D. Y. Graham (2001). Gastric intestinal metaplasia: subtypes and natural history. *J. Clin. Pathol.,* **54**: 679-683.

Filipe, M. I., N. Munoz, I. Matko, I. Kato, V. Pompe-Kirn, A. Juersek, S. Teuchmann, M. Benz and T. Prijon (1994). Intestinal metaplasia types and the risk of gastric cancer: a cohort study in Slovenia. *Int.J.Cancer.,* **57**: 324-329.

Fjeldbo, C. S., I. Bakke, S. E. Erlandsen, J. Holmseth, A. Laegreid, A. K. Sandvik, L. Thommesen and T. Bruland (2012). Gastrin upregulates the prosurvival factor secretory clusterin in adenocarcinoma cells and in oxyntic mucosa of hypergastrinemic rats. *Am J Physiol Gastrointest Liver Physiol,* **302**(1): G21-33.

Fox, J. G., M. Blanco, J. C. Murphy, N. S. Taylor, A. Lee, Z. Kabok and J. Pappo (1993). Local and systemic immue responses in murine Helicobacter felis active chronic gastritis. *Infect.Immun.,* **61**: 2309-2315.

Fox, J. G., X. Li, R. J. Cahill, K. Andrutis, A. K. Rustgi, R. Odze and T. C. Wang (1996). Hypertrophic gastropathy in Helicobacter felis-Infected wild type C57BL/6 mice and p53 hemizygous transgenic mice. *Gastroenterology.,* **110**: 155-166.

Fox, J. G., T. C. Wang, A. B. Rogers, T. Poutahidis, Z. Ge, N. Taylor, C. A. Dangler, D. A. Israel, U. Krishna, K. Gaus and R. M. Peek, Jr. (2003). Host and microbial constituents influence Helicobacter pylori-induced cancer in a murine model of hypergastrinemia. *Gastroenterology,* **124**(7): 1879-90.

Fujii, Y., K. Yoshihashi, H. Suzuki, S. Tsutsumi, H. Mutoh, S. Maeda, Y. Yamagata, Y. Seto, H. Aburatani and M. Hatakeyama (2012). CDX1 confers intestinal phenotype on gastric epithelial cells via induction of stemness-associated reprogramming factors SALL4 and KLF5. *Proc Natl Acad Sci U S A,* **109**(50): 20584-9.

Goldenring, J. R., K. T. Nam, T. C. Wang, J. C. Mills and N. A. Wright (2010). Spasmolytic polypeptide-expressing metaplasia and intestinal metaplasia: time for reevaluation of metaplasias and the origins of gastric cancer. *Gastroenterology,* **138**(7): 2207-10, 2210 e1.

Goldenring, J. R., G. S. Ray, R. J. Coffey, P. C. Meunier, P. J. Haley, T. B. Barnes and B. D. Car (2000). Reversible drug-induced oxyntic atrophy in rats. *Gastroenterology.,* **118**: 1080-1093.

Goldenring, J. R., G. S. Ray, C. J. Soroka, J. Smith, I. M. Modlin, K. S. Meise and R. J. Coffey, Jr. (1996). Overexpression of transforming growth factor-alpha alters differentiation of gastric cell lineages. *Dig.Dis.Sci.,* **41**: 773-784.

Grandi, D., F. C. Shenton, P. L. Chazot and G. Morini (2008). Immunolocalization of histamine H3 receptors on endocrine cells in the rat gastrointestinal tract. *Histol Histopathol,* **23**(7): 789-98.

Halldorsdottir, A. M., M. Sigurdardottir, J. G. Jonasson, M. Oddsdottir, J. Magnusson, J. R. Lee and J. R. Goldenring (2003). Spasmolytic polypeptide expressing metaplasia (SPEM) associated with gastric cancer in Iceland. *Dig.Dis.Sci.,* **48**: 431-441.

Hattori, T. (1986). Development of adenocarcinomas in the stomach. *Cancer,* **57**: 1528-1534.

Hattori, T. and S. Fujita (1979). Tritiated thymidine autotradiographic study on histogenesis and spreading of intestinal metaplasia in human stomach. *Pathol. Res. Practice,* **164**: 224-237.

Hattori, T., B. Helpap and P. Gedigk (1982). The morphology and cell kinetics of pseudopyloric glands. *Virchows Arch B Cell Pathol Incl Mol Pathol,* **39**(1): 31-40.

Hinkle, K. L. and L. C. Samuelson (1999). Lessons from genetically engineered animal models. III. Lessons learned from gastrin gene deletion in mice. *Am J Physiol,* **277**(3 Pt 1): G500-5.

Hirayama, F., S. Takagi, H. Kusuhara, E. Iwao, Y. Yokoyama and Y. Ikeda (1996). Induction of gastric ulcer and intestinal metaplasia in mongolian gerbils infected with Helicobacter pylori. *J Gastroenterol,* **31**(5): 755-7.

Hirschowitz, B. I. (1967). The control of pepsinogen secretion. *Ann N Y Acad Sci,* **140**(2): 709-23.

Hochberg, Y. and Y. Benjamini (1990). More powerful procedures for multiple significance testing. *Stat Med,* **9**(7): 811-8.

Honda, S., T. Fujioka, M. Tokieda, T. Gotoh, A. Nishizono and M. Nasu (1998a). Gastric ulcer, atrophic gastritis, and intestinal metaplasia caused by Helicobacter pylori infection in Mongolian gerbils. *Scand J Gastroenterol,* **33**(5): 454-60.

Honda, S., T. Fujioka, M. Tokieda, R. Satoh, A. Nishizono and M. Nasu (1998b). Development of Helicobacter pylori-induced gastric carcinoma in Mongolian gerbils. *Cancer Res,* **58**(19): 4255-9.

Houghton, J., C. Stoicov, S. Nomura, J. Carlson, H. Li, A. B. Rogers, J. G. Fox, J. R. Goldenring and T. C. Wang (2004a). Gastric cancer originating from bone marrow derived cells. *Science,* **306**: 1568-1571.

Houghton, J., C. Stoicov, S. Nomura, A. B. Rogers, J. Carlson, H. Li, X. Cai, J. G. Fox, J. R. Goldenring and T. C. Wang (2004b). Gastric cancer originating from bone marrow-derived cells. *Science,* **306**(5701): 1568-71.

Huh, W. J., E. Esen, J. H. Geahlen, A. J. Bredemeyer, A. H. Lee, G. Shi, S. F. Konieczny, L. H. Glimcher and J. C. Mills (2010). XBP1 controls maturation of gastric zymogenic cells by induction of MIST1 and expansion of the rough endoplasmic reticulum. *Gastroenterology,* **139**(6): 2038-49.

In, J. G. and P. L. Tuma (2010). MAL2 selectively regulates polymeric IgA receptor delivery from the Golgi to the plasma membrane in WIF-B cells. *Traffic,* **11**(8): 1056-66.

Ito, K., L. S. Chuang, T. Ito, T. L. Chang, H. Fukamachi, M. Salto-Tellez and Y. Ito (2011). Loss of Runx3 is a key event in inducing precancerous state of the stomach. *Gastroenterology,* **140**(5): 1536-46 e8.

Jain, R. N., A. A. Al-Menhali, T. M. Keeley, J. Ren, M. El-Zaatari, X. Chen, J. L. Merchant, T. S. Ross, C. S. Chew and L. C. Samuelson (2008). Hip1r is expressed in gastric parietal cells and is required for tubulovesicle formation and cell survival in mice. *J Clin Invest,* **118**(7): 2459-70.

Jain, R. N., C. S. Brunkan, C. S. Chew and L. C. Samuelson (2006a). Gene expression profiling of gastrin target genes in parietal cells. *Physiol Genomics,* **24**(2): 124-32.

Jain, R. N. and L. C. Samuelson (2006b). Differentiation of the gastric mucosa. II. Role of gastrin in gastric epithelial cell proliferation and maturation. *Am J Physiol Gastrointest Liver Physiol,* **291**(5): G762-5.

Jat, P. S., M. D. Noble, P. Ataliotis, Y. Tanaka, N. Yannoutsos, L. Larsen and D. Kioussis (1991). Direct derivation of conditionally immortal cell lines from an H-2Kb-tsA58 transgenic mouse. *Proc Natl Acad Sci U S A,* **88**(12): 5096-100.

Johnson, L. R. (1977). New aspects of the trophic actions of gastrointestinal hormones. *Gastroenterology.,* **72**: 788-792.

Judd, L. M., B. M. Alderman, M. Howlett, A. Shulkes, C. Dow, J. Moverley, D. Grail, B. J. Jenkins, M. Ernst and A. S. Giraud (2004). Gastric cancer development in mice lacking the SHP2 binding site on the IL-6 family co-receptor gp130. *Gastroenterology,* **126**(1): 196-207.

Karam, S. M. (1993). Dynamics of epithelial cells in the corpus of the mouse stomach. IV. Bidirectional migration of parietal cells ending in their gradual degeneration and loss. *Anat.Rec.,* **236**: 314-332.

Karam, S. M. and C. P. Leblond (1992). Identifying and counting epithelial cell types in the "corpus" of the mouse stomach. *Anat Rec,* **232**(2): 231-46.

Karam, S. M. and C. P. Leblond (1993a). Dynamics of epithelial cells in the corpus of the mouse stomach. I. Identification of proliferative cell types and pinpointing of the stem cell. *Anat Rec,* **236**(2): 259-79.

Karam, S. M. and C. P. Leblond (1993b). Dynamics of epithelial cells in the corpus of the mouse stomach. I. Identification of proliferative cell types and pinpointing of the stem cells. *Anat.Rec.,* **236**: 259-279.

Karam, S. M. and C. P. Leblond (1993c). Dynamics of epithelial cells in the corpus of the mouse stomach. II. Outward migration of pit cells. *Anat.Rec.,* **236**: 280-296.

Karam, S. M. and C. P. Leblond (1993d). Dynamics of epithelial cells in the corpus of the mouse stomach. III. Inward migration of neck cells followed by progressive transformation into zymogenic cells. *Anat.Rec.,* **236**: 297-313.

Karam, S. M. and C. P. Leblond (1993e). Dynamisc of epithelial cells in the corpus of the mouse stomach. V. Behavior of entero-endocrine and caveolated cells:general conclusions of cell kinetics in the oxyntic epithelium. *Anat.Rec.,* **236**: 333-340.

Karam, S. M., T. Straiton, W. M. Hassan and C. P. Leblond (2003). Defining epithelial cell progenitors in the human oxyntic mucosa. *Stem Cells,* **21**(3): 322-36.

Katz, J. P., N. Perreault, B. G. Goldstein, L. Actman, S. R. McNally, D. G. Silberg, E. E. Furth and K. H. Kaestner (2005). Loss of Klf4 in mice causes altered proliferation and differentiation and precancerous changes in the adult stomach. *Gastroenterology,* **128**(4): 935-45.

Keeley, T. M. and L. C. Samuelson (2010). Cytodifferentiation of the postnatal mouse stomach in normal and Huntingtin-interacting protein 1-related-deficient mice. *Am J Physiol Gastrointest Liver Physiol,* **299**(6): G1241-51.

Kidd, M., L. H. Tang, K. Miu, G. P. Lawton, A. Sandor and I. M. Modlin (1996). Autoregulation of enterochromaffin-like cell histamine secretion via the histamine 3 receptor subtype. *Yale J Biol Med,* **69**(1): 9-19.

Koelz, H. R., S. J. Hersey, G. Sachs and C. S. Chew (1982). Pepsinogen release from isolated gastric glands. *Am J Physiol,* **243**(3): G218-25.

Koh, T. J., J. R. Goldenring, S. Ito, H. Mashimo, A. S. Kopin, A. Varro, G. Dockray and T. C. Wang (1997). Gastrin deficiency results in altered gastric differentiation and decreased colonic proliferation. *Gastroenterology.,* **113**: 1015-1025.

Kohn, E. A., Z. Du, M. Sato, C. M. Van Schyndle, M. A. Welsh, Y. A. Yang, C. H. Stuelten, B. Tang, W. Ju, E. P. Bottinger and L. M. Wakefield (2010). A novel approach for the generation of genetically modified mammary epithelial cell cultures yields new insights into TGFbeta signaling in the mammary gland. *Breast Cancer Res,* **12**(5): R83.

Lamprecht, M. R., D. M. Sabatini and A. E. Carpenter (2007). CellProfiler: free, versatile software for automated biological image analysis. *Biotechniques,* **42**(1): 71-5.

Langley, J. N. (1882). On the Histology of the Mammalian Gastric Glands and the Relation of Pepsin to the Granules of the Chief-Cells. *J Physiol,* **3**(3-4): 269-91.

Lee, A., J. G. Fox, G. Otto and J. Murphy (1990). A small animal model of human Helicobacter pylori active chronic gastritis. *Gastroenterology.,* **99**: 1315-1323.

Lee, A., J. O'Rourke, M. C. De Ungria, B. Robertson, G. Daskalopoulos and M. F. Dixon (1997). A standardized mouse model of Helicobacter pylori infection: introducing the Sydney strain. *Gastroenterology,* **112**(4): 1386-97.

Lee, H. J., K. T. Nam, H. S. Park, M. A. Kim, B. J. Lafleur, H. Aburatani, H. K. Yang, W. H. Kim and J. R. Goldenring (2010). Gene expression profiling of metaplastic lineages identifies CDH17 as a prognostic marker in early stage gastric cancer. *Gastroenterology,* **139**(1): 213-25 e3.

Lee, J. R., T. M. Baxter, H. Yamaguchi, T. C. Wang, J. R. Goldenring and M. G. Anderson (2003). Differential protein analysis of spasomolytic polypeptide expressing

metaplasia using laser capture microdissection and two-dimensional difference gel electrophoresis. *Appl Immunohistochem Mol Morphol,* **11**(2): 188-93.

Lee, S., S. W. Hong, B. H. Min, Y. J. Shim, K. U. Lee, I. K. Lee, M. Bendayan, B. J. Aronow and I. S. Park (2011). Essential role of clusterin in pancreas regeneration. *Dev Dyn,* **240**(3): 605-15.

Lefebvre, O., M. P. Chenard, R. Masson, J. Linares, A. Dierich, M. LeMeur, C. Wendling, C. Tomasetto, P. Chambon and M. C. Rio (1996). Gastric mucosa abnormalities and tumorigenesis in mice lacking pS2 trefoil protein. *Science,* **274**: 259-262.

Lennerz, J. K., S. H. Kim, E. L. Oates, W. J. Huh, J. M. Doherty, X. Tian, A. J. Bredemeyer, J. R. Goldenring, G. Y. Lauwers, Y. K. Shin and J. C. Mills (2010). The transcription factor MIST1 is a novel human gastric chief cell marker whose expression is lost in metaplasia, dysplasia, and carcinoma. *Am J Pathol,* **177**(3): 1514-33.

Leys, C. M., S. Nomura, E. Rudzinski, M. Kaminishi, E. Montgomery, M. K. Washington and J. R. Goldenring (2006). Expression of Pdx-1 in human gastric metaplasia and gastric adenocarcinoma. *Hum Pathol,* **37**(9): 1162-8.

Li, Q., S. M. Karam and J. I. Gordon (1996). Diphtheria toxin-mediated ablation of parietal cells in the stomach of transgenic mice. *J Biol Chem,* **271**: 3671-3676.

Lindstrom, E., D. Chen, P. Norlen, K. Andersson and R. Hakanson (2001). Control of gastric acid secretion:the gastrin-ECL cell-parietal cell axis. *Comp Biochem Physiol A Mol Integr Physiol,* **128**(3): 505-14.

Liu, Z., E. S. Demitrack, T. M. Keeley, K. A. Eaton, M. El-Zaatari, J. L. Merchant and L. C. Samuelson (2012). IFNgamma contributes to the development of gastric epithelial cell metaplasia in Huntingtin interacting protein 1 related (Hip1r)-deficient mice. *Lab Invest,* **92**(7): 1045-57.

Marazuela, M., A. Acevedo, M. A. Garcia-Lopez, M. Adrados, M. C. de Marco and M. A. Alonso (2004a). Expression of MAL2, an integral protein component of the machinery for basolateral-to-apical transcytosis, in human epithelia. *J Histochem Cytochem,* **52**(2): 243-52.

Marazuela, M. and M. A. Alonso (2004b). Expression of MAL and MAL2, two elements of the protein machinery for raft-mediated transport, in normal and neoplastic human tissue. *Histol Histopathol,* **19**(3): 925-33.

Marazuela, M., F. Martin-Belmonte, M. A. Garcia-Lopez, J. F. Aranda, M. C. de Marco and M. A. Alonso (2004c). Expression and distribution of MAL2, an essential element of the machinery for basolateral-to-apical transcytosis, in human thyroid epithelial cells. *Endocrinology,* **145**(2): 1011-6.

Matozaki, T., C. Sakamoto, M. Nagao, H. Nishizaki, Y. Konda and S. Baba (1988). Involvement of Ca2+ influx in F(-)-stimulated pepsinogen release from guinea pig gastric chief cells. *Biochem Biophys Res Commun,* **152**(1): 161-8.

Matsumoto, Y., T. G. Blanchard, M. L. Drakes, M. Basu, R. W. Redline, A. D. Levine and S. J. Czinn (2005). Eradication of Helicobacter pylori and resolution of gastritis in the gastric mucosa of IL-10-deficient mice. *Helicobacter,* **10**(5): 407-15.

McDaniel, N., A. J. Pace, S. Spiegel, R. Engelhardt, B. H. Koller, U. Seidler and C. Lytle (2005). Role of Na-K-2Cl cotransporter-1 in gastric secretion of nonacidic fluid and pepsinogen. *Am J Physiol Gastrointest Liver Physiol,* **289**(3): G550-60.

McDonald, S. A., L. C. Greaves, L. Gutierrez-Gonzalez, M. Rodriguez-Justo, M. Deheragoda, S. J. Leedham, R. W. Taylor, C. Y. Lee, S. L. Preston, M. Lovell, T. Hunt, G. Elia, D. Oukrif, R. Harrison, M. R. Novelli, I. Mitchell, D. L. Stoker, D. M. Turnbull, J. A. Jankowski and N. A. Wright (2008). Mechanisms of field cancerization in the human stomach: the expansion and spread of mutated gastric stem cells. *Gastroenterology,* **134**(2): 500-10.

McLaughlin, L., G. Zhu, M. Mistry, C. Ley-Ebert, W. D. Stuart, C. J. Florio, P. A. Groen, S. A. Witt, T. R. Kimball, D. P. Witte, J. A. Harmony and B. J. Aronow (2000). Apolipoprotein J/clusterin limits the severity of murine autoimmune myocarditis. *J Clin Invest,* **106**(9): 1105-13.

Minegishi, Y., H. Suzuki, M. Arakawa, Y. Fukushima, T. Masaoka, T. Ishikawa, N. A. Wright and T. Hibi (2007). Reduced Shh expression in TFF2-overexpressing lesions of the gastric fundus under hypochlorhydric conditions. *J Pathol,* **213**(2): 161-9.

Misra, V., S. Misra, M. Dwivedi, U. P. Singh, V. Bhargava and S. C. Gupta (2000). A topographic study of Helicobacter pylori density, distribution and associated gastritis. *J Gastroenterol Hepatol,* **15**(7): 737-43.

Modlin, I. M., Z. Zhu, L. H. Tang, M. Kidd, G. P. Lawton, K. Miu, R. E. Powers, J. R. Goldenring, D. Pasikhov and C. J. Soroka (1996). Evidence for a regulatory role for histamine in gastric enterochromaffin-like cell proliferation induced by hypergastrinemia. *Digestion,* **57**(5): 310-21.

Mohammadi, M., S. Czinn, R. Redline and J. Nedrud (1996). Helicobacter-specific cell-mediated immune responses display a predominant Th1 phenotype and promote a delayed-type hypersensitivity response in the stomachs of mice. *J Immunol,* **156**(12): 4729-38.

Molet, S., C. Belleguic, H. Lena, N. Germain, C. P. Bertrand, S. D. Shapiro, J. M. Planquois, P. Delaval and V. Lagente (2005). Increase in macrophage elastase (MMP-12)

in lungs from patients with chronic obstructive pulmonary disease. *Inflamm Res,* **54**(1): 31-6.

Morson, B. C. (1955). Intestinal metaplasia of the gastric mucosa. *Br J Cancer,* **9**(3): 365-76.

Muallem, S., C. J. Fimmel, S. J. Pandol and G. Sachs (1986). Regulation of free cytosolic Ca2+ in the peptic and parietal cells of the rabbit gastric gland. *J Biol Chem,* **261**(6): 2660-7.

Mulder, H., H. Schachter, M. De Jong-Brink, J. G. Van der Ven, J. P. Kamerling and J. F. Vliegenthart (1991). Identification of a novel UDP-Gal:GalNAc beta 1-4GlcNAc-R beta 1-3-galactosyltransferase in the connective tissue of the snail Lymnaea stagnalis. *Eur J Biochem,* **201**(2): 459-65.

Murayama, Y., J. Miyagawa, S. Higashiyama, S. Kondo, M. Yabu, K. Isozaki, Y. Kayanoki, S. Kanayama, Y. Shinomura, N. Taniguchi and et al. (1995). Localization of heparin-binding epidermal growth factor-like growth factor in human gastric mucosa. *Gastroenterology,* **109**(4): 1051-9.

Murayama, Y., J. Miyagawa, S. Higashiyama, S. Kondo, M. Yabu, S. Kanayama, Y. Shinomura and Y. Matsuzawa (1994). Localization of heparin-binding epidermal growth factor-like growth factor (HB-EGF) in human gastric mucosa. Gastroenterology. **106:** A622.

Nakamura, E., T. Kataoka, K. Furutani, K. Jimbo, T. Aihara, S. Tanaka, A. Ichikawa, H. Ohtsu and S. Okabe (2004). Lack of Histamine Alters Gastric Mucosal Morphology: Comparison between Histidine Decarboxylase-deficient and Mast Cell-deficient Mice. *Am J Physiol Gastrointest Liver Physiol*.

Nam, K. T., H. J. Lee, H. Mok, J. Romero-Gallo, J. E. Crowe, Jr., R. M. Peek, Jr. and J. R. Goldenring (2009). Amphiregulin-deficient mice develop spasmolytic polypeptide expressing metaplasia and intestinal metaplasia. *Gastroenterology,* **136**(4): 1288-96.

Nam, K. T., H. J. Lee, J. F. Sousa, V. G. Weis, R. L. O'Neal, P. E. Finke, J. Romero-Gallo, G. Shi, J. C. Mills, R. M. Peek, Jr., S. F. Konieczny and J. R. Goldenring (2010). Mature chief cells are cryptic progenitors for metaplasia in the stomach. *Gastroenterology,* **139**(6): 2028-2037 e9.

Nam, K. T., R. L. O'Neal, R. J. Coffey, P. E. Finke, N. Barker and J. R. Goldenring Spasmolytic polypeptide-expressing metaplasia (SPEM) in the gastric oxyntic mucosa does not arise from Lgr5-expressing cells. *Gut,* **61**(12): 1678-85.

Nam, K. T., A. Varro, R. J. Coffey and J. R. Goldenring (2007). Potentiation of oxyntic atrophy-induced gastric metaplasia in amphiregulin-deficient mice. *Gastroenterology,* **132**(5): 1804-19.

Neuburger, P., M. Lewin, C. de Recherche and S. Bonfils (1972). Parietal and chief cell populations in four cases of the Zollinger-Ellison syndrome. *Gastroenterology,* **63**(6): 937-42.

Nishizawa, T., H. Suzuki, T. Masaoka, Y. Minegishi, E. Iwasahi and T. Hibi (2007). Helicobacter pylori eradication restored sonic hedgehog expression in the stomach. *Hepatogastroenterology,* **54**(75): 697-700.

Nomura, S., S. Baxter, T. Yamaguchi, C. Leys, A. B. Vartapetian, J. G. Fox, J. R. Lee, T. C. Wang and J. R. Goldenring (2004a). Spasmolytic polypeptide expressing metaplasia (SPEM) to pre-neoplasia in *H. felis*-infected mice. *Gastroenterology,* **127**: 582-594.

Nomura, S., T. Baxter, H. Yamaguchi, C. Leys, A. B. Vartapetian, J. G. Fox, J. R. Lee, T. C. Wang and J. R. Goldenring (2004b). Spasmolytic polypeptide expressing metaplasia to preneoplasia in H. felis-infected mice. *Gastroenterology,* **127**(2): 582-94.

Nomura, S., S. H. Settle, C. Leys, A. L. Means, R. M. Peek, Jr., S. D. Leach, C. V. E. Wright, R. J. Coffey and J. R. Goldenring (2005a). Evidence for repatterning of the gastric fundic epithelium associated with Menetrier's disease and TGFa overexpression. *Gastroenterology,* **128**: 1292-1305.

Nomura, S., H. Yamaguchi, M. Ogawa, T. C. Wang, J. R. Lee and J. R. Goldenring (2005b). Alterations in gastric mucosal lineages induced by acute oxyntic atrophy in wild-type and gastrin-deficient mice. *Am J Physiol Gastrointest Liver Physiol,* **288**(2): G362-75.

Nomura, S., H. Yamaguchi, T. C. Wang, J. R. Lee and J. R. Goldenring (2004c). Alterations in gastric mucosal lineages induced by acute oxyntic atrophy in wild type and gastrin deficient mice. *Amer.J.Physiol.,* **288**: G362-G375.

Noto, J. M., T. Khizanishvili, R. Chaturvedi, M. B. Piazuelo, J. Romero-Gallo, A. G. Delgado, S. S. Khurana, J. C. Sierra, U. S. Krishna, G. Suarez, A. E. Powell, J. R. Goldenring, R. J. Coffey, V. W. Yang, P. Correa, J. C. Mills, K. T. Wilson and R. M. Peek, Jr. (2013). Helicobacter pylori promotes the expression of Kruppel-like factor 5, a mediator of carcinogenesis, in vitro and in vivo. *PLoS One,* **8**(1): e54344.

Nozaki, K., M. Ogawa, J. A. Williams, B. J. LaFleur, V. Ng, R. I. Drapkin, J. C. Mills, S. F. Konieczny, S. Nomura and J. R. Goldenring (2008). A molecular signature of gastric metaplasia arising in response to acute parietal cell loss. *Gastroenterology.,*(134): 511-521.

Nozaki, K., V. Weis, T. C. Wang, A. Falus and J. R. Goldenring (2009). Altered gastric chief cell lineage differentiation in histamine-deficient mice. *Am J Physiol Gastrointest Liver Physiol,* **296**(6): G1211-20.

Ogawa, M., S. Nomura, A. Varro, T. C. Wang and J. R. Goldenring (2006). Altered metaplastic response of waved-2 EGF receptor mutant mice to acute oxyntic atrophy. *Am J Physiol Gastrointest Liver Physiol,* **290**(4): G793-804.

Ogawa, T., K. Maeda, S. Tonai, T. Kobayashi, T. Watanabe and S. Okabe (2003). Utilization of knockout mice to examine the potential role of gastric histamine H2-receptors in Menetrier's disease. *J Pharmacol Sci,* **91**(1): 61-70.

Ohtsu, H., S. Tanaka, T. Terui, Y. Hori, Y. Makabe-Kobayashi, G. Pejler, E. Tchougounova, L. Hellman, M. Gertsenstein, N. Hirasawa, E. Sakurai, E. Buzas, P. Kovacs, G. Csaba, A. Kittel, M. Okada, M. Hara, L. Mar, K. Numayama-Tsuruta, S. Ishigaki-Suzuki, K. Ohuchi, A. Ichikawa, A. Falus, T. Watanabe and A. Nagy (2001). Mice lacking histidine decarboxylase exhibit abnormal mast cells. *FEBS Lett,* **502**(1-2): 53-6.

Oshima, H., K. Hioki, B. K. Popivanova, K. Oguma, N. Van Rooijen, T. O. Ishikawa and M. Oshima (2011). Prostaglandin E signaling and bacterial infection recruit tumor-promoting macrophages to mouse gastric tumors. *Gastroenterology,* **140**(2): 596-607 e7.

Oshima, H., A. Matsunaga, T. Fujimura, T. Tsukamoto, M. M. Taketo and M. Oshima (2006). Carcinogenesis in mouse stomach by simultaneous activation of the Wnt signaling and prostaglandin E2 pathway. *Gastroenterology,* **131**(4): 1086-95.

Oshima, H., M. Oshima, K. Inaba and M. M. Taketo (2004). Hyperplastic gastric tumors induced by activated macrophages in COX-2/mPGES-1 transgenic mice. *EMBO J,* **23**(7): 1669-78.

Oshima, M., H. Oshima, A. Matsunaga and M. M. Taketo (2005). Hyperplastic gastric tumors with spasmolytic polypeptide-expressing metaplasia caused by tumor necrosis factor-alpha-dependent inflammation in cyclooxygenase-2/microsomal prostaglandin E synthase-1 transgenic mice. *Cancer Res,* **65**(20): 9147-51.

Pisani, P., D. M. Parkin, F. Bray and J. Ferlay (1999). Estimates of the worldwide mortality from 25 cancers in 1990. *Int J Cancer,* **83**: 18-29.

Quiding-Jarbrink, M., S. Raghavan and M. Sundquist (2010). Enhanced M1 macrophage polarization in human helicobacter pylori-associated atrophic gastritis and in vaccinated mice. *PLoS One,* **5**(11): e15018.

Ramnarayanan, S. P., C. A. Cheng, M. Bastaki and P. L. Tuma (2007). Exogenous MAL reroutes selected hepatic apical proteins into the direct pathway in WIF-B cells. *Mol Biol Cell,* **18**(7): 2707-15.

Ramnarayanan, S. P. and P. L. Tuma (2011). MAL, but not MAL2, expression promotes the formation of cholesterol-dependent membrane domains that recruit apical proteins. *Biochem J,* **439**(3): 497-504.

Ramsey, V. G., J. M. Doherty, C. C. Chen, T. S. Stappenbeck, S. F. Konieczny and J. C. Mills (2007). The maturation of mucus-secreting gastric epithelial progenitors into digestive-enzyme secreting zymogenic cells requires Mist1. *Development,* **134**(1): 211-22.

Raufman, J. P., S. Berger, L. Cosowsky and E. Straus (1986). Increases in cellular calcium concentration stimulate pepsinogen secretion from dispersed chief cells. *Biochem Biophys Res Commun,* **137**(1): 281-5.

Raufman, J. P. and L. Cosowsky (1987). Interaction between the calcium and adenylate cyclase messenger systems in dispersed chief cells from guinea pig stomach. Possible cellular mechanism for potentiation of pepsinogen secretion. *J Biol Chem,* **262**(13): 5957-62.

Raufman, J. P., D. K. Kasbekar, R. T. Jensen and J. D. Gardner (1983). Potentiation of pepsinogen secretion from dispersed glands from rat stomach. *Am J Physiol,* **245**(4): G525-30.

Rizzi, F. and S. Bettuzzi (2010). The clusterin paradigm in prostate and breast carcinogenesis. *Endocr Relat Cancer,* **17**(1): R1-17.

Roth, K. A., S. B. Kapadia, S. M. Martin and R. G. Lorenz (1999). Cellular immune responses are essential for the development of Helicobacter felis-associated gastric pathology. *J Immunol,* **163**(3): 1490-7.

Samuelson, L. C. and K. L. Hinkle (2003). Insights into the regulation of gastric acid secretion through analysis of genetically engineered mice. *Annu Rev Physiol,* **65**: 383-400.

Sato, T., R. G. Vries, H. J. Snippert, M. van de Wetering, N. Barker, D. E. Stange, J. H. van Es, A. Abo, P. Kujala, P. J. Peters and H. Clevers (2009). Single Lgr5 stem cells build crypt-villus structures in vitro without a mesenchymal niche. *Nature,* **459**(7244): 262-5.

Schmidt, P. H., J. R. Lee, V. Joshi, R. J. Playford, R. Poulsom, N. A. Wright and J. R. Goldenring (1999). Identification of a metaplastic cell lineage associated with human gastric adenocarcinoma. *Lab.Invest.,* **79**: 639-646.

Shapiro, S. D., N. M. Goldstein, A. M. Houghton, D. K. Kobayashi, D. Kelley and A. Belaaouaj (2003). Neutrophil elastase contributes to cigarette smoke-induced emphysema in mice. *Am J Pathol,* **163**(6): 2329-35.

Sharp, R., M. W. Babyatsky, H. Takagi, S. Tagerud, T. C. Wang, D. E. Bockman, S. E. Brand and G. Merlino (1995). Transforming growth factor alpha disrupts the normal program of cellular differentiation in the gastric mucosa of transgenic mice. *Development.,* **121**: 149-161.

Shipley, J. M., R. L. Wesselschmidt, D. K. Kobayashi, T. J. Ley and S. D. Shapiro (1996). Metalloelastase is required for macrophage-mediated proteolysis and matrix invasion in mice. *Proc Natl Acad Sci U S A,* **93**(9): 3942-6.

Slaughter, D. P., H. W. Southwick and W. Smejkal (1953). Field cancerization in oral stratified squamous epithelium; clinical implications of multicentric origin. *Cancer,* **6**(5): 963-8.

Soroka, C. J., C. S. Chew, D. K. Hanzel, A. Smolka, I. M. Modlin and J. R. Goldenring (1993). Characterization of membrane and cytoskeletal compartments in cultured parietal cells: immunofluorescence and confocal microscopic examination. *Eur J Cell Biol,* **60**(1): 76-87.

Sugimura, T., N. Matsukura and S. Sato (1982). Intestinal metaplasia of the stomach as a precancerous stage. *IARC Sci Publ,*(39): 515-30.

Sutliff, V. E., J. P. Raufman, R. T. Jensen and J. D. Gardner (1986). Actions of vasoactive intestinal peptide and secretin on chief cells prepared from guinea pig stomach. *Am J Physiol,* **251**(1 Pt 1): G96-102.

Takizawa, T. and M. Koike (1998). Minute gastri carcinoma from pathomorphological aspect - reconsideration concerning histogenesis of gastric carcinomas. *Stomach and Intestine,* **23**: 791-800.

Tan, I. B., T. Ivanova, K. H. Lim, C. W. Ong, N. Deng, J. Lee, S. H. Tan, J. Wu, M. H. Lee, C. H. Ooi, S. Y. Rha, W. K. Wong, A. Boussioutas, K. G. Yeoh, J. So, W. P. Yong, A. Tsuburaya, H. Grabsch, H. C. Toh, S. Rozen, J. H. Cheong, S. H. Noh, W. K. Wan, J. A. Ajani, J. S. Lee, M. S. Tellez and P. Tan (2011). Intrinsic subtypes of gastric cancer, based on gene expression pattern, predict survival and respond differently to chemotherapy. *Gastroenterology,* **141**(2): 476-85, 485 e1-11.

Tanaka, S., K. Hamada, N. Yamada, Y. Sugita, S. Tonai, B. Hunyady, M. Palkovits, A. Falus, T. Watanabe, S. Okabe, H. Ohtsu, A. Ichikawa and A. Nagy (2002). Gastric acid secretion in L-histidine decarboxylase-deficient mice. *Gastroenterology,* **122**(1): 145-55.

Tang, L. H., F. D. Gumkowski, D. Sengupta, I. M. Modlin and J. D. Jamieson (1996). rab3D protein is a specific marker for zymogen granules in gastric chief cells of rats and rabbits. *Gastroenterology,* **110**(3): 809-20.

Tashima, K., S. Zhang, R. Ragasa, E. Nakamura, J. H. Seo, A. Muvaffak and S. J. Hagen (2009). Hepatocyte growth factor regulates the development of highly pure cultured chief cells from rat stomach by stimulating chief cell proliferation in vitro. *Am J Physiol Gastrointest Liver Physiol,* **296**(2): G319-29.

Tian, X., R. U. Jin, A. J. Bredemeyer, E. J. Oates, K. M. Blazewska, C. E. McKenna and J. C. Mills (2010). RAB26 and RAB3D are direct transcriptional targets of MIST1 that regulate exocrine granule maturation. *Mol Cell Biol,* **30**(5): 1269-84.

Tsunoda, Y., H. Takeda, T. Otaki, M. Asaka, I. Nakagaki and S. Sasaki (1988). A role for Ca2+ in mediating hormone-induced biphasic pepsinogen secretion from the chief cell determined by luminescent and fluorescent probes and X-ray microprobe. *Biochim Biophys Acta,* **941**(1): 83-101.

Tu, S. P., M. Quante, G. Bhagat, S. Takaishi, G. Cui, X. D. Yang, S. Muthuplani, W. Shibata, J. G. Fox, D. M. Pritchard and T. C. Wang (2011). IFN-gamma inhibits gastric carcinogenesis by inducing epithelial cell autophagy and T-cell apoptosis. *Cancer Res,* **71**(12): 4247-59.

Varon, C., P. Dubus, F. Mazurier, C. Asencio, L. Chambonnier, J. Ferrand, A. Giese, N. Senant-Dugot, M. Carlotti and F. Megraud (2011). Helicobacter pylori Infection Recruits Bone Marrow-Derived Cells that Participate in Gastric Preneoplasia in Mice. *Gastroenterology*.

Wang, L., E. J. Wilson, J. Osburn and J. DelValle (1996). Epidermal frowth factor inhibits carbachol stimulated parietal cell function via protein kinase C. *Am.J.Physiol.*

Wang, T. C., C. A. Dangler, D. Chen, J. R. Goldenring, T. Koh, R. Raychowdhury, R. J. Coffey, S. Ito, A. Varro, G. J. Dockray and J. G. Fox (2000). Synergistic interaction between hypergastrinemia and Helicobacter infection in a mouse model of gastric cancer. *Gastroenterology,* **118**: 36-47.

Wang, T. C., J. R. Goldenring, C. Dangler, S. Ito, A. Mueller, W. K. Jeon, T. J. Koh and J. G. Fox (1998). Mice lacking secretory phospholipase A2 show altered apoptosis and differentiation with Helicobacter felis infection. *Gastroenterology.,* **114**: 675-689.

Watanabe, T., M. Tada, H. Nagai, S. Sasaki and M. Nakao (1998). Helicobacter pylori infection induces gastric cancer in mongolian gerbils. *Gastroenterology,* **115**(3): 642-8.

Wei, J., T. A. Nagy, A. Vilgelm, E. Zaika, S. R. Ogden, J. Romero-Gallo, M. B. Piazuelo, P. Correa, M. K. Washington, W. El-Rifai, R. M. Peek and A. Zaika (2010). Regulation of p53 tumor suppressor by Helicobacter pylori in gastric epithelial cells. *Gastroenterology,* **139**(4): 1333-43.

Weis, V. G., J. F. Sousa, B. J. Lafleur, K. T. Nam, J. A. Weis, P. E. Finke, N. A. Ameen, J. G. Fox and J. R. Goldenring (2013). Heterogeneity in mouse spasmolytic polypeptide-expressing metaplasia lineages identifies markers of metaplastic progression. *Gut*.

Whitehead, R. H. and J. L. Joseph (1994). Derivation of conditionally immortalized cell lines containing the Min mutation from the normal colonic mucosa and other tissues of an "Immortomouse"/Min hybrid. *Epithelial Cell Biol,* **3**(3): 119-25.

Whitehead, R. H. and P. S. Robinson (2009). Establishment of conditionally immortalized epithelial cell lines from the intestinal tissue of adult normal and transgenic mice. *Am J Physiol Gastrointest Liver Physiol,* **296**(3): G455-60.

Whitehead, R. H., P. S. Robinson, J. A. Williams, W. Bie, A. L. Tyner and J. L. Franklin (2008). Conditionally immortalized colonic epithelial cell line from a Ptk6 null mouse that polarizes and differentiates in vitro. *J Gastroenterol Hepatol,* **23**(7 Pt 1): 1119-24.

Xia, H. H., J. S. Kalantar, N. J. Talley, J. M. Wyatt, S. SAdams, K. Cheung and H. M. Mitchell (2000). Antral-type mucosa in the gastric incisura, body and fundus (antralization): A link between Helicobacter pylori infection and intestinal metaplasia. *Am. J. Gastroenterol.,* **95**: 114-121.

Xiao, C., R. Feng, A. C. Engevik, J. R. Martin, J. A. Tritschler, M. Schumacher, R. Koncar, J. Roland, K. T. Nam, J. R. Goldenring and Y. Zavros Sonic Hedgehog contributes to gastric mucosal restitution after injury. *Lab Invest,* **93**(1): 96-111.

Yamaguchi, H., J. R. Goldenring, M. Kaminishi and J. R. Lee (2002). Association of spasmolytic polypeptide expressing metaplasia (SPEM) with carcinogen administration and oxyntic atrophy in rats. *Lab. Invest.,* **82**: 1045-1052.

Yamaguchi, H., J. R. Goldenring, Kaminishi.M. and J. R. Lee (2001). Identification of spasmolytic polypeptide expressing metaplasia (SPEM) in remnant gastric cancer and surveillance postgastrectomy biopsies. *Dig.Dis.Sci.,* **47**: 573-578.

Yamamoto, T., M. Kita, T. Ohno, Y. Iwakura, K. Sekikawa and J. Imanishi (2004). Role of tumor necrosis factor-alpha and interferon-gamma in Helicobacter pylori infection. *Microbiol Immunol,* **48**(9): 647-54.

Yoshizawa, N., Y. Takenaka, H. Yamaguchi, T. Tetsuya, H. Tanaka, M. Tatematsu, S. Nomura, J. R. Goldenring and M. Kaminishi (2007). Emergence of spasmolytic polypeptide-expressing metaplasia in Mongolian gerbils infected with Helicobacter pylori. *Lab Invest,* **87**(12): 1265-1276.

Zavros, Y., K. A. Eaton, W. Kang, S. Rathinavelu, V. Katukuri, J. Y. Kao, L. C. Samuelson and J. L. Merchant (2005). Chronic gastritis in the hypochlorhydric gastrin-deficient mouse progresses to adenocarcinoma. *Oncogene,* **24**(14): 2354-66.

Zavros, Y., M. Waghray, A. Tessier, L. Bai, A. Todisco, L. G. D, L. C. Samuelson, A. Dlugosz and J. L. Merchant (2007). Reduced pepsin A processing of sonic hedgehog in parietal cells precedes gastric atrophy and transformation. *J Biol Chem,* **282**(46): 33265-74.

Zimmerhackl, B., E. Wunsch, M. Classen, V. Schusdziarra and W. Schepp (1993). In man histamine and muscarinergic mechanisms are essential mediators of acid secretion in response to synthetic human gastrin (1-17). *Regul Pept*, **46**(3): 583-92.